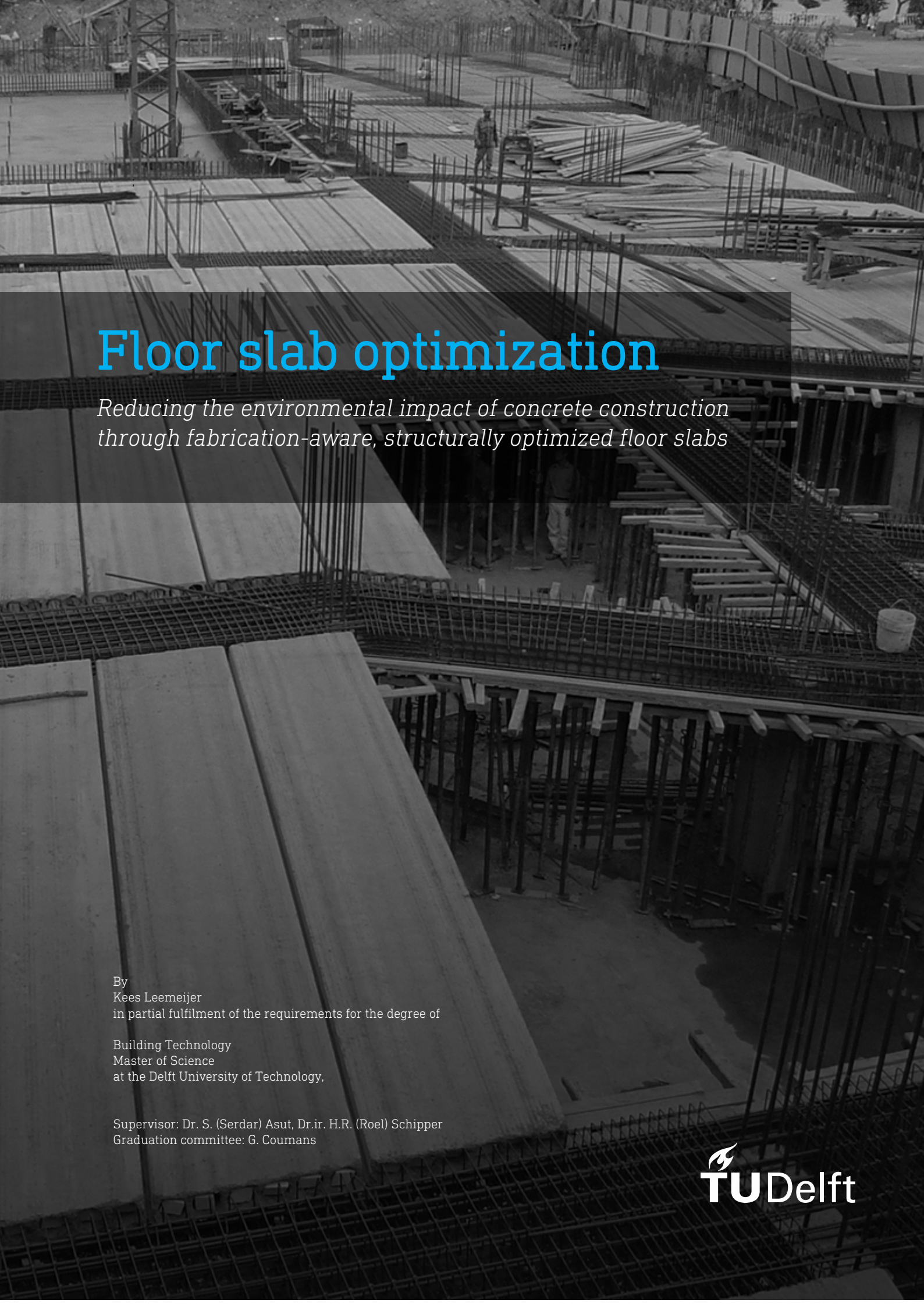

Floor slab optimization

Reducing the environmental impact of concrete construction through fabrication-aware, structurally optimized floor slabs

By
Kees Leemeijer
in partial fulfilment of the requirements for the degree of

Building Technology
Master of Science
at the Delft University of Technology,

Supervisor: Dr. S. (Serdar) Asut, Dr.ir. H.R. (Roel) Schipper
Graduation committee: G. Coumans

TU Delft

Nervi on concrete construction

"Although reinforced concrete has been used for over a hundred years and with increasing interest during the last decades, few of its properties and potentialities have been fully exploited so far. Apart from the unconquerable inertia of our own minds, which do not seem to be able to adopt freely any new ideas, the main cause of this delay is a trivial technicality: The need to prepare wooden frames." – Pier Luigi Nervi, 1956

Abstract

The building sector is responsible for 40% of worldwide carbon emissions, of which 8% can be attributed to concrete construction. With an increased demand for housing, this percentage is bound to increase. This thesis sheds light on strategies for reducing the environmental impact of concrete construction by investigating the potential of structural optimization and additive manufacturing. It concludes that in its current state, additive manufacturing is not able to address the environmental impact. Therefore, other potential strategies were explored, resulting in the following hypothesis: Fabrication-aware, structurally optimized floor slabs can significantly reduce the environmental impact of concrete construction.

This hypothesis resulted in a derivative-free – fabrication aware – optimization methodology combining shape and size optimization to find the optimal form of a thin-shell inspired flooring system. A life cycle assessment resulted in an overall environmental footprint reduction that ranges from 60.1% to 79.8% compared to conventional flooring systems in a hypothetical office building. This shows the effectivity of flooring systems that take advantage of membrane action and the impact of increasing structural efficiency to reduce the environmental footprint of concrete structures.

Table of Contents

1 Introduction ..... A
1.1 Preface ..... A
1.2 Thesis structure ..... A

2 Background 1
2.1 Reimagining formwork as a critical design-motivator 1
2.2 Energy use, environmental emissions, and material efficiency 2
2.3 Environmental impact of concrete 2
2.4 Problem statement 3

3 Research methodology 5
3.1 Research objective 5
3.2 Main research question 5
3.3 Research method 5

4 Section I: Literature study 9
4.1 Theoretical framework 9
4.2 Additive manufacturing processes 11
4.3 Structural optimization 25
4.4 Concrete manufacturing process 35
4.5 Literature research: Conclusion 40

5 Section II: Optimization of the floor slab 43
5.1 Defining the scope 44
5.2 The hypothesis 47
5.3 Proposed method: Creating a floor slab inspired by thin shells 48
5.4 Boundary conditions 50
5.5 Integration of the material 56
5.6 Environmental analysis 62
5.7 Research through design process 66
5.8 Resulting floor slabs of optimization 79
5.9 Section II: Summary and key findings 83

6 Section III: Comparison and evaluation 85
6.1 LCA analysis of the new floor 85
6.2 LCA analysis of conventional floors 88
6.3 LCA analysis of a hypothetical office building 91
6.4 Comparison of flooring systems (3600 mm x 5400 mm) 96
6.5 Comparison of the flooring systems in a hypothetical office building 99
6.6 Section III: Conclusion and key findings. 101

7 Discussion 103
7.1 Limitations and suggestions for further research 103
7.2 Future research 103

8 Conclusions 106
8.1 Revisiting the research questions 106
8.2 Conclusions on hypothesis-driven design 107
8.3 Societal relevance 107
8.4 Scientific relevance 107
8.5 Concluding remarks 107

9 References 108

10 Appendix 115

Introduction

Motivation behind the thesis

Image Source: https://www.rileycon.com/tag/bubbledeck/

1 Introduction

1.1 Preface

During my Bachelor studies in Bouwkunde at the Technical University of Delft and my internship at Bentvelsen Fleer Architectuur en Stedenbouw (BFAS), I have come to appreciate the great potential of using digital tools as an architect. When working on a project, the structural calculations and the manufacturability are usually only being checked after the design phase. The shift towards an integrated digital workflow through programs such as Dynamo, Revit, Rhino, and Grasshopper allows for an integrated and thus more efficient design approach. This realization, coupled with the fact that the current building sector is highly inefficient (Barbosa, Woetzel, Mischke, et al., 2017), led to my fascination with computational design and robotic – or possibly automated – fabrication.

Figure 1 3D-printed floor slab of ETH Zurich

In November 2019, I visited the ETH Zürich. One of their institutes that greatly inspires me is "Digital Building Technologies." They focus on the seamless integration of computational design methods, digital fabrication, and new materials. The 3D-printed floor slab that they fabricated is an excellent example of the impact you can have with their approach. This floor slab resulted in a reduction of 70% of the material compared to conventional floor slabs (M Rippmann, Van Mele, & Block, 2018) (figure 1).

Their project showed the potential of informed (e.g., fabrication-aware, structurally optimized) design. It led me to ask: Can we use innovative fabrication methods, and an informed design approach to adapt to the changing conditions in the building sector?

1.2 Thesis structure

This thesis is written within the framework of the "sustainable design graduation studio," which is part of the two-year Building Technology Master's program at the Delft University of Technology. The graduation thesis consists of three parts:

- *Introduction*
  It starts with the driving forces behind the thesis topic and the topic's current relevance. The introduction builds up to the problem statement and is then followed up by an elaboration of the research methodology.

- *Body*
  The body of the thesis consists of three sections. Section I contains the research phase; this is a literature study providing relevant background information on the addressed topics; it results in the formulation of initial conclusions as well as in the hypothesis that will be tested in Section II.

  Section II focuses on testing the hypothesis that *fabrication-aware, structurally optimized floor slabs can significantly reduce the environmental impact of concrete construction.* It does so by creating a floor slab inspired by thin shells, which is not only structurally efficient, but constructed using materials with a low environmental impact, compatible with economical construction and that can be built using a methodology that is replicable and robust. Section III focuses on the evaluation of the results in a hypothetical office building and a comparison to other flooring systems, thereby illustrating the effectiveness of thin-shell flooring systems.

- *Conclusions*
  The conclusions of the thesis consist of a discussion of the results, a conclusion, and further recommendations. Here, the main research question will be answered, and the hypothesis will be discussed, further evaluated, and validated. This all results in conclusions and further recommendations.

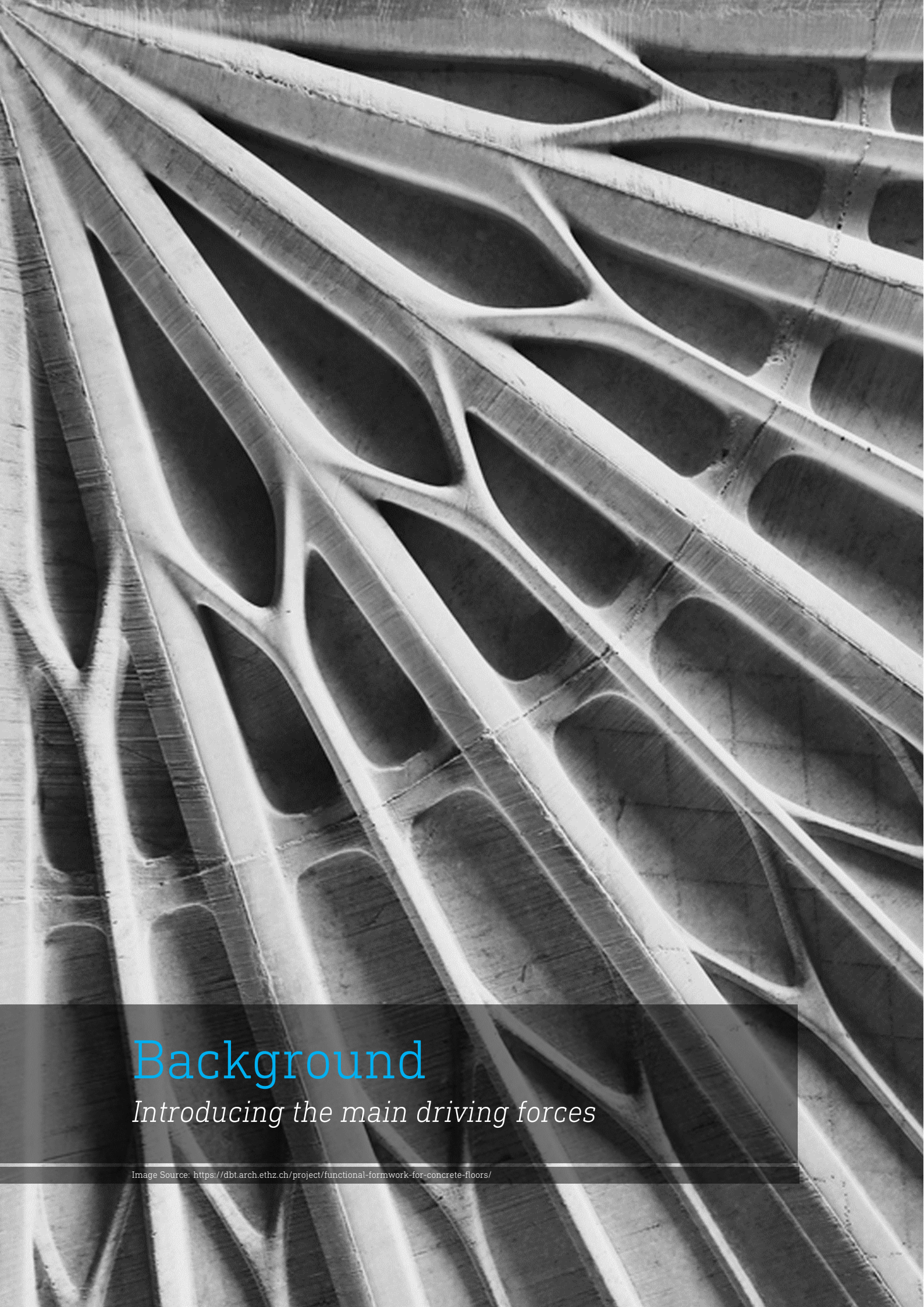

Background

Introducing the main driving forces

Image Source: https://dbt.arch.ethz.ch/project/functional-formwork-for-concrete-floors/

2 Background

To mitigate the increasing severity of climate change, we need to reduce greenhouse gas emissions by 55–85% before 2050 (Fisher & Nakicenovic, 2007). Looking at our current period-specific cultural patterns, the motivation to reduce emissions exists, but that does not automatically result in a reduction of emissions. The scope of this thesis is defined by the urgency to have more tools at hand to reduce greenhouse gas emissions, combined with three underlying driving factors in the building sector:

- Reimagining formwork as a critical design-motivator (in concrete construction)
- Optimizing energy use, reducing emissions, and increasing material efficiency
- Reducing the pollution in concrete construction

2.1 Reimagining formwork as a critical design-motivator

The cost of formwork is estimated to make up between 35 and 60% of the overall cost of concrete construction (Lloret et al., 2015). Figure 2 illustrates the cost distribution of building with concrete. Similarly, the formwork accounts for 53% of the cost (A. Jipa et al., 2019). The cost distribution of construction highlights the importance of optimizing the current process.

Currently, geometrical simplicity is preferred over efficient material use. One of the reasons for this is that the cost is a significant driving force for design in construction. Often geometry is standardized and post-rationalized to reduce the amount and complexity of formwork required.

Besides this, formwork is a significant source of waste; all formwork is discarded sooner or later, contributing to an increasing amount of waste in the world (Llatas, 2011). Reducing the amount of waste originating in the construction sector is essential as *"80 % of the total worldwide waste is generated in the construction industry" (Sanjayan & Nematollahi, 2019).*

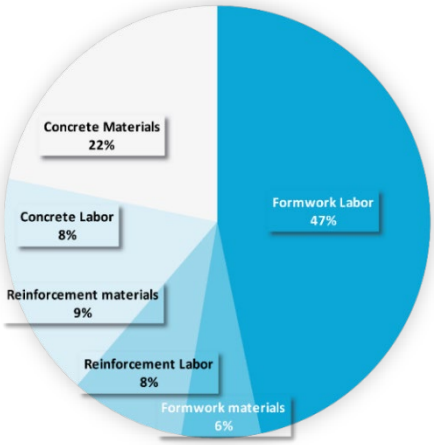

Figure 2 - Cost distribution of concrete construction. Based on: (A. Jipa et al., 2019)

Currently, our economy shifting from a linear model to a circular one. The financial aspects of adopting the Ellen MacArthur model (circular economy) are becoming more feasible as people become aware of the current resource depletion and waste production.

Figure 3 Formwork required to build the Building Academy in Salzburg. Source: Diversaire.nl

Figure 3 show the construction of the foyer and entrance of the Building Academy in Salzburg (Hafele, 2012). This project showcases the amount of formwork required to generate complex shapes, however, the question that arises is how sustainable is it to build a building twice?

With the increasing level of awareness of the impact of the building sector, it can be expected that environmental reasons will drive the future of the industry. A reduction in the amount of waste and decrease in cost by eliminating formwork, by reducing the amount of required labor or making formwork reusable, could be game-changing.

2.2 Energy use, environmental emissions, and material efficiency

When looking at the future of the building sector, material efficiency will become a critical driving force for design (Ruuska & Hakkinen, 2014). According to the Global Status Report by the United Nations Environment Program, the building sector accounts for 40% of energy-related carbon-dioxide (CO_2) emissions and 36% of global total global energy use (*Global Status Report: Towards a zero-emission, efficient and resilient buildings and construction sector*, 2018). The European Commission created a roadmap to a more sustainable, resource-efficient Europe. In this roadmap, the building sector forms one of the three key sectors for improvement (*Roadmap to a Resource Efficient Europe* 2011). According to the European Commission, the building sector can realize a reduction of:

- 42% of final energy consumption
- 35% of the greenhouse gas emissions
- 50% of all extracted materials

The European Commission mainly considered research, which focuses on the end of a building's lifecycle. Most research focuses on reducing waste, extending life spans, recycling materials, and reusing materials, as solutions to the problem. However, most pollution currently comes from concrete as a building material.

2.3 Environmental impact of concrete

Concrete – mainly used in the building sector - is the world's second most consumed material, after water. Today, concrete industry alone is estimated to account for 8% of total annual global CO_2 emissions (Andrew, 2019).

To put this number into perspective, aviation represents approximately 2% to 3% of the total annual global CO_2 emissions (McCollum, Gould, & Greene, 2010). Reports from *The Guardian* state that if the cement (the binder in concrete) industry were a country, it would be the third-largest emitter of CO_2 in the world (Watts, 2019).

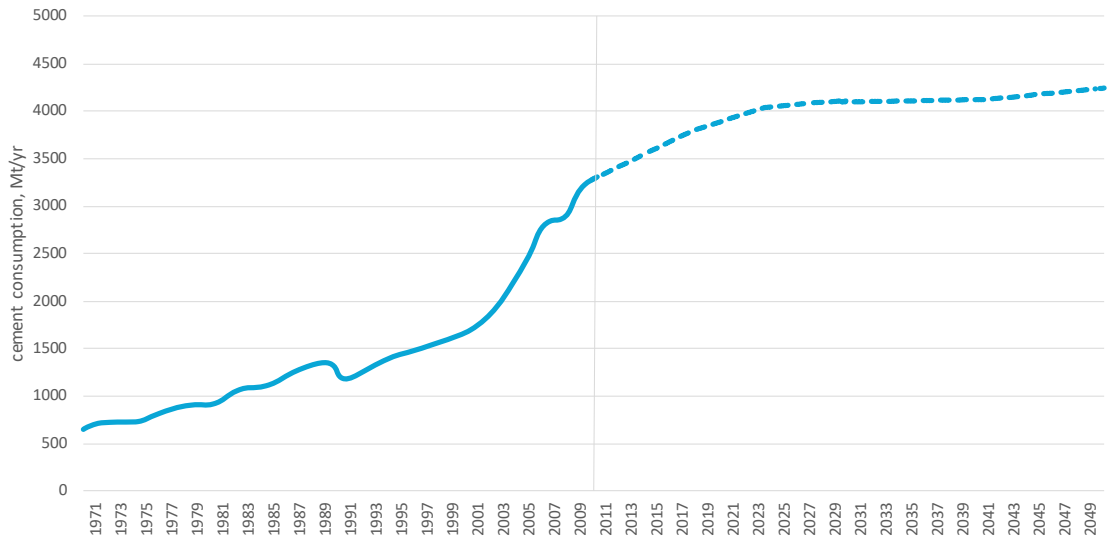

Figure 4 – Graph of the global cement consumption and the (conservative) prediction of consumption up to 2050. Based on: (Ruijven et al., 2016)

(Van Ruijven et al., 2016) predicted future cement consumption until 2050 (Figure 4) whereby the production is set to increase to 4500 Mt/year in 2050. The International Building Agency (2017) noted similar numbers. On a business as usual trajectory, the global cement production is set to increase to 5000 Mt/year in 2050 (Johanna Lehne & Felix Preston, 2018).

The increase in cement consumption is not in line with the amount of reduction in environmental pollution required. Furthermore, global building floor area in 2016, which was around 235 billion square meters, is projected to double over the next 30 years (Johanna Lehne & Felix Preston, 2018). When taking the growth of global floor area into account, cement consumption presented by Ruijven and by Johanna Lehne & Felix Preston could be considered as conservative estimates.

2.4 Problem statement

Based on the background study on driving forces within the current state of the construction industry, there is a need to reduce the environmental impact of concrete (Van Ruijven et al., 2016), as well as to change production methods (due to the cost and waste related to formwork) (Sanjayan & Nematollahi, 2019). Moreover, the overall emissions of the building sector need to be reduced. (Abergel, Dean, Dulac, & Hamilton, 2017)

These driving forces, combined with the potential of digitalization and automation in the building industry, define the topic for this thesis.

Potential solution: Additive manufacturing and topology optimization

Timothy Wangler from the ETH Zurich stated that additive manufacturing (AM) can eliminate the use of formwork (Wangler et al., 2016). Moreover, the use of robotics and additive methods have the potential to increase the efficiency of the building industry greatly (Barbosa, Woetzel, & Mischke, 2017) and topology optimization can result in reducing material use by 70%, thereby also reducing emissions by 70% (M Rippmann et al., 2018).

As geometrical simplicity is still the primary design motivator and the intricate "optimized" geometrical shapes resulting from topology optimization are hard to fabricate, we still need to solve several problems.. Challenges that arise are:

- Can we reduce the amount of material while considering fabrication constraints?
- Can we use innovative fabrication methods to fabricate intricate shapes?
- Can we further reduce the impact of the building sector by looking at the design process?

The second challenge is especially fascinating, because additive manufacturing (AM), and topology optimization (TO) can complement one another other. Topology optimization provides a powerful method for generating the optimized models, while AM enables a cost-effective fabrication of geometrically complex shapes (J. Wu, Aage, N., Lefebvre, S., & Wang, C., 2017).

The complementary relationship between AM and TO and the applicability of innovative fabrication methods are at the heart of this thesis. The research starts by investigating the possibilities of reducing material usage by innovative fabrication methods. If direct application does not seem feasible, it will focus on the reducing environmental impact with the use of existing techniques.

Research methodology

Research through process design

Image Source: https://dbt.arch.ethz.ch/project/topology-optimisation-concrete-slab/

3 Research methodology

3.1 Research objective

The objective of this research is to develop an efficient design-to-fabrication method that can be used for making large-scale, optimized, complex building components. The aim is to create insights into the possibilities of reducing (environmental) impact through an integrated design approach. As noted in Chapter 1, this is especially significant for building materials that are difficult to recycle (e.g., concrete, the most used building material).

3.2 Main research question

The main research question that results from the background study and the objective is:

In what manner can we use structural optimization and additive manufacturing in the building sector to address the environmental impact of concrete construction?

This will result in a comprehensive design-to-fabrication workflow illustrating the possibility of reducing the environmental impact by an integrated design approach.

3.3 Research method

The research method applied here can be categorized as a research-through-design approach with a central focus on the process. The research begins with a literature study to gain insights into potential solutions to the primary research question. This research phase is followed up by a design-to-fabrication workflow addressing the hypothesis produced by the insights gained during the research phase. The thesis concludes with a validation and comparison of the developed results. Figure 5 summarizes the interactive way the research process works within the thesis.

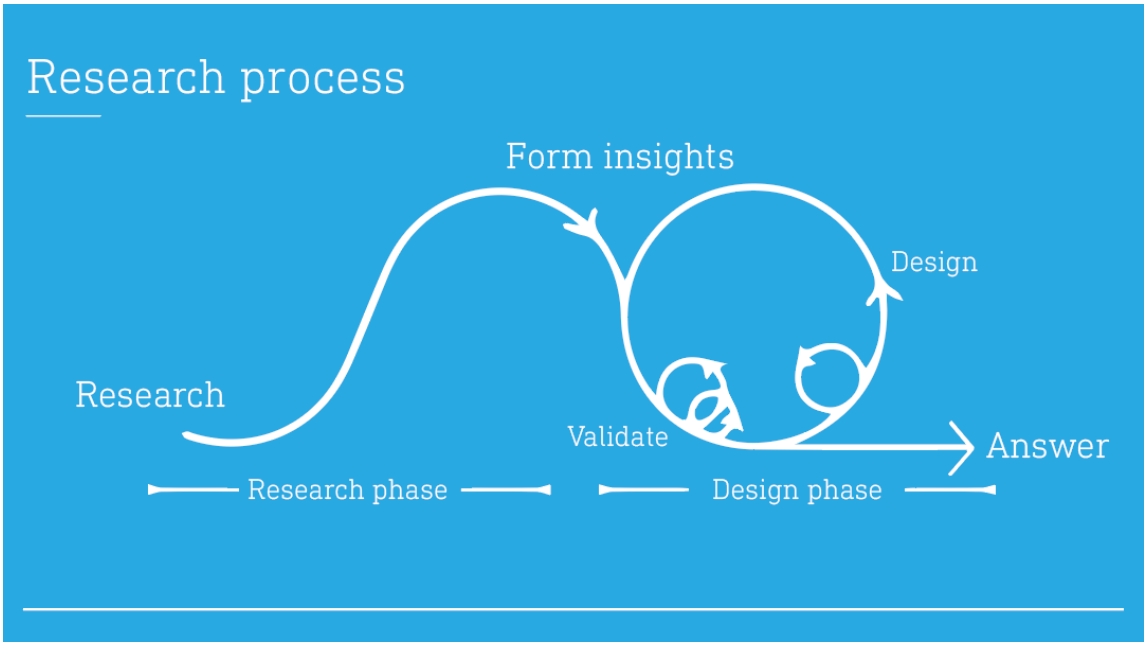

Figure 5 Illustration of the cyclic character of the research and design process

As described in the introduction, the thesis is divided into an introductory problem analysis, a main body that includes the literature research, and finally, the thesis conclusions consisting of the validation, reflection, and discussion of the research results.

Figure 6 illustrates the research process in further detail, which is based on the theory of inventive problem-solving and the systematic approach by Pahl and Beitz, (Malmqvist, Axelsson, & Johansson, 1996) which forms the basis of this thesis. The approach starts with a problem analysis followed up by the main body, conclusions, and recommendations. The main body consists of literature research, research through interactive process design, evaluation and comparison. The different sections of the main body will be elaborated on in Chapter 3.3.1, 3.3.2, and 3.3.3.

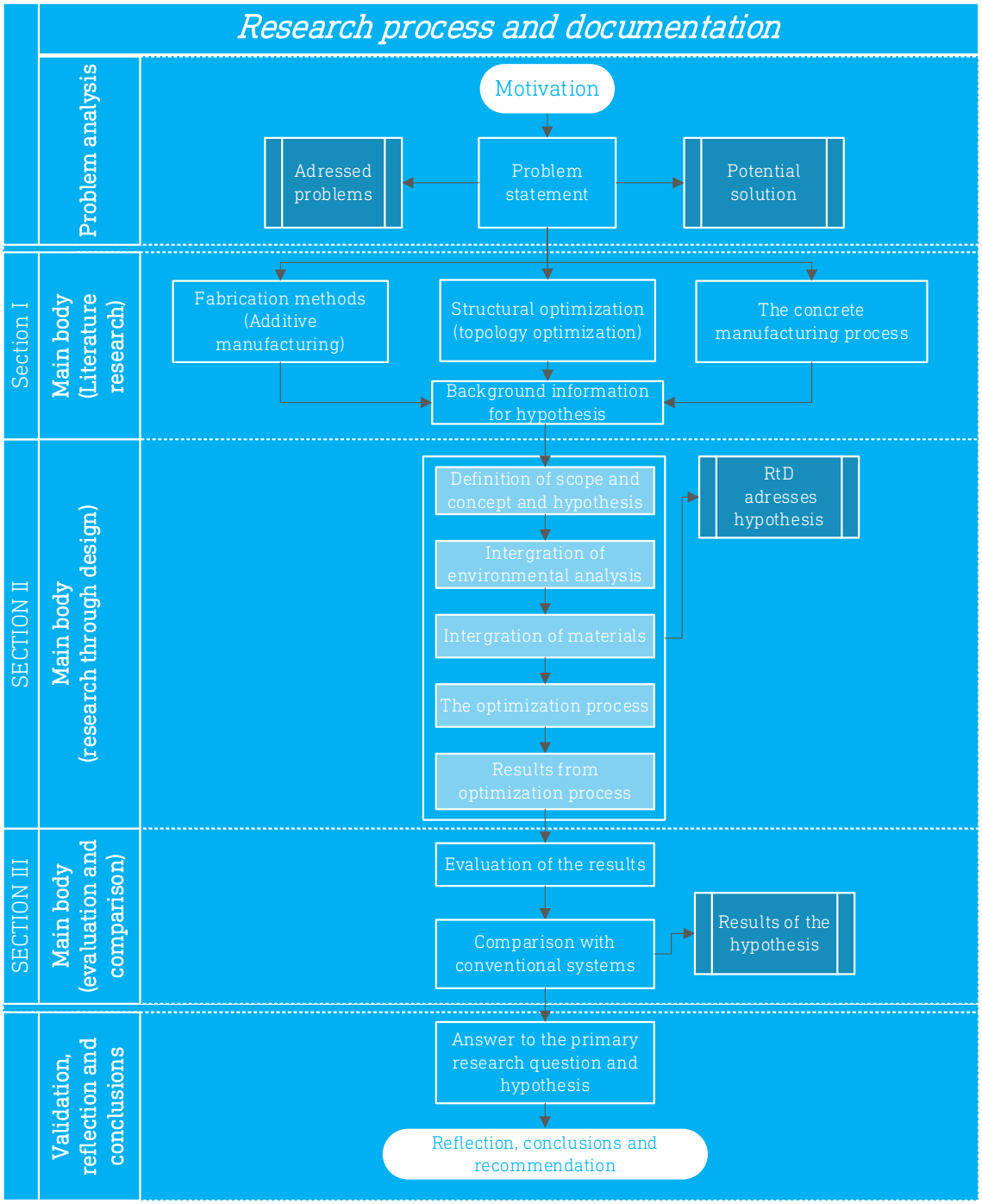

Figure 6 - Flowchart of the research methodology of this graduation thesis

3.3.1 Section I: Literature research

To answer the primary question, literature research is done in three main areas. The primary goal of the literature research is to check the viability of the proposed solution and to produce a hypothesis. The main research question addresses three subdomains highlighted in the question underneath.

In what manner can we use structural optimization and additive manufacturing in the building sector to address the environmental impact of concrete construction?

The literature research tries to find answers regarding the issues addressed in the thesis, and to propose potential solutions. This is done in three areas of literature:

- Structural optimization
- Fabrication methods (additive manufacturing)
- Concrete manufacturing process (and the environmental impact of concrete)

Each area consists of a brief summary. Instead of comprehensive analysis, the literature study aims to uncover the relevancy to the problems of this study and insights into potential solutions. Further questions that relate to the primary research question will be formulated and answered, resulting in the necessary background information to formulate an informed hypothesis for the research-through-design (RtD) part, Section II.

3.3.2 Section II: Optimization of a floor slab

Section II seeks to find an answer to the main research question by addressing the hypothesis formulated in Section I with a research-through-design (RtD) approach. It starts with a definition of the scope and of the boundaries for the optimization process. Section II results in a fabrication-aware design to fabrication workflow. The section consists of three areas, which will be further elaborated on in section II:

- Introduction
- Optimization process
- Results of the optimization methods

Section II results in an optimized design that addresses the environmental impact of concrete construction. The optimized design forms the basis for evaluation and comparison.

3.3.3 Section III: Evaluation and comparison

To find an answer to the main research question, the results need to be compared. Section III aims to evaluate the results and to compare them with conventional systems. Evaluations will be made that will form the basis for the discussion and conclusions, thereby also providing recommendations for further research.

Literature study

Compiling a theoretical background

Image Source: https://dbt.arch.ethz.ch/wp-content/uploads/2020/06/Fast-Complexity_0.jpg

4 Section I: Literature study

The goal of the literature study is to provide a theoretical background for the research topic which in turn exists to provide theories as the basis for a solution to the stated problem. The main aim is to create a succinct summary of each field. Instead of a comprehensive analysis, the literature study is focused on the relevancy to the problems of this study and insights into potential solutions. In the end, the literature study is synthesized into conclusions. The conclusions form the basis for the research-through-design (RtD) approach. The primary goal is to get all the necessary information to address the research question:

In what manner can we use structural optimization and additive manufacturing in the building sector to address the environmental impact of concrete construction?

4.1 Theoretical framework

This research builds upon recent research in different fields. Some fields are distinctive yet interconnected within the scope of this thesis. The fields studied are:

- Fabrication methods
- Structural optimization
- Concrete manufacturing processes

As stated before, the Chapter will form the basis for the research-through-design (RtD) approach, which is described in section II. A description of the comprehensive analysis of each field would exceed the scope of this thesis. Instead, questions will be formulated and individually answered at the end of the research. Furthermore, innovative examples of the application of each of the fields will be elaborated on concisely throughout the literature study.

The theoretical framework will try to find answers to questions in relation to the primary research question:

- In what manner can we use additive manufacturing to address the environmental impact of concrete construction?
- In what manner can we use structural optimization to address the environmental impact of concrete construction?
- What are the different ways are there to address the environmental impact of concrete construction?

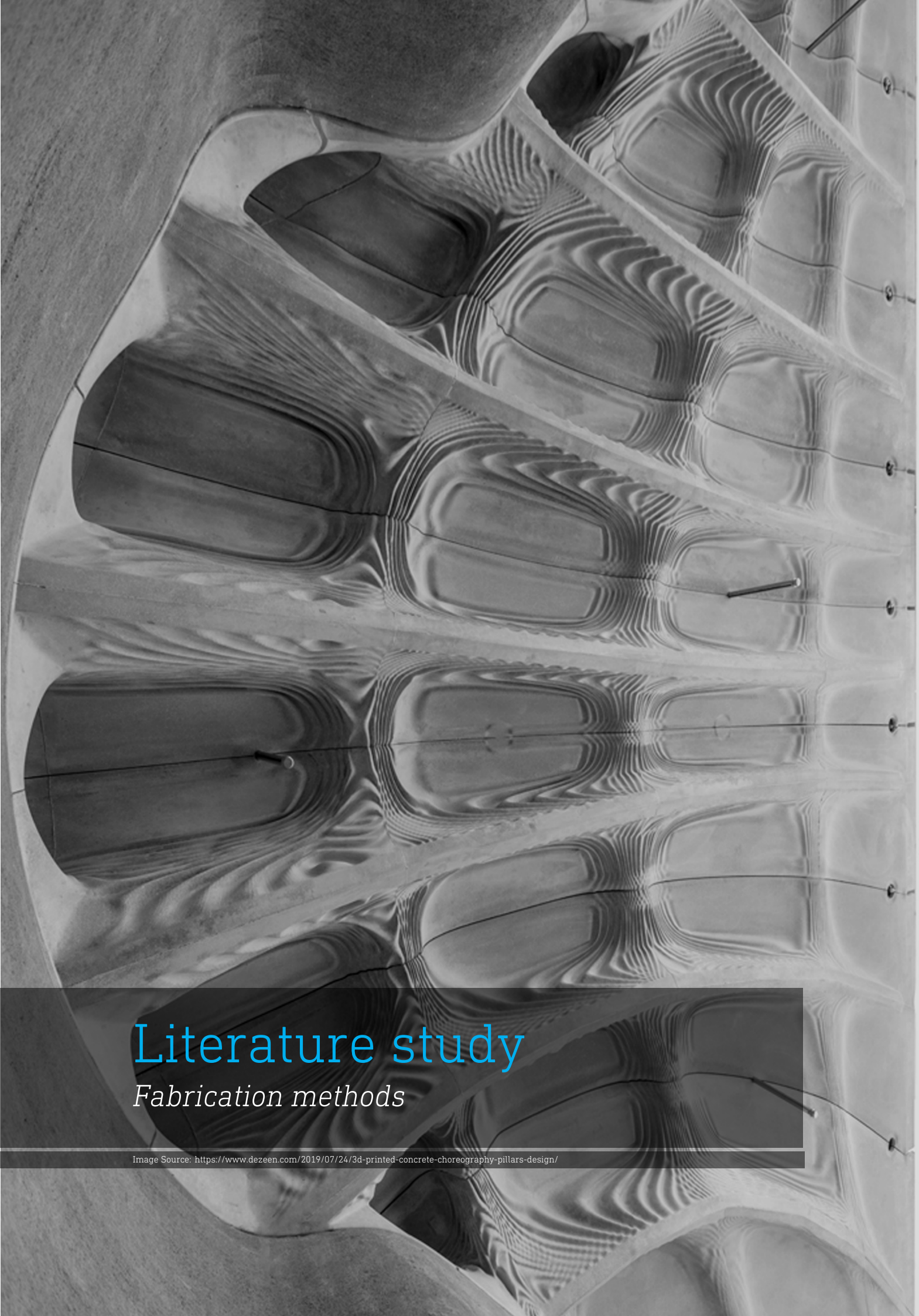

Literature study

Fabrication methods

Image Source: https://www.dezeen.com/2019/07/24/3d-printed-concrete-choreography-pillars-design/

4.2 Additive manufacturing processes

Additive methods can be divided into seven categories: material extrusion, material jetting, binder jetting, powder bed fusion, directed energy deposition, vat photopolymerization, and sheet lamination (Figure 7) ("ISO/ASTM 17296 Standard on additive manufacturing (AM) Technologies," 2015).

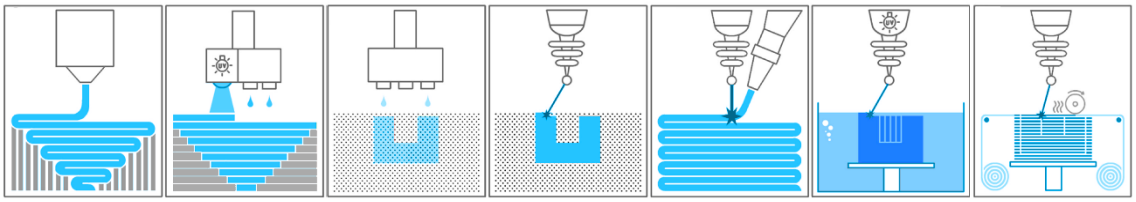

Figure 7 – Illustration of additive manufacturing methods. From left to right: material extrusion, material jetting, binder jetting, powder bed fusion, direct energy deposition, vat photopolymerization, and sheet lamination. Based on: (Ahangar, Cooke, Weber, & Rosenzweig, 2019)

Most additive manufacturing processes are hard to scale up and are, therefore, not applicable to the building sector. After a short introduction to the general categories of additive manufacturing processes, this research will focus on the potential applications of additive manufacturing within the building sector. After this, the manufacturing methods with the most potential will be elaborated in-depth.

- *Material extrusion*
  Material extrusion is a process in which material is extruded in a layer-by-layer manner, and is usually used for plastics. The process has been commercialized as Fused Deposition Modeling (FDM). It is a relatively cheap process which is reflected in the variety of inexpensive, personal 3D printers available (Gibson, Rosen, & Stucker, 2014).

- *Material jetting*
  In material jetting, droplets are selectively deposited at predetermined locations. The technology shares many similarities to common inkjet printers. The printed material consists of a combination of a photopolymer and wax which is cured by ultraviolet lighting. A good example of material jetting is the PolyJet technology from Stratasys (Gibson et al., 2014).

- *Binder jetting*
  In binder jetting, a powdered material is added layer-by-layer manner. Within each layer, a liquid-binding agent is selectively applied to bind the powder together at the desired location. This method's primary advantage is that the unbound particles support the powder on top, enabling prints with overhangs. Binder jetting was originally developed at MIT under the name 3D printing (3DP) (Gibson et al., 2014).

- *Powder bed fusion*
  Similar to binder jetting, in powder bed fusion, a fine powder is selectively bonded to create prints. However, instead of a liquid binder agent, the powder is fused by thermal energy, typically in the form of a laser or an electron beam.

- *Direct energy deposition*
  In direct energy deposition, a material is fused by thermal energy in a manner similar to that as with powder bed fusion. The difference is that in the case of direct energy deposition, the material is melted together while being deposited. This technology's primary application is used to repair and rebuild damaged components.

- *Vat photopolymerization*
  In vat photopolymerization, a liquid, light-activated polymer is selectively cured with a laser. During curing, the platform moves down (into the liquid) so that a new layer of liquid forms on top. The main advantage of this process is that it allows for a very high printing resolution.

- *Sheet lamination*
  In sheet lamination, an object is formed by successively shaping and bonding layers of sheet material on top of each other. These sheets are made of coated paper, metals, or plastics. A laser is usually used to cut the sheet material to the desired form.

With the focus on addressing the environmental impact of concrete construction, several other potential applications of additive manufacturing can be imagined. To examine which of these additive manufacturing methods are applicable to concrete construction, the following section will take a broader look at manufacturing methods in the construction sector, focusing on digital fabrication as this is where additive manufacturing excels.

4.2.1 manufacturing methods in digital fabrication with concrete

Digital fabrication and additive manufacturing methods are on the rise within the construction sector. Just recently (August 2020), a comprehensive process classification framework for defining and describing the process of digital fabrication with concrete was proposed (Richard A Buswell et al., 2020). Buswell describes five primary classes – particle binding, material extrusion material jetting, solidification and deformation – which can be divided into three types of manufacturing:

- *Additive manufacturing*
  Additive manufacturing is an additive process in which an object is built "layer-by-layer." Each layer consists of material that is placed on the previous layers. The most commonly used additive manufacturing processes for the digital fabrication of concrete are: *particle-bed binding, material extrusion, and material jetting.*

- *Subtractive manufacturing*
  The process of subtractive manufacturing is a subtractive method in which an object is made by removing material from a solid piece of material (typically called stock). It can be done manually by cutting away material, but is mostly done in a pre-programmed manner by machines. Although subtractive manufacturing processes do not generally find widespread application in concrete construction, milling is the most frequently used process when it comes to digitally supported manufacturing processes in concrete fabrication, and it is often used to generate formwork.

- *Formative manufacturing*
  This type of manufacturing is a formative process where an object is shaped through a compression or consolidation process. This includes methods such as injection molding, die casting, pressing, and stamping to form material into the desired shape. The formative processes related to digital fabrication of concrete can be divided into two categories: *solidification and deformation.*

While all manufacturing methods can be described as distinctive and separate processes, hybrid methods are seen more often when more complexity or certain qualities are required. This is mostly done to combine the advantages of different processes. Within the construction sector, the term "hybrid manufacturing" is used to denote the intentional combinations of processes to achieve better results (Richard A Buswell et al., 2020).

One example of an hybrid process is the topology-optimized beam in Figure 9, which is developed by 3D printing company start-up Vertico and Ghent University in 2019.

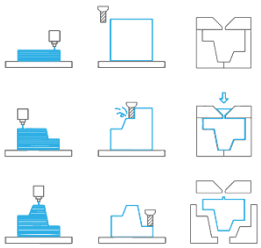

Figure 8 - Additive, subtractive and formative manufacturing

4.2.2 Hybrid manufacturing

The shape of the girder was optimized using topology optimization (Chapter 4.3) In the optimization process, not only the position of the concrete was optimized, but the shape, position, and curvature of the post-tensioning cable (Figure 9) (Menna et al., 2020).

This minimizes the displacement at the top surface of the girder caused by the combined action of the external loads and the post-tensioning tendon. Figure 10 show the fabricated girder and the 3D printed formwork.

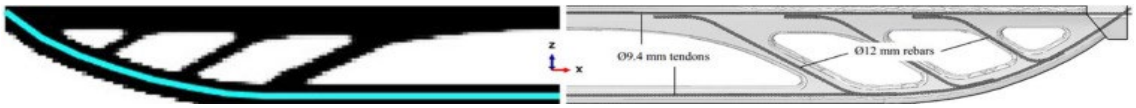

Figure 9 Topology optimization results positioning of the post-tension cable, and the final rebar of the girder (image by Menna, Mata-Falcon et al. 2020)

The collaborative project between Vertico and Ghent University showcases the potential of additive manufacturing in offering optimized alternatives for existing building elements. It results in the reduced cost of fabricating complex shapes by using additive methods to generate the formwork and the ease of reinforcement in formative methods (casting).

Figure 10 - Picture of the final topology optimized girder, on the right: 3D printed formwork by Vertico (image by Menna, Mata-Falcon et al. 2020)

4.2.3 Additive manufacturing: Potential

In recent years, there has been a vast increase in research on additive manufacturing for building components. This development can be attributed to the digitalization of the building industry and the opportunities associated with additive manufacturing.

A paper by the TU Eindhoven, "Additive manufacturing of concrete in construction: potentials and challenges of 3D concrete printing" says that digital processes hold the potential to increase the efficiency of buildings and help lower their environmental impact (Bos, Wolfs, Ahmed, & Salet, 2016). In combination with additive manufacturing, it can result in multiple significant benefits to the current construction industry, such as increasing geometrical flexibility, adding multi-functionalities, eliminating the use of formwork, and a considerable reduction in construction cost and time (Wangler et al., 2016) Similarly, Benjamin Dillenburger from the ETH Zurich states that:

> Additive manufacturing promises the fully automated fabrication of building components where customization and complexity comes at no extra cost (Lowke et al., 2018)

According to Lowke, et al. (2018) and Wangler (2016), additive manufacturing has significant potential. From Chapter 4.2.2 onwards, the current applications of additive manufacturing in the industry will be explored. Furthermore, the different potentials of additive manufacturing will be analysed in-depth, and the additive manufacturing methods with the most potential will be further evaluated.

4.2.4 Additive manufacturing: Applications in the building sector

The first attempt to use additive manufacturing technologies in construction dates back to 1997. The process stacked sand with Portland cement in a layer-by-layer manner using cement as the adhesive. Final consolidation was performed by applying steam in a pressurized steam chamber (Pegna, 1997). Since then, additive manufacturing has seen an increase in usage in the building sector.

Table 1 offers an overview of currently applied additive manufacturing technologies in research facilities and in the construction industry (2019). Furthermore, it includes the material used in the processes.

When looking at the potential of different methods described in literature, material extrusion seems to be the clear frontrunner with respect to both the level of overall technological readiness and economic viability (Mechtcherine et al., 2020). 3D particle-bed methods are the most suitable when it comes to geometric complexity, as this complexity does not result in additional costs of fabrication (Lowke et al., 2018).

Table 1: Overview of additive manufacturing technologies in the construction industry (Craveiroa, Duartec, Bartoloa, & Bartolod, 2019)

PRINTER TYPE	ADDITIVE MANUFACTURING METHODS AND MATERIALS USED					
	Extrusion based technologies				Selective Binding / Particle-bed 3D printing	
	in-situ	Material used	Prefab	Material used	Prefab	Material used
ROBOT-ARM SYSTEM	Aachen University	*Cement-based*	Bruil	*Sand-based*		
	Apis Cor	*Cement-based*	CON3D	*Cement-based*		
	Batiprint3D	*Polymer-based*	CYBE	*Cement-based*		
	Branch Technology	*Polymer-based*	SIKA	*Cement-based*		
	ETH Zurich	*Cement-based*	Pennsylvania University	*Geopolymer-based*		
	ETH Zurich	*Polymer-based*	Vertico	*Cement-based*		
	MIT -	*Polymer-based*	Xtreee	*Cement-based*		
	SC3DP	*Geopolymer-based*				
	Spectavia	*Cement-based*				
GANTRY SYSTEM	Betabram	*Cement-based*	3D print canal house	*Polymer-based*	3Dealise	*Sand-based*
	HuaShang Tengda	*Cement-based*	3D printhouse	*Cement-based*	CONCR3DE	*Sand-based*
	TotalKustom	*Cement-based*	BAAM	*Polymer-based*	D-Shape	*Sand-based*
			Concrete printing	*Cement-based*	Emerging Objects	*Polymer-based*
			Contour crafting	*Cement-based*	ETH Zurich	*Sand-based*
			G3DP2	*Glass*	Pegna	*Cement-based*
			RapidConstruction	*Cement-based*	Pierre et al.	*Cement-based*
			Southeast University China	*Cement-based*	Swinburne university	*Geopolymer-based*
			TU Eindhoven	*Cement-based*	TUM	*Cement-based*
			Winsun	*Cement-based*	Sydney university	*Cement-based*
ROBOT / GANTRY SYSTEM	Fusion of high melting point materials					
	Prefab	Material used	Prefab	Material used	Prefab	Material used
	FreeFAB Wax	*Polymer-based*	Arup	*Metal*	Skansa	*Polymer-based*
	MX3D	*Metal*	MST	*Glass*	Solar Sinter	*Glass*
	Arup	*Metal*	Nematox	*Metal*	TU Dresden	*Cement-based*

Table 1 demonstrates that the number of companies that apply additive manufacturing in the building sector is still limited. It is noteworthy that the company called D-shape (selective binding) was founded as early as 2008, and it is often described as the first company to apply additive manufacturing in the building sector.

4.2.5 Additive manufacturing: Application potential

In recent years, the number of applications of additive manufacturing has slowly increased. Currently, there are more than 20 different companies and research institutes focusing on the application of additive manufacturing (Table 1). For additive manufacturing for the digital fabrication of concrete there are two applications:

- *The fabrication of structures*
  The on- and off-site manufacturing of the functional building element

- *The fabrication of formwork*
  The additive manufacturing process for the fabrication of formwork

The primary reason for the use of multiple methods is that the design of an object also needs to take fabrication constraints into account. Constrains can be grouped into four main categories; fabrication constraints, material constraints, construction constraints and design constraints (Austern, Capeluto, & Grobman, 2018).

Cement-based materials are known for low cost, good strength, exceptional durability, as well as excellent fire-resistance (Gursel & Ostertag, 2017). This explains why most applications use cement-based material. The application of polymer-based methods is often focused on hybrid methods in which it is used as formwork. The future Tree by Joris Burger is an excellent example of this (Chapter 4.2.6). When looking at non-hybrid methods, extrusion-based additive manufacturing (Chapter 4.2.7) and particle-bed additive manufacturing techniques (c Chapter 4.2.8) show the most potential.

4.2.6 Additive manufacturing: Fabrication of the formwork

One of the challenges in digital fabrication with concrete is reinforcement. The fabrication constraints of 3D printing with concrete are still the primary reason for the choice of manufacturing the formwork instead of the product. The topology-optimized girder (in Chapter 4.2.1) is an excellent example of how the difficulty of including steel reinforcement often represents the deciding factor for using additive manufacturing as a means of producing formwork (Menna et al., 2020).

For the digital fabrication of concrete, the material used to 3D print the formwork does not have to comply with the qualities required of building components. The change in design constraints (e.g., long-term durability, fire safety) allows for the application of other additive manufacturing techniques and materials.

Fused Deposition Modeling with plastics is becoming a possibility due to changing design constrains. This is often seen as a sustainable method, as only a minimal amount of 3D-printed plastic is required to deliver a very thin, stable shell as formwork (Andrei Jipa et al., 2019). Difficulties occur when extra strength is required due to scaling up the built volume and primary height because this results in increased hydrostatic pressure.

Figure 11 Future Tree, showcasing ultra-thin 3D-printed formwork, in combination with set-on-demand concrete and steel reinforcement. From: (Menna et al., 2020)

A great example of solving a design constraint by a change in material is the Future Tree designed by Joris Burger. (Figure 11) The problem of increasing hydrostatic pressure is solved using set-on-demand concrete. Here the (quicker) hardening properties of concrete limit the build-up of hydrostatic pressure to values that the formwork is able to support.

This allows for an ultra-thin 3D-printed formwork, which the researchers describe as the Eggshell Method. The Eggshell Method allows for the digital fabrication of complex columns in a continuous casting process. The use of conventional procedures and manufacturing methods permits direct application, since the structural element complies with existing building regulations (Menna et al., 2020).

4.2.7 Extrusion-based additive manufacturing: 3D concrete printing

For the digital fabrication of concrete structures, extrusion-based additive manufacturing, often referred to as 3DCP (3D concrete printing), currently seems to be the clear frontrunner with respect to both the level of overall technological readiness and economic viability (Mechtcherine et al., 2020) (Chapter 4.2.3).

The application of current methods of extrusion-based AM is reported to be more efficient in terms of cost, time, and material usage, as well as in the amount of labor required when compared to conventional construction. (P. Wu, Wang, & Wang, 2016)

In extrusion-based additive manufacturing with concrete, mortar is forced through a nozzle/extruder, while it moves along a defined path (Figure 12). An object is built layer-upon-layer, which is in many ways similar to the well-known process of "fused deposit modeling."

Figure 12 Extrusion-based 3D printing of a bicycle bridge at TU Eindhoven

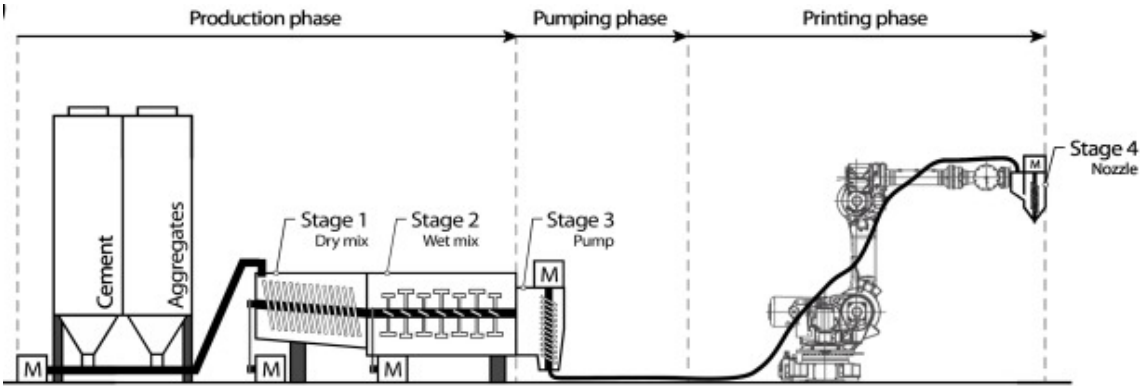

Figure 13 - Image showing the different stages and phases in the 3DCP manufacturing process

When describing the process of extrusion-based AM, a distinction can be made between three phases throughout 3DCP: the production phase, pumping phase, and printing phase (Figure 13). Throughout this process, different properties from the to-be-printed material are necessary.

4.2.7.1 3D concrete printing: Process-related material requirements

In additive manufacturing, the rheological properties of the used materials are fundamentally important. The four key characteristics of the material as defined by Lim et al. (2012) are:

- Pumpability: Ease and reliability with which material is moved through the delivery system
- Printability: Ease and reliability of depositing material through a deposition device
- Buildability: Resistance of deposited wet material to deformation under load
- Open time: Period where the above properties are consistent within acceptable tolerances

All key characteristics are determined by the rheology and hydration properties of the material in the 3DCP process. Much research has been conducted on optimal material properties, but throughout the construction process, the requirements of the design and therefore the demands from the material are at odds with one another: (Malaeb et al., 2015) (Figure 14)

Maximizing workability <-> Maximizing compressive strength

Maximizing buildability <-> Maximizing extrudability

Maximizing speed of setting <-> Maximizing inner-layer bonding

Considering all the contradictions within the manufacturing process and the demands of the end-product, the process is more complex than it may appear at first. The pumpability, printability, buildability, and open time requires the addition of viscosity-modifying agents, superplasticizers, accelerators, and other admixtures to ensure good results.

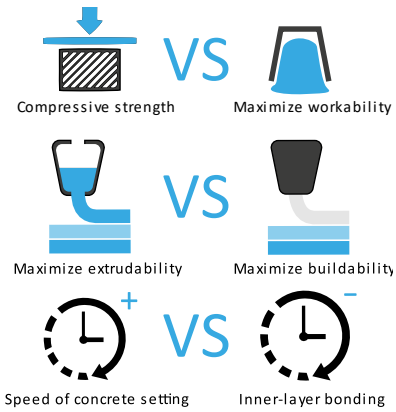

Figure 14 - 3DCP: Contradictions within material design

4.2.7.2 3D concrete printing: Buildability requirements

Figure 15 Failure mechanisms of buildability elastic buckling (left), plastic collapse (right) source: (Suiker, Wolfs, Lucas, & Salet, 2020)

Difficulties in 3D concrete extrusion mostly relate to buildability requirements. At present, elastic buckling and plastic collapse are the primary failure mechanisms for buildability for 3DCP (Figure 15). They are both strongly related to the strength development of the concrete, which is, in turn, dependent on the thixotropy and setting properties of the material (Reiter, Wangler, Roussel, & Flatt, 2018). The absence of formwork requires a controlled structural build-up to reach a certain height (Figure 16).

The strength of the material should evolve faster than the hydrostatic pressure of layers placed later to end up with a successfully printed 3D object. Therefore, an understanding of how the yield stress develops at the microstructural level is needed (Reiter, Wangler, Roussel, & Flatt, 2018). Figure 16 illustrates the necessary changes in yield stress. Furthermore, Figure 17 shows the time-dependent strength development of set-on-demand concrete. In essence, materials for 3D concrete extrusion require a specific evolution of yield stress and shear modulus over time, depending on the rate at which components are built (Mechtcherine et al., 2020).

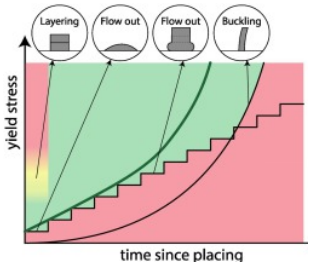

Figure 16 Yield stress evolution required for layered extrusion as a function of age after placing, taking into account the process limiting factors of layering, flow out, and buckling for a single layer. From: (Reiter, Wangler, Roussel, & Flatt, 2018)

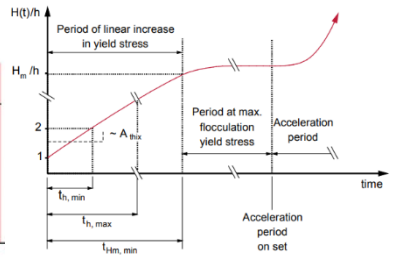

Figure 17 Element height vs. time. Initial strength correlates to a yield stress limited by flocculation processes. The Figure shows the strength development set-on-demand concrete. From: (Wangler et al., 2016)

There are two potential ways to control the strength development of the buildability of 3DCP: Controlled setting and setting-on-demand. The controlled setting method meets the buildability requirements by the continuous preparation of small quantities of high early-age strength concrete. In contrast, in setting-on-demand, a larger batch of concrete is prepared and activated during the extruding process. Generally, setting-on-demand concrete offers more freedom in the overall process.

The strength build-up during the early age of concrete is directly proportional to the rate of hydration. Therefore, the hydration kinetics need to be adjusted to match the corresponding requirements of the respective process step (Mechtcherine et al., 2020). Additionally, higher yield stress results in difficulty in pumping. The pumping pressure is proportional to the fourth power of the yield stress, according to the Buckingham-Reiner equation (De Schutter & Feys, 2016). In other words, setting-on-demand concrete makes it easier to meet the pumpability constraints of the fabrication process by setting the concrete where the higher yield stress is required.

4.2.7.3 3D concrete printing: Flowchart

To better understand the process, a flowchart illustrates the many steps of the 3DCP process from a material perspective (Figure 18). This allows for insight into the different methods of addressing the material-related requirements throughout the process. An example of this is changing material properties by adding accelerators/retarders to influence the open time.

At the top of the flowchart, a material is selected that is pumpable towards the nozzle. Particle segregation, de-homogenization, and blockage needs to be prevented. The next step is the printing of the material. The printability defines the ability of the material to be extruded through the nozzle without considerable cross-sectional deformation and with an acceptable degree of splitting/tearing.

The material needs to be buildable. Good buildability means that no significant deformation should occur under the weight of the stacked layers. Finally, the open time should be long enough to ensure the buildability and good interlayer bonding to minimize the anisotropic behavior of the 3D printed object.

All of the steps above need to be coordinated by a good printer setup.

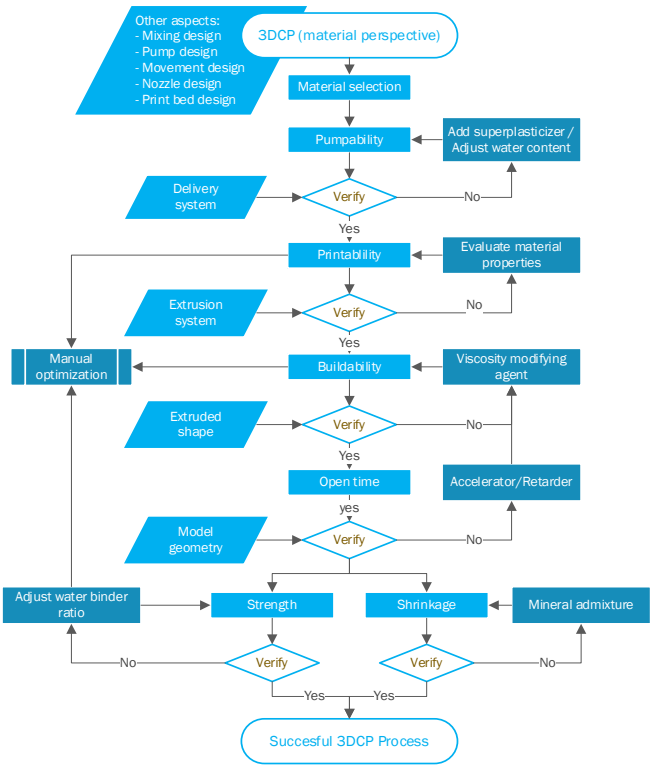

Figure 18 - 3DCP process from a material perspective and potential measures to meet the requirements of the process.

4.2.7.4 3D concrete printing: Drawbacks

While extrusion-based additive manufacturing is relatively easy to explain and seems straight forward as a process, process-related requirements make it challenging. Extrusion-based additive manufacturing with concrete has five major drawbacks in regard to the main research question here: its process-related material requirements (sustainability), anisotropic behavior, requirements of formwork for overhangs, reinforcement, robustness, and repeatability:

- *Process-related material requirement*
  Process-related material requirements to achieve the key characteristics of 3DCP (pumpability, printability, buildability, open time) result in concrete mixtures that contain a significantly higher amount of Ordinary Portland Cement (OPC) (Beersaerts, Lucas, & Pontikes, 2020). In a comparison of different research papers, on average, the binder content was higher than 800kg/m^3 (Mohan, Rahul, Van Tittelboom, & De Schutter, 2020). (For comparison, regular floor slabs with XC1 require an average binder content of 260kg/m^3.)

- *Requirements of formwork*
  Complexity with in 3DCP comes at a cost. Overhangs are challenging to print due to eccentric loading on each subsequent layer. This results in the need for additional formwork. Failure also occurs in the collapse of straight-walled structures. A recommendation in regards the buildability of straight walled structure is a recent paper by Suiker et al. (2020), wherein he successfully predict the layer at which elastic buckling and plastic collapse occurs of straight-walled 3DCP structures. (Figure 19)

  Some of the buildability requirements can be met with the use of set-on-demand concrete. In an experimental study, Brun et al. (2020) succeeded in printing 17.5° degree overhangs. They used a cement: fly ash ratio of 70%:30%, plus 1% superplasticizer and 0.5% accelerator (Brun, Gaspar, Mateus, Vitorino, & Diz, 2020). For printing overhangs without an accelerator, it is likely that additional support structures will be required.

- *Anisotropic behavior*
  All extrusion-based processes are likely to result in anisotropic structures or components (R. A. Buswell, Silva, Jones, & Dirrenberger, 2018), which means that 3DCP objects exhibit a difference in transverse versus longitudinal strength (Figure 20). This anisotropic behavior arises from the adhesion strength of the printed layers. Weak adhesion within structural layers is often caused by cold jointing and results from the contradictory requirements in the process. One of the contradictions, for example, is the fast-setting concrete, which is advantageous for meeting the buildability requirements, but increases the risk of insufficient layer adhesion.

- *Reinforcement*
  Conventional reinforcement solutions are incompatible with extrusion-based additive manufacturing (Asprone et al., 2018). Several difficulties stem from the printing process. It results in uncertainties regarding the reinforcement-to-matrix bonding, preventing the optimal use of the reinforcement. (Menna et al., 2020) Furthermore, cavities around the reinforcement are likely, due to a lack of compaction around the reinforcement (Bos, Dezaire, Ahmed, Hoekstra, & Salet, 2020). The difficulty of reinforcement was also the primary motivation to develop a post-tensioned structure, combined with hybrid manufacturing for the post tensioned Insufficient knowledge on the durability behavior of digitally fabricated concrete (3DCP) is a major obstacle to its application. At the current stage of development, extrusion-based additive manufacturing cannot sufficiently guarantee product quality and design code compliance in many practical cases (Menna et al., 2020). 3DCP therefore requires design by testing and higher safety factors, which due to the increased resource utilization, unfortunately mitigates any environmental benefit in the short term.

For an in-depth review of the processes, production steps, and the underlying physics, the recent paper *Extrusion-based additive manufacturing with cement-based materials – Production steps, processes, and their underlying physics: A review* by Mechtcherine et al. (2020) can be recommended. The rest of this chapter will focus on particle-bed additive manufacturing.

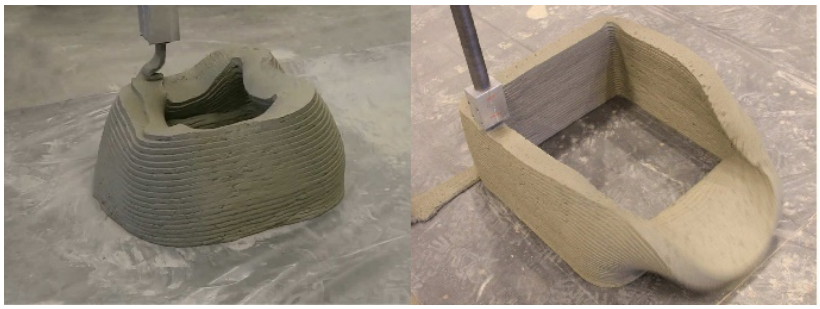

Figure 19 Failure modes: left, elastic buckling and right, plastic collapse. Source of images: (Suiker, Wolfs, Lucas, & Salet, 2020)

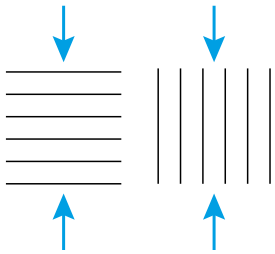

Figure 20 Transverse (left) and longitudinal (right) loading results in different strengths

4.2.8 Particle-bed AM

Particle-bed 3D additive manufacturing – often referred to as binder jetting – shares the similarity with 3DCP that it relies on the build-up of successive layers to form a structure. According to (Loweke et al., 2018), three techniques are relevant in the case of additive manufacturing with concrete::

- *Selective binder activation (2 step process)*
  In the selective binder activation technique, step one consists of forming layers of very fine aggregate and a binder. Step two is the printing of the activator.

- *Selective paste intrusion (2 step process)*
  In the selective paste intrusion technique, step one consists of the placement of aggregate particles (typically with an average diameter ≤ 5 mm) without a binder. Step two is the process of printing a binder paste consisting of a mixture of binder and activator.

- *Binder jetting (2 step process)*
  In binder jetting, step one consists of forming layers of very fine aggregates. Step two is the printing of a liquid binder. The binder is typically a resin which reacts with a hardener component in the particle bed.

Figure 21 explains the difference between selective binder activation, selective paste intrusion, and binder jetting. The primary difference is the position of the binder (B), the activator (A), and the aggregates (AG). Selective binder activation applies an aqueous solution to a particle bed of binder and aggregates (left). In selective paste intrusion, a liquid binder is applied to an aggregate bed (center), In the case of binder jetting, a binder is applied to a particle bed containing the activator (right) (Lowke et al., 2018).

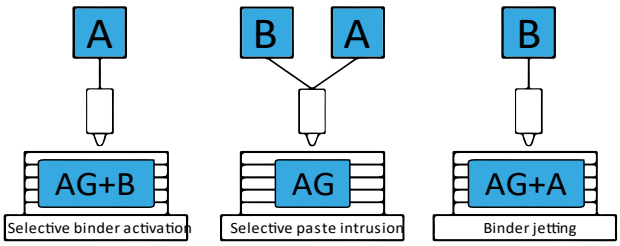

Figure 21 Selective binder activation, selective paste intrusion and binder jetting. image adapted from: (Lowke et al., 2018)

4.2.8.1 Particle-bed AM: Explanation general process

All particle-bed 3D printing processes are based on the same process steps (Figure 21). The process starts with the application of a new layer of particles/aggregates. The next step is to set the right layer height based on the particle sizes and binder properties. In the last step, the activator/binder is selectively printed. This results in a finished layer that sets where the binder is applied. Then the process starts again, untill the full cross-section is printed.

Figure 22 - From left to right: Application of a new layer of particles/aggregates; setting the right layer height; Selectively printing the binder/activator, the finished layer, the process starts over again after the full cross-section is printed. Source: (Lowke, et al 2018)

In general, most particle-bed 3d printing processes are carried out using the steps suggested by Lowke et al. (2018) (Figure 22). Figure 21 shows a section of the printer used by Odaglia, Pietro, et al. in "Advances in Binder-Jet 3D Printing of Non-cementitious Materials" (Odaglia, Voney, Dillenburger, & Habert, 2020). When looking at particle-bed printing methods, the printer usually consists of three main components: (1) A peristaltic pump to apply the right amount of binder at the right time, (2) a roller (or a blade) to ensure enough compaction, and (3) the proper layer height of the particles and a particle/aggregate spreading system (pneumatic actuated shutter). (Figure 23)

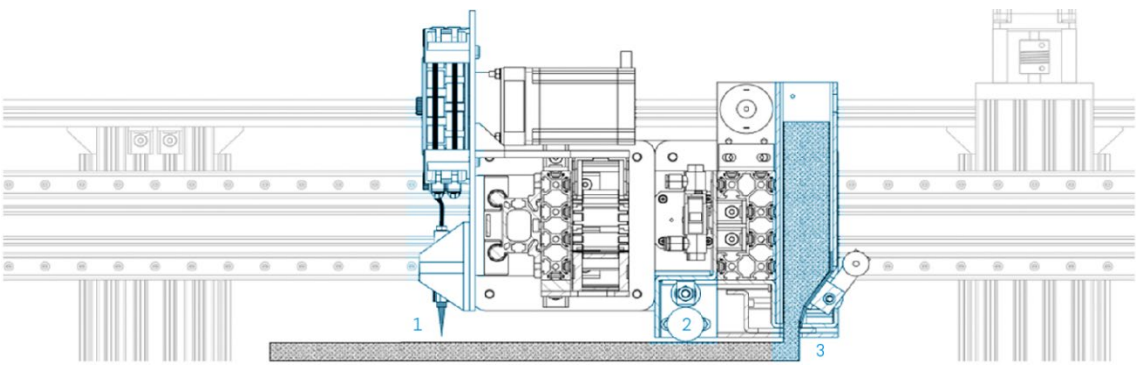

Figure 23 Main components in particle bed 3D printing (from left to right): (1) anti-pulse peristaltic pump and nozzle,(2) compacting roller, (3) sand spreading system (pneumatic actuated shutter). Source: (Odaglia et al., 2020)

4.2.8.2 Particle-bed AM: Material requirements

Particle-bed 3D printing is a process in which many different printer, process, and material parameters govern the quality of the result. For an economical, robust, and repeatable process, most research focuses on a smaller scale in controllable environments. The biggest particle-bed system that showcases a robust and repeatable process is the VX4000 with a print bed volume of 4 m x 2 m x 1 m. It is mainly used to print moulds for NASA and Space X. The concrete-construction innovation company D-shape proposed the first particle-bed system for the building industry in 2008 (Figure 24). Until now, this machine has only been used for prototypes.

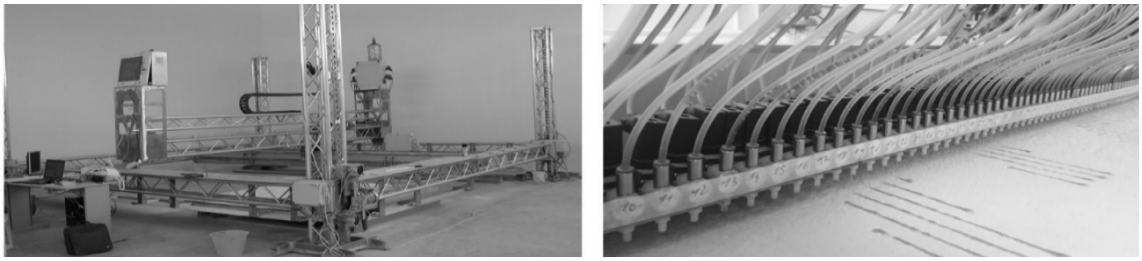

Figure 24 D-shape printer (left) and the nozzles of the printer (right). This setup allowed for printing up to a width of 6m. source: (Lowke et al., 2018)

The process of particle-bed 3D printing is complex. Flowability, spreadability, packing density, reactivity, green strength, depositability, printability, and wettability are all described as fundamental requirements of particle-bed 3D printing. These, in turn, are influenced by material parameters such as the morphology, particle size, density porosity, and droplet penetration behavior. These parameters also define the printer and process parameters such as layer thickness, binder saturation, and drying time (Butscher, Bohner, Hofmann, Gauckler, & Müller, 2011).

The quality of the print is primarily defined by the powder and aggregate (e.g., morphology, mean size, and distribution) as well as the binder characteristics (deposition, drying, and curing) (Mostafaei et al., 2020). The most critical material and binder properties are as follows:

- *Powder – Morphology*
  Morphology (the shape of the powder) determines the packing density, flowability, and spreadability. Together with the used compaction method and the binder (dispersion/distribution of the binder/activator), the morphology has a significant influence on the consistency and density of the particle-bed. Figure 9 showcases different powder morphologies; in general, it can be said that rounder particles result in better flowability, spreadability, and packing density.

- *Powder – Mean size and distribution*
  The size and distribution of the particles, combined with their morphology, defines the powder flowability and possible packing densities. The mean distribution and size also influence the powder-binder interaction Smaller particles show higher reactivity and interaction due to more contact surface and deeper penetration depth of the binder. This means that particle size also has an influence on the printing layer height The layer height is usually three times larger than the mean particle size. This relationship between mean size and layer height is also applicable to for selective paste intrusion. Powders as fine-grained as 5 µm can be processed (Figure 24). Smaller particles are generally not used due to safety issues (Mostafaei et al., 2020). This results in a minimal theoretical layer height (and thereby accuracy of the print) of 0.003 mm.

- *Powder – Segregation*
  Segregation describes the separation powders during the particle-bed 3D printing. Segregation can occur during the material preparation, while feeding the material into the printer or during the spreading process on the particle bed. Understanding the behavior of segregation is complex. To minimize segregation, the influential factors of materials, handling, operational and environmental parameters need to be documented and understood (Meier, Weissbach, Weinberg, Wall, & Hart, 2019). For example, in binder jetting, oscillation of the hopper is followed by roller, and compaction is often more effective than a powder dispensing method using only a roller as this could lead to powder segregation during the placement of the particle layer.

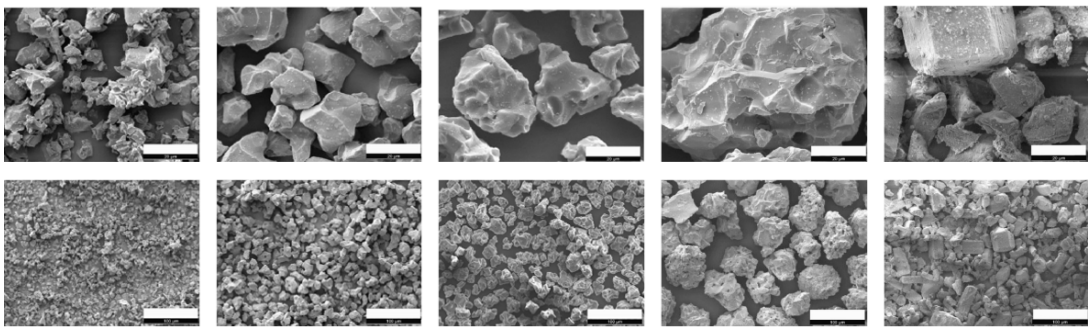

Figure 25 Overview of particle size and morphology of different powder fractions (top row scale bar = 100 µm) and close up (bottom row, scale bar = 20 µm). Powder size varies from 5 µm (left) to 40 µm (right) Note the difference in morphology in the two materials

- *Binder – deposition*
  The deposition of the binder affects the bonding of the powder particles, the integrity of the print, and the quality of the particle-bed surface. For proper deposition of the binder, it must have enough speed to overcome the surface tension and a maximum velocity to prevent splashing (Derby, 2010).

  The proper deposition can be based on the number of the fluid predicted by Reynolds, Weber, and Ohnesorge (Oh) (Figure 26). This, in turn, is defined by density, dynamic viscosity, and the surface tension of the binder.

  There is also a mechanical interaction between the binder and the powder bed. When a binder is jetted with high velocity from the nozzle/printhead, it disrupts the particle bed, forming elevated parallel tracks on the powder. Interestingly, a recent study shows that a more homogeneous particle bed does not result in higher printing strength (Lowke et al., 2020).

  Insufficient binder usage results in weak bonds that might cause delamination. Excessive binder, due to the capillary working, may cause overspreading, which will lead to bad dimensional accuracy in the print. (Miyanaji, Zhang, & Yang, 2018)

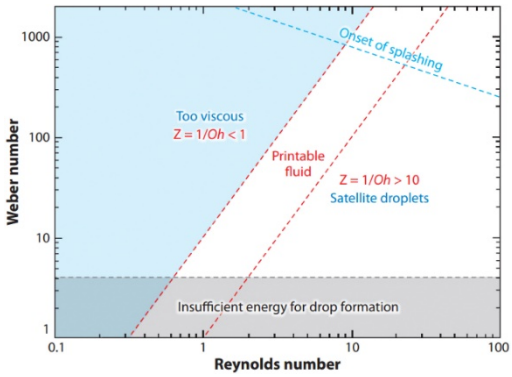

Figure 26 The printability of the binder falls in the area within the four dashed lines. Outside of this area, the binder is not suitable for printing because of its high viscosity, splashing, production of satellite droplets, and insufficient energy for drop formation (Derby, 2010)

- *Binder – Drying time during printing*
  To prevent delamination or anisotropic behavior, the solidification or polymerization needs to be carefully controlled. Additionally, the powder should not clog the nozzle or stick to the roller. Binder drying time is also an important parameter as it influences the overall print speed and quality of the print. The time each layer takes to print can vary between several seconds to minutes, depending on the saturation and the energy required for solidification, evaporation, or polymerization.

- *Binder – Curing time*
  Curing time is defined as the drying time during printing. It determines the time and energy required for the binder to cure, both during and after printing. The ideal binder should set instantaneously upon impact. This can be achieved with two component binders that are highly reactive with one another. To achieve this, the powder is often premixed, which could affect the chemistry of the printed product. Two-component binders increase the risk of clogging due to their high reactivity.

- *Binder – Green part strength*
  A binder should be selected that has enough early age strength (green part strength). Early age strength is especially significant for thin-walled structures or parts with fine features. If the printed product has insufficient green strength, it can easily break during the depowdering process. Much research is used to improving the green strength, as it is a critical factor in increasing process reliability and affordability. Increasing the green strength is crucial to making the process cost-efficient. Careful handling of the parts between printing, depowering, and densification is currently expensive and highly labor-intensive.

4.2.8.3 Particle-bed AM: Print process parameters

The three main print processing parameters are: layer thickness (between 20–300 µm, in the case of binder jetting), binder saturation (between 40–200%), and drying time (between 0–60 s). These parameters are all interrelated by the powder characteristics and the binder (Mostafaei et al., 2020). Together they define the quality of the print.

An excellent example of the relationship between printing parameters and powder characteristics is the relationship between the powder particle size and minimum layer thickness. In general, it can also be said that a higher binder saturation and drying time is required for binders with smaller particle sizes (at the same layer height) (Mostafaei et al., 2020). The higher saturation, in turn, causes excessive binding, which results in geometrical differences. This means that a smaller layer height does not always result in higher accuracy and detail. The same interdependency between material and binder can be observed in the powder spreading process.

In short, all printer parameters are interdependent with the used material and binder. Moreover, much research still needs to be done to determine the optimum conditions in reference to powder and binder characteristics. When looking at existing applications, the powder and binder are often proprietary to companies building the machines that provide print process parameters for their delivered printers. Open-source information is vital to move the market further.

4.2.8.4 Particle-bed AM: Innovative examples

All particle-bed 3D printing processes share similar advantages over extrusion-based methods. The primary strength of binder jetting is that the unbound particles function as a for support for subsequent layers. This results in a lower required green strength and enormous geometric flexibility, with limited to no extra cost. A good example is digital Grotesque II by Benjamin Dillenburger, in which he explored a new kind of architecture that leaves behind traditional paradigms of rationalization and standardization. Instead, it emphasizes the viewer's perception, evoking curiosity and bewilderment (Dillenburger & Hansmeyer, 2019).

Figure 27 Digital grotesque II: An example of a single building block, which were stacked with others to form the final structure. Source: (Dillenburger & Hansmeyer, 2019)

Figure 28 Digital grotesque II. Source: (Dillenburger & Hansmeyer, 2019)

The structure consists of stackable sand-printed elements, resulting in a total height of 3.45 m. In total, the structure consists of 7 tons of printed sandstone and very detailed ornaments with a 280 µm print accuracy. (Figure 28)

The project also shows the drawback of particle-bed methods. Although the maximal working space of the printer (Voxeljet VX4400) is 4 m x 2 m x 1 m, the handling made printing the structure in one go difficult. Therefore, the final structure is composed of stackable bricks to overcome the limited green strength and handleability. (Figure 27)

Post-processing included the infiltrating the structure with an epoxy resin. While giving considerable strength and durability to the structure, epoxy is not known for its positive environmental features. (La Rosa et al., 2014)

What is noteworthy is the construction speed. The final structure was produced on-site by two people in less than a day. This illustrates the ease of construction and potential in cost reduction, resulting from the high geometrical accuracy.

Figure 29 Four-point bending test of the binder jetted floor by the Block research group. Source: (Matthias Rippmann et al., 2018)

Figure 30 Failure. Source: (Matthias Rippmann, Liew, Van Mele, & Block, 2018)

Another example that shows the potential of binder jetting is a floor slab made by the Block research group. In 2018, the Block research group explored the design, fabrication and testing of discrete 3D printed floor slabs.

The design was guided by process constraints and resulted in three optimized structures. The structures consist of five interlocking elements, with the total dimensions of 2.0 m × 1.4 m × 0.16 m.

After the construction of the floors, the research group tested the structural integrity through a four-point bending test (Figure 28). Failure of the floors was initiated by cracks propagating across the width on the underside, combined with crushing and spalling of the material on the topside (Figure 30) (Matthias Rippmann, Liew, Van Mele, & Block, 2018). However, two of the three floors sustained the designed load. The deflections exceeded the design limit by 20–80% due to hinging at the interfaces between the interlocking elements (Matthias Rippmann et al., 2018), which made the floor slabs unsuitable for direct use. The project shows that particle bed methods can result in structurally integer elements and that once scalability is no longer an issue, binder jetting of complete floors is possible.

The project Digital Grotesque II and the floor designed by the Block research group were highlighted here because they are excellent examples of the interaction between the fabrication process, material, and on-site construction (Figure 30) (Dillenburger & Hansmeyer, 2014). What makes both projects stand out is the integrated approach to taking full advantage of possibilities, while considering the drawbacks of the process and the material. Primary advantages for construction using particle bed processes are:

- Geometrical freedom and range of feature sizes
- High production accuracy and quality
- No added cost for integration of multi functionalities
- Construction with environmentally friendly materials
- Reduction of the labor required

While still in the early stages, it can be said that particle-bed methods show much potential. At this day and age, it is already highly suitable for the manufacturing of small-scale building components.

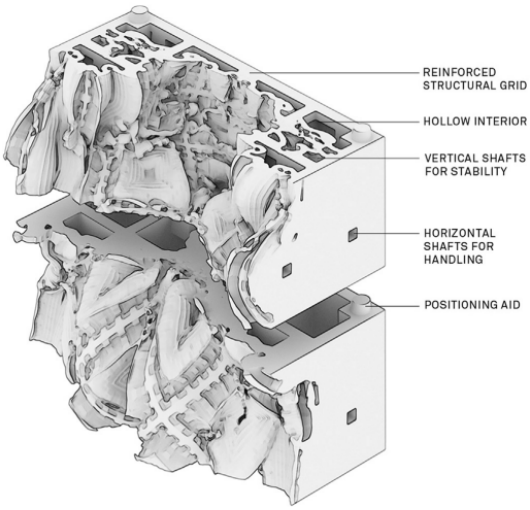

Figure 31 Integration of different elements throughout the construction of Digital Grotesque II.Note the integration of horizontal shafts for handling and the positioning aid for construction. Source: (Dillenburger & Hansmeyer, 2019)

4.2.8.5 Particle-bed AM: Drawbacks

Throughout this Chapter, several innovative examples have been showed of the application of particle-bed additive manufacturing. Nevertheless, when it comes to the cost-efficient application of particle-bed methods, several drawbacks can be noted:

- Reliability
  Particle-bed additive manufacturing methods are still at an early stage. The main challenge for future applications is the understanding and control of the parameters involved. Where companies such as D-shape envisioned in-situ particle-bed processes, their implementation shows that a low-maintenance, reliable multi-nozzle print head for cementitious slurries is still too challenging and expensive to apply. For smaller-scale production, different research groups have shown that it is possible to get reliable results in smaller controlled environments. However, this process is still highly labor-intensive, costly, and hard to scale-up.

- Scalability, green strength, and cost
  Fabrication with particle-bed processes is limited by the size of the printer bed. Additionally, a controlled environment is required for the process to become reliable and repeatable. Thus, the construction of a full-scale building would require a large printer and a controlled environment. Currently, the largest particle-bed system with a robust and repeatable process is the VX4000 with a print bed volume of 4 m x 2 m x 1 m. The initial investment cost of binder jetting is high, as the price of the VX4000, for example, runs over 1.5 million euros. Additionally, the handling of products (limited green strength), difficulty in depowdering, and post-processing requirements make the process labor-intensive and costly.

- Clogging
  In a personal conversation with Vera Voney (researcher at the ETH working on particle-bed printing) at Digital Concrete 2020, the reproducibility and maintenance of particle-bed systems was discussed, specifically, the printing with geopolymer concretes which is more sustainable than with conventional concrete. Voney noted that, due to the higher viscosity of the sodium/potassium silicate binder, the minimal nozzle size required for reproducible results was 0.2 mm. Otherwise, clogging during the printing process would become problematic. Furthermore, the nozzle had to be throughout the process, although a larger nozzle was used in the end to prevent clogging. Clogging seems to be an inherent problem, which still needs to be solved in binder jetting (The reason for asking Vera Voney this question was my personal experience at Concr3de, where I worked on the binder jetting of window sills, throughout which printing clogging occurred).

- Difficulties of reinforcement
  Similar to extrusion-based additive manufacturing, conventional reinforcement methods are incompatible with particle-bed methods. The combination of wire arc additive manufacturing of reinforcement together with particle-bed methods are being explored, but remains in an experimental and costly stage. More background information on the difficulties of reinforcement can be found in the section on extrusion-based additive manufacturing. In both manufacturing methods, the same drawbacks apply.

- Depowdering
  Depowdering is still a labor-intensive process that drives up the cost of fabrication with particle-bed methods. Another issue is the impossibility of removing materials if enclosed voids exist within the structure. This could offset the advantages of structural optimization and should be taken into account in the optimization process.

4.2.9 Additive manufacturing: Summary and key findings

This chapter began by giving an overview of the different digital fabrication methods and their potential in the building sector. This was followed by a study of the state-of-the-art applications and exploration of the potential of additive manufacturing methods, particularly extrusion-based and particle-bed additive manufacturing methods. By looking at innovative examples and a study of the manufacturing process, the potential and drawbacks of the additive manufacturing methods were explored.

Key findings from the literature study are given below:

- Additive manufacturing is on the rise within the construction sector, but the difficulty of integrating reinforcement, the process-related material requirements, and drawbacks related to specific printing methods prevent the application of one specific manufacturing method as the optimal solution to sustainability in the building sector.

- There is no clear advantage of a singular manufacturing process. State-of-the-art projects show that hybrid manufacturing, combining the advantages of additive, subtractive, and formative processes, often lead to innovative solutions. Casting remains to be an effective method of construction with concrete. Most successfully applied methods of additive manufacturing contain hybrid processes with casting.

- Extrusion-based additive manufacturing and particle-bed additive manufacturing show the most potential when it comes to the fabrication of building components. Fused Deposit Modeling shows potential when it comes to the fabrication of formwork.

- Current drawbacks of additive manufacturing prevent the large-scale application of additive manufacturing methods as a solution to the environmental impact of concrete. Extrusion-based methods result in higher cement usage, which in turn end up in higher emissions. Particle-bed methods are not currently at the level of maturity that would allow them to be reliable scaled-up and applied.

- A reduction of the amount of material or required formwork does not automatically reduce environmental impact. Process-related material requirements or the investment of machinery could result in higher CO_2 emissions of the product while using less material The extra CO_2 emissions emitted by increased cement content in extrusion-based additive manufacturing is an excellent example of this.

- Several challenges need to be solved before additive manufacturing will be the solution to environmental-related issues. The drawbacks are process-dependent as explained above in the literature study. In general, they relate to reinforcement, scalability, life cycle cost, and process-related material requirements.

4.2.10 Additive manufacturing: Conclusions and future research

For additive manufacturing to become game-changing, reinforcement, scalability, life cycle cost, and process-related material requirements need to be solved. Without solutions to these challenges, it is unlikely that innovative manufacturing methods will disrupt the industry in the short term towards a more sustainable paradigm (P. Wu et al., 2016). Based on the current state of additive manufacturing methods, it seems that conventional manufacturing methods (casting), combined with innovative formwork solutions, might be the best way to address the environmental impact of concrete..

Future research should focus on hybrid methods and integration of the material process into the optimization loop. While hybrid methods such as thin-formwork seem to be the perfect solution to fabricating intricate shapes, the set-on-demand concrete required to prevent hydrostatic pressure might make the environmental impact by reducing the amount of formwork required neglectable. This example illustrates that it is essential in the selection of a fabrication method to look at other constraints. The following constraints are essential:

- Fabrication constraints
- Material constraints
- Construction constraints
- Design constraints

Only a holistic approach that takes into account these four constraints will result in a solution that addresses the environmental impact of the building sector and thereby concrete construction.

Literature study

Structural optimization

Image source: youtube.com/watch?v=8Rf-D-d-OhI 3D-Printed Formwork for Bespoke Concrete Stairs: From Computational Design to Digital Fabrication

4.3 Structural optimization

This Chapter starts with a brief introduction to structural optimization, followed up by an overview of the most common structural optimization methods – shape, size, and topology optimization. After the introduction, it focuses on topology optimization and explores the potential in fabrication-oriented structural optimization. This is done to find an answer to the primary research question:

In what manner can we use structural optimization and additive manufacturing in the building sector to address the environmental impact of concrete construction?

After the exploration of structural optimization, the Chapter explores the difference between structural optimization and form-finding methodologies. This part starts with the history of structural form-finding through physical models, which are explained by examples of great engineers like Heinz Isler and Antione Gaudi. The Chapter closes with an elaboration on a parametric design approach as a solution to the difficulty of integrating design and manufacturing constraints within structural optimization processes.

4.3.1 Structural optimization

A structure in mechanics is defined by J.E. Gordon [17] as "any assemblage of materials which is intended to sustain loads." The design of optimal structures is becoming increasingly important due to the limited material resources, environmental impact, and technological competition, all of which demand lightweight, low-cost, and high-performance structures (Huang & Xie, 2010).

Given Gordon's definition of structures, structural optimization can be described as optimal material distribution for a given load-case, which results in an optimal layout of material in a linear elastic structure. The structural optimization process can be expressed mathematically and involves an objective function, design variables, and state variables (Christensen & Klarbring, 2008). They are defined as:

- Objective function (*f*)
  A function that classifies the design options, with respect to a quantifiable objective. This function returns a numerical value that represents the quality of the design regarding set criteria. In the case of structural optimization problems, *(f)* often describes weight, maximum displacement, strain energy, or cost of a design.

- Design variables (*x*)
  A vector that describes the design in numerical values; in the case of structural optimization problems, the design variable often represents the topology, nodal positions, cross-sectional arias, or the material.

- State variables (*y*)
  For a given design with the design vector x, the variable *y* represents the response of the structure, that is, how well the structure performs in terms of the evaluation criteria (e.g., deformation).

This results in the following general definition of optimization:

$$\begin{cases} \min\limits_{\boldsymbol{x}} & f(\boldsymbol{x}, \boldsymbol{y}(\boldsymbol{x})) \\ \text{subject to} & \begin{cases} \text{design constraint on } \boldsymbol{x} \\ \text{state constraint on } \boldsymbol{y}(\boldsymbol{x}) \\ \text{equilibrium constraint} \end{cases} \end{cases}$$

In the optimization process for a structure, the function *g*(*y*) representing the given variables ('(*y*)') can be introduced. This state function can be included as a constraint in the optimization task. An example is a discrete finite element approach in which the state variable for displacement is defined by *g*(*u*(*x*)) (the displacement vector).

This results in an equilibrium that needs to be solved. In finite element modeling, the equilibrium is solved by equalizing the stiffness matrix of the structure and its deformations to the forces applied. This produces a so-called nested formulation in which the equilibrium constraint is taken care of by the state function. The equilibrium constraint is:

$KU = F$

- K = Stiffness matrix of the structure
- U = Displacement vector
- F = Force vector

In the formulation of a structural optimization *x* and *y* are generally treated as independent variables. Such formulation is called a "simultaneous formulation" since the equilibrium of state function is solved simultaneously with the optimization problem. In (most) structural optimization problems, the variable *y* is a result of a given *x*. This allows for a nested formulation expressed in functions of *x*.

4.3.1.1 Structural optimization: Shape, Size, and Topology

In structural optimization, the variable *x* in the objective function usually defines geometrical features. In this case, three types of structural optimization classes exist (Christensen & Klarbring, 2008):

- *Sizing optimization*
  Here, *x* represents a variable of a member of a structure, for example, the cross-sectional area of a truss member or the thickness distribution of a sheet.

- *Shape optimization*
  In this instance, *x* represents the form or contour of some part of the boundary of the structural domain. For example, the state of a solid body is described by a set of partial differential equations. The optimization consists of choosing the integration domain for the differential equations in an optimal way. Note that the connectivity of the structure is not changed by shape optimization; new boundaries are not formed. This is a two-dimensional shape optimization problem.

- Topology optimization
  In topology optimization, *x* is usually defined as a density-like variable that can take the value 0 or 1 (in the case for 2D, this can be a range between 0 and a set maximum thickness). It allows for a change of the connectivity of the structure, thereby changing the topological definition of the shape.

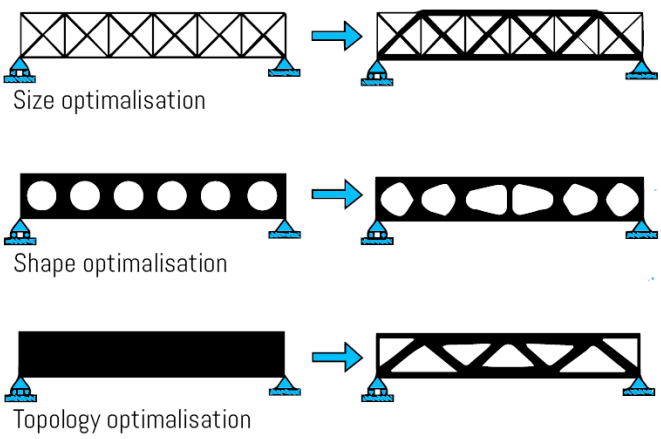

Figure 32 Illustration showing the principles of size, shape, and topology optimization. Source: (Gebisa & Lemu, 2017)

Figure 32 shows various different optimization processes. The primary difference between sizing and shape optimization and topology optimization is that sizing and shape optimization cannot change the structural topology during the solution process. This means that size and shape optimization methods will always result in solutions with topologically equivalent domains.

Topology allows for a change in the number of genuses. In geometric topology, a genus is the topology of an orientable geometry that describes the number of holes in the geometry in the case of 2D shapes (Y. Zhang, Wang, & Hughes, 2012).

The possibility of changing the number of holes can be defined as the essential difference between topology and shape optimization. (Bendsoe & Sigmund, 2013). Figure 33 shows this difference more clearly in that the upper image shows topologically equivalent domains, while the lower image illustrates simple, two-fold, and three-fold connected domains (zero, one and two genuses) (Eschenauer & Olhoff, 2001).

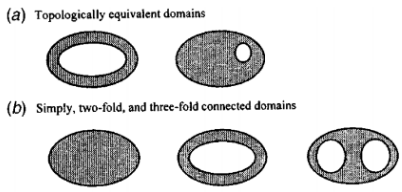

Figure 33 Illustration of (a) topologically equivalent domains and(b) a change in topologies with the addition of genuses. Source: (Eschenauer & Olhoff, 2001)

4.3.1.2 Structural optimization: Topology

As described earlier, topology optimization aims at finding the optimal distribution of material under a given set of constraints (Bendsoe & Sigmund, 2013). Topology optimization dates back to 1989. The most common applications of topology optimization are density-based methods and level set methods.

- Density-based methods
  The density approach was first introduced by (Bendsøe, 1989) under the name Solid Isotropic Material with Penalization (SIMP). In density-based methods, the geometry is described by the distribution of the material in two or more phases, in which one usually represents no material, (i.e., the void phase) (van Dijk, Maute, Langelaar, & Van Keulen, 2013). The optimization process leads to material distribution that provides the optimal layout (including topology, shape, and size) of a structure for a given design loading.

- Level set method
  The level set method was first introduced by (Osher & Sethian, 1988). Level set methods involve a redesign of a structure based on the stress distribution in the previous design state, removing material in the regions where the stress is low and adding material where the stress is high.

Since 1989, many new topology methods have been introduced. Those related to fabrication-oriented methods are of special interest here (Chapter 4.3.4). For a detailed analysis of the different topology optimization methods, I refer to the work of Ole Sigmund in 2013 on "Topology optimization approaches"(Sigmund & Maute, 2013).

4.3.1.3 Structural optimization: Fabrication-oriented topology optimization

Structural optimization often results in complex, intricate shapes that pose challenges during the fabrication of the elements. In recent years, significant research has been carried out on fabrication-oriented topology optimization using both density-based methods and level-set methods. The primary focus is on topology optimization that considers additive manufacturing constraints as they are viewed as a complementary pair:

> Topology optimization provides a powerful method for generating the optimized models, while AM enables a cost-effective fabrication of geometrically complex shapes. (J. Wu, Aage, N., Lefebvre, S., & Wang, C., 2017)

Current research shows that the statement above is not entirely true. Extrusion-based methods have problems with printing overhang bigger than 17.5 degrees (Chapter 4.2), and in particle bed methods, enclosed voids cannot be depowered (Chapter 4.2). This has as the result that a lot of literature research is done on bridging this gap.

The current literature research on fabrication-oriented topology optimization, considering additive manufacturing constraints and characteristics primarily focus on:

- Overhang angle (J. Wu, Aage, Westermann, & Sigmund, 2017)
- Material anisotropy due to layered manufacturing (P. Zhang, Liu, & To, 2017)
- Infill structures (Fu, Li, Gao, & Xiao, 2019) (Sigmund, Clausen, Groen, & Wu, 2017)
- Thermal residual stresses (Allaire & Jakabčin, 2018)

One noteworthy example of fabrication-aware optimization is recent work published by Weiming Wang: *Space-Time Topology Optimization for Additive Manufacturing. (Wang, Munro, Wang, van Keulen, & Wu, 2020).* This research paper presents a novel topology optimization formulation which concurrently optimizes the structure and the fabrication sequence. In this paper, three fabrication related aspects are considered: the self-weight of the intermediate structure, the process-dependent loads resulting from a moving manufacturing platform, and process time-dependent material properties (Wang et al., 2020) (Figure 34).

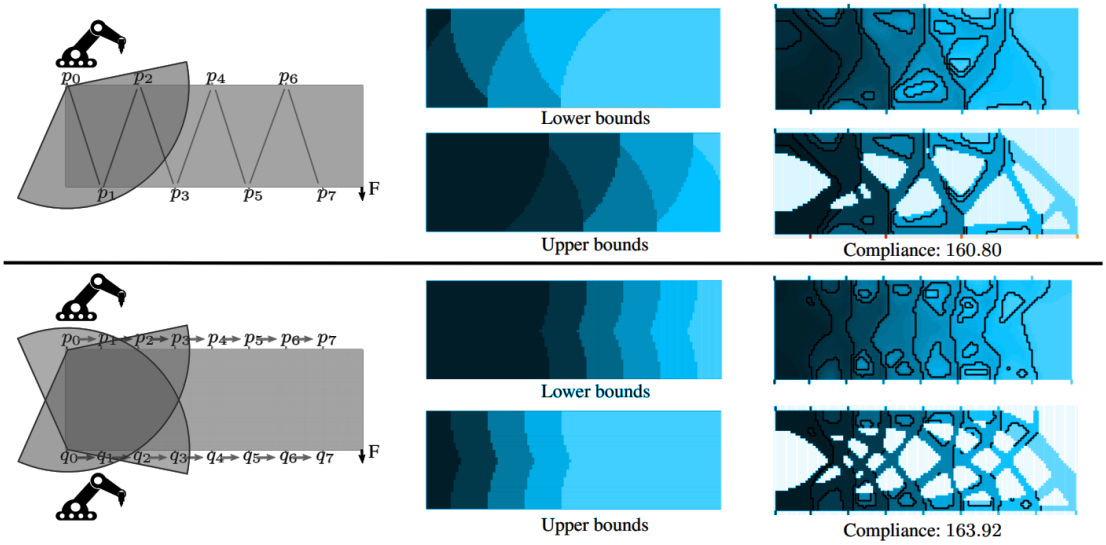

Figure 34 The illustration shows the intermediate manufacturing stages and different potential positions for the robotic fabrication platform throughout the process. Source: (Wang et al., 2020)

The concurrent optimization processes in Wang's work show the potential of imposing manufacturing constraints into topology optimization, while still increasing structural efficiency. New challenges arise in the implementation of not only fabrication constraints, but also in design and material constraints within the optimization process, which results in compromises in structural optimality.

A good summary of different manufacturability-oriented topology optimization methods can be found in (...) *Current and Future Trends in Topology Optimization for Additive Manufacturing* by (Liu et al., 2018). Process-related material requirements still outweigh the potential structural optimality for the application of additive manufacturing topology optimization methods. Before successful topology optimization methods can be applied to address the environmental impact of concrete, the additive manufacturing constraints need to be better understood, and recent studies needs to be integrated with one another.

While there is much potential in the combination of topology optimization and additive manufacturing, at the current time, there is more potential in the integration of conventional methods based on safety factors of uncertainty related to additive manufacturing.

4.3.2 Form finding: Funicular structures

Concrete is known for the excellent properties in compression and for being relatively weak in tension. Due to these properties, concrete can be effective in structures where the exposed loads purely result in axial or in-plane forces, reducing the amount of bending that occurs, and thereby tension. Structures that primarily work in compression are described as funicular structures.

The generation of funicular structures is often produced through a form finding process. The difference between structural optimization and form finding is not always precisely defined in literature. Moreover, form finding is extensively used to describe any optimization problem that involves a change of shape (Coenders & Bosia, 2006).

The primary difference between structural optimization and form finding is that form finding methods use force-active structural systems in which an initial form deforms under load into an equilibrium state. This method of finding optimal structures through deformation is often described as "Form follows force" (Adriaenssens, Block, Veenendaal, & Williams, 2014).

Structural engineers who are known for the application of form finding throughout history are Heinz Isler, Frei Otto, and Antoni Gaudi. They also used force-active methods, but without the potential of computation. Instead, they utilized physical models to find optimal structural forms. Three different types of models can be distinguished, all using different equilibrium states:

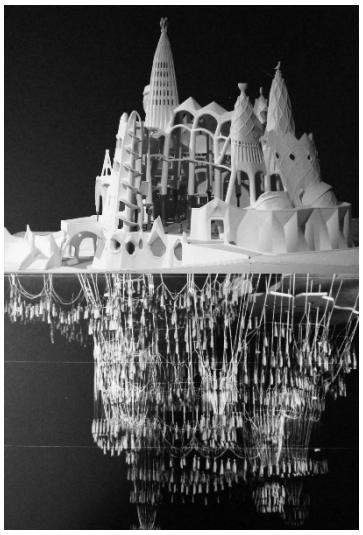

Figure 35 Model of the form-finding process by Antoni Gaudi using hanging chains. (Image by Nathalie Petersen)

- *Hanging models*
  Hanging models find an equilibrium state that forms under gravity loading. Early examples are the "La Sagrada di Familia" designed by Gaudi, which was created using the principles of the inverted catenary chain (Figure 35). Isler is also famous for his application of hanging models in the design of thin concrete structures (Figure 36) .

- *Tension models*
  Tension models find an equilibrium state with internal stresses within the structure. The membranes derive an equilibrium that result in shapes with the minimal material surface. Otto pioneered this technique with physical models made from soap film or gauze (Figure 37).

- *Pneumatic models*
  Pneumatic models find an equilibrium state under differences in air pressure. Here, air-tight membranes are inflated to form the structure based on the differences in pressure.

WFigure 36 depict structures resulting from the use of physical models as a tool for structural optimization by Isler. By combining the material's excellent compressive strength integrated with form-finding using hanging models, Isler succeeded in creating spans of more than 60 meters of relatively thin concrete shells. Remarkable is that these structures were both created without the use of computational tools.

Figure 36 Funicular shell designs by Heinz Isler:top, the SICLI company building under construction in Geneva, Switzerland, by Heinz Isler (1969);bottom , the Deitingen Service Station by Heinz Isler in Deitingen, Switzerland (1968) Photos by (Matthias Rippmann, 2016).

4.3.2.1 Form finding: Computational

The development of the computer allowed for form finding processes to be solved in a quantitative way, which resulted in the transition from physical models to mathematical ones. Since the 1980's, many different form finding methods have been developed.

Veenendaal et al. (2012) compiled an extensive and comprehensive overview of numerical form finding methods (Adriaenssens et al., 2014). Here, the form finding methods are based on three different principles: stiffness matrix methods, geometric stiffness methods, and dynamic equilibrium methods. (figure 38)

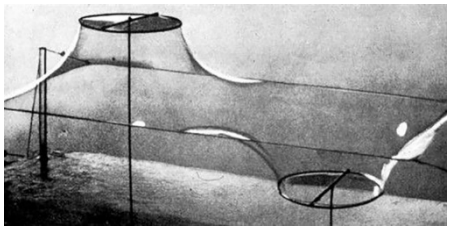

Figure 37 Form finding using soap by Frei Otto.

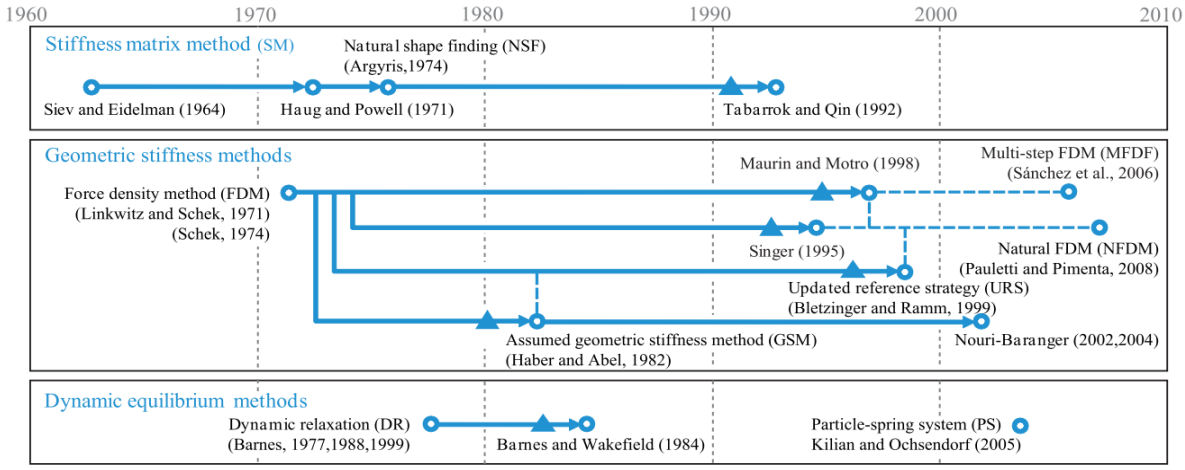

Figure 38 Development and categorization of form finding methods with key references. Arrows denote descendance, and dotted lines denote independent but related methods and triangles a first formulation using surface elements. Source: (Veenendaal & Block, 2012)

All three methods often rely on relatively simple input parameters consisting of a set of boundary conditions, defined design loads, an initial stress state, and "method specific" parameters. While simple, the input parameters required are often the main weak point of form finding methods. For example, stiffness matrix methods include material properties which is computational costly when designing with one specific material (Haber & Abel, 1982).

In comparison, geometric stiffness methods result in shapes that are difficult to fabricate and consist of variables that are counter-intuitive (Barnes, 1999), which makes it difficult to predict an optimal outcome. Dynamic equilibrium methods have the same problem. Nour-Baranger (2004) stated that it relies on too many parameters that are fictitious towards the actual structure and have no physical representation (Nouri-Baranger, 2004).

Much research has been devoted to solving these inherent problems of specific form finding techniques. Veenendaal et al. (2012) compiled a chart showing the development of various form finding methods.

All the form-finding methods described above can be linked back to the physical methods used by Otto, Gaudi, and Isler. Thus, they have inherited the limitations of the physical methods that they simulate.

The primary difficulty of applying stiffness matrix methods, geometric stiffness methods, and dynamic equilibrium methods is their monofunctionally. All the form-active methods come with the difficulty of integrating fabrication constraints, material constraints, construction constraints, design constraints, and multiple stress states into the optimization process.

While being highly effective at finding funicular structures, it is likely that the application of form finding methodologies needs to be combined with structural optimization methodologies to overcome the integration of constraints and multiple stress states.

Figure 39 shows the expected position of form finding within computational structural optimization. Here, a combination of structural optimization together with force-active form finding techniques is likely to converge quickly into a good result. In this schematic representation, the "modeling" stage should include fabrication-related constraints.

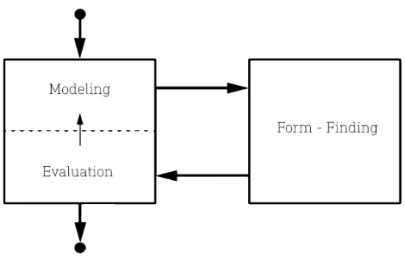

Figure 39 Figure 39 –Form-finding remains a tool and requires the manual processes for a holistic evaluation.

Because existing form finding methods currently do not allow for the inclusion of fabrication-related constraints, the rest of this thesis research will focus on the potential integration process of multiple optimization techniques within a parametric framework. For more background on force-active form finding methods, I refer to the work of (Veenendaal & Block, 2012) and the book *Shell Structures for Architecture: Form-Finding and Structural Optimization* by (Adriaenssens et al., 2014).

4.3.3 Integration of constraints

As shown in Chapter 4.3.4, new challenges arise in the implementation of not only fabrication constraints but also in design, material, and construction constraints within the optimization process. Currently, there is no method of structural optimization that integrates the required fabrication-related aspects and material properties. Similarly, there is no form finding method that allows for the integration of multiple load cases. Is there another solution to this problem?

To successfully explore the solution space regarding the primary research question, a model needs to be built that answers the primary research question and integrates not only the fabrication-related aspects but also design, material and construction constraints. Performance-based-design engineers often refer to this as parametrics.

4.3.4 Parametric design

Parametric design can be described as an (algorithmic) process that enables the expression of parameters and rules that together define, encode, and clarify the relationship between design intent and design response (Jabi, 2013). The hanging model by Gaudi is an excellent example of a parametric approach to structural design (Figure 34). In his physical model, he could influence the position of the towers and arches by changing the position of weights, which in turn, influenced the structural behavior of the structure. Gaudi's model helped him to explore the potential solution space (Figure 39).

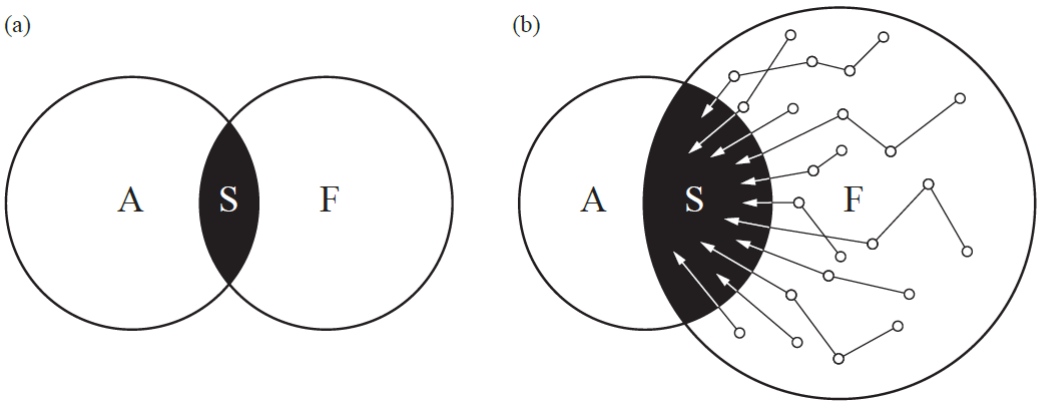

Figure 40 Design and solution space: (a) The space (S) depicts solutions to a problem. (b) By applying correct parameters, the solution space of a design problem is enlarged. Space A represents acceptable design solutions, while F represents potential funicular

A parametric model can also be used as a search tool that allows the process to navigate the design space efficiently (Motta, 1999). In this case, the model needs to be set in accordance to a set of criteria that reflects the fabrication, material construction, and design constraints. Figure 40 shows the influence of successfully set parameters that enlarge the solution space of a given design problem.

To successfully explore the solution space according to a set of criteria, the right parameters need to be set. This is especially true when focusing on performance-oriented design, where the design expresses a meaningful range of variations on key aspects affecting the analyzed performance criteria (Turrin, Von Buelow, & Stouffs, 2011).

New challenges arise when addressing (multi-objective) design questions with the implementation of parametric models. The explicit formulation of the objective function and its gradient often becomes unavailable and results in difficulties in exploring the solution space (Turrin et al., 2011). Results need to be generated and evaluated from the parametric model to find a solution (Oxman, 2006). which also often proves to be difficult. Turrin et al. (2011) mentioned the same problem as "difficulties in exploring the solution space are a definite drawback when using parametric techniques."

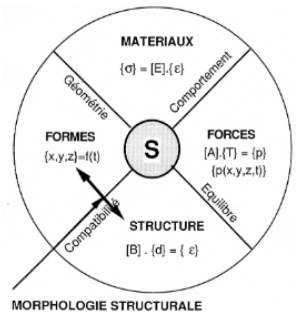

Figure 41 - In structural morphology, many structural engineers list and process the design of a structure in the relation between material, forces, forms and structure. Other parameters should also be considered and are often non-tacit. Source: (Motro, 2009)

The difficulty of searching the solutions space is primarily due to the unavailability of the objective function and its gradient. Why is the explicit formulation of the objective function unavailable?

In architectural design-related problems, the explicit formulation of the objective function is often impossible due to the complexity of the problem. Here, choices regarding the set parameters are based on non-tacit knowledge. Structural engineers often know the relationship between material, forces, form, and structure (Figure 41). However, they are not able to explicitly define other design parameters or their relationship in a formula (Motro, 2009).

To overcome the problem of not having a set formula, finite element analysis can be used to get objective values and approximate the unknown objective function (known as simulation-based-design). In mathematics, the problem of not having an objective function is often described as derivative-free, or black-box, optimization problems.

4.3.5 Black-box optimization: Derivative free optimization

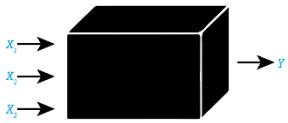

Figure 42 - In a black box optimization process, only the inputs and outputs are known.

In mathematics, optimization methods that address problems without a known objective function are called black-box optimization. Similar to general optimization problems (described in 4.3.1), the goal in this case is to minimize or maximize an objective function defined on a continuous search space. However, in the case of black box optimization, the only available information about the objective function *f*(".") is the resulting values of *f*(*x*) for a given input (Figure 42).

The question then arises: How do you find an optimum in a black box problem?

For background on optimization in the field of engineering, I refer to the work of Yang on *Engineering Optimization: An Introduction with Metaheuristic Applications (X.-S. Yang, 2010).* In this book, Yang gives a clear overview of the different types of optimization problems and how to solve them. Parametric design problems in construction with multiple variables often result in multiple local optima, due to the non-linear dependencies between the different variables (Attia, Hamdy, O'Brien, & Carlucci, 2013). Therefore, all optimization methods considered in this thesis are global methods that search for an overall optimum.

Black box optimization: Three global approaches

When looking at the relevant global approaches to black-box optimization problems, three approaches can be distinguished: metaheuristic, direct search, and model-based methods (Wortmann & Nannicini, 2016).

- *Metaheuristic methods*
  A metaheuristic optimization algorithm is an optimization algorithm in combination with a generative model that is used to guide the development of the optimization (Beheshti & Shamsuddin, 2013). Meta-heuristics are often inspired by nature. Beheshti & Shamsudiin (2013) give a comprehensive overview of metaheuristic methods; the different methods are summarized in Figure 43, Genetic algorithms are currently the most common (metaheuristic) optimization methods used in the building sector (Oxman, 2006).

- *Direct search methods*
  Direct search methods examine design candidates according to a deterministic strategy and thus, they do not try to approximate the objective function. This is advantageous when computation of the derivative is impossible (e.g., involving noisy functions or unpredictable discontinuities) or difficult (i.e., high complexity or high computation cost) (Wright, 1996). State-of-the-art direct search methods typically outperform metaheuristics in scientific tests by orders of magnitude (Rios & Sahinidis, 2013)., although they are rarely applied in an architectural context (Wortmann & Nannicini, 2016). This might be because they are not standard integrated into parametric design tools such as Grasshopper and Dynamo.

- Model-based methods
  Model (or surrogate)-based optimization methods are known for finding optima with a relatively small number of simulations (Costa & Nannicini, 2014). They do this by constructing a simplified mathematical model from the evaluated variants and use this model to guide further exploration (Koziel & Yang, 2011). The optimization process results in an interpolated surface between a set of strategically chosen design variants and thus a mathematical approximation of the design space (Wortmann, Costa, Nannicini, & Schroepfer, 2015).

When comparing the three approaches, metaheuristics and especially genetic algorithms are currently the most common optimization methods used in the building sector (Oxman, 2006). The primary reason for their popularity is the integration in visual programming software packages such as Grasshopper – Galapagos in Grasshopper is a genetic algorithm – and Design Builder (Wortmann & Nannicini, 2016). The advantage of metaheuristic methods is that they can be applied to any problem type, are easy to implement, and are suited to perform multi-objective optimizations (Lin & Gerber, 2014).

When it comes to the optimization community, most people are sceptical of metaheuristic methods. This is primarily due to the generally poor performance of metaheuristics and the lack of mathematical rigor (Rios & Sahinidis, 2013). Conn, Scheinberg, & Vicente, 2009, p. 9) even refer to them as the "methods of last resort."

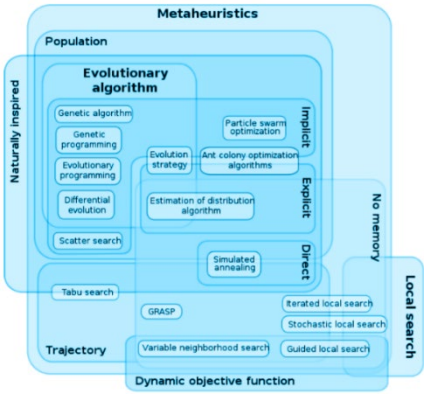

Figure 43 - Classification of all the different meta-heuristic algorithms (2013). Adapted from: (Beheshti & Shamsuddin, 2013)

Most metaheuristic methods require the evaluation of tens of thousands of design candidates to find a high-quality solution (Hasançebi, Çarbaş, Doğan, Erdal, & Saka, 2009) .

The question that arises is: What is the optimal way of solving black-box optimization problems? The answer finds itself in the No Free Lunch Theorem, which has logically proven that there is no optimal solving technique that solves all optimization problems (Wolpert & Macready, 1997).

In the case of structural optimization with the use of finite element analysis, slow convergence needs to be avoided, as each calculation is computationally costly. This requires the model to converge to an optimum relatively quickly. In these problems, model-based methods excel as they converge more rapidly to an optimum in most optimization problems.

Similar results can be found in the paper "Derivative-free Methods for Structural Optimization" by (Ilunga & Leitão, 2018) in which they concluded that metaheuristic methods do not appear to be the best choice for structural optimization. Instead, they found that direct and global model-based algorithms outperform other methods. In the case of structural optimization problems, model-based algorithms excel.

4.3.6 Visual programming: Interdisciplinary advantage

Parametric design thinking often consists of four different steps. First, the right parameters for the problem should be identified. Second, the related constrains to the set parameters must be recognized and implemented. Third, the objectives should be investigated and considered. Finally, based on the type of parameters, constraints, and objectives, a suitable optimizer needs to be found (Saremi, Mirjalili, & Lewis, 2017).

For structural engineering related problems, model-based algorithms seem to excel as literature shows that they converge relatively quickly. However, the question remains: How can we effectively include all the parameters, constraints, and objectives in a script, within a relatively short time-span, and without a Master's degree in computer programming?

Recently, computer-aided design (CAD) packages started introducing visual programming environments that allow for an algorithmic approach to design without the need for coding. The main characteristic of the visual programming environment is the "box-and-wire" analogy (Figure 44), which can be described as the hierarchical organization of elements that can be grouped to form subunits. Visual programming has many advantages (Celani & Vaz, 2012). These are:

- Making an algorithmic approach more accessible.
- Allowing for the visualization of the logic (like a flow chart)
- Allowing for the rapid development of code
- Offering a less steep learning curve than regular programming
- No syntax errors

Visual programming within CAD packages can be beneficial for shape exploration through the real-time generation of parametric variations (Celani & Vaz, 2012). Examples of software that include visual programming with CAD packages are: Grasshopper, Generative Components, and Dynamo.

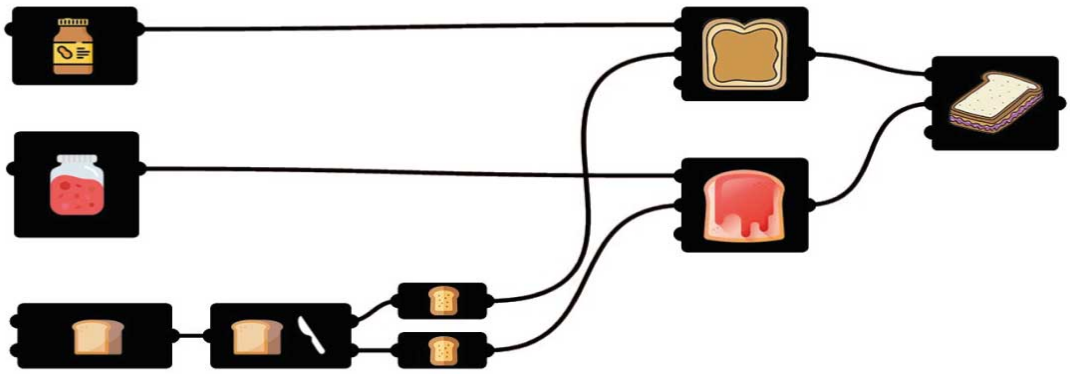

Figure 44 - visual programming of a peanut butter jelly sandwich.Illustration from twitter.com/_m_juliani).

Turrin et al. (2011), in her paper on "Design explorations of performance driven geometry in architectural design using parametric modeling and genetic algorithms," states that integrating interdisciplinary knowledge and early numeric performance evaluations is a key development to addressing design decisions. In this case, visual programming allows for interdisciplinary collaboration through an almost flowchart-like process (Figure 44), giving insight into an algorithmic process for people without a programming background. In addition, Turrin et al. (2011) conclude that:

> Parametric approaches enhance an early structure of the design problems by forcing the designer to decompose complex design aspects and their interrelations at an early stage. It also challenges the designer, by requiring a consistent early abstract thinking, for which computationally supporting the reusability of knowledge during the parameterization process is crucial states that a parametric approach. Turrin et al. (2011)

4.3.7 Structural optimization: Summary and key findings

This Chapter began by giving an overview of the different methods of structural optimization – size, shape, and topology optimization, which was followed by fabrication-aware structural optimization. It was found that new challenges arise in the implementation of not only fabrication constraints, but also in design and material constraints, resulting in compromises in structural optimality. It also showed that the field is still in a relatively early stage of development, whereby relevant concurrent optimization processes for the fabrication with concrete have not been explored yet.

The Chapter also elaborated on form finding methods of structural optimality of compression-only structures, the primary difference between structural optimization and form finding being the use of force-active methods. It found that a combination of structural optimization together with force-active form finding techniques is likely to converge quickly to a good result. However, current form finding methods do not allow for the inclusion of fabrication-related constraints.

Because of this, a parametric design approach was explored that incorporates the use of a visual programming language and black-box optimization algorithms. While the clear objective function cannot be defined, which results in optimization-related problems, this seems to be the most effective method to integrate fabrication, material, construction, and design constraints.

Key findings from the literature study are:

- Before successful structural optimization methods can be applied to address the environmental impact of concrete, the additive manufacturing constraints need to be better understood and documented.
- Research in manufacturability-oriented structural optimization is relatively young (mostly after 2015). When it comes to additive manufacturing, overhang angle, material anisotropy due to layered manufacturing, infill structures are considered, but there is no research yet on concurrent optimization that considers all the fabrication constraints of a process and the material properties required.
- The explicit formulation of the objective function is often impossible due to the complexity of the problem when considering fabrication, material, construction, and design constraints. This makes manufacturability-oriented structural optimization with sustainability in mind exceptionally difficult and results in black-box optimization problems.
- Force-active methods are highly effective in creating funicular structures, but need to be combined with structural optimization methodologies to overcome the difficulty of integration of constraints and multiple stress states.
- A parametric design approach allows for the integration of structural optimization and form-finding methodologies while considering fabrication, material, construction, and design constraints. Parametric design approaches seem to be effective in overcoming the difficulty of structural optimization problems.
- Surrogate-based optimization solvers are likely the most effective method of solving "derivative-free" structural optimization problems, as they exhibit faster convergence, with fewer optimization cycles. This is particularly important for processes with computational costly optimization cycles (e.g., structural optimization).
- The use of visual programming tools facilitates interdisciplinary collaboration early on in the process and a better understanding for people without a programming background. This is especially relevant when sustainable design problems, as they benefit from an interdisciplinary approach.

4.3.8 Structural optimization: Conclusions and future research

For structural optimization to become game-changing, key challenges related to the integration of fabrication, material, construction, and design constraints need to be solved. While much effort is put into concurrent optimization with a clearly defined objective function, this research is still in an early phase and cannot be directly applied.

Because tackling sustainability-related issues requires an interdisciplinary approach and since it is difficult to formulate an explicit objective function as design decisions are often non-tacit, a new direction for manufacturability-oriented structural optimization is required. Potential can be found in interdisciplinary collaboration using visual programming tools. A parametric approach forces people to deconstruct complex design problems into parameters, while visual programming allows people to collaborate without needing programming knowledge.

In this situation, the focus should be on applying surrogate-based solvers for black-box optimization problems, as they have the most potential regarding computational costly optimization processes.

Literature study

Concrete manufacturing process

Image Source: https://block.arch.ethz.ch/brg/research/3d-printed-floor-system

4.4 Concrete manufacturing process

Every year we use more than 10 billion tons of concrete, which makes it the second most commonly used material on earth after water. Questions that arise ask if we can make concrete manufacturing more sustainable or if we should use less concrete? Given its environmental impact, why do we use so much concrete?

The primary reason that we use so much concrete is that very few materials have the ease of construction, low cost, versatility, and durability of concrete. In addition, very few materials can resist environmental extremes in the way concrete can. When looking at the building sector, high thermal mass and low air infiltration help to reduce the energy demand required to heat and cool buildings (Tuojy, McElroy, & Johnstone, 2005).

Considering the excellent manufacturability, cost, and the qualities it offers to buildings, the major question is if we can minimize the environmental impact while maintaining these advantages. The following Chapter goes into depth into the concrete manufacturing process and analyses if we can lower the environmental footprint of concrete construction while maintaining its advantages.

4.4.1 Concrete manufacturing: Description of process

Concrete is a composite material created by mixing chemically inert aggregates (e.g., sand, gravel, and stone) with a binder (cement), additives, and water. The process of concrete production is time-sensitive and usually takes place in facilities called concrete plants.

The product chain of the generation of concrete is primarily defined by the generation process of the binder – cement. Figure 44 illustrates the fabrication process of cement.

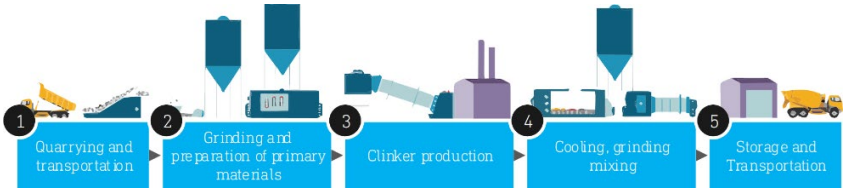

Figure 45 - Illustration of the different stages inf cement production, from quarrying to transportation.

The production of concrete can be divided into five stages involving the the manufacturing process and the chemistry of concrete (Figure 45):

- *(1) Quarrying and transportation*
  The production of cement starts with raw material extraction and quarrying of the material. Quarrying is the process of crushing the materials into smaller workable pieces. The primary ingredient of concrete is limestone (80%). Other required materials include clay, shale, fly ash, mill scale, and bauxite.

- *(2) Crushing and grinding: preparation of primary materials*
  The limestone is crushed and mixed with the other materials and prepared for pyro-processing in the kiln. The crushing facilitates good reactivity between the minerals in the raw materials. The chemical composition of the two primary materials is: limestone → $CaO + CO_2$, clay → $SiO_2 + Al_2O_3 + Fe_2O_3$.

- *(3) Clinker processing*
  Clinker processing is the process of generating the binder known as clinker. The process is shown in Figure 46. The raw materials are heated to a high temperature (around 1,450 °C) in a kiln. Chemical reactions occur between the clay and the limestone which result in the clinker. Limestone + clay → (C_3S, C_2S, C_3A, C_4AF) = clinker.

- *(4) Cooling grinding and mixing*
  The clinker is cooled and mixed with small amounts of gypsum and other finely ground materials. This mixture ultimately defines the type of cement that is produced. This is one of the measures where the carbon footprint of concrete construction can be reduced. More information on different types of cement can be found in Chapter 5.6, which goes in-depth into the material process and building codes.

- *Storage and transportation (5)*
  The cement clinker is then transported to the building site or concrete producers. Mixing clinker together with water, aggregates, and additives will result in hardened concrete.

Within the whole concrete manufacturing process, clinker processing is the most defining. Figure 46 illustrates in detail the pyro-processing of clinker (Van Oss & Padovani, 2002). Note the critical position of CO_2 in the process and the requisite temperature of 1,450 °C (Here, blue annotates the processes with high environmental impact.)

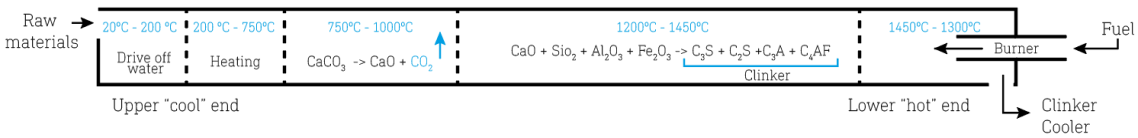

Figure 46 – The process of clinker production and pyro- processing in a rotary kiln. Image based on: (Van Oss & Padovani, 2002)

4.4.2 Concrete manufacturing: The emissions of production

In 2010, the cement industry accounted for more than 2800 million tons of greenhouse gases. This corresponds to 8% of global CO_2 emissions (Marchal et al., 2011). As shown in Chapter 2, the number is expected to grow as the worldwide cement demand for cement-based products increases (Johanna Lehne & Felix Preston, 2018).

In general, there are three types of emissions that can be distinguished in the process of creating cement:

- Direct process emissions
- Emissions from the combustion of fuel
- Smaller indirect emissions

When looking at the concrete manufacturing process, 50% of emissions are related to the calcination process of limestone (Benhelal, Zahedi, Shamsaei, & Bahadori, 2013). These are considered direct process emissions.

About 40% of emissions are thermal-related emissions caused by the combustion of fuel. The emissions are high, because coal is still the primary energy source of the sector (Rahman, Rasul, Khan, & Sharma, 2015).

Process and thermal emissions are both related to the calcination process of clinker, which makes it responsible for around 90% of emissions (Tregambi, Salatino, Solimene, & Montagnaro, 2018).

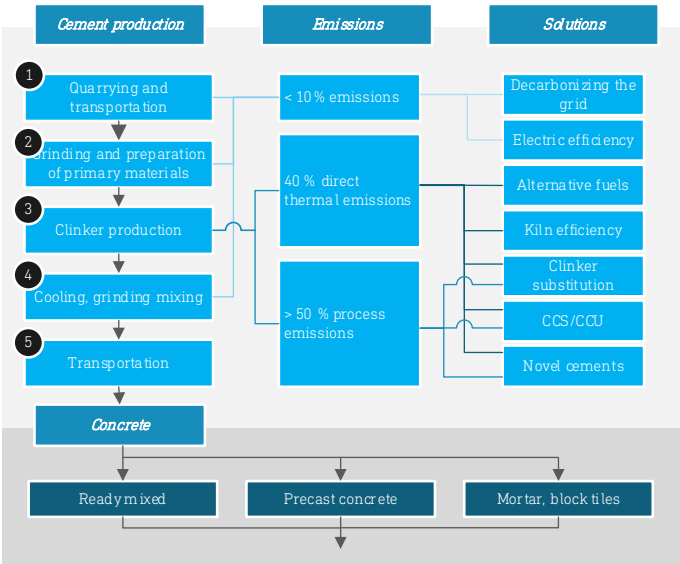

Figure 47 - Cement production with the related emissions and mitigation solutions. image based on research by (J. Lehne & F. Preston, 2018)

McKinsey & Co. published an article in 2020 called "Laying the foundation for zero-carbon cement" (2020) with a similar study that broke down the carbon emissions throughout the fabrication process of cement (Figure 48).

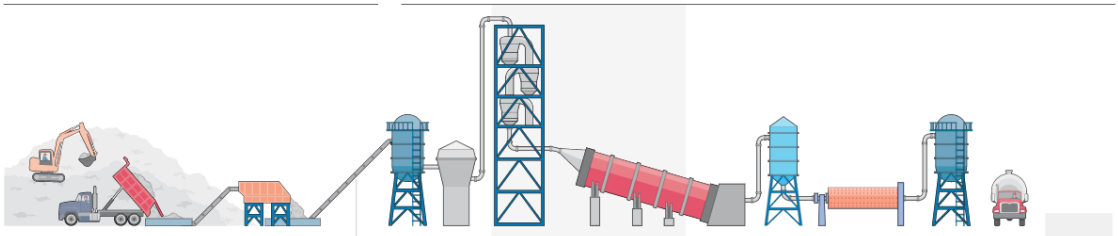

	Quarry	Crusher	Transport[1]	Raw mill	Kiln and preheater/ precalcinator[2]		Cooler[3]	Cement mill	Logis-tics[4]	**Total**
Energy, mega-joule/ton	40	5	40	100	3,150		160	285	115	3,895
CO_2, kilogram/ton	3	1	7	17	479 Calcination process	319 Fossil fuels	28	49	22	925

Figure 48 - Breakdown of the co2 emissions and energy used within the process of generating cement., similarly +/- 90% of the emissions are related to the calcination process of the klinker in the Kiln and cooler. Source: https://www.mckinsey.com/industries/chemicals/our-insights/laying-the-foundation-for-zero-carbon-cement

As pointed out by the studies of Lehne & Preston and McKinsey & Co., the emissions of concrete are primarily due to the calcination process of the clinker. The next Chapter focuses on effective methods to reduce the environmental impact of concrete production. Figure 48 offers potential methods which range from increasing efficiency, use of alternative fuels, to clinker substitution and use of novel cement types.

4.4.3 Concrete manufacturing: Strategies to reduce the environmental impact

Four strategies can be identified to reduce the environmental impact of concrete construction (Favier, De Wolf, Scrivener, & Habert, 2018) optimizing the clinker production process; optimizing the mix design of concrete and; optimizing the application; (i.e., reducing the quantity of concrete required; optimizing a structure to use concrete mortar with less binder)

All these strategies are indirectly based on the clinker production process. Figure 46 lists potential improvements and their respective emissions in the clinker production phase. Different initiatives have already been started, and major producers have begun to devote substantial efforts toward reducing their climate impact. The different methods of reducing the environmental impact are:

- *Decarbonizing transportation*
  In the transition towards a more sustainable footprint, it is essential to think about the transport of materials from their origin location to the construction site. While currently accounting for around 5% (Kajaste & Hurme, 2016), this percentage might go up as other process-related emissions become smaller. Methods of reducing the emission of transport include local production and decarbonizing transport using alternative fuels.

- *Electricity efficiency*
  Emissions are produced by the generation of electricity to power grinding machinery and cooling of the clinker in the process. Grinding accounts for, on average, 100 kWh per ton of clinker, whereby the current energy efficiency is around 5% to 10% (M. Taylor, Tam, & Gielen, 2006). By designing smarter plants, upgrading machines and mills with variable speed drives, this energy can be used more efficiently.

- *Alternative fuels*
  Switching away from fossil fuels to renewable alternatives can generate a significant reduction in emissions. Coal is still the predominant fuel burned in cement kilns (Rahman et al., 2015). The International Renewable Energy Agency (IRENA) monitors the price of renewable energy sources. In their report, they show a cost decline in Solar photovoltaics (PV) energy of 82% over the period of 2010–2019 (International Renewable Energy Agency, 2020), making it cheaper per kWh than fossil fuel energy. Figure 48 shows the price history of several renewable energy sources. Due to recent investments into sustainable energy sources, it may become cost-effective to switch to sustainable energy for cement production. As 50% of the environmental pollution comes indirectly from heating, this would have a significant impact on the environmental impact of concrete.

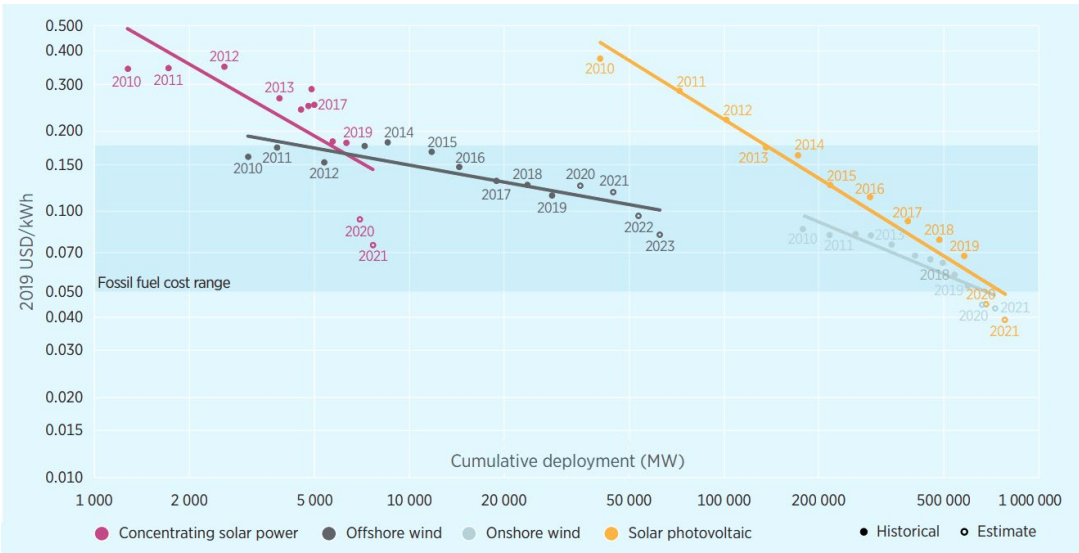

Figure 49 Figure showing the cost development of investments in fossil fuels versus renewable sources, Note the steep decline in price of solar photovoltaic energy. Source: (International Renewable Energy Agency, 2020)

Furthermore, cement manufacturing can be used to stabilize energy grids based on wind and solar. Energy storage is currently costly, which results in low prices when the production is higher than the demand. Cement producers can take advantage of the fluctuation.

- *Kiln efficiency*
  The kiln is, directly and indirectly, responsible for 90% of environmental emissions (Tregambi et al., 2018). Shifting towards higher efficiency systems, combined with machine learning to improve the process actively, can make a big difference in consumption and emissions. A state-of-the-art dry-kiln with pre-calciner results in a reduction of emissions of 50% (Szabó, Hidalgo, Císcar, Soria, & Russ, 2003), as compared to wet kilns. Furthermore, energy recovery in existing systems can result in a reduction of emissions of about 33% (Irungu, Muchiri, & Byiringiro, 2017).

- *Clinker substitution*
  As described earlier, the clinker process takes place in the kiln and is responsible for about 90% of the emissions of concrete manufacturing. Replacing ordinary Portland clinker with other binders is thus a highly efficient way to reduce the environmental impact of concrete construction. A recent study by (Vizcaíno-Andrés et al., 2015) showed a reduction of 50% of the mass of clinkers without compromising performance.

- *Novel types of cement*
  J. Lehne & F. Preston (2018) studied the potential of different alternative binders in concrete. Figure 50 shows the results of different alternative binders studied by Lehne & Preston. London Imperial College did similar research in the economic viability of alternative binders and concluded that BPC, BYF, CCSC, and MOMS, are also economically viable solutions to replace ordinary Portland cement. (Gartner & Sui, 2018) On the other hand, the ETH Zurich annotates that without economies of scale, and considering technical application difficulties, it is unlikely that alternative will become economically viable. (Favier et al., 2018) (figure 50)

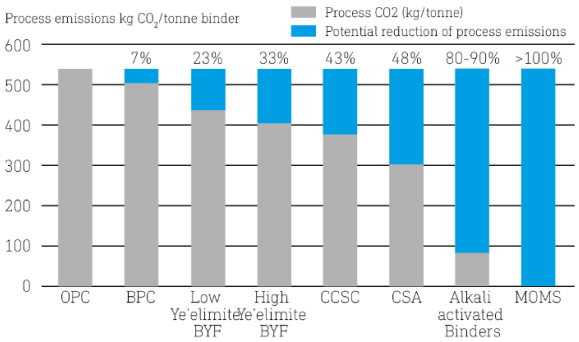

Figure 50 - Potential reduction of CO_2 emission of several novel cement types based on alternative binders. Source: (Johanna Lehne & Felix Preston, 2018)

- *Carbon capture and storage (CSS)*
  Carbon capture and storage (CSS) is a measure that can be taken as the last step to reduce the impact of concrete construction. Carbon capture is an effective way to deal with the chemical process emissions. Effort in upcycling the CO_2 in greenhouses has high potential. It mitigates CO_2 emissions while increasing the productivity of greenhouses. This partly solves the cost related to CO_2 storage (Lilliestam, Bielicki, & Patt, 2012).

4.4.4 Concrete manufacturing: Theoretical decarbonization

In the study by Lehne & Felix Preston (2018), on the effectiveness of the different decarbonization methods for cement production, they state that the effectiveness of clinker substitution and the impact of novel cement types illustrate that relatively inexpensive paths that could lead to the decarbonization of the production process of cement and thereby concrete (J. Lehne & F. Preston, 2018). It does come with the difficulty of certification. Figure 51 summarizes the theoretical decarbonization potential of different reduction methods.

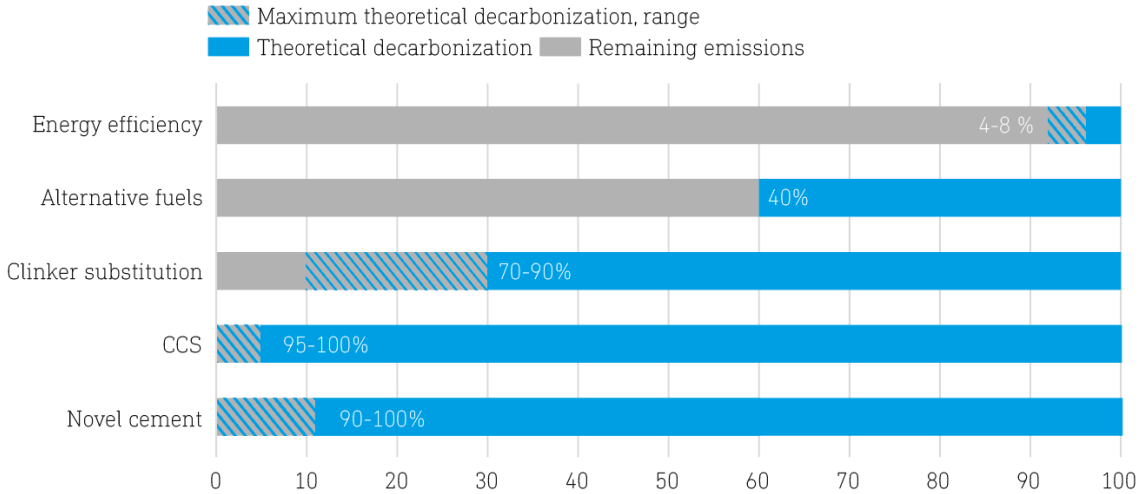

Figure 51 - Theoretical decarbonization in % of concrete production by different measures. Source: (J. Lehne & F. Preston, 2018)

The United Nations environmental program (2018) carried out a similar study in the decarbonization potential of concrete manufacturing and concluded that there are two key areas that can deliver a substantial reduction in environmental emissions. These are:

- Use of clinker substitutes (SCMs) in Portland clinker-based cement
- More efficient use of Portland cement clinker in mortars and concretes

Additionally, carbon capture and storage are effective but costly. The UN (2018) expects that Portland clinker cement will still dominate in the near future due to the economy of scale, level of process optimization, availability of raw materials, and market confidence in these products (Environment, Scrivener, John, & Gartner, 2018). In the longer term, other emerging alternatives could play a vital role in the mitigation of environmental emissions (e.g., novel cement types).

4.4.5 Concrete manufacturing: Summary and key findings

This Chapter began by giving insight into the manufacturing process of concrete, with a focus on the production of the binder. A breakdown of the emissions of concrete and strategies to reduce the environmental impact showed that 90% of the emissions are related to the fabrication process of the binder. By looking at strategies to reduce the environmental impact and optimize the process, three main strategies could be identified to address the environmental impact of concrete construction.

a. Optimizing the clinker production process
b. Optimizing the mix design of concrete
c. Optimizing the application

Several measures to reduce the environmental impact of concrete were studied: decarbonizing transportation, increasing the electricity efficiency, using alternative fuels, increasing the efficiency of the kiln, clinker substitution of concrete, and the use of novel cement.

The key findings of the research were:

- In the process of clinker generation, 90% of the emissions can be allocated to the calcination process of the limestone. Optimization and an increase in energy efficiency together with carbon capture and storage and the use of renewable energy could play a vital role in reducing the environmental impact of concrete.

- Improving the energy efficiency of the grinding and kiln can reduce the environmental impact by more than 50%, compared to existing methods (wet kiln processes). Thereby the primary source of energy for existing kilns is still coal. With the expectancy for solar energy to become cheaper than fossil fuels, switching to renewable energy sources combined with heat recovery could set out the future of sustainable concrete.

- While novel cement types show many potentials, the state-of-the-art binders are not allowed within existing legislation. The economy of scale, level of process optimization, availability of raw materials, and market confidence in these products prevent the application in the short term.

- The most effective methods of reducing the environmental impact in the short term are the use of clinker substitutes (SCMs) in Portland cement clinker-based cement and more efficient use of Portland cement clinker in mortars and concretes.

- As CO_2 emissions are embedded within the clinker process, carbon capture and storage need to be applied for concrete as the last step for concrete to become sustainable. To reduce the cost, innovative synergies can be applied (e.g., upcycling the CO_2 in greenhouses).

4.4.6 Concrete manufacturing: Conclusion and future research

The clinker production process causes 90% of the concrete-related emissions. Luckily, many strategies exist to reduce the environmental impact of the clinker production process and, thereby, concrete. More effective use of clinker within concrete plays a vital role in further reducing the environmental pollution of the sector. Additionally, a lot of the current sector still relies on coal as its primary energy source. With the expectancy for solar energy to become cheaper, electrification of the kiln processes becomes vital.

Further research should be in R&D regarding the electrification of the clinker production process, Energy produced by solar photovoltaics is becoming cheaper, and concrete plants have the potential to stabilize the energy grid in a shift towards renewable energy sources.

As stated in the introduction (Johanna Lehne & Felix Preston, 2018), the global building floor area is projected to double over the next 30 years. Most importantly is to focus on methods that are directly applicable, which is optimizing the use of clinker in cement, optimizing the amount of cement in concrete, and minimizing concrete with innovative construction concepts.

4.5 Literature research: Conclusion

Three primary research directions, structural optimization, additive manufacturing, and the environmental impact of concrete construction, were studied, resulting in key findings and potential for further research. This chapter aims to create a succinct summary of the relationship between the different subfields and the primary research question. for the conclusions and key findings I would like to refer to:

- Chapter 4.2.10 (additive manufacturing processes)
- Chapter 4.3.8 (structural optimization)
- Chapter 4.4.6 (concrete manufacturing)

4.5.1 Answer to the related sub-questions

The goal of the literature study was to provide a theoretical background for the research topic and form the basis for the research-through-design approach. The primary research question is: *In what manner can we use structural optimization and additive manufacturing in the building sector to address the environmental impact of concrete construction?*

In this section, the sub-questions related to the primary research question will be answered, resulting in the necessary background information to formulate an informed hypothesis for the research-through-design part.

- *In what manner can we use additive manufacturing to address the environmental impact of concrete construction?*

  Additive manufacturing is unlikely to address the environmental impact of concrete construction in the short term. Reinforcement, scalability, life cycle cost, and process-related material requirements need to be solved before additive manufacturing methods can be applied to address the environmental impact of concrete construction. Two primary methods can be found to address the environmental impact with the construction of building elements;

  a. 3D concrete printing
  b. Particle-bed additive manufacturing

  Particle-bed methods are currently not at the level of maturity that it can be reliably, upscaled, and applied. Furthermore, 3D concrete printing required higher cement content to overcome the buildability constraints, which, in turn, results in higher environmental emissions. Therefore 3D concrete printing is an ineffective way to address environmental emissions. In the case of formwork production, thin formwork seems to be a perfect solution to fabricate intricate shapes. The problem is that set-on-demand concrete, required to overcome hydrostatic pressure breaking the formwork, might make the environmental impact by reducing the amount of formwork required neglectable.

  Long story short, innovative manufacturing methods will not disrupt the industry in the short term towards a more sustainable paradigm. It could find a specific application where it might lead to more sustainable construction. Most often, this will be in a hybrid process where the integration of the fabrication, material, construction, and design constraints need to be considered from the beginning of the design process.

- *In what manner can we use structural optimization to address the environmental impact of concrete construction?*

  Structural optimization is highly effective in addressing the environmental impact of concrete construction. Favier, et al. (2018) state in the research: *'A sustainable future for the European Cement and Concrete Industry Technology assessment for full decarbonization of the industry by 2050'* that structural optimization for low-carbon cement could result in a reduction of more than 50% of the environmental impact, and thereby forms a critical part addressing the environmental impact of concrete construction.

  For structural optimization to become game-changing key challenges related to the integration of fabrication, material, construction, and design constraints need to be solved. There are not many research papers that concurrently consider multiple constraints. This is since research in manufacturability-oriented structural optimization is relatively young, and it's relatively complex to integrate all the aspects within the optimization. Concurrent optimization needs to happen, or boundaries need to be set, which take the fabrication constraints into account.

  In the short term, there is a lot of potential in parametric modeling to integrate the fabrication, material, construction, and design constraints, combined with black-box optimization tools. The parametric approach allows for an integration of constraints, the use of structural optimization, and overcomes the loss in structural optimality in post-processing and fabrication. In the long-term concurrent optimization methods, as proposed by Weiming Wang (2020) (Chapter 4.3.4), show much potential.

- *What are the different strategies to address the environmental impact of concrete construction?*

In addressing the environmental impact of concrete, three main strategies could be identified; optimizing the clinker production process, optimizing the mix design of concrete, optimizing the application. All these strategies are indirectly based on the clinker production process. The clinker production process accounts for about 90% of the pollution of concrete. Two reasons can be noted;

a. The concrete sector primary relies on coal as its energy source
b. Within the chemistry of clinker production is CO_2 embedded.

With the expectancy for renewable energy to become cheaper, electrification of the processes becomes vital. Additionally, several measures can be taken to reduce the environmental impact of clinker production further (e.g., Decarbonizing of the transportation, Increasing the electrical efficiency, Novel clinker types, and addressing the efficiency of the Kiln, etc.). Investments in a dry-kiln can already result in a reduction of emissions of 50% (Szabó et al., 2003) and are thereby highly effective in reducing the environmental impact of concrete.

The most effective strategy of reducing the environmental impact in the short term is the use of clinker substitutes (SCMs) in Portland clinker-based cement; more efficient use of Portland cement clinker in concretes and optimize structures for the use of these low emission type of cement.

SECTION II

Optimization of the floor slab

Image Source: https://www.tugraz.at/index.php?id=36358

5 Section II: Optimization of the floor slab

Whereas Section I provided the necessary background information to formulate an informed hypothesis, Section II seeks an answer to the main research question. The second section focuses on formulating a hypothesis and addressing it using a research-through-design (RtD) approach (Figure 52).

Section II starts with a definition of the scope of this thesis. Along with the literature study, it identifies the most effective way of addressing the primary research question (Chapter 5.1) and results in the final design hypothesis: *Fabrication-aware, structurally optimized floor slab, can significantly reduce the environmental impact of concrete construction* (Chapter 5.2). A major focus of the primary research question is the integration of:

- Material (Chapter 5.5)
- Integration of the life cycle assessment of the product stage (Chapter 5.6)
- The research-through design process (the design of the process vs. the product) (Chapter 5.7)

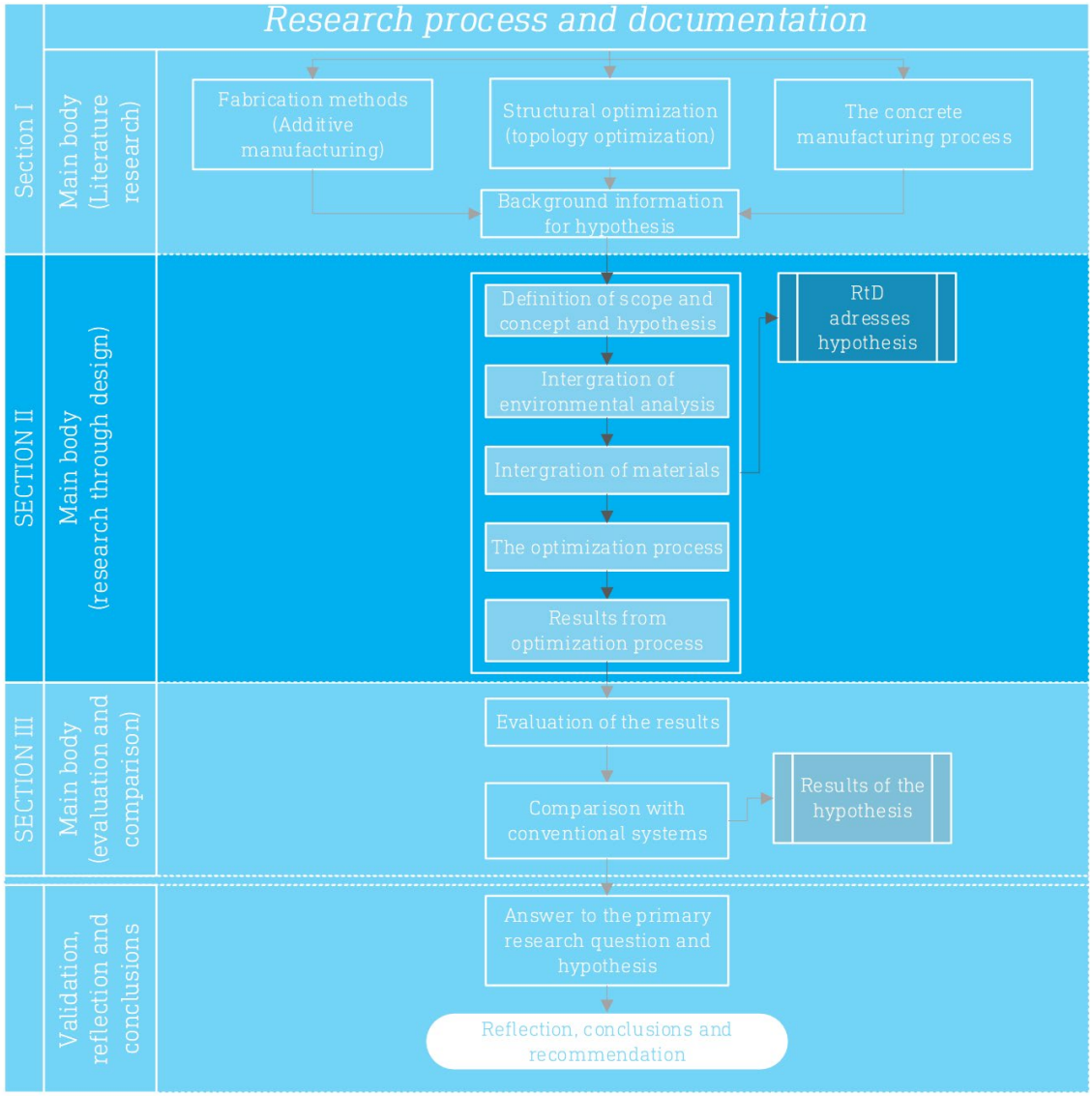

Figure 52 The position of Section II in the body of the research process

When a hypothesis has been formed, the solution of creating a floor slab inspired by thin shells will be elaborated on (Chapter 5.3) based on shell theory (Chapter 5.4). This will result in an optimized design of two-floor spans (2400 mm x 3600 mm and 5400 mm x 3600 mm) with the aim of reducing the emissions of concrete construction.

5.1 Defining the scope

In addressing the environmental impact of concrete construction, three main strategies have been identified in the literature research:

- Optimizing the clinker production process
- Optimizing the mix design of concrete
- Optimizing the application

While much research focuses on the optimization of the clinker production process, a gap exists in the integration of the mix design in the optimization process of concrete construction. When designing for sustainability, there is potential for the integration of fabrication, material, construction, and design constraints in the optimization process.

An integrated approach results in a structure that is not only structurally efficient, but also in one that is constructed using materials with a low environmental impact, compatible with economical construction, and can be designed and built using a methodology that is repeatable and robust.

5.1.1 Scope: Why design a floor slab?

In concrete construction, 50% of concrete, on average, is used for building construction and 30% for civil engineering structures (Favier et al., 2018). In civil engineering, each structure is individually calculated, which in general results in an optimized amount of concrete. This is not the case in building construction, where engineering offices take less time to optimize the design (Favier et al., 2018).

Hence, it makes the most sense to optimize building construction. In buildings, concrete floor slabs account for 59% of the total mass (table 2) (Wight & MacGregor, 2009). A reduction of the weight of the floor slab also addresses the amount of concrete required in the foundation[1] (22%). For this reason, it would be wisest to optimize floor slabs. Georgopoulos & Minson (2014) also came to this same conclusion. The largest potential lies in optimizing floor slabs in multi-story buildings of concrete because 85% of the weight and cost are related to the construction of floor slabs (Georgopoulos & Minson, 2014).

TABLE 2: DISTRIBUTION OF CONCRETE IN A BUILDING (WIGHT & MACGREGOR, 2009)

Building element	Percentage of concrete
Floor slabs	59%
Foundation	22%
Other elements	10%
Columns	5%
Load-bearing walls	4%

5.1.2 Scope: Casting as a primary fabrication method

As stated earlier, a sustainable floor system must not only be structurally efficient but should also be economically feasible, quickly applicable, and avoid using carbon-intensive materials. Direct applicability, together with the ability to upscale, define the chosen fabrication method "casting." Casting remains highly effective for the fabrication of concrete. Conversely, reinforcement, scalability, and primarily process-related material requirements prevent additive manufacturing from being an effective method[2]

Additionally, the number of buildings is expected to double in the next 30 years.[3] (Johanna Lehne & Felix Preston, 2018). With the current state of regulations, it might take years before innovative methods reach the market.

5.1.3 Scope: Simplicity over complexity

Currently, the shape of the slabs is dictated by the cost of formwork. Slabs optimized for a reduction of material come at a very high cost by the increased complexity of the formwork. One of the primary reasons is the one-time use of the formwork (Anton, Jipa, Reiter, & Dillenburger, 2020); another reason is not taking into account the fabrication constraints in the optimization process. This is also the case for existing systems optimized for floor slabs.

[1] In the case of highrise optimization with lightweight structures, too much of a reduction in weight results in tensile forces in the foundation, due to lateral loading, which is problematic for foundation design and results in an increase in steel.

[2] This does not exclude the use of additive manufacturing in a hybrid application, similar to the future tree (Chapter 4.2.6).

[3] From 2016 to 2036, the expected building floorarea worldwide is expected to double from 235 billion m^2 to 470 billion m^2.

Existing slabs that aim to reduce the building material often require complex formwork solutions, multiple digital fabrication, and concrete processes. Examples are the Smart Slab and the functionally integrated funicular slab, both fabricated by the ETH (Anton et al., 2020). The Smart Slab is a great example of applying complex solutions.

Figure 53 – The fabrication process of the Smart Slab. Source: (Meibodi et al., 2018)

The optimized floor slab shown in Figure 53 ended up with a final material reduction of 70% (Meibodi et al., 2018) and is often cited as the example of the potential for digital fabrication to create more sustainable structures. But is this actually true?

The fabrication of the Smart Slab started with the binder jetting of the formwork. The surface of the formwork was infiltrated with polyester resin, which was followed up by a release agent. This allowed for the application of fiber-reinforced shotcrete (Figure 54). After this, laser-cut plywood panels were used to cast the concrete for the beams (Figure 54). When the plywood formwork was in place, fused deposit modeling was required to create the guides for the post-tensioning system. This allowed for the casting process inside the formwork on top of the shotcrete layer.

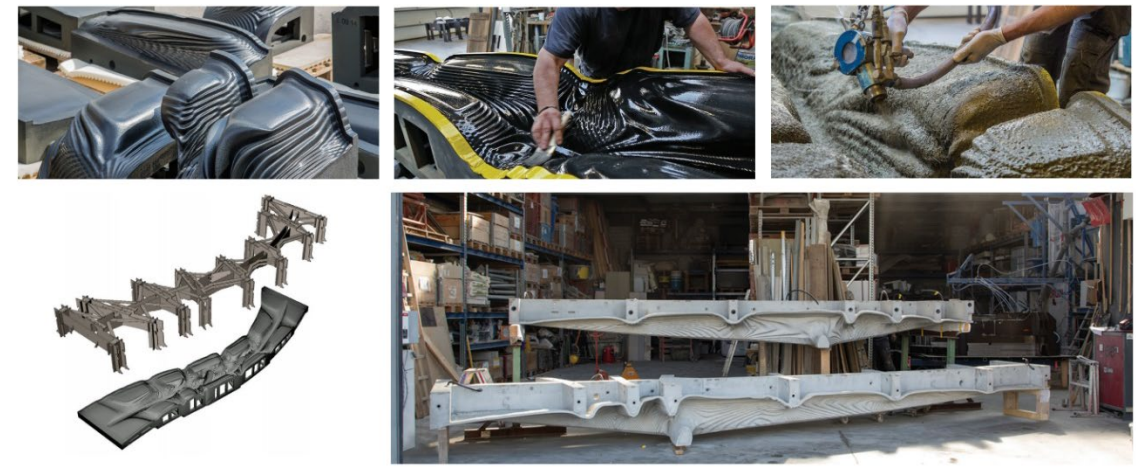

Figure 54 - Different stages of the fabrication process of the Smart Slab. Source: (Meibodi et al., 2018)

Regarding the fabrication procedure, a question that arises is if the 70% material reduction makes up for the extensive fabrication process (e.g., epoxy resulting in unrecyclable formwork, the clinker content required by shotcrete, the single-use laser-cut formwork, etc.). Hybrid digital fabrication techniques may have advantages and disadvantages, but digital fabrication cannot be categorized as a sustainable or cost-effective production technique in its current form.

For now, digital fabrication needs to include concurrent optimization for design, material, and construction constraints resulting in a repeatable and straightforward fabrication process, if it is to be applied in the construction sector.

5.1.4 Scope: Prefabrication and modularization

Conventional on-site construction is described as labor-intensive, wasteful, and inefficient (Mao, Shen, Shen, & Tang, 2013). In turn, prefabrication and modularization have emerged as promising construction methods that address traditional construction challenges (Mao et al., 2016). Prefabrication and modularization are associated with: a reduction in cost and labor cost compared to conventional construction (Jaillon & Poon, 2009); a reduction in necessary formwork by reusability (Tam, Tam, & Ng, 2007); a reduction in general construction waste (Lu & Yuan, 2013); an increase in productivity and safety (Pan, Gibb, & Dainty, 2012); and a reduction in environmental emissions (López-Mesa, Pitarch, Tomás, & Gallego, 2009).

The advantages make prefabrication and modularization key strategies in moving the building sector forward. What is often not described is the additional sustainability benefits that prefabrication could bring to the table. Here, two aspects are noteworthy:

- Carbon sequestration in the curing process[1]
  Tam et al. (2020) studied the potential of utilizing different technologies to reduce the environmental impact of concrete, with a focus on recycled aggregates. They found two primary methodologies effective in the sequestration of CO_2 in concrete-based products – carbon-curing and carbon conditioning. Carbon-curing is particularly interesting within the scope of this thesis because it involves sequestering CO_2 into new concrete's cement paste. In the process of carbon-curing, carbon dioxide (CO_2) becomes chemically converted into a mineral.

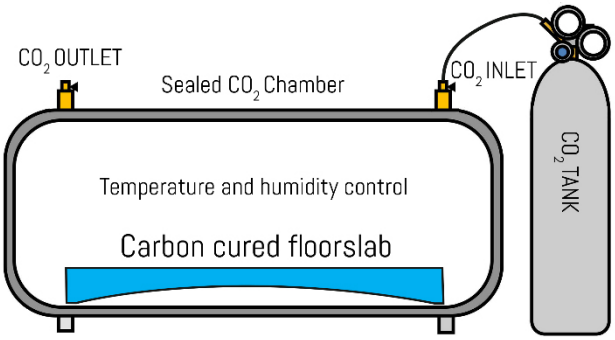

Figure 55 - proposed curing method for the floor slab based on (Tam, Butera, Le, & Li, 2020)

  CO_2 mineralization in a structure reduces the carbon emissions of the concrete by 6.0% in in-situ application. In temperature and humidity-controlled environments, the effectivity of carbon curing results in a further reduction of 12.3 to 30.7% (Seo et al., 2018). This reduction provides a good argument for prefabrication to reduce the environmental impact of the building sector further. Figure 55 shows the proposed curing method of the floor slab, whereby the CO_2 can be upcycled from the clinker process of the binder.

- Strength development of sustainable concretes
  For in-situ fabrication, the construction speed defines the type of cement. Often the selection of the concrete mixture is not based on the final strength but on the two-day strength, as this allows for faster in-situ construction and reduces associated labor costs. Prefabrication and modularisation allow for a decoupling of curing speed from fabrication speed and is in general, associated with faster rates of construction (Pan et al., 2012).

  Additionally, with prefabrication, the process is no longer guided by the early strength development of concrete, thus allowing for more sustainable cement. As noted in the literature study of this thesis, one of the key measures that can be carried out to reduce the carbon footprint is to replace ordinary Portland cement by alternative binders. Novel cement types usually result in a lower initial strength, but a longer strength development. Figure 56 shows the strength development of different types of cement; the percentage behind the cement type shows the amount of ordinary Portland clinker (Wijte, 2019).

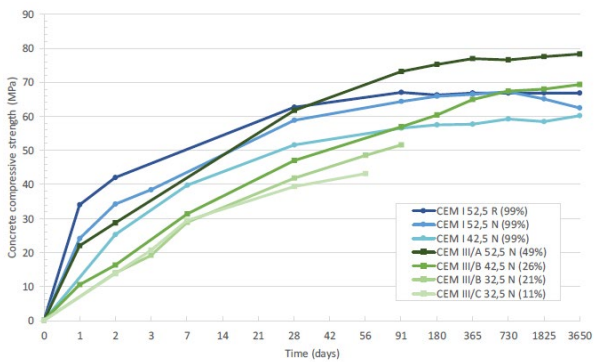

Figure 56 - Strength development of different types of cement. Source: (Wijte, 2019)

  Notice the difference in strength development of CEMIII/B and CEMI 52.5. CEMIII/B has a significantly slower strength development, but the strength development continues for a longer period, resulting in a final strength similar to CEMI 52.5, but with a reduced clinker content of 74%.

[1] While outside of the scope of this thesis, it is interesting to note that Jacobsen and Jahren (2002) estimated that 16% of CO_2 emissions in cement production are reabsorbed by concrete due to carbonation during its life cycle(Jacobsen & Jahren, 2002).

5.1.5 Scope: Life cycle assessment analysis: Product stage A1–A3

The fabrication procedure of Smart Slab shows that a significant reduction in the material of the floor is not automatically equivalent to a reduction in environmental impact. Similarly, the girder from TU Ghent presented earlier resulted in 20% less concrete, but the paper did not state the cement content required to fabricate its intricate shape. Extrusion-based 3D concrete printing requires significantly higher amounts of Ordinary Portland Cement (Beersaerts et al., 2020); therefore, the environmental impact will be higher, even with less material.

In the optimization process, material optimization, together with a life cycle assessment method, is integrated to prevent wrong conclusions. Within concrete construction, the product stage A1–A3 (materials and processing) accounts for 60% to 80% of the environmental impact (Gervasio & Dimova, 2018). Additionally, the European Union aims to make all new buildings nearly zero-energy by 2020 (Recast, 2010). This means that as the operational energy of buildings is reduced, materials and embodied energy become increasingly important. More information about the LCA analysis can be found in Chapter 6.6.

5.1.6 Scope: Conforms to building regulations

The floor slab has to conform to current building regulations to address the environmental impact of concrete. Dutch building regulations for concrete construction are the basis here for the optimization of the floor slab. The material selection will be in accordance with NEN-EN 13670, the Dutch interpretation of the current European standard of manufacturing with concrete, and NEN-EN 206 + NEN 8005. NEN-EN 206 + NEN 8005 describes the specifications, performance, production, and conformity of concrete. Likewise, the loading is defined in accordance with NEN-EN 1991-1-1+C1+C11:2019/NB:2019, with a primary focus on office buildings aimed at future adaptability as they require a higher load case than residential buildings. The partial safety factors are based on NEN-EN 1990+A1+A1/C2:2019.

5.2 The hypothesis

The primary goal of the research hypothesis is to address the primary research question: *In what manner can we use structural optimization and additive manufacturing in the building sector to address the environmental impact of concrete construction?* The literature research in this thesis shows that a gap exists between the integration of mixed design of mortars in the optimization process and the fabrication-related material constraints. This is important because the materials have a high impact on the environmental footprint of the product. This resulted in the formulation of the following hypothesis:

> Fabrication-aware, structurally optimized floor slabs, can significantly reduce the environmental impact of concrete construction.

This hypothesis is the driving force of the research-through-design process in this thesis. The primary emphasis is on casting of the floor slab, focusing on simplicity over complexity, prefabrication and modularization, and a life-cycle-assessment of product stage A1–A3, all of which conforms to the current building regulations. Hence, the optimized floor slab should not only be structurally efficient but also constructed using materials with a low environmental impact, compatible with economical construction, and can be designed and built using a methodology that is repeatable and robust.

5.2.1 Verification of the hypothesis

The new designed floor system developed in this thesis will be compared in a hypothetical office building to validate the result. This fabrication-aware, structurally optimized floor slab will be compared initially to two conventional flooring systems: lattice girder floor slabs and hollow-core slabs. Later, the floor slab will be compared to 10 additional conventional flooring systems.

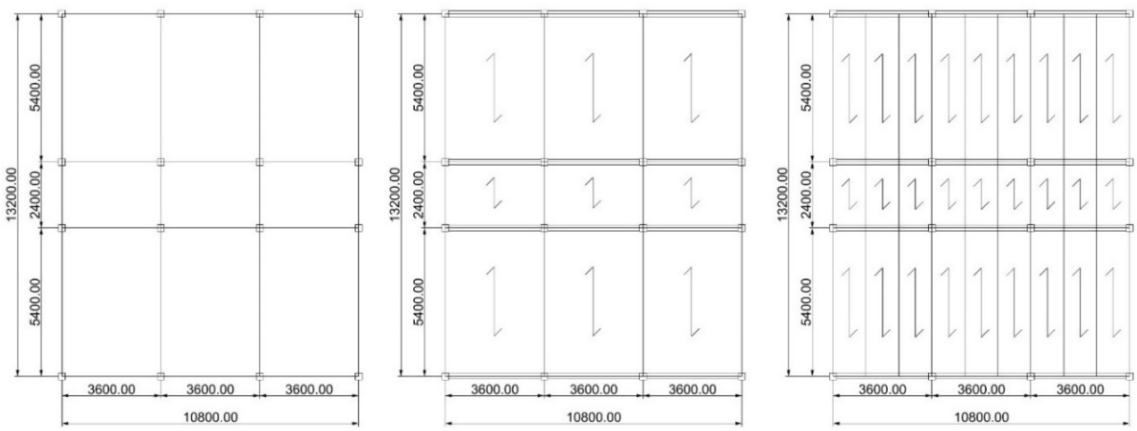

Figure 57 - Floorplan of three hypothetical office building: left, the new designed floor system proposed in this thesis; center, lattice girder floor system; righ,: hollow-core slabs.

5.3 Proposed method: Creating a floor slab inspired by thin shells

Today, the entire construction industry is facing a large challenge by being responsible for a significant part of global emissions, resources, energy consumption, and waste. Before going into the optimization process of floor-slabs, it is interesting to note the impact:

- Concrete is responsible for around 8% of the worldwide environmental emissions (Andrew, 2019)
- 50% of the concrete is used in the building sector (Favier et al., 2018)
- 59% of the concrete in building engineering is used in flooring [1] (Wight & MacGregor, 2009)

This makes concrete floors responsible for around 2.39% of worldwide environmental emissions. To put this number into perspective, the Netherlands accounts for 0.42% and Germany 1.99% of global emissions, while international aviation emits only 1.49% [2] (Crippa et al., 2019).

A thin shell-based flooring system

The most common floor type is the reinforced concrete flat slab. This is due to its low structural depth, architectural flexibility, and simple formwork requirements. The average stress in concrete in a regular reinforced concrete slab is 2.5 Mpa (Hawkins, 2019). This is far under the design strength of concrete. Thus, existing floor slabs are far from optimal.

Several measures have already been taken to increase the efficiency of floor slabs. The introduction of column heads resulted in a 19.5% reduction in embodied emissions (Griffin, Reed, Hsu, & Cruz, 2010). The introduction of beam-slab systems produced a reduction of 30% (Miller, Doh, & Mulvey, 2015), while post-tensioning, on average, 34.9% (Miller et al., 2013). While these measures are already an effective way to reduce the energy of floor slabs, a different approach might be more effective, as evidenced by the Smart Slab.

All existing floor systems use bending to resist loads. The solution proposed in this thesis is to create a floor slab inspired by thin shells, which will resist loads using membrane action and result in significantly greater carrying capacity primarily by using axial forces (S. Taylor, Rankin, & Cleland, 2001). Additionally, such a floor slab minimizes tensile stresses within the structure and takes full advantage of the properties of concrete. The comparison between existing floor slabs and the proposed flooring system is shown in Figure 58.

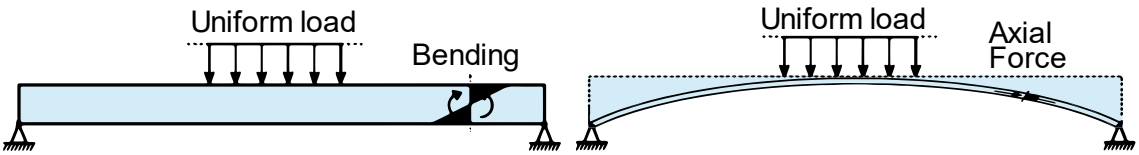

Figure 58 – Left, Current flooring systems, which primarily act in bending, resulting in stress concentration in the structure. Right, in a thin shell-based flooring system, membrane action results in a significant increase in load carrying capacity.

The concept of thin shell-based flooring is inspired by the work of Heinz Isler, Carlos Guastavino, and the block research group (Figure 59), who are primarily known for structures that derive strength through their geometry. The rest of this chapter will focus on the principles of the optimization process. It starts with the theory behind thin shells, followed up by aspects that lead to potential failure, the parametric approach, and the design considerations.

Figure 59 Inspiration for this Masters thesis. From left to right: Heinz Isler – Heimberg Tennis Center; Carlos Guastavino – structural test of the thin-shell tile vault; Block research group – Integrated funicular floor

[1] The 59% excludes the percentage that could be saved in the foundation by reducing the weight of buildings, even more for multi-story buildings. Georgopoulos & Minson (2014) estimate that 85% of concrete is used in the construction of flooring. (Georgopoulos & Minson, 2014)

[2] Due to availability of data, the comparison is made for CO_2 emissions.

5.3.1 Background information: The theory of shells

The word shell is a generalization of non-planar isotropic homogeneous plates. In the case of plates, out-of-plane loads generate moments and transverse shear forces. Instead, a shell can carry out-of-plane loads by in-plane membrane forces due to its curvature. The ability to carry out-of-plane loads by in-plane membrane forces are the primary reason why shells are strong and economic structures (Blaauwendraad & Hoefakker, 2013).

Shells are described by their local coordinate system, whereby the z-direction is perpendicular to the normal plane, while x and y are defined by the tangents to this point. The curvature of a shell is described by Gaussian curvature, which is the the product of the reciprocal of the radius in the x and y plane. The product can have positive, zero, or negative curvature, thereby defining the form of the shell (Figure 59).

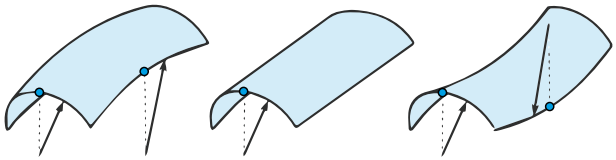

Figure 60 - Types of Gaussian curvature: left, positive Gaussian curvature; center, zero Gaussian curvature; right, negative Gaussian curvature. Adapted from: (Blaauwendraad & Hoefakker, 2013)

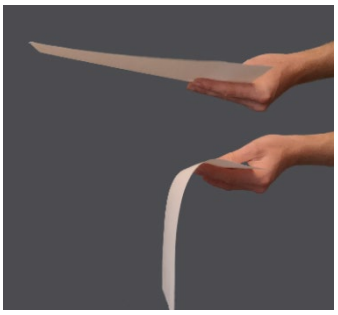

Figure 61 - Bending a sheet of paper is a good example of the influence on the stiffness of an increased Gaussian curvature. Optimizing the shape by bending it allows for membrane action to carry the gravitational force.

The Gaussian curvature has structural significance. Forms with a positive or negative Gaussian curve require more external energy to be deformed, as they allow for out-of-plane loads to be carried by in-plane membrane forces. Thus, buckling stability is gained by an increase in shell curvature. An excellent example of this is shown in Figure 61, whereby an increase in Gaussian curvature results in a stiffer structure, This is particularly interesting as one of the primary failure modes of thin-walled structures is buckling.

As you can imagine, it is difficult to calculate the exact behavior of shells. Many theories have been developed to accurately predict mechanical behaviour. The best known is the membrane theory, which assumes that only in-plane membrane forces are present. As multiple load cases dictate the design of a floor slab, it is likely that the floor will not only act by axial forces. Therefore, a theory is required that will take both membrane and bending action into account. One of the possible theories that does this is the Donnell theory, in which the expression for a change in curvature due to bending moments from the theory of flat plates is borrowed. This theory only works for small curvatures.

Figure 62 shows the forces that act on a point in the shell where bending and axial forces occur. For the optimization of the floor slab, it is desirable to minimize the moment and shear forces as they will most likely result in failure of the structure due to the limited tensile capacities of concrete. Therefore, the structure will be optimized to work by membrane forces. The structure will exhibit mostly positive Gaussian curvature because gravitational force results in axial compression when the Gaussian curvature is positive. An example of a structure using positive Gaussian curvature to minimize the effect of moment and shear forces is *"Parapluie"* (Figure 63).

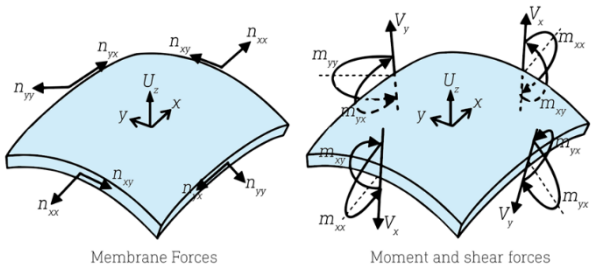

Figure 62 - Forces and moments on a shell element of arbitrary curvature. For optimizing structures, the structure should act primarily in membrane forces. Adapted from: (Blaauwendraad & Hoefakker, 2013)

Even though the material thickness compared to its span is very small, a Gaussian structure can carry its self-weight and extra loading through efficient use of membrane action (Eisenbach, 2017). The question is how we find these structures using mostly membrane action. With continuum structures, the theory of shells is based on three sets of equations – the kinematic, constitutive, and equilibrium equations (Figure 64). Multiple load cases and complex surfaces will not lead to simple analytical solutions. Instead, both the analysis for the membrane theory and bending theory are evaluated using finite element analysis. Here, the focus is on design-specific aspects and the points that require extra attention for thin-shell design. For more theory on shells, I refer to the book *Structural Shell Analysis: Understanding and Application'* (Blaauwendraad & Hoefakker, 2013).

Figure 64 Test loading of the installed Parapluie prototype as verification of feasibility. Source: (Eisenbach, 2017)

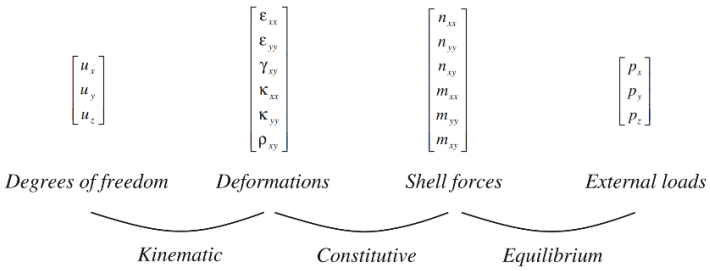

Figure 63 Scheme of relations within structural mechanics. Source: (Blaauwendraad & Hoefakker, 2013)

5.4 Boundary conditions

As floor slabs are guided multiple load cases, analytical approaches to calculate the shells are difficult. As stated earlier, the analysis and optimization will be done here applying an integrated parametric model using finite element analysis. This will be further described in Chapter 5.3.5. The subsection here starts by stating the primary focus of the research:

- This research focuses on the integration of the construction material in the optimization of rectangular floor slabs. The focus is on a standard office floorplan in two spans of 2400 mm x 3600 mm and 5400 mm x 3600 mm, respectively. This floor slab will be evaluated based on an LCA analysis and compared to conventional flooring systems.

- The primary focus is on the aspects of structural design, optimization, and analysis. The construction methods and detailing of the corners will be elaborated on shortly, for firesafety proposes. (chapter 5.4.3)

- The structural design is based on the Eurocode. For the design and calculations of the structure, the loading, and the material requirements the Dutch national annex is applied.

- The environmental impact analysis will limit itself to the product stage (cradle-to-gate), since most of the energy consumption of floor slab systems comes from the product stage, and this percentage is set to increase with the aim of the European Union to make all new buildings nearly zero-energy by 2020 (Recast, 2010).

- The structural optimization will focus on linear analysis to calculate the stresses and displacements. If resulting displacements are within the margin of the serviceability limit state, a linear analysis will likely predict the correct behavior of the shell. A recent study by (Hawkins, 2019) showed that a linear approach was conservative, compared to structural testing.

When looking at structural performance, the design will be analysed according to the Eurocode. This results in two different limit states regarding the structural performance of the floor slab:

- *Ultimate Limit State (ULS)*:
  the state where the structure is at the limit of failure

- *Serviceability Limit State (SLS)*:
  the state where the structure is at the limit of not satisfying the requirements for normal use

The primary focus in this thesis is on the design within the Dutch standards. This means that the risk of exceeding any possible ultimate limit state is satisfactory low. Hence, the compressive strength, tensile strength, and modulus of elasticity of the material are guiding. Time-dependent stress-strain behavior is not considered. Several points require extra attention when designing for thin shells using membrane action:

- *Concentrated loads*
  Shell structures are highly efficient due to three-dimensional in-plane resistance to external forces, thereby resulting in little to no bending. A consequence of this is that the structure is relatively thin, therefore making it vulnerable to concentrated loads (Figure 64). Concentrated loads will likely result in bending moments, as a product of the thrust line being eccentric from the neutral axis. Therefore, minimal shell thickness is one of the design constraints throughout the optimization process.

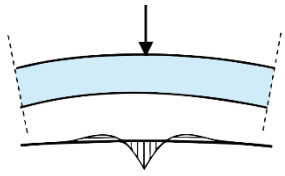

Figure 65 Tensile stresses as a result of a concentrated load on thin-walled structures.

- *Support conditions*
  The membrane working of a shell is highly dependent on the support conditions. Fixed boundary conditions are incompatible with the requirements of pure membrane action. Therefore, the shell edge should be thick enough to withstand the possibility of a bending moment at the edges. Moreover, to prevent the likelihood of localized edge effects, thickening the edge or smart design of the corner is required. Otherwise, tensile stresses will result in the failure of thin shell structures of concrete (Figure 65).

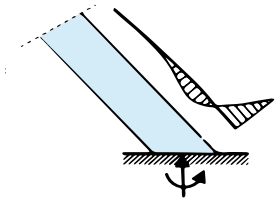

Figure 66 Localized edge effects might result in failure in thin shells.

- *Buckling behavior*
  In general, it can be said that Gaussian curvature results in extra buckling resistance. Nevertheless, the optimized shell might become thin, making it susceptible to buckling. Therefore, buckling behavior is one of the main design criteria for thin shells. The effective thickness of the shell needs to be optimized, and throughout the design process, buckling behavior should be evaluated. Three types of shell buckling should be considered: symmetrical bucking, asymmetrical bucking, and snap-through buckling.

5.4.1 Designing a fabrication-aware, structurally optimized flooring system.

The aim of this thesis is to create a floor slab that derives its strength through its geometry, carrying forces primarily through axial compression (Figure 70). It aims to decouple tensile and compression forces, which is illustrated here with steel in tension (blue) and concrete in compression (black) (Figure 71). This aims to take advantage of the material-specific advantages of concrete.

The proposed floor slab is supported at four corner points, which consists of steel "shoes" to prevent localized edge effects, and failure due to punching shear. (chapter 5.4.4) The shoes are connected by steel tension ties to absorb the horizontal trust generated by the shell. Figure 68 shows a plan view and Figure 69 an isometric view of the proposed flooring system.

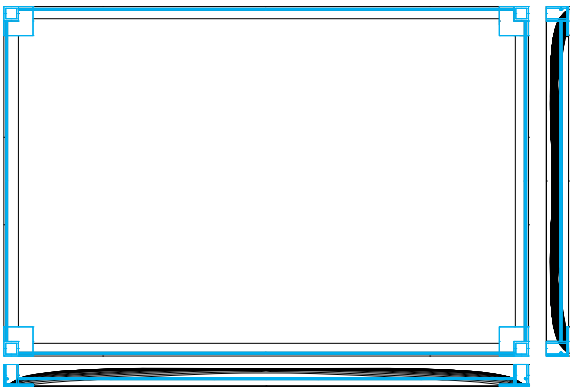

Figure 67 Plan view of the proposed floor system. The aim is to decouple tensile and compression forces. The black lines represent the concrete shell, the steel tension ties, while "shoes" are shown in blue. Notice the steel corners to prevent localized edge effects

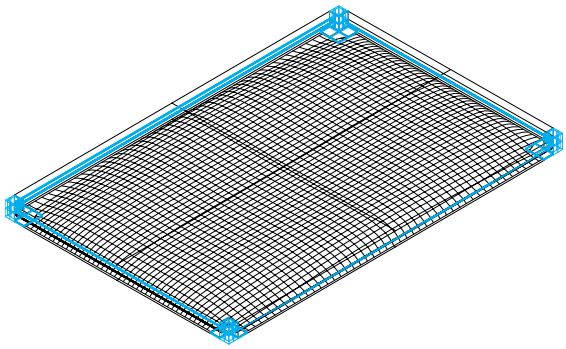

Figure 69 Isometric view of the proposed flooring system. As before, the aim is to decouple tensile and compression forces. The black lines represent the concrete shell, the steel tension ties, while "shoes" are shown in blue.

The floor itself consists of a concrete shell with a positive Gaussian curvature that allows for membrane action resulting in axial compression forces (Figure 70). Incidental point loads might result in bending forces. Therefore, the shell will exhibit variable thickness, becoming thicker at the edges. The self-weight of the material minimizes bending by bending the trust line towards the support points. Additionally, this will offer extra stiffness if required, and limits the risk of high stresses due to localized edge effects. (Figure 71)

This research focuses on a standardized office floorplan resulting in spans of 2400 mm x 3600 mm and 5400 mm x 3600 mm. This floor slab will be evaluated with an LCA analysis and compared to conventional flooring systems in Section III. The optimization process happens through a parametric approach in combination with finite element analysis. The integration of material optimization for sustainability, the fabrication constraints, and a life cycle analysis of the product stage (A1–A3) are guiding.

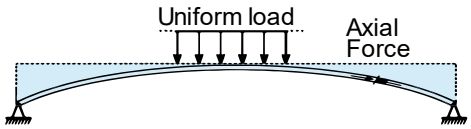

Figure 68 Transferring load through axial force

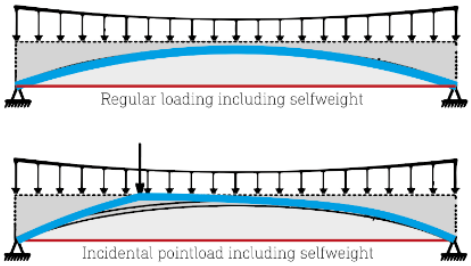

Figure 70 The increased self-weight at the edges due to an increased thickness, which helps bending the trust line towards the support point, both for the Q-load and incidental point loads

5.4.2 Externalized steel tension cords

The floor falls under the safety class CC2, resulting in 60 minutes required fire safety. To comply with the fire safety requirements, reinforcement steel needs a concrete coverage layer of 20mm. In initial design studies, this was integrated into the optimization process. This initial design with integrated reinforcement already resulted in a significant reduction of mass. However, since groin-vault systems are known for strong structural performance across deflection, vibration, and buckling (Hawkins, 2019), externalizing the steel tension members appears to be overall more advantageous. Due to the groin-vault system's shape, the use of this system does inherently not allow for the encasement of reinforcement steel; however, the newly won space enables the integration of building installations. Moreover, decoupling materials generally allows easier end-of-life recyclability and a longer lifespan of the structure. The firesafety approach is further described in chapter 5.4.3

Additionally, externalizing steel has several other significant advantages when it comes to the environmental impact of concrete construction. With traditional reinforced concrete, a higher clinker percentage is required to prevent the steel from corroding by mitigating the decline in pH level through the "alkaline reserve" in the concrete. This buffering capacity of the "alkaline reserve" plays a pivotal role in the long-term durability reinforced concrete. (Andrade, 2019) Additionally, by externalizing the steel, no passivation of the reinforcement is required, which allows for concrete with lower clinker percentage, which, in turn, significantly lowers the environmental footprint (Valeri et al., 2020). When looking at the Dutch building code it allows for a reduction of clinker content from 260kg to 200kg, which then translates to a 15% to 20% reduction of the environmental impact of the total structure.

5.4.3 Fire safety

According to EN 1993-1-2:2005 Eurocode 3, structural steel retains about 50% of its ambient temperature strength at temperatures of 500-600 °C. By externalizing the steel from the concrete, other fire safety measures than concrete encasement have to be found. This chapter gives an overview of the potential approaches to the fire safety for the externalized steel, with a primary focus on the integration of thermal barriers in the design. Traditionally, there is a range of commercially available options that encapsulate steel structures, such as calcium silicate, gypsum plaster board, cementitious spray-on systems or fire blankets. (Lucherini & Maluk, 2019) But these conventional measures are often described as aesthetically unpleasant and therefore are not the most desirable choice for structures with visible steel. (Challener, 2007) This resulted in intumescent coatings to be the mainstream solution to protect steel in load-bearing structures for fire, (Mariappan, 2016) including the fire proofing of steel tension rods. (Häßler, Häßler, Hothan, & Krüger, 2019) Figure 71 shows the fire safety concept of the steel shoe and the tension rods.

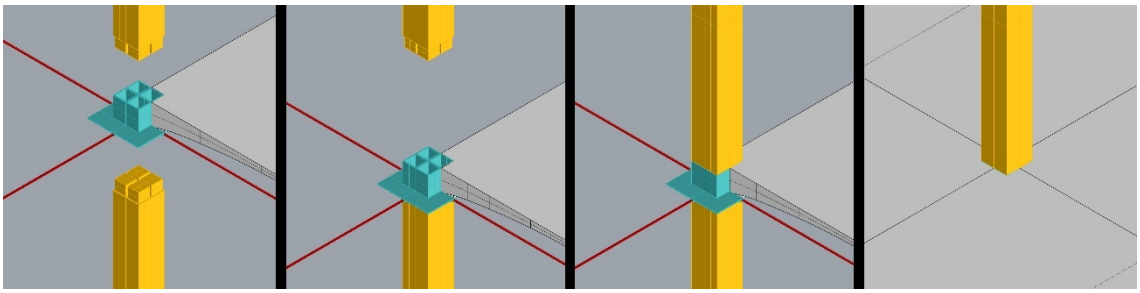

Figure 71 - proposed construction sequence of the floor, from the top perspective. Notice the full encasement of the steel shoe.

Here, the construction starts by placing the concrete floors and steel shoes, one by one, on the wooden column (for visibility reasons the other flooring systems are not shown). The next step is to place the upper columns on top which then results in a full coverage of the steel. Thereby, the fire safety is provided through the encasement of the steel shoe. Figure 72 shows the fire safety concept from the bottom perspective.

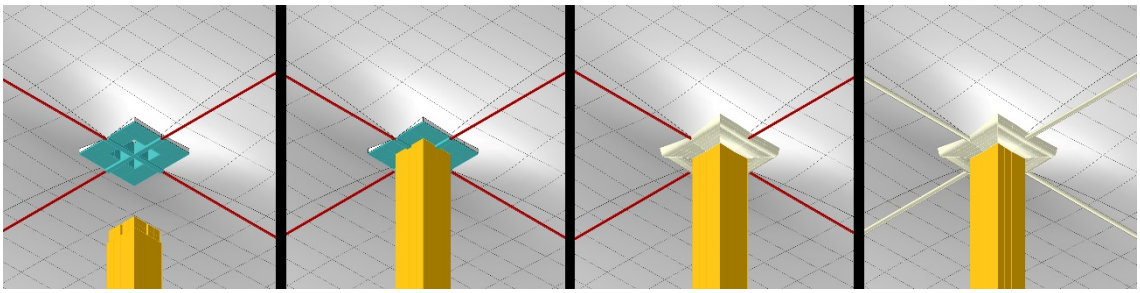

Figure 72 - proposed construction sequence of the floor, from the bottom perspective. Notice the steps on the right, fireproofing the steel.

Here, the example shows how fire safety can be achieved by covering the steel with low thermal conductive material and thereby reducing the temperature increase in the steel elements. (Buchanan & Abu, 2017) Additionally, a thin film of intumescent coating can be used if visible steel is the most desirable choice.

5.4.4 Punching shear

The proposed floor slab is supported at four corner points. For the design of flat slabs with similar supporting conditions, the column-slab connection is usually the decisive factor because of the concentration of shear stresses in this region, which, in turn, might lead to punching (figure 73). This is a undesired failure mode, as it results in brittle failure. Punching shear therefore is one of the critical failure mechanisms of flat slab flooring systems, and the exact behavior is complex and cannot be accurately approximated without taking into account non-linear effects (e.g. cracking, crushing and plasticity). Therefore, post-analysis checks should be carried out to ascertain that a shear failure mode is not overlooked. Punching shear failures can be reasonably predicted with a non-linear FEM approach of 3D solid models. (Amir, 2014)

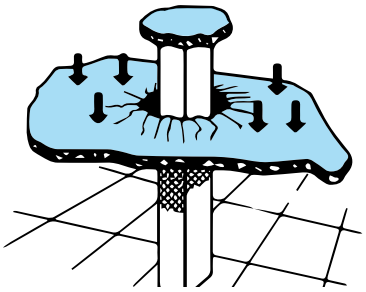

Figure 73 - Punching shear of a floor slab. Adapted from: Civilsnapshot.com

It should be noted that punching shear failure is not the expected failure mode of the proposed system, as systems which work on compressive membrane action lead to an increase in the bearing capacity of the slab and it fails at a load much higher than predicted by the standard yield line theory. (Amir, 2014) Additionally, it has been demonstrated in tests that membrane action leads to a significant increase in flexural and shear capacity. (Chana & Desai, 1992) An example of this is t structural investigation of the 1978 collapse of the Kimberley-Clark warehouse by Vecchio and Collins in 1990. In this study, the tested floor slabs were able to carry 4.5 times the design load (48kN/m^2). (Vecchio & Collins, 1990) They concluded that this was primarily due to the effects of the horizontal

restraint by neighboring slabs resulting in membrane action. In the proposed flooring system, the tension cords provide the horizontal restraint, therefore making punching shear failure at the column-floor connection unlikely.

It is important to note that currently no design codes make use of the beneficial effects of compressive membrane action. Eurocode 2 gives conservative results since it considers a very low contribution of the in plane forces. (Amir, van der Veen, Walraven, & de Boer, 2015) The reason that it is not integrated is the difficulty of assessing the boundary conditions and the lateral restraint in buildings, which is required in order for the membrane action to occur. The integration of the tension cords within the structural floor slab allows for clear boundary conditions for estimating the effects of the membrane action on the punching shear. This can be correctly modeled using non-linear finite element approaches. (Amir, 2014) It is important to realize that the E-modulus of the tension cord and the stiffness of the column are the decisive factors; relying on neighboring floor slabs for horizontal restraint is illogical since the failure of one slab might then result in the collapse of the whole building system.

Additionally, critical shear could occur at locations of highly concentrated point loads where the floor is the thinnest. Within the linear model, this did not show greater forces than 1.5 Mpa in the bottom layer. In an unreinforced concrete shell, shear due to concentrated loads and punching shear might be critical. To overcome this, textile reinforcement could be applied. Reinforcing the bottom layer would provide not only ductile failure modes (Tsangouri, Van Driessche, Livitsanos, & Aggelis, 2020), but also additional robustness by providing alternative load paths through local bending in the concrete shell.

5.4.5 Performance-driven computational design: Workflow

The optimization process is based on a performance-driven conceptual design. Firstly, the shell structure will be generated as an input for finite element analysis. Karamba3D (FEM software) is used to calculate the structural performance and further optimize the shell using size optimization. After this step, a rationalization step will carried out to optimize the shell for the fabrication constraints. The rationalized shell is used to generate objective values. Evaluation of the objective values is made with a model-based optimization script (Figure 74).

The primary goal of the performance-driven methods is to generate a tool that can be used by architects using familiar computer-aided design software (Rhinoceros3D) without background knowledge in structural optimization. The performance-driven method is implemented within the parametric modeling environment Grasshopper3D. Chapter 5.4.3 gives background information on the software used throughout the process, while Chapter 5.4.6 focuses on the input and output variables. More information on the optimization method can be found in Chapter

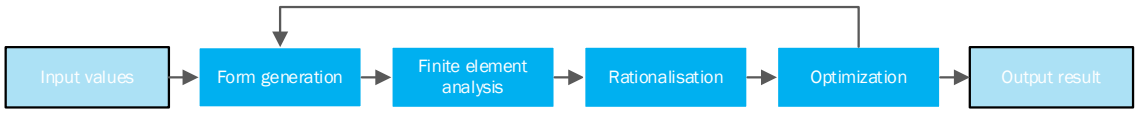

5.4.7. Afterwards, the optimization process itself will be documented, resulting in optimized floor slabs (Chapter 5.8).

Figure 74 Simplified flowchart of the optimization driven design process,

5.4.6 Performance-driven computational design: Software used

The optimization process for this thesis was primarily carried out using Rhinoceros3D, with the help of the visual programming environment Grasshopper3D. In total, five different software packages were used: (Figure 75)

- *Rhinoceros 6*
  Rhinoceros or Rhino3D is a computer-aided design (CAD) and 3D modeling application developed by Robert McNeel & Associates. (Rutten, 2015). Rhino3D allows for modeling based on NURBS (non-uniform rational B-splines) geometry, which allows for the precise mathematical presentation of forms (Piegl & Tiller, 2012). The strength of NURBS modeling is the accuracy of the mathematical description, thereby allowing for a repeatable and accurate process. This is especially significant when multiple optimization loops occur throughout the process.

- *Grasshopper3D*
  Grasshopper is an easy-to-use visual programming language and environment that runs within the Rhinoceros 3D computer-aided design (CAD) application. The program was created by David Rutten at Robert McNeel & Associates. (Rutten, 2015). Grasshopper is focused on the algorithmic design of objects. Its user-friendly interface facilitates an easy exploration of complex geometry by manipulating logic elements (Figure 43). Its primary strength is in the user community behind it and the wide variety of plug-ins available.

- *Kangaroo*
  Kangaroo is a live physics engine that gives the possibility to create particle-spring systems within the grasshopper environment. Kangaroo is a plug-in for Grasshopper developed in 2008 by Daniel Piker, a trained architect who works with the Specialist Modelling Group (SMG) at Foster + Partners (Piker, 2013). The particle-spring system is a dynamic equilibrium method to find funicular shells. This is particularly interesting within the scope of this thesis. More background information on computational form-finding can be found in literature study (Chapter 4.3.2.1).

- *Karamba3D*
  Karamba3D is a parametric finite element analysis plug-in embedded in the grasshopper environment, which was developed by Clemens Preisinger in cooperation with Bollinger und Grohmann ZT GmbH (Preisinger, 2015). Karamba3D provides accurate finite element analysis that allows for parametric structural engineering of shell structures.

- *Opposum*
  Opposum is a model-based optimization plug-in embedded in grasshopper, which was developed by T. Wortmann (Wortmann & Nannicini, 2016). Opposum integrates surrogate-model based optimization algorithms within a parametric environment. This is significant as they converge to optimal solutions quickly. More background information on black-box optimization algorithms, computational form-finding can be found in the literature study (Chapter 4.3.5).

- *Ansys Mechanical*
  Ansys Mechanical is a software suite that focuses on finite element analysis. In this Masters thesis, Ansys is used to verify the results from the grasshopper3D/rhino3D environment. The primary strength of Ansys is that it is freely available for students and allows for solid finite element analysis. Currently, there is no finite element analysis tool that works with solids in a Grasshopper environment.

The software and plug-ins selected for application and analysis in this Masters thesis are based on their wide use within the market, their ease of use, and their performance. Other approaches, such as volumetric modeling, together with iso-geometric analysis, have many potentials, but currently cannot be integrated easily within CAD environments.

Figure 75 Overview of the software used throughout the optimization process

5.4.7 Input parameters

Understanding the interdependence of the design geometry, material properties, and process characteristics is essential within the optimization process of a floor slab for the minimization of environmental impact. The focus is on the design of a repeatable process here instead of the design of a product is central to the integration of materials, environmental impact analysis, and the structural tests of the floor slab within the optimization process. The most important parameters that guide the optimization process are:

- *Geometry*
  The geometry parameters define the initial shape and space of the floor slab system. The parameter values consist of the minimal height of the floor slab, maximal height of the floor slab, and values for the span to be designed. The geometry values can be manually set by the user for the maximal and minimal height. Reference values can be found with a smaller mesh, which allows for a good indication of structural optimality and faster optimization process.

- *Cross-sectional properties*
  The cross-sections are defined by the sizing optimization process. The cross-sectional values that can be manually set are the minimal cross-sectional thickness and the step size. The reason for doing this manually is the influence it has on the required material properties, the acoustic performance, and the robustness of the flooring system. An excellent example of this is the aggregate size and content, which is guided by minimal feature thickness. Smaller aggregates result in higher water content which, in turn, results in more cement for the same strength.

- *Material properties*
  The material parameters are mostly calculated manually for this process. The material properties are primarily defined by the Dutch implementation of Eurocode and minimizing the cement content for environmental impact. The optimization script is written in a way that it can be updated easily, but for now, the regulations, with a maximum cement content of 260kg/m^3 CEMIII/B, form the guidelines followed throughout the process. More information about the calculations of the required materials according to Eurocode can be found in Chapter 5.5.

- *Boundary conditions*
  The parameters of the boundary conditions are largely defined by structural optimality of flat slabs. In an exploratory study, linear supports resulted in a significant bending moment in the support structure (Chapter 5.5.6). Elliptic paraboloid surfaces, on the other hand, allow for a stress concentration at the corners and minimal bending throughout the surface (Blaauwendraad & Hoefakker, 2013), resulting in an efficient structural system, as stress concentrates on the corner points.

- *Loading conditions*
  The Dutch implementation of Eurocode defines the parameters of the loading conditions. Interestingly, for flooring systems that do not act on bending, the concentrated load criteria become guiding, while in conventional flooring systems, the distributed Q-load is often guiding. More information about the set load cases can be found in Chapter 5.7.1.

- *Environmental impact analysis*
  The parameters of the environmental impact analysis are mainly manually calculated and focuses on the material related environmental emissions. More information about the integration of the environmental impact, analysis can be found in Chapter 5.6.

- *Finite element analysis*
  The parameters for the finite element analysis (FEM) need to be accurately set. Central to this is the definition of the mesh. The mesh largely defines the accuracy of the optimization solution and has a great influence on computation time. In some instances, a doubling of computing time improves accuracy by only 1%. As a rule of thumb, it can be said that for a two-dimensional shell element, the mesh should be 1 to 2 times the thickness of the structure.

The optimization script will result in multiple fabrication-aware optimized floor slabs if all input variables are set accurately. The optimized floor slabs, in turn, can be evaluated on other qualities not integrated within the optimization script. The geometry generation also allows for a verification of the structure in finite element or iso geometric analysis software packages.

Before going into depth on the optimization process, the material selection process for environmental impact, and the integration of the environmental impact will be discussed.

5.5 Integration of the material

The material selection within this thesis is in accordance with NEN-EN 13670 and EN-EN 206 + NEN 8005. The NEN-EN 13670 is the Dutch interpretation of the current European standard of manufacturing with concrete. NEN-EN 206 + NEN 8005 describes the specifications, performance, production, and conformity of concrete. The main aim of this chapter is to succinctly describe the selection process of the material.

The interdependencies between shape, manufacturing process and material need to be understood in order to reduce the environmental impact of a flooring system. If a design with less material results in a concrete mix that requires a higher amount of cement content, the final environmental impact might end up worse than the non-optimized version.

It is essential to integrate material related aspects. The necessary workability, design, and fabrication method influence the required properties of the material and hence, the environmental impact and the design.

It can be said that the design for environmental impact is a dialogue between manufacturing requirements and material properties. Considering the relationship between the fabrication process, the material, and the final shape in the optimization process results in the highest reduction in environmental impact.

From a material perspective, the environmental impact can be reduced by many factors which are described in the literature study. From a shape perspective, environmental impact can be reduced by:

- Optimizing the shape, resulting in a reduction of material
- Using higher-strength concrete, thereby further reducing the amount of material used
- Optimizing the shape based on workability requirements (e.g,. minimal thickness influences grain size which, in turn, influences the water content required)

To find the optimal relationship between shape and material, the process needs to be understood. The digital design to fabrication process starts with the selection process of materials and material-dependent variables, followed by the technical requirements for use and the resulting system boundaries. This chapter will conclude with the integration of the material and shape requirements needed in the optimization process.

5.5.1 Selection of concrete mixture

As described, the mix design is dependent on the rheology requirements which is, in turn, dependent on the manufacturing process and the final shape of the floor. The selection of material usually consists of four phases: choosing the required material properties, calculating the composition of the mixture, calculating the amount of required material, and verification of the results. This process is described in in table 3.

TABLE 3: METHOD OF ASSEMBLING CONCRETE MORTAR FOR THE OPTIMISATION OF A FLOORSLAB

PHASE	Description	Explanation
PHASE 1	Choosing the required properties	Define the technical properties of the concrete (according to NEN-EN 206): - Exposure class - Strength class - Consistency class - Mass
PHASE 2	Select cement and calculate the composition	1. Select fitting binder based on Phase 1 2. Determine the water cement factor (wcf/wbf) based on: - Target compressive cement strength - Environmental class concrete - Fabrication requirements (slumb/de-molding) 3. Select grading of aggregates, water requirements, cement type 4. Select excipients and additives (if necessary)
PHASE 3	Calculate the amount of required material	1. Determine the quantities of the materials used 2. Calculate the volume based on volumetric mass 3. Calculate the water content based on wcf/wbf
PHASE 4	Verification of the results	1. Verification of mixture (by a concrete technologist)

5.5.2 Phase 1: Choosing the material properties

Selection of the right material starts with the manufacturing requirements and the technical properties required of the end product. The technical properties described in Eurocode refer to three aspects: exposure class, strength class, and consistency class.

5.5.2.1 Exposure class

The exposure classes are described in NEN-EN 206. In this case, the exposure classes are related to different mechanisms of deterioration of concrete construction. These consist of corrosion induced by carbonation or chlorides, freeze/thaw attacks, and chemical attacks. The exposure classes have an impact on the minimum cement content, the maximal w-c ratio, the minimum grade of concrete, and the coverage of steel reinforcement.

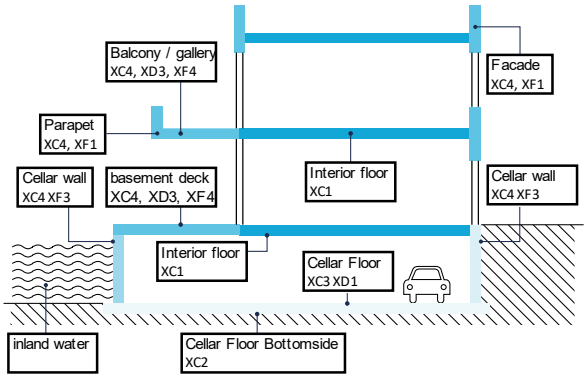

Figure 72 - Exposure classes in a building. Based on: (VOBN, 2013)

The exposure class is dependent upon the conditions in which the concrete is used and any potential special requirements for future use. For general reinforced buildings, the different classes based on their position in a building are illustrated in Figure 72 (for reinforced concrete).

The resulting exposure classes– with their minimum strength class, the minimum water to cement factor, and the minimum amount of cement – are shown in table 4.

TABLE 4: EXPOSURE CLASSES RELATED TO ENVIRONMENTAL CONDITIONS IN ACCORDANCE WITH EN 206-1

CLASS	Class	Description	Concrete strength class	w/c factor	Minimal cement content
	X0	No risk of corrosion or attack	C12/20	-	-
CARBONATION	XC1	Carbonation - Dry or permanently wet	C20/25	0.65	260
	XC2	Carbonation - Wet, rarely dry	C20/25	0.60	280
	XC3	Carbonation - Moderate humidity	C30/37	0.55	280
	XC4	Carbonation - Cyclic wet & dry	C30/37	0.5	300
CHLORIDES	XD1	Chlorides - Moderate humidity	C30/37	0.55	300
	XD2	Chlorides - Wet or rarely dry	C30/37	0.5	300
	XD3	Chlorides - Cyclic wet & dry	C35/45	0.45	300
SEAWATER	XS1	Sea water - Airborne salts	C30/37	0.5	300
	XS2	Sea water - Permanently submerged	C30/37	0.45	300
	XS3	Sea water - Tidal splash & spray zones	C35/45	0.45	320
FREEZE / THAW ATTACK	XF1	Freeze/thaw attack - Moderate water saturation without de-icing agent	C30/37	0.55	300
	XF2	Freeze/thaw attack - Moderate water saturation with de-icing agent	C30/37	0.55	300
	XF3	Freeze/thaw attack - High water saturation without de-icing agent	C30/37	0.45	300
	XF4	Freeze/thaw attack - High water saturation with de-icing agent or sea water	C30/37	0.5	320
CHEMICAL ATTACK	XA1	Chemical attack – Slightly aggressive	C30/37	0.55	300
	XA2	Chemical attack – Moderate aggressive	C30/37	0.5	320
	XA3	Chemical attack – Highly aggressive	C35/45	0.45	340

To maximize impact, this thesis will focus on the most common floor type, interior floors. This results in concrete with an XC1 class, as shown in Figure 72. Eurocode does not allow for the use of X0 in floor slabs. Without Eurocode-externalizing reinforcement, steel in flooring would make sense as this allows no risk for carbonation.[1]

[1] The carbonation process is associated with material shrinkage and corrosion of steel reinforcement. Carbonation increases both the tensile and compressive strength of concrete, but results in shrinkage. Externalizing steel will prevent cracking due to differential shrinkage. It also has a positive impact on recyclability.

5.5.2.2 Strength class

The strength class used is defined by the exposure class and the required structural properties of the material. Within NEN-EN1992, concrete classes are named after their cylindric and cubical compression strengths. The properties of different strength classes are shown in table 5.

TABLE 5: STRENGTH CLASSES OF CONCRETE IN ACCORDANCE WITH NEN-EN 1992-1-1

VALUE	Description	C16/20	C20/25	C25/30	C30/37	C35/45	C45/55	explanation
F_{CK} (MPA)	Cylinder compressive strength	16	20	25	30	35	45	5% fractile 28 days
$F_{CK,CUBE}$ (MPA)	Cube compressive strength	20	25	30	37	45	55	5% fractile 28 days
F_{CM} (MPA)	Mean compressive strength	24	28	33	38	43	53	$F_{cm} = f_{ck} + 8$ (MPa)
F_{CTM} (MPA)	Mean tensile strength	1,9	2,2	2,6	2,9	3,2	3,8	F_{ctm} (MPA) = $0.30 \cdot F_{ck}^{2/3}$
$F_{CTK,0,05}$ (MPA)	5th precentile tensile strength	1,3	1,5	1,8	2,0	2,2	2,7	$F_{ctk,0.05} = 0.7 \cdot F_{ctm}$
FCD (MPA) [1]	Design compressive strength	16	20	25	30	35	45	$EF_{cd} = \alpha_{cc} \cdot f_{ck} / \gamma_c$ EN1992-1-1 3.1.6(3)
F_{CTD} (MPA)[1]	Design tensile strength	1,3	1,5	1,8	2,0	2,2	2,7	$EF_{cd} = \alpha_{cc} \cdot f_{ck} / \gamma_c$ EN1992-1-1 3.1.6(3)
ECM (GPA) [2]	Modulus of elasticity	29	30	31	33	34	36	E_{cm} (GPa)= $22 \cdot (f_{cm} / 10 \text{ MPa})^{0.3}$

If the exposure class results in higher strength concrete due to the required water to cement ratio or minimal cement content per m^3, it might be best to optimize the floor for higher strength concrete, depending on the future use.

5.5.2.3 Consistency class and water content

The consistency class describes the properties of mortar during mixing, transporting, pouring, compacting, and finishing. Consistency class is described by three factors: compaction, slump, and flowability (Figure 76).

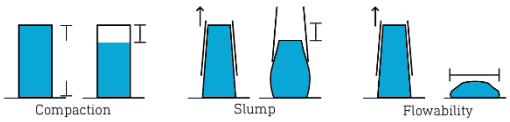

Figure 76 - Illustration of compaction, slump and flowability. Based on: (VOBN, 2013)

The water content and grain build-up are the defining factors when it comes to the workability (compaction, slump, and flowability) of the mixture.

Grain build-up influences the required amount of water content which, in turn, influences the cement content based on the water to cement ratio required.[3] In regard to grain build-up, in accordance to the Eurocode, the largest grain size shall not exceed:

- the free space between parallel tensioning channels
- 1/5 of the shortest distance between formwork walls
- 2/5 of the floor or pressure layer thickness for floors
- 3/4 of the smallest reinforcement bar spacing

TABLE 6: WATER CONTENT (KG/M³) BY CONSISTENCY CLASS AND MAXIMUM GRAIN SIZE

	Consistency	Compaction, slump and flowability	D_{max} 8mm	D_{max} 11mm	D_{max} 16mm	D_{max} 22mm	D_{max} 32mm
CONSISTENCY CLASS	Very stiff	C0	155	150	145	140	135
	Stiff	C1, S1, F1	170	165	155	150	145
	Half-plastic	C2, S2, F2	185	180	170	165	160
	plastic	C3, S3, F3	200	195	185	180	175

When constructing for sustainability, it is desirable to minimize water content. Table 6 shows the relationship between grain size, consistency class, and water content. These data do not show the help of plasticizers, which can further reduce the required water content by around 12%.

[1] f_{cd} is a function of the reduction coefficient a_{cc}. The appropriate value for a_{cc} for tension and compression is given in accordance with EN1992-1-1 §3.1.6(3). This is based on the use of FEA and the number of safety factors.

[2] This is according to EN1992-1-1 3.1.3 (2). The e-modulus varies depending on the aggregates used. Sandstone results in a reduction of 30% and limestone 10%, while basalt increases the e-modulus by 20%.

[3] This may result in a higher environmental impact

5.5.3 Phase 2: Calculate the composition of the mixture

The future use of the floor results in exposure class XC1, which is calculated using a maximal water-cement factor of 0.65, minimal 260kg/m^3 and a minimum strength class of C20/25. To meet the required target strength, a binder is needed; cement is the binder in concrete. Table 7 shows the different types of cement currently allowed in the Netherlands.

Table 7: Cement classes allowed in the Netherlands with strength coefficients for w/c factor formula.

Cement class	Description	α,	*b*	*c*
CEM I	Portland Cement	0,85	33	62
CEM II/A-S	Portland Slag Cement	-	-	-
CEM II/B-S	Portland Slag Cement	-	-	-
CEM II/A-V	Portland Fly-ash Cement	-	-	-
CEM II/B-T	Portland slate Cement	-	-	-
CEM III/A	Blast Furnace Cement	0,8	25	45
CEM III/B	Blast Furnace Cement	0,75	18	33

The calculations in this thesis are based on two types of cement, Ordinary Portland Cement (CEM I) and CEMIII/B, [1] selected for their environmental requirements and on their properties. CEM I result in high early strength, while CEMIII/B has excellent environmental properties.

5.5.3.1 Water–cement factor

For CEM I and CEMIII/B cement-based concrete, the water–cement factor is a good indicator of strength development. Based on the exposure class XC1, F_{ck} at 28-days should be higher than 20N/mm^2. The strength of concrete by the water-cement factor can be calculated with the following formula:

$$F_{CM} = \alpha N_n + \frac{b}{wcf} - c \qquad (1)$$

Herein is:

- F_{CM} = Mean compressive strength at N-days [N/mm^2]
- N_n = The standard strength of the cement used at N-days
- Wcf = Water–cement factor
- α, *b*, *c* = Coefficients based on the cement class

The calculation of the strength is based on an average concrete compressive strength F_{ccm} [N/mm^2]. The F_{cm} is calculated by adding a fixed value of 8 N/mm^2 to the characteristic cylindrical compressive strength F_{ck} [N/mm^2]. This is done in order to get to the 95th percentile of the strength.

$$F_{CM} = F_{CK} + 8 \qquad (1.1)$$

Herein is:

- F_{CM} = Mean compressive strength at N-days [N/mm^2]
- F_{CK} = Characteristic cylindrical compressive strength [N mm^2]

The resulting wcf based on the minimal required strength of C20/C25(XC1), with the cement types CEM I and CEM III/B [2] is:

- - CEMI (N-28 = 67 N/mm^2) = 0.86727 wcf (-)
- - CEMIII/B (N-28 = 48.85 N/mm^2) = 0.6828 wcf (-)

The maximum wcf for the durability class XC1 (0.65) is lower than the calculated value and, therefore, decisive. For the calculation of the concrete composition, the wtc is lowered by adding a safety margin of 0.02. This is done due to possible inaccuracies during the mixing and fabrication process. This results in a maximal wcf of 0.63.

[1] EMIII/B has the advantage that it has more than 20% clinker, which allows it for direct use according to the Dutch building codes. Besides this, it has a high amount of blast furnace slag which reduces the environmental impact of the concrete mixture.

5.5.3.2 Water requirements

The quantity of water required is determined based on the consistency class: half-plastic (C2, S2, F2) and the maximum grain size (D_{max} of 16mm[1]). A superplasticizer is used to increase workability and further reduce water content. There is the potential to further reduce the cement content by the use of a plasticizer. This results in the following effective water requirement.

Minimal water requirement half-plastic D_{max} 16mm	: 170 kg/m^3	(Table 6)
Reduction of water content with superplasticizer	: 12%	

- Effective water requirement M_{Water} : 170 * 0.88 = 149,6 kg/m^3

5.5.3.3 Cement content based on water requirements and wcf

To calculate the amount of cement content M_{cement} [kg/m^3], the wcf and the effective water requirement M_{Water} [kg/m^3] are:

$$M_{cement} = \frac{M_{water}}{wcf} \qquad (2)$$

The resulting cement content M_{cement} for XC1 with the cement types CEM I and CEM III/B [2] is:

- - CEMI = 172 kg/m^3
- - CEMIII/B = 219 kg/m^3

The minimum cement content for the durability class XC1 (260 kg/m^3) is higher than the calculated value and therefore decisive.

5.5.4 Phase 3: Calculation of the amount of materials required

Phase 3 consists of calculating the amount of materials required for the concrete mortar. The properties of the mixture are summarized below:

- Strength class = C20/25
- Exposure class = XC 1
- Consistency class = C2, S2, F2
- Maximal w/c factor = 0.65
- Design w/c factor = 0.63
- Minimal cement content = 260 kg/m^3
- Design cement strength = 260 kg/m^3
- Cement types used = CEM I and CEM III/B 42,5 N
- Aggregate size = 4/16 design area I
- Plasticizer (water reduction) = 12%g

The grain size, quantity of cement per m^3, and the required water content is given. An additional percentage of 2% air is used to calculate the additional volume of the mixture.

CEM I	260	kg	(density 3000 kg/m^3)	= 0.086 m^3
CEM III/B 42,5 N	260	kg	(density 2750 kg/m^3)	= 0.095 m^3
Water	149,6	kg	(density 1000 kg/m^3)	= 0.150 m^3
Air content	(2%)			= 0.020 m^3

- CEM I = 0.256 m^3 binder volume (cement paste)
- CEM III/B = 0,265 m^3 binder volume (cement paste)
- 4/16 mm agreggates = 0.744 m^3 binder volume (cement paste)
- 4/16 mm agreggates = 0.735 m^3 binder volume (cement paste)

In regard to the classification of concrete based on aggregates and their specific density, in normal concrete, aggregate weight ranges from 1,520 to 1,680 kg/m^3. Aggregates of 1600 kg/m^3 results in concrete weight of:

- CEM I Concrete = 1860 kg/m^3
- CEM III/B 42,5 *N* concrete = 1845.6 kg/m^3

based on 0.086 CEM I, 0.095 CEMIII/B, 0.150 water, and 0.744 (CEMI) or 0.735 (CEMIII/B) aggregates.

---

[1] 2/5 of the minimal floor thickness = 50 mm

Optimizing the aggregates used for minimal weight makes sense in floor slabs that work on bending, as self-weight is significant in floor construction. In funicular flooring systems, the weight helps to bend the trust line towards the support points, increases the membrane action, and reduces the amount of steel required and allows for less concrete required in the floor slab to meet the design loads.

5.5.5 Phase 4: Verification of the mixture

Phase 4 consists of the verification of the minimal cement binder content, The amount of fine material, the chloride content, and the alkali content of the mixture. The exposure class demands a cement content of higher than 260 kg/m^3, which is true for both the CEM I and the CEM III/B mixture. NEN 8005 also defines a minimal amount of fine material of 0,125 of the mixture for a maximum grain size of 16mm. Furthermore, NEN-EN206 defines a maximum chloride percentage of 0,4 for reinforced structures and a maximum alkali content of 3 kg.

The effects of the fine material, chloride percentage, and Akali content have a neglectable impact on the environmental impact and are therefore not further specified.

5.5.6 optimizing the material selection

Central within the optimization process is of material is meeting the design constraints and providing maximum strength. Usually, for in-situ fabrication, the early age strength of concrete is important, as slower curing of the concrete results in longer building times, which in turn is associated with higher costs.

When looking at optimizing for sustainability, the goals should be minimizing the amount of cement content within the mixture. For the optimization process of the floor slab, Eurocode is still guiding when it comes to the amount of cement content. Optimization for alternative cement types should be central, which has lower clinker content.

As the 260kg/m^3 is the minimum amount of cement required by Eurocode, it does not make sense to integrate a variable mixture within the optimization. A minimal feature thickness should be used to allow for 16mm aggregates combined with a process that allows for CEMIII/B cement. If quick demolding is required for fabrication in-situ optimization for minimizing stresses due to self-weight of the structure should be integrated. For now, the calculation above is guiding, resulting in 260kg/m^3 CEMIII/B with 16/4mm aggregates as a building material.

5.6 Environmental analysis

The general requirements for the sustainability assessment of buildings are described in the Eurocode: EN 15643-1, central within this is the Life Cycle Assessment (LCA). LCA was initially developed for the assessment of simple products or processes and later translated to the building scale. LCA is a tool used for the quantitative assessment of materials used, energy flows, and environmental impact. There are three main reasons why LCA studies are performed:

- check if a product complies with regulations
- evaluation method of the environmental impact of a design
- Compare the sustainability properties of/with existing products

Within this graduation, the LCA focusses on the comparison of existing products with a newly designed product, a floor slab. A complete LCA following ISO 14040 and 14044 is, for most projects, too time-consuming and expensive. The main difficulties for performing an LCA is obtaining complete environmental impact data for the elements and materials used. To make this easier, EN 15643-1 has categorized the processes of a product into modules: A1-A3 is the product stage, A4-A5 is the construction stage, B1-B7 is the use stage, C1-C4 is the end-of-life stage. (figure 77)

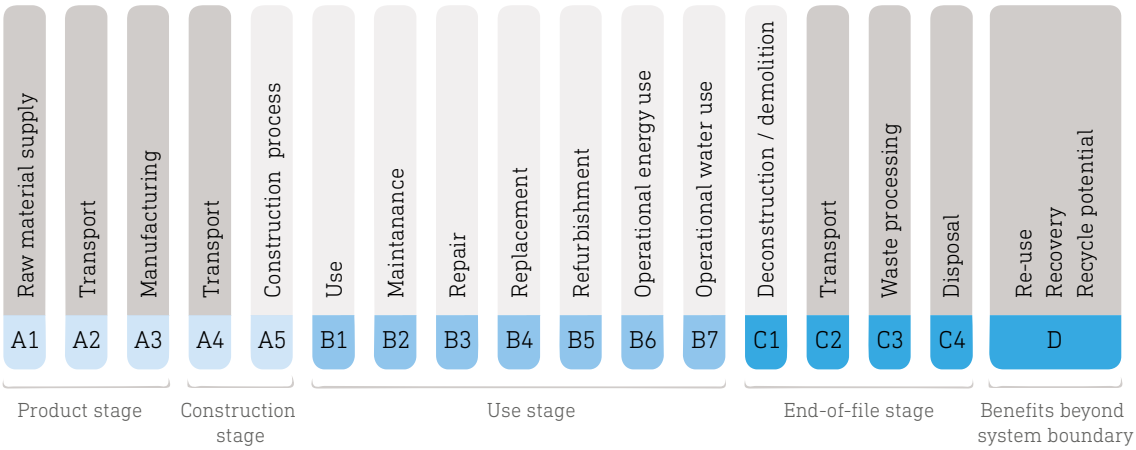

Figure 77 - figure illustrating the different environmental impact categories for a building, from the product stage to the benefits beyond the system boundaries

Considering all these stages for buildings within a complete LCA analysis shows the complexity of a full analysis. Within the framework of this master thesis, many challenges arise performing an LCA analysis:

- Floors exist in a broader framework (building), which consists of complex interdependent structures with many different materials, components, and products.
- The environmental impact of manufacturing, transportation, fabrication, and construction processes are location dependent.
- Quantitative data on the environmental impact of building products are limitedly available.
- The data is often limited to the production phase, as our current economy still works in a cradle-to-gate approach.
- A complete LCA analysis is extremely time-consuming and difficult to perform.

As stated above, a formal, classical, 'full' LCA in accordance with ISO 14040 and ISO 14044 requires much time (at least 2 – 3 months) is associated with high costs (Vogtlander, 2016). Due to its time consuming and costly character, LCA studies are often not used in the early design phase. Therefore 'Fast track' LCA studies were invented. FastTrack LCA is commonly used when there is no time to perform a full LCA, e.g., for comparing design alternatives. It uses the data produced by classical LCA studies as an input. In order to perform a FastTrack LCA, five steps must be taken, according to Voigtlander (2016):

- Define the scope and the goal of the analysis
- Define the system boundaries and functional unit (what do you want to measure?)
- Quantify the materials, energy used, in the system
- Calculate the environmental impact
- Interpret the results

There are concerns regarding FastTrack LCA as (1) The quality of the LCA is highly dependent on the underlying source data (classical LCA studies). (2) The availability of life cycle data of specific building products/materials (3). the comparability of the LCA data - as they are location specific – and there are more than 30 different methods: (e.g. AWARE, CML 1992, CML 2001, CML 2 baseline 2000, Eco-indicator 95/99, EDIP/UMIP 97, EPD (2008), ReCiPe, enz.) which are not all comparable.

5.6.1 Shadow cost and focus

Due to the number of LCA studies, a critical review is required regarding the underlying source data and the methods applied within the life cycle assessment. Regarding the availability of LCA data, there are different international databases (e.g., ELCD, USDA, Ecoinvent). For Dutch environmental impact assessments, the Nationale Milieu Database was created (NMD). It is based on CML evaluation. The NMD database will also be the one used within this graduation thesis.[1] For the environmental impact of different types of content, the main contributors will be further studied by analyzing the raw material compositions. When the environmental impact is clear, the shadow cost will be calculated. The shadow cast is a monetary value assigned to currently unknowable or difficult-to-calculate costs related to environmental emissions. This allows for an easier comparison of different environmental profiles.

The environmental profiles and background information of NMD are not publicly available but are accessible via the tools which are based on the database: such as GPR, MRPI Free tool, MPGCalc, One Click LCA, and DuboCalc. Within this graduation MPG, calc (1.21) by Consultancy agency DGMR is used. MPG calc contains all materials and systems that are included in the National Environmental Database (NMD). For the calculation of the environmental impact of the concrete mixture, the date from the National Environmental Database will be verified and compared with data from ENCI, a Dutch cement manufacturer.

As stated earlier, the product stage A1-A3 (materials and processing) accounts for 60% to 80% of the environmental emissions (H. Gervasio & S. Dimova, 2018). Additionally, the European Union aims to make all new buildings nearly zero-energy by 2020 (Recast, 2010). Therefore, the focus of this graduation thesis is on the product stage.[2]

It should be noted that the floor also limits the weight of the structure compared to conventional systems (transportation accounts for 10% to 20%) and that concrete structures, in general, have a positive influence on the energy consumption of buildings, as they provide thermal mass. Studies report a reduction of yearly energy consumption of 7% to 22% (Shafigh, Asadi, & Mahyuddin, 2018) Lastly, carbonation of concrete over its lifetime (100 years) correspondents with 18% to 21% of the CO_2 emissions of the product stage (K.-H. Yang, Seo, & Tae, 2014)

5.6.2 LCA impact categories

The environmental impact categories are defined by EN 15643-1. Table 8 summarizes the environmental impact categories and their associated shadow cost.

Table 8: LCA environmental impact categories according to EN 15643-1 (source: HTTPS://ECOCHAIN.COM/KNOWLEDGE/IMPACT-CATEGORIES-LCA/

	ABRR.	Environmental category	Units	Shadow cost	Description
1	GWP	Global Warming Potential	kg CO 2 eq.	0.057 €	Indicator of potential global warming due to emissions of greenhouse gases to the air
2	ODP	Ozon Depletion Potential	kg CFC-11 eq.	30.4 €	Indicator of emissions to air that destroys the stratospheric ozone layer
3	HTP	Human Toxicity Potential	kg 1,4-DCB eq.	0.21 €	Impact on humans of toxic substances emitted to the environment (Dutch version of EN15804 only)
4	FWAE	Fresh Water Aquatic Ecotoxicity	kg 1,4-DCB eq.	0.04 €	Impact on freshwater organisms of toxic substances emitted to the environment (Dutch version of EN15804 only)
5	MEA	Marine Aquatic Ecotoxicity	kg 1,4-DCB eq.	0.0074 €	Impact on seawater organisms of toxic substances emitted to the environment (Dutch version of EN15804 only)
6	TE	Terrestrial Ecotoxicity	kg 1,4-DCB eq.	8.69 €	Impact on land organisms of toxic substances emitted to the environment (Dutch version A of EN15804 only)
7	PO	Photochemical Oxidation	kg C 2 H 4 eq.	2.1 €	Indicator of emissions of gases that affect the creation of photochemical ozone in the lower atmosphere (smog) (catalyzed by sunlight)
8	AP	Acidification Potential	kg SO 2 eq.	5.4 €	Indicator of the potential acidification of soils and water due to the release of gases such as nitrogen oxides and sulfur oxides
9	EP	Eutrophication Potential	kg PO4 eq.	3.11 €	indicator of the enrichment of the aquatic ecosystem with nutritional elements, due to the emission of nitrogen or phosphor.
10	ADP	Abiotic Depletion Potential	kg Sb eq.	0.16 €	Indicator of the depletion of natural non-fossil resources

The categorization allows for a scientific approach to quantitively measure the environmental performance of a product or system over its life span. At the same time, the shadow cost results in a realization of the cost. And so more aware of the impact of a given a choice, both will be integrated within the optimization process. The rest of this Chapter will focus on the integration of fast track LCA studies in the optimization and evaluation process of the floor slab.

[1] One of the main reasons for going for the NMD as a primary source is the inclusion of 'VBI 150mm groen' hollow-core slabs. These are Hollow-core slabs optimized for a low environmental impact.

[2] Additionally the number of unknown variables increase by having a bigger scope for the LCA analysis, one of the key factors besides the emissions of concrete production in the product phase is the availability of data.

5.6.3 Intergration of materials within the optimization process

The LCA study takes the A1-A3 product stage into account. This is often referred to as the cradle-to-gate approach. It includes the emissions resulting from all the processes involved in the production of the material. The floor slabs will be evaluated based on the reduction in all 10 LCA environmental impact categories, A special focus will be on CO_2 reduction, and the reduction in shadow costs. The calculation of the shadow cost is primarily based on the *Environmental prices handbook 2017, methods, and numbers for valuation of environmental impacts.* (De Bruyn et al., 2018).

Table 9: LCA environmental impact of different materials.

	ABRR.		CEM I cement 260 kg	CEM III/B cement 260 kg	Reinforcement steel ecoinvent 3.4, 1000 kg	NMD 2.3 Concrete mortar C20/25 XC1 1000 kg	Betonhuis: Concrete mortar c20/25 XC1 1000 kg	Shadow cost per eq.
1	GWP	kg CO_2 eq.	228,02	68,64	1,358	66,30	94.50	0.057
2	ODP	kg CFC-11 eq.	0	0	0	$5{,}82*10^{-6}$	$4.55*10^{-6}$	30.4
3	HTP	Kg 1,4-DCB eq.	11,67	5,67	182	15,31	12.8	0.21
4	FWAE	kg 1,4-DCB eq.	0,367	0,13	3,20	0,34	0.299	0.04
5	MEA	kg 1,4-DCB eq.	262,60	138,06	22600,0	2112,79	2060.00	0.0074
6	TE	kg 1,4-DCB eq.	0,427	0,236	1,70	0,16	0.298	8.69
7	PO	kg C_2H_4 eq.	0,027	0,012	5,40	0,03	0.03	2.1
8	AP	kg SO_2 eq.	0,356	0,146	0.60	0,30	0.31	5.4
9	EP	kg PO_4 eq.	0,092	0,028	0	0,05	0.026	3.11
10	ADP	kg PO_4 eq.	0,434	0,192	8,60	0	0.36	0.16

The LCA data has the following sources.

- *CEM I cement 260 kg*
  The lifecycle assessment data is provided by ENCI, a Dutch cement manufacturer. Whereby the environmental emissions are based on an LCA analysis in accordance with the MRPI review scheme. [1]

- *CEM III/B cement 260 kg*
  The lifecycle assessment data is provided by ENCI, a Dutch cement manufacturer. Whereby the environmental emissions are based on an LCA analysis in accordance with the MRPI review scheme.[1]

- *Reinforcement steel 1000 kg*
  The environmental emissions of reinforcement steel is based on the NMD 2.3, accessed through MPGcalc v1.2. Code: 28.06.016. This data is based on ecoinvent.

- *Heavy construction steel 1000 kg*
  The environmental emissions of reinforcement steel is based on the NMD 2.3, accessed through MPGcalc v1.2. Code: 28.06.016. The data itself is provided by (Bouwen met staal).

- *NMD 2.3 Concrete mortar C20/25 XC1 1000 kg*
  The environmental emissions of the concrete mortar is based on the NMD 2.3, accessed through MPGcalc v1.2. Code: 28.06.00039 It consists of 280kg/m^3 CEMIII cement.

- Betonhuis: Concrete mortar C20/25 XC1 1000 kg
  This concrete mortar is calculated with the design tool "Groenbeton" realized by the CUR-commission 1759. The data is based on NMD, and it includes transport and waste treatment at the end of life of the concrete.[2]

When looking at Table 9 the impact of the cement is clearly visible. CEM I cement has almost 3.3 times the amount of CO_2 emissions than CEMIII/B. This shows the impact you can have when optimizing the process and the product to be built with more sustainable cement. Additionally it is interesting to see that the NMD 2.3 concrete mortar results in lower environmental emissions than the CEMIII/B cement manufactured by ENCI while using 20kg more CEMIII cement. Several reasons can be named for this difference, but for a clear evaluation or the reason for the difference, the data behind LCA studies should be evaluated, which is not publicly available.

[1] The data is provided by Peter de Vries, part of technical marketing at the HeidelbergCementGroup (ENCI)

[2] The calculation was done with the help of Martin Verweij, the innovation & development manager of cementbouw.

5.6.4 Integration of the LCA analysis.

Within grasshopper3D, a script is written to integrate the lifecycle assessment studies within the optimization process. Due to the regulatory requirements and the availability of LCA data, the integration happened on minimizing volumes of the concrete and steel required. Therefore the amount of steel required in the tension cords due to the tensile forces have to be calculated (Chapter 5.5.6).

The data used within the calculation of the environmental impact is primarily from the NMD 2.3. The concrete mixtures used are the NMD 2.3 and Betonhuis mixture calculated by cementbouw. For the steel reinforcement, the data of NMD is used (Table 9). Additionally the flooring concepts will be compared to floor systems by 'Nederlands Instituut voor Bouwbiologie en Ecologie' (NIBE) milieuclassificaties'. They perform LCA analysis for 5.4m span floor slabs, and state the percentage of the impact in the product stage. Therefore the shadow cost of the production stage can be accurately calculated. NIBE uses a TWIN model based on CML 2 to perform their life cycle assessment, The results of this methodology are inline with the results of the NMD. Additionally NIBE is on the list of recognized LCA experts. In the final comparison, the source of the data will be annotated with the product.

Figure 78 shows the integration of the life cycle impact analysis in the script. The impact of the steel reinforcement is also exported separately, The primary optimization was on reducing the amount of concrete, in further optimization processes a reduction of the reinforcement required could also be integrated, as exploratory studies showed that it is significant (around 50% of the environmental impact is caused by the steel reinforcement).

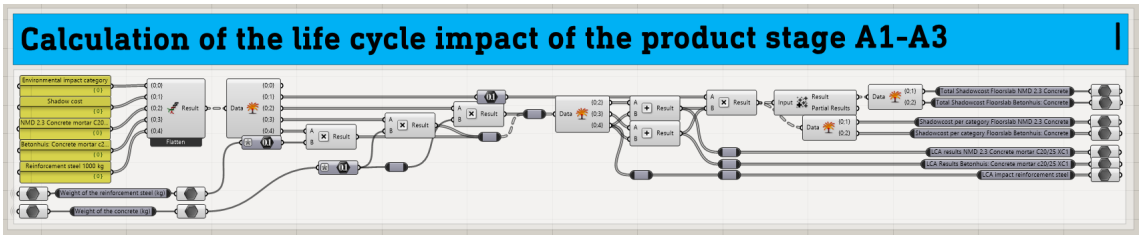

Figure 78 - integration of lca analysis within the optimization algorithm, So the direct impact from the floor is updated realtime during the optimization process

Additionally, the integration of the material mixtures showed the difference in impact. While both mixtures are optimized to reduce the environmental impact, the betonhuis mixture shows less CO_2 emissions, and the NMD 2.3 mixture resulted in a lower shadow cost and, thereby a lower overall environmental footprint. If more sustainable mixtures (or steel fabrication methods) will be developed, they can be integrated easily within the script.

5.6.5 Calculation of the amount of steel required

A grasshopper script was developed based on data provided by euro cable. The selection of wire was the DIN3064 6x36 warrington-seale+steelcore cable due to the high e-modulus of the steel wire. Table 10 shows the diameters, strength, weight and e-modulus of the cable.[1]

The Table was imported in grasshopper, and based on the horizontal trust within the support points. The right cable diameter was selected. In turn, the span determined the amount of steel required (Figure 79). The steel required in the structural nodes (steel shoes) was estimated conservatively with a wall thickness of 20mm. This resulted in roughly 0.012 M^3 steel, with a density of 700 kg/m^3. The volume of the steel in the structural nodes could be further reduced in the future, but is outside of the scope of this thesis due to the complexity of calculating the optimal thickness.

Table 10: Cable diameter, weight and strength and e-modulus.

Diameter (mm)	Weight (kg/m)	Strength (kN)	E-modulus (N/mm^2)
8	0,27	49,1	105.000
9	0,34	62,3	105.000
10	0,42	76,8	105.000
11	0,51	93	105.000
12	0,6	111	105.000
13	0,71	130	105.000
14	0,82	151	105.000
15	0,94	173	105.000
16	1,07	197	105.000
17	1,21	222	105.000
18	1,36	249	105.000
19	1,51	277	105.000
20	1,67	307	105.000

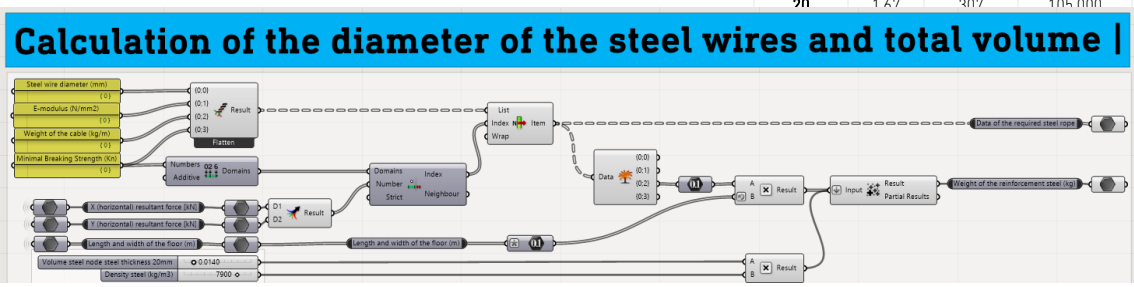

Figure 79 - calculation process of the thickness required of the tensions cables based on the data from eurocable. Additionally it shows the intergration of the steel nodes

[1] An interesting further study would be the influence of the e-modulus of the steel wire on the structural nodes and thereby the structural integrity of shell inspired flooring systems.

5.7 Research through design process

The Research through design optimization process consists of four parts. This chapter explains the process in detail. In the appendix, there is a full flowchart, that describes the the optimization process. (appendix DD)

The digital design to fabrication workflow for the generation of optimized floor slab can be described as a four-step process:

- A | Definition of the boundary conditions
- B | Fabrication-aware optimization process
- C | Design to fabrication
- D | Fabrication

Herein the primary focus within the graduation is on the fabrication-aware optimization process. Figure 80 shows the final optimization script generated in the visual programming environment grasshopper3D.

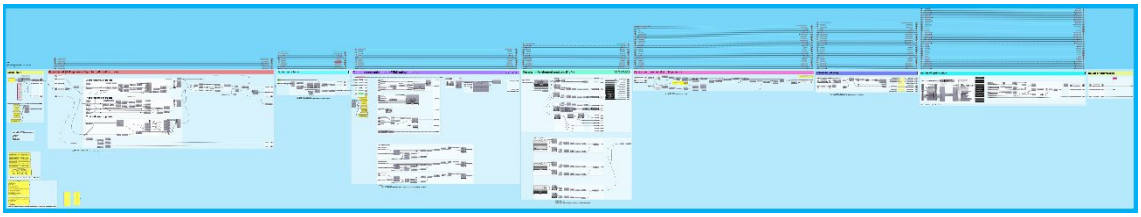

Figure 80 The fabrication aware optimization script in the visual programming language Grasshopper3D. (a higher resolution version can be found in the appendix)

Throughout the next chapter, each subsection will be explained by flowcharts. The full flowchart of the final optimization script can be found in the appendix. The description of the process in the form of flowcharts is done in order to allow for reproducibility, insight on the process, and further optimization in a later stage. The idea is to generate a mostly automated process, whereby the initial definition of the floor slab, minimal height, and maximal height would be enough to perform an optimization.

5.7.1 A | Definition of boundary conditions

The definition of the boundary conditions is primarily a manual process. It consists of a definition of the floor use, span, the load cases which result from the use, the material properties, the mesh size, and the safety factors. Additionally, a definition of topology[1] is required when using funicular form-finding methods. Figure 81 shows the process of the definition of the boundary conditions. As noted before, this optimization process will be guided by the Dutch Eurocode, with a primary focus on reducing the environmental emissions of concrete construction, by addressing floor slab construction, as it accounts for 2.37% of the worldwide CO_2 emissions (Chapter 5.3).

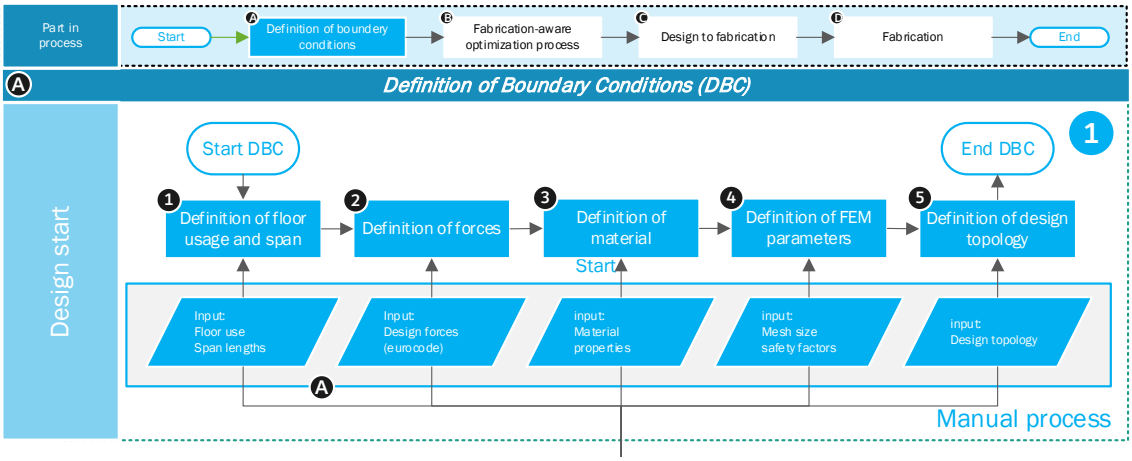

Figure 81 Definition of boundary conditions, part of the overall workflow of the fabrication aware optimization process presented in appendix ..

[1] Topology in this case defines the connectivity of patterns of the particle spring network, which is in direct relation to architectural and structural requirements, not topology as defined by structural engineers.

5.7.1.1 Definition of the floor usage and span

This research focusses on a standardized office floorplan resulting in spans of 2400x3600 and 5400x3600mm. The dimensions were largely guided by the maximum office depth, and daylight requirements into office spaces. Figure 82 showed the proposed floorplan of the offices. It is based on the vision of Le Corbusier in 1914 to showcase the future of the buildings. It was called the dom-ino system, hyphenated from "Domus" and "innovation" and showcases a future of housing in an era of standardization. (Samuel, 2007)

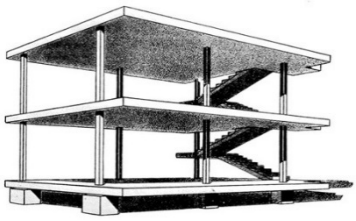

Figure 82 Drawing of le Corbusier of the dom-ino system source: (Samuel, 2007)

The reason to go for office floorplans is easy for transformation. Offices allow for a more straightforward transformation towards residential housing, as the critical design loads are higher within Eurocode.

5.7.1.2 Definition of the design force (Eurocode)

The design of structural floor slabs in the Netherlands must be in accordance with the Dutch annex of Eurocode. The design force results from the given load case. The variable and permanent load is defined according to NEN-EN 1991-1-1+C1+C11:2019/NB:2019. Partial safety factors have been used in accordance with NEN-EN 1990+A1+A1/C2:2019. These are 1.35 for permanent loading and 1.5 for variable loading. This results in the following design values.

The additional 1.2 kN/m^2 is based on light movable partition walls, required in open plan office buildings.

Additionally, NEN-EN 1991-1-1+C1+C11:2019/NB:2019 requires the testing of incidental point loads of 2kN for offices. While not being a critical design load in floor-slabs that work in bending, in thin shells, concentrated loads are expected to be guided throughout the process

TABLE 11: LOADING IN ACCORDANCE WITH NEN-EN 1990 AND EN 1991

CATEGORY	Load in kN/m^2	safety factor (-)	Resulting load in kN/m^2
Office CC2	2.5 kN/m^2	1.5	3.75 kN/m^2
Additional loading	1.2 kN/m^2	1.35	1.62 kN/m^2
Self Weight (SW)	Structure defines SW	(-)	SW
		TOTAL:	5.37 kN/m^2 + SW

5.7.1.3 Material properties (Eurocode)

The material selection within this graduation thesis is in accordance with NEN-EN 13670 and EN-EN 206 + NEN 8005. The NEN-EN 13670 is the Dutch interpretation of the current European standard of manufacturing with concrete. NEN-EN 206 + NEN 8005 describes the specifications, performance, production, and conformity of concrete. The required material mixture for the design is calculated manually based on cement types: CEM I and CEMIII/B 42,5 N. Therefore, the following strength, exposure and consistency classes were guiding:

- Strength class = C20/25
- Exposure class = XC 1
- Consistency class = C2, S2, F2
- Maximal w/c factor = 0.65
- Design w/c factor = 0,63
- Minimal cement content = 260 kg/m3
- Design cement strength = 260 kg/m3
- Cement types used = CEM I and CEM III/B 42,5 N

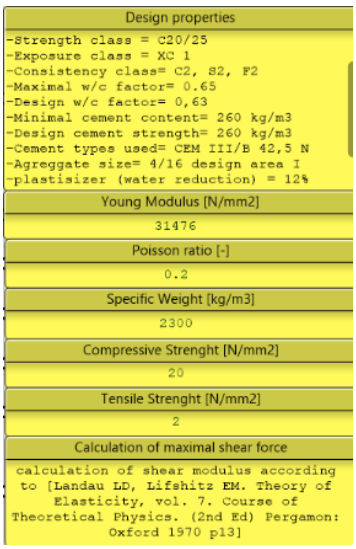

Figure 83 Material properties within the VPL grasshopper

Figure 83 shows the resulting material values used for the parametric optimization of the two floor-slabs within grasshopper. Currently, this is still based on hand calculations, with a set weight of 2300 kg/m^3 due to the availability of the aggregates.

An exciting next step would be an integration of cement type and aggregates within the optimization process, thereby also optimizing the weight of the concrete and the integration of higher strength. Chapter 5.6.3 gives more background information on the calculation process of the material and the impact of using CEMIII/B cement.

5.7.1.4 Definition of FEM parameters and safety factors.

Different input parameters define the quality and the outcome of the finite element analysis. Most importantly is the fineness of the mesh. As described earlier, a rule of thumb is that the size of the element should be at least 2 times the minimal thickness of the shell. The minimal shell thickness is guided by the material related constraints and is 5/2th of the design aggregate size 16mm, resulting in a minimal floor thickness of 50mm. This would result in a minimal element size of the mesh of 100mm. Additionally, it is vital that the NURBS surface is correctly approximated as then shell structures exhibit the NURBS surface is correctly approximated as thin shell structures exhibit significant imperfection sensitivity (Gee, Ramm, & Wall, 2005)

The above resulted in the fineness of the final mesh of 70mm. A doubling of the mesh to 140mm resulted in a difference in result by 6,98%. Taking the imperfection sensitivity into account it shows that the results are fairly accurate, for the final optimization the mesh size was further reduced to 50mm.

In the rationalization of the final structure for casting constraints, additional material is added, which results in an increased stiffness at the edges and lower stress concentrations in the structure. Solid finite element analysis of the post rationalized structure verified this assumption. Therefore, no additional safety factors were integrated. The integrated safety factors within the process are 1.35 for permanent loading and 1.5 for variable loading, 0,75 as a material factor for the compression stress. In turn, the tensile stress is calculated based on this value with an additional safety factor of 0.7 ($0{,}7 * (0.30 \cdot F_{ck}^{2/3})$).

5.7.1.5 Design topology and support conditions

Several methods were tested to find the optimal shape for the flooring system. For the form-finding procedure using dynamic equilibrium methods to find the initial shape, the network of springs (topology) defines the outcome of the optimal structural system. Figure 84 shows the relationship between different topologies (spring networks) and the optimal shape in the equilibrium condition.

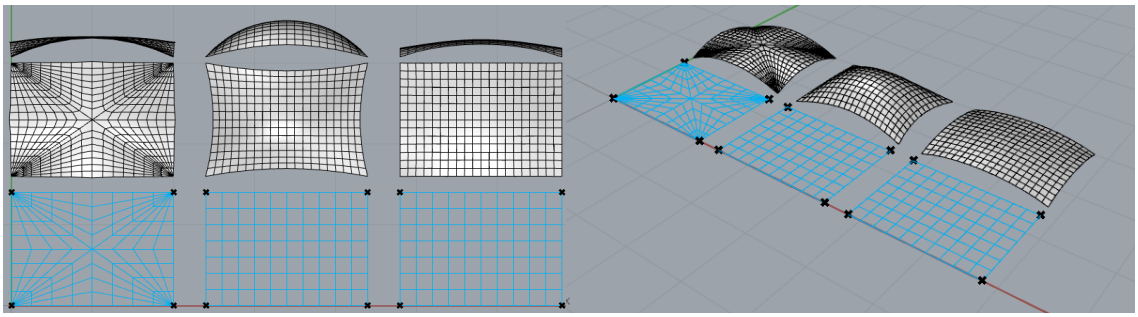

Figure 84 relationship between 2D topology and the effect on the structural form, on the left a groin vault inspired topology, middle a quad-mesh topology, on the right a quad mesh topology with constrained edges. When looking at structural optimality the groin vault shows equal performance compared to the quad mesh, the quad mesh with constrained edges performs worse.

The comparison shows that dynamic equilibrium methods do not automatically converge to the optimal solution. In the case of the optimization for a floor slab for a distributed load, a groin vault inspired shape has higher structural optimality as its boundary after convergence is the initial boundary of the spring network.

Integrating a variable material thickness in the optimization process of the floor slab using funicular form-finding methods (particle-spring methods) is difficult as this is represented by the stiffness of the individual springs. Additionally, it does not allow for the integration of multiple load cases in the same optimization process. Therefore, it might be more optimal to generate a parametric model that includes a general shape optimization process with a shell of variable thickness.

The support conditions were primarily defined by the structural optimality of the flat slab. In an explorative study, two different support mechanisms were tested.

- Linear supports like hollow-core-slabs
- Point supports in the corner

The explorative study showed that the structural optimality of the floor slab increased with the use of linear supports, but the support conditions result in the need for buttresses or a steel profile, which neglects all the material saved in the floor slab (Figure 85).

The explorative study concluded that corner supports are more effective, as it results in concentrated forces in the corner points that allow for an axial transmission, and thereby a better utilization of the steel within the floor slab.

Figure 85 Calculation of the steel beam required for the resultant Q-load in the line support.

5.7.2 B | Fabrication-aware optimization process

The second step of the process is fabrication-aware structural optimization. It builds upon the defined boundary conditions and consists of 5 steps; verification of the design input, generation of shell and finite element analysis, results of the finite element analysis and Fabrication-aware design, black-box optimization process and structural verification

5.7.2.1 Verification of the design input

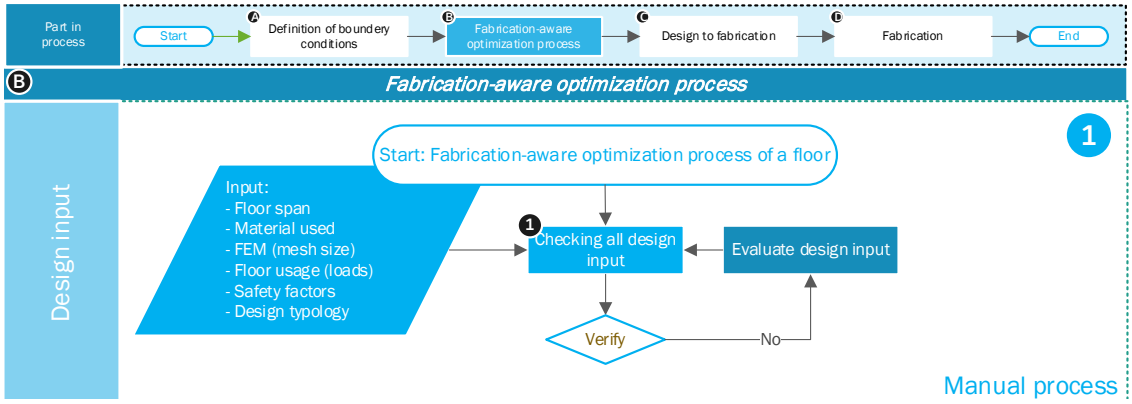

Figure 86 Flowchart of the design to fabrication workflow: Verification of the design input

The optimization process of the floor-slab starts by checking the boundary conditions earlier defined. The primary inputs that need to be checked are; the floor span, the materials required, the fineness of the mesh, the load cases, and the set safety factors and design topology (in the case of funicular form-finding methods) If all input variables are correct. The optimization can start. For the optimization of the floor-slabs for verification, two sets were tested:

– Floor span:	3600x2400mm	3600x5400mm
– Material used:	C20/25 CEM III/B	C20/25 CEM III/B
– Fineness of mesh:	7mm max element length	7mm max element length
– Floor usage:	Office CC2	Office CC2
– Safety factors:	According to Eurocode	According to Eurocode
– Form finding method:	Optimized NURBS based surface	Optimized NURBS based surface
– Design topology:	"no topology required"	"no topology required."

5.7.2.2 Generation of shell and finite element analysis

When the input for the optimization is correctly defined, and the input parameters are correct, the optimal shape of the floor can be calculated. This process consists of three steps, generation of the shell (form-finding), the definition of the forces, and finite element analysis (thickness optimization). (figure 87)

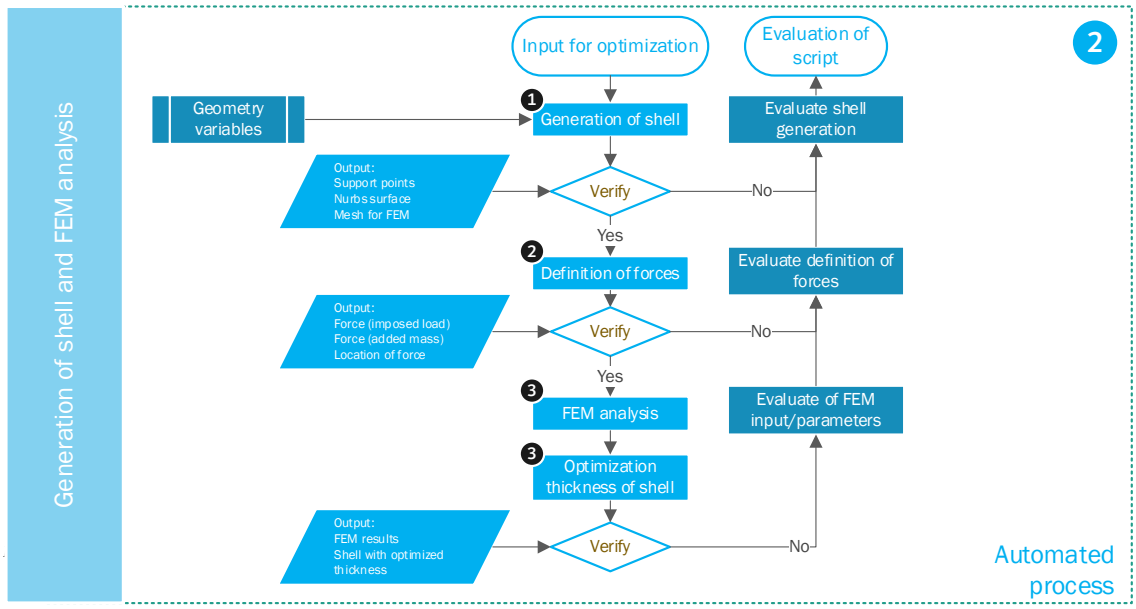

Figure 87 - Generation of the shell and FEM input

5.7.2.3 Generation of the shell

Throughout this graduation thesis, several methods of structural optimization were explored. As the strength of concrete is dominant in compression, topology optimization will not result in the addition of a genus and therefore does not make sense, additionally for a floor slab, the topology is predefined by the exposed q-load. Four different approaches have been explored to generate the shell within the optimization process:

- Catenary based optimization
- Particle spring optimization
- Groin vault, Bezier curve based.
- Variable NURBS surface

WForm finding: Catenary based optimization

Catenary-based optimization was the first approach to generating an optimized shell in compression (funicular shells), by hanging chain models within grasshopper3D. The words currently used for finding compressions only structures refer back to the analog form-finding methods by Gaudi (Figure 31) and Varigon (Figure 88). The worth catenary is derived from the Latin word for "chain." Similarly, the word funicular originates from the Latin word funiculus, meaning "cord, rope."

Figure 88 shows different funicular forms created by hanging ropes. The catenary is a hanging rope/chain without any additional weights attached, optimized for its self-weight or a distributed Q-load. The primary loading conditions of a floor is a distributed Q-load, resulting in the same optimal shape.

The optimization method consisted of catenary curves between the corner support points with variable length. This resulted in three variables defining the structure. This allowed for a variable shell that could be optimized for a uniform stress distribution for the given shell thickness.

Figure 89 shows the generated script for catenary based optimization. Figure 90 shows the resulted shell from the script.

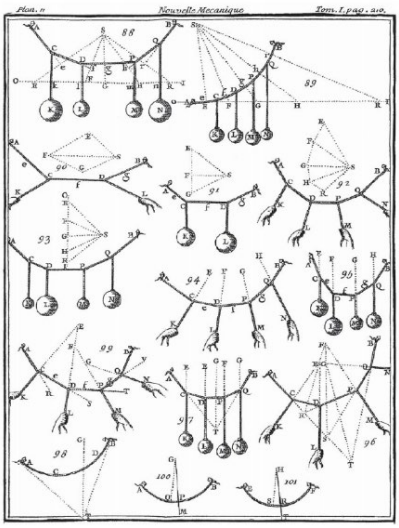

Figure 88 funicular form finding using hanging chains. Source: (Varignon, 1725)

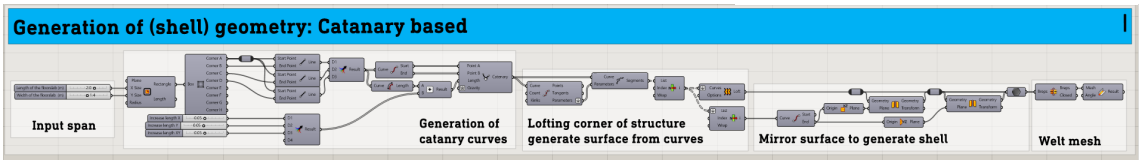

Figure 89 - Script for the optimized catenary based shell, with only 5 variables optimal groin vaults, could be found for the distributed Q-load.

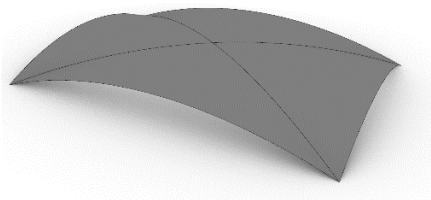

Figure 90 - Optimized form created by the catenary approach

The catenary method has five variables; the three-rope length between the support points, and the width and length of the floor. The small number of variables combined with the principles of the catenary allowed the structure to converge relatively fast to a good solution for the distributed Q-load. Therefore, giving you a good initial idea of the optimal solution for the shell with constant thickness. If the shell would be optimized for variable thickness, which makes sense for a floor slab (total height as low as possible), other form-finding methods had to be explored.

Form finding: Particle spring optimization

The second approach was based on physical-based modeling, with the use of dynamic relaxation. In contrast to the catenary based method, physics-based modeling allows for a more guided form-finding process. As shown earlier, the topology of the spring network allows you to change the outcome of the structural system (Figure 90), The difficulty of integrating a logical topology (with variable spring thickness) to take the variable thickness of the shell into account opted against this solution. This confirms the conclusions of the paper from Nouri-Baranger (2004). Additionally, the difficulty of integrating multiple load-cases, showcased that the initial assumption of the literature study was correct. It is more optimal to generate a parametric model that includes a general shape optimization process with a shell of variable thickness and multiple loading conditions.

Form finding: Bezier curve

As funicular form-finding methods did not converge to optimal solutions due to their pre-set solution space, a parametric approach combining shape optimization with a size optimization for the primary load-case (distributed Q-load) is explored. The Bezier curve-based surface was the first explorative study, inspired by groin vaults.

The final parameterization of the Bezier-based shell was based on three planar Bezier curves, which in turn is defined by four control points (Figure 91), These Bezier curves were lofted into a surface and mirrored, resulting in the form of the shell. To optimize the optimization process, relationships were defined between the points which build the Bezier curve:

- Point C2 defines the maximum range for C1 and C3
- Point C defines the maximum range for B and A
- The maximum range of point A is defined by point B.

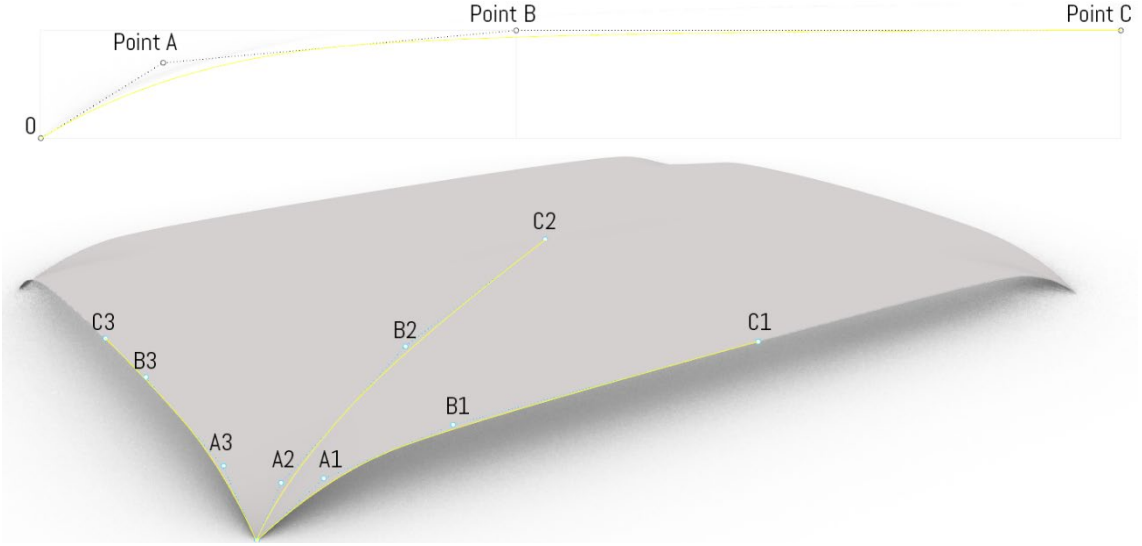

Figure 91 The control points of the bezier based shell

Additionally, the ranges of the x y and z coordinates could be remapped to guide the optimization process further, (Figure 82) this allowed for an interactive optimization process whereby the range of possible positions could be set based on previous results. This allowed for an optimization of the optimization process, before doing accurate finite element analysis with a fine mesh. Figure 88 also shows the script that generates the Bezier curves and the computational relationship between the points. Notice that the X and Y domains of point A are being remapped based on the Z coordinate and Y coordinate of point B, this allows for greater detail where required, with fewer parameters.

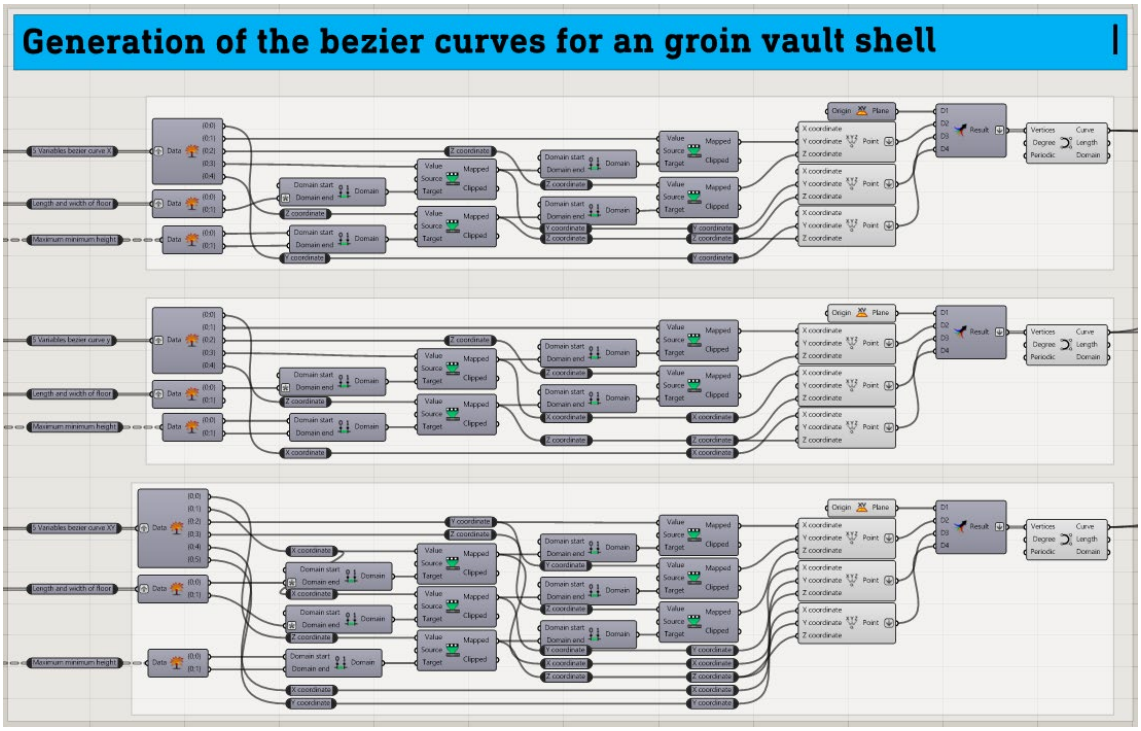

Figure 88 - script which showcases the ability to remap the numbers to nudge the process towards optimal results

The primary drawback of the Bezier based optimization was the difficulty of creating a consistent mesh as the input for the finite element analysis. Thin shells are imperfect sensitivity, and the methodology of Bezier based optimization required the mesh to be consistently re-meshed without resulting in imperfections throughout the optimization loop. This is where the strength shows of NURBS based geometry. Meshes need to be approximated by a computer while NURBS based surfaces give an exact solution for a given position.

The quad-mesh for the finite element analysis was based on a NURBS surface that approximated the form found mesh to get a robust process. This made the optimization loop longer. The Bezier based method did show a fast convergence due to the set relationship between the parameters (2 hours).

Form finding: NURBS based surface

The final optimization is based on NURBS (non-uniform rational basis splines) surfaces. The surface, in turn, is defined by 36 control points. (figure 92) The surface was not bound by "any" assumption of optimal curvature. Therefore, it does also not constrain the potential solution set. While the optimization process might take longer, it ensures that the optimal solution is within the solution space.

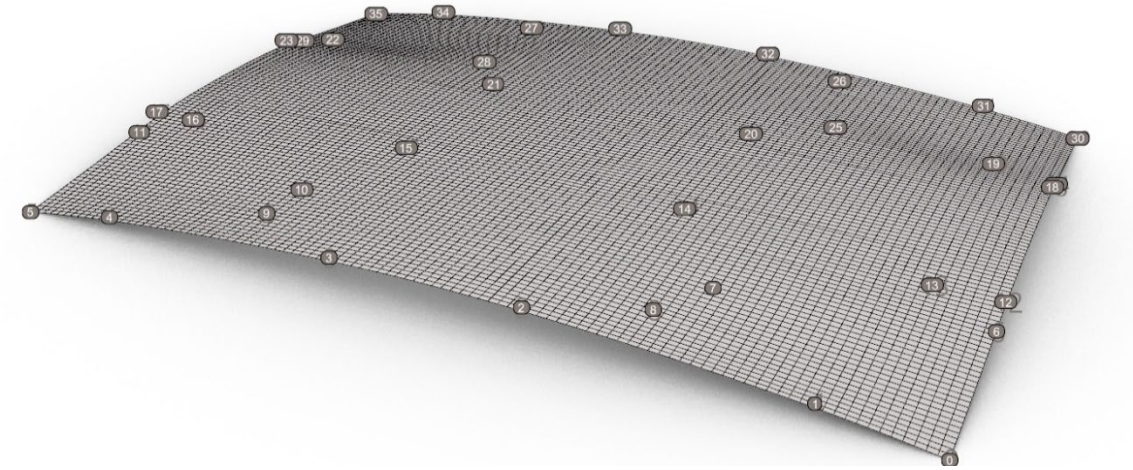

Figure 92 one of the optimal solutions of the floor span 5400x3600mm. It is unlikely that Bezier based or catenary based solutions would converge to a similar solution.

Figure 93 shows one of the optimized shells using NURBS based optimization. Interestingly, the optimal shell surface has negative gaussian curvature at the short edges (between points 0 and 6). This sounds counterintuitive. Two potential reasons could be named; the curvature allows for better distribution of forces in the corner by using the short edge to help the longer edge carry the forces. Additionally, it allows for an increase of Gaussian curvature in the corner.

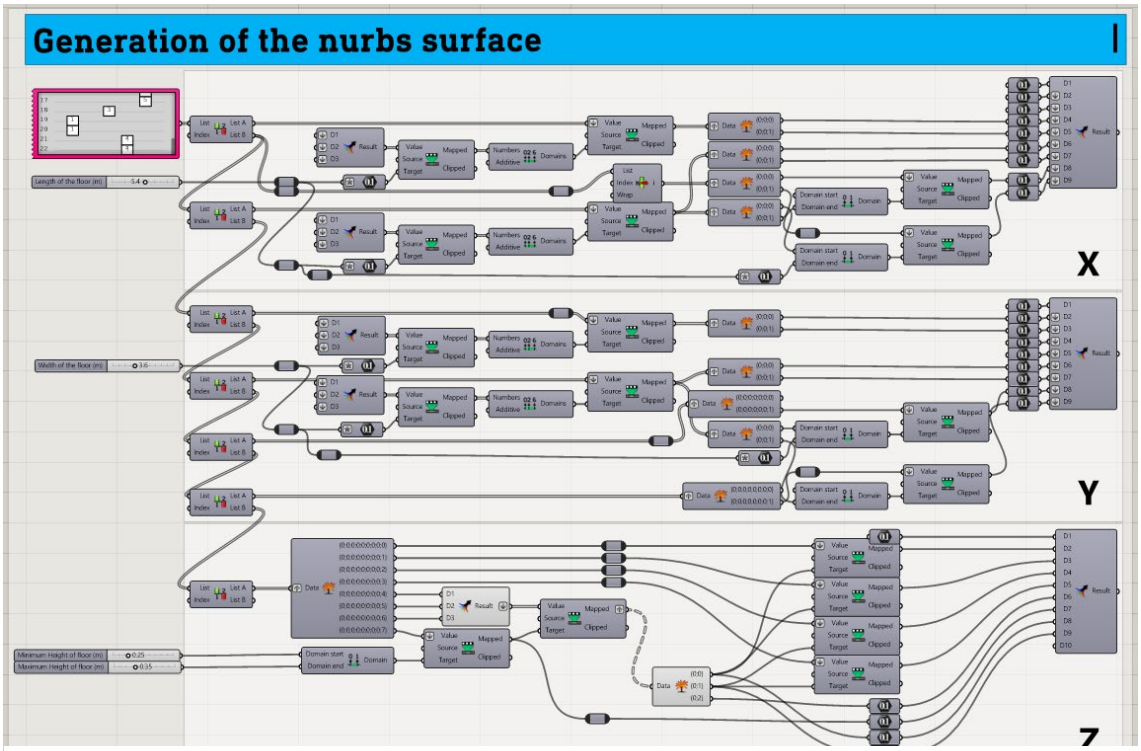

Figure 93 - Script for the generation of the coordinates of the 36 points defining the NURBS surface.

To conclude it can be said that funicular form-finding methods do not converge to optimal solutions due to their pre-set solution space. Bezier based optimization allows for the integration of multiple load cases but has difficulties in generating a robust process as it is based on the approximation of meshes. Therefore, the final optimization consists of a parametric approach combining shape optimization with a size optimization whereby the initial shell is based on a variable NURBS surface in turn defined by 36 control points. The solution space will be optimized by rougher meshes resulting in faster convergence.

5.7.2.4 Definition of forces

As stated earlier. The design of structural floor slabs in the Netherlands must be in accordance with the Dutch annex of Eurocode. The variable and permanent load is defined according to NEN-EN 1991-1-1+C1+C11:2019/NB:2019, and the safety factor is based on NEN-EN 1990+A1+A1/C2:2019. Additionally, NEN-EN 1991-1-1+C1+C11:2019/NB:2019 requires the testing of incidental point loads of 2kN. This results in the following load cases:

- Q-load 5.37 kN/m^2
- Concentrated point load 2 kN (100x100mm)
- Self-weight of the floor by the structure

While the definition of the Q-load and the concentrated point load is straightforward, the self-weight of the infill of the shell needs to be integrated. This is done by taking the surface of the projected Voronoi, times the difference in height with the top surface of the floor, minus the top side of the shell thickness (Figure 94). The resulting distribution of self-weight of the structure and infill is shown in Figure 95.

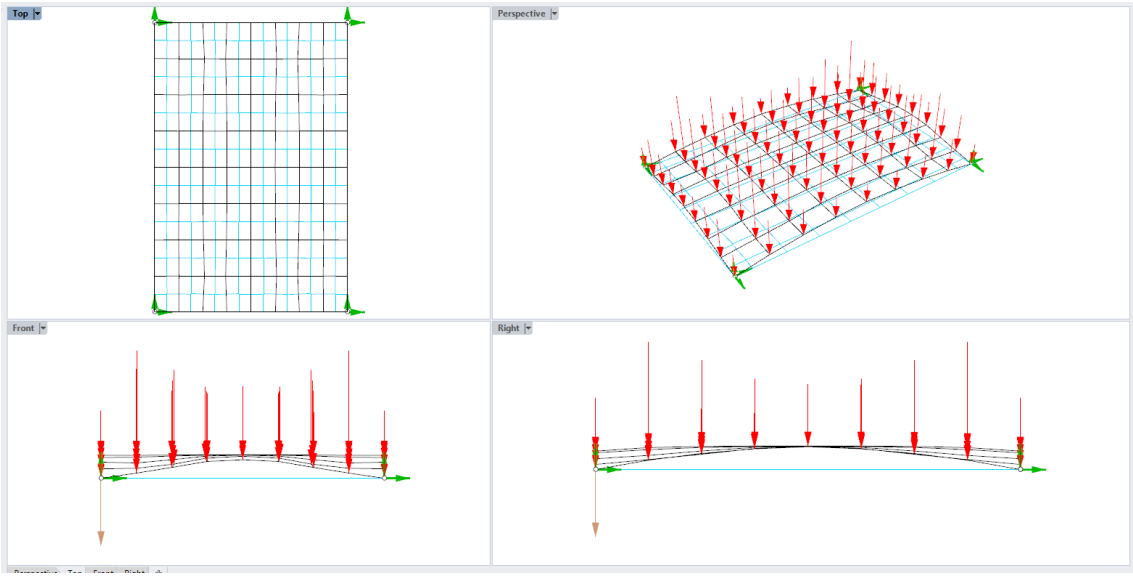

Figure 95 Exposed loading on the floor, the Q-load from the structural infill is calculated by taking the projected Voronoi of the structural nodes on the horizontal surface (blue) times the height difference between the structural node and the top surface of the

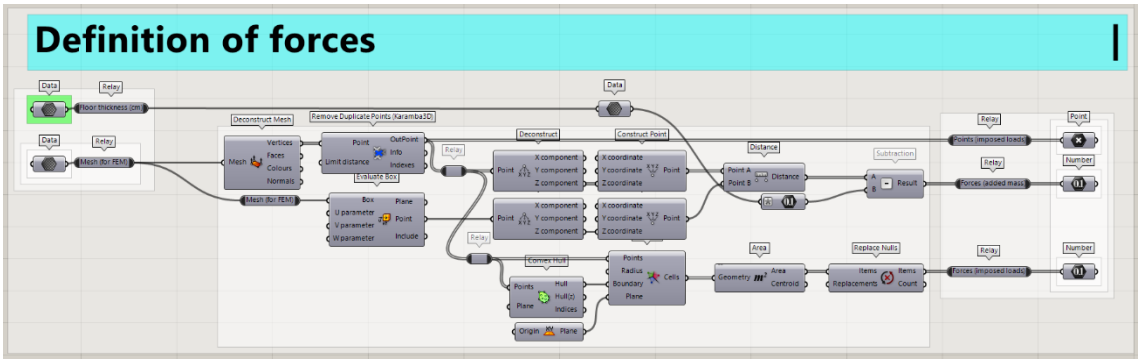

Figure 94 The grasshopper script that calculates the forces shown in Figure 92.

Explorative testing of optimized floor slabs resulted in three ultimate limit states to consider, Combined loading of the concentrated load, Q-load and self-weight, the self-weight of the structure without additional loading, and the self-weight combined with concentrated point loads for critical points on the shell. In the process of taking into account the concentrated point loads, the critical locations have to be found. This is further described in Chapter 5.7.2.5

5.7.2.5 Finite element analysis and thickness optimization.

The structural optimization process is done using the finite element method with karamba3D. In total, 17 earlier defined parameters define the input for the finite element analysis resulting in shell elements, the range of cross-sections, the related material properties, support conditions, and the loading conditions (Figure 96).

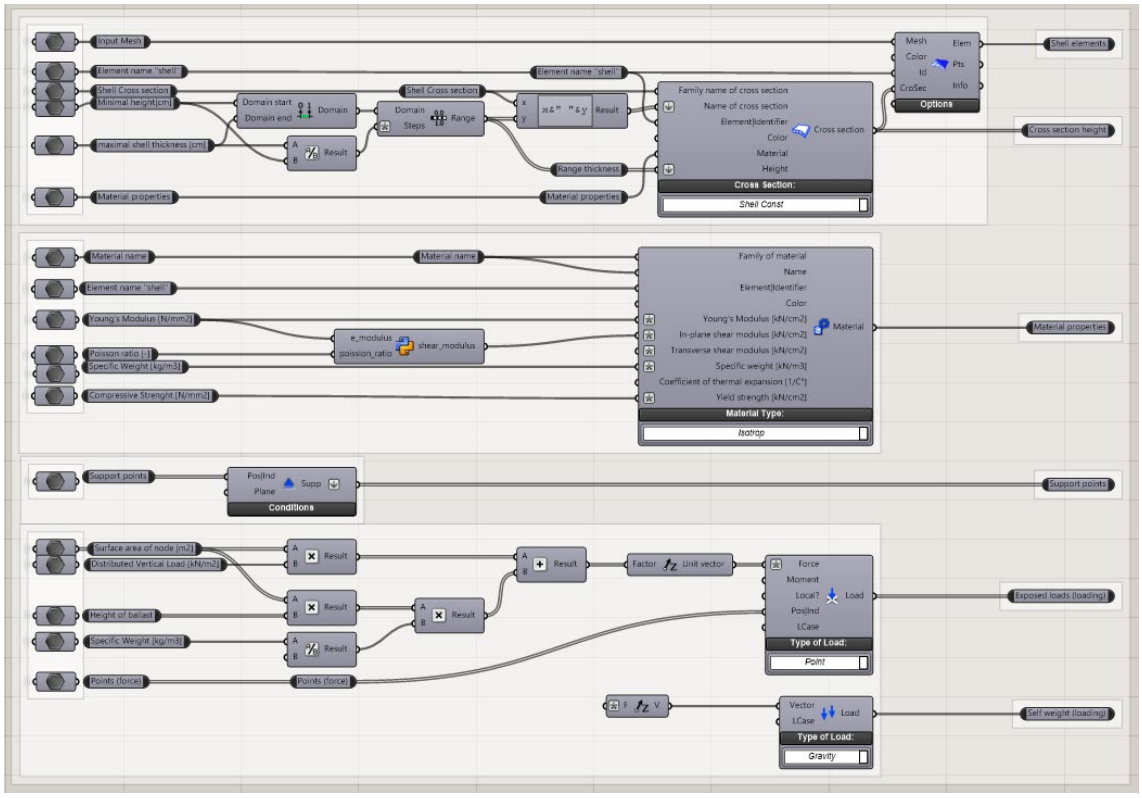

Figure 96 Definition of the boundary conditions of the finite element analysis in Karamba3D

Additionally, the critical position for the concentrated point load has to be found to integrate within the optimization process. The prediction is that the concentrated load is critical, where the thickness of the shell is minimal in the middle. Another critical location could be one/forth of the span at the edges, as there is limited membrane action, and for shallow arches of a constant thickness, this is the critical position. (Plaut, 2015)

As the inclusion of multiple loading conditions in the optimization process significantly slows the optimization, a model-based optimization script was built to test the critical positions of the concentrated loads. This test verifies the assumption stated above, resulting in the following critical states for the shell:

- At One/forth of the span at the outer edges (LC1).
- At The middle of the outer edges, where the shell is the thinnest.
- At The middle point of the shell where the shell is the thinnest.

A Solid finite element analysis (in Ansys) is done to verify the criticality of the loading conditions in the rationalized shell. The finite element analysis showed that LC1 was not critical. The primary explanation is that the eccentricity of the point force results in a better distribution of the force over a larger area of the shell that works in membrane action. Additionally, the increased thickness results in a stronger shell. For the middle point of the shell and the middle point of the outer edges, the shell thickness did not increase. Therefore, they must be included in the optimization process. Figure 97 shows different load cases which will be used in the optimization.

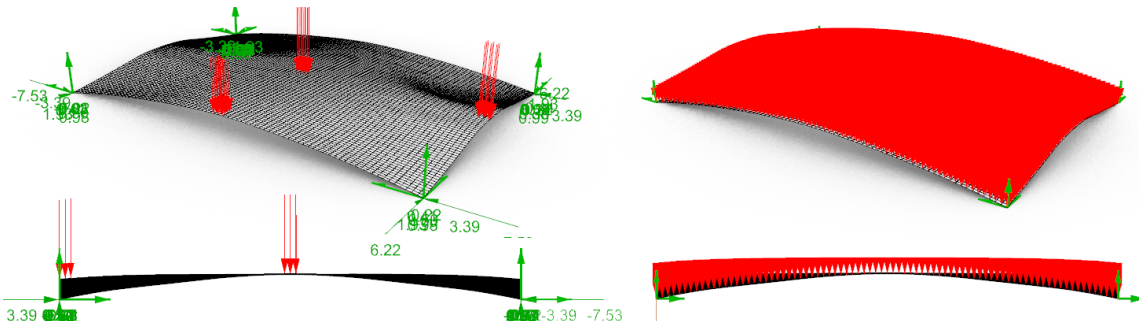

Figure 97 the four critical loading conditions which need to be taken into account. The thickness optimization happens on the primary loadcase (right image)

Size optimization of the shell

One of the guiding measures in regular floor-slabs is the structural height. For thin shell floor slabs casting constraints will add extra material in the outer edges of the shell. In a shell optimized for constant thickness, the concrete is the least effective in this position as the location is above the neutral axis. Therefore, a variable thickness shell has been introduced, which will be optimized based on the rationalized geometry for casting.

The size optimization process results in multiple finite element analyses optimizing the utilization of each element of the shell by changing the thickness. To integrate the size optimization, one of the functions of parametric FEM software karamba3D was used. Karamba3D has a build-in tool to optimize steel sections (Figure 95). Steel is equally strong in tension and compression. A utilization factor was introduced as an additional variable in the overall optimization process, as concrete is more potent in compression than tension.

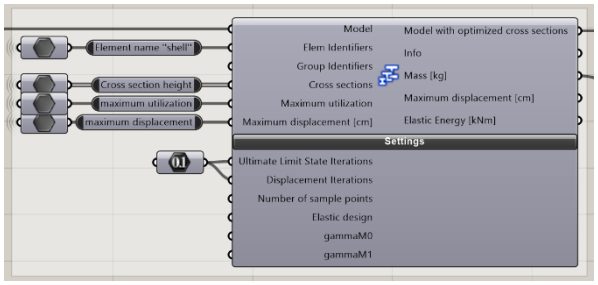

Figure 95 – Karamba3D, the tool used for optimizing the cross section of the shell

The shell with optimized thicknesses formed the basis for the final Finite element analysis, which evaluates the structural performance. These results formed the bases for the fabrication-aware design.

5.7.2.6 Results of the finite element analysis and Fabrication-aware design

After the final finite element analysis is performed, the results need to be extracted. This includes the maximum displacement, maximum compression, and tensile forces, the resultant forces in the supports, and the results from the other load cases. Additionally, Karamba3D allowed for the export of the shell with a projection of the utilization. This gives insight into the way the structural shell performs; in the explorative studies, this was used in remapping the ranges of the parameters defining the shell.

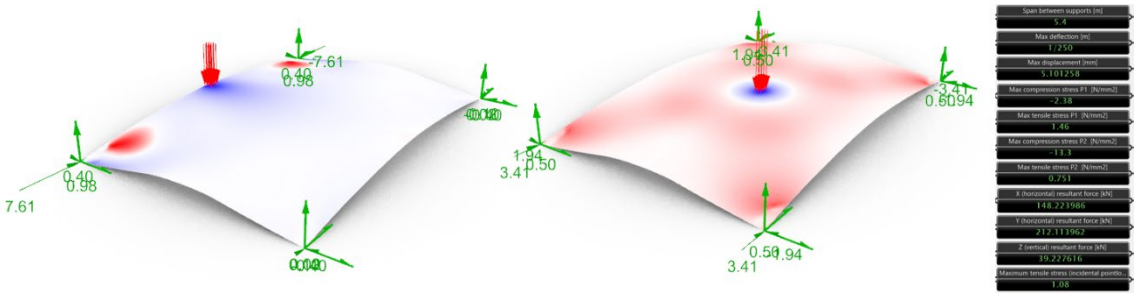

Figure 98 Visualisation of the force flow in the lower surface of the shell for two load cases, in initial studies this was used to optimize the solution space of the shell

Fabrication aware geometry

The next step is the rationalization for casting, whereby points are projected towards the bottom surface of the shell, resulting in a NURBS surface. This surface forms the bottom surface on which the floor will be cast during fabrication.

The casted floor is represented by a solid b-rep guided by the NURBS surface and the top of the floor (Figure 99). This surface was generated by projecting points towards the bottom surface of the thickness optimized mesh. The volume of this solid is calculated and gives a good indication on the amount of concrete that is required to build the floors slab.

This volume later forms one of the primary objective variables, and allows for the integration of the casting constraints within the optimization process.

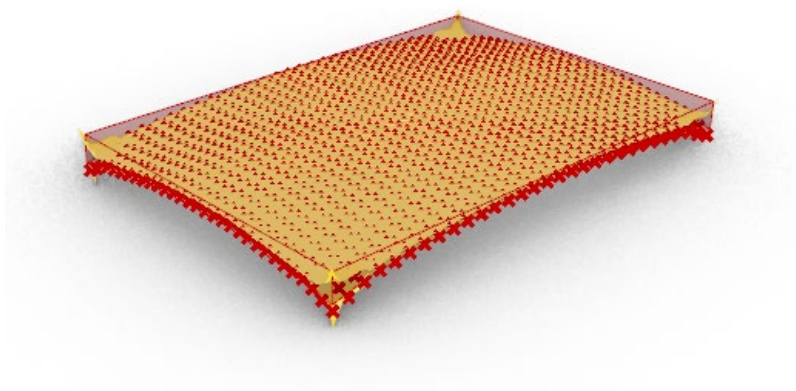

Figure 99 the solid b-rep of the to be cast floor, which is based on the shell geometry with variable thickness

5.7.2.7 Black-box optimization process

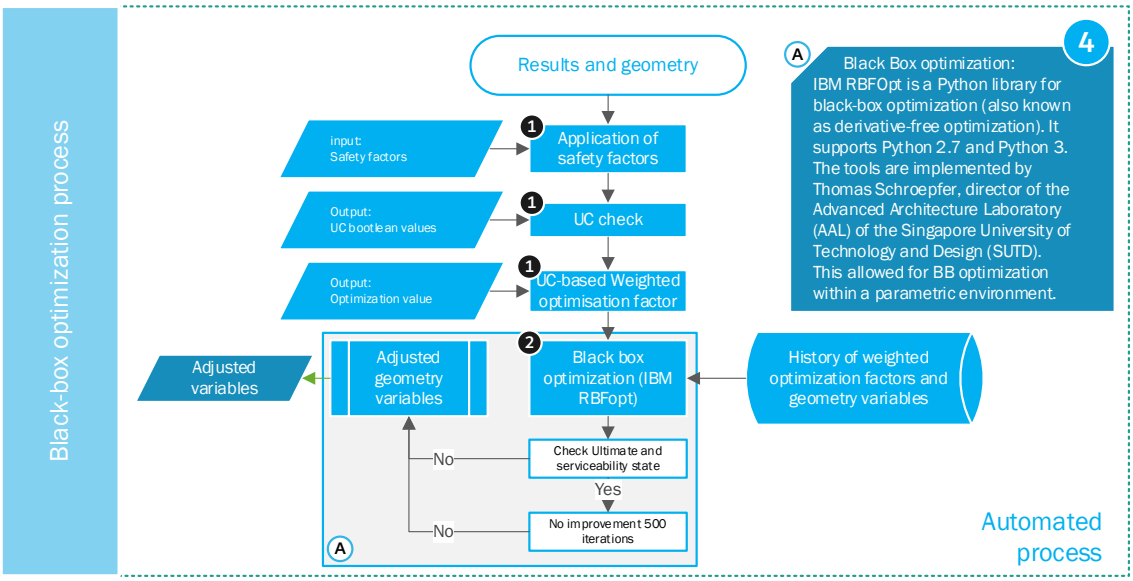

Figure 100 Flowchart of the black box optimization process: Finding the best floor slab

Based on the volume of the fabrication-aware structure and the results of the size optimization process, an objective value can be formulated. A single objective optimization solver is used for the optimization process. In this process, the unity checks of the structural calculations are integrated as Boolean variables. The objective value increases in the case the objective values do not pass the UC checks. (Figure 100)

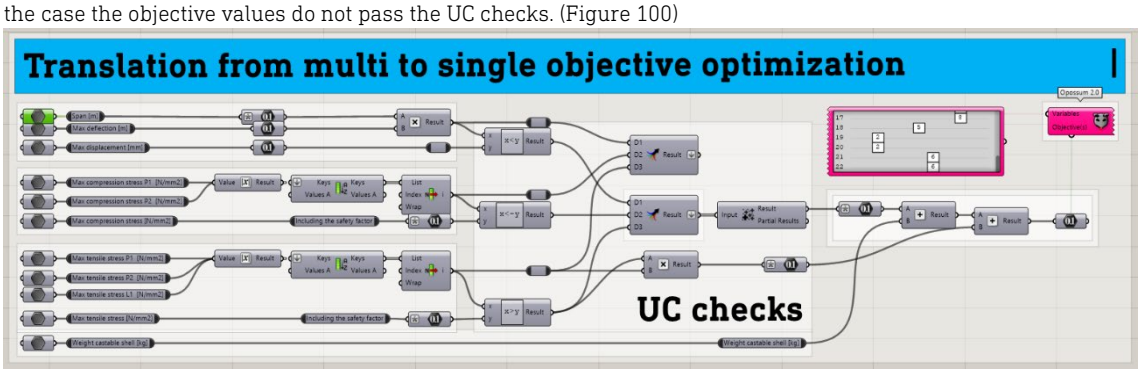

Figure 101 Grasshopper3D script, which translates the unity checks, together with the weight of the structure into a single objective value for the optimization process.

As concluded in the literature study, model-based optimization processes promise to converge quickly towards optimal results. Within the grasshopper3D environment, the plug-in Opossum allows for model-based optimization, using RFBOpt, a surrogate model-based machine learning algorithm. The algorithm is based on the Radial Basis Function method initially proposed by Gutmann (Gutmann, 2001), which builds and refines a surrogate model that approximates the unknown objective function. This allows for faster convergence when evaluations are costly.

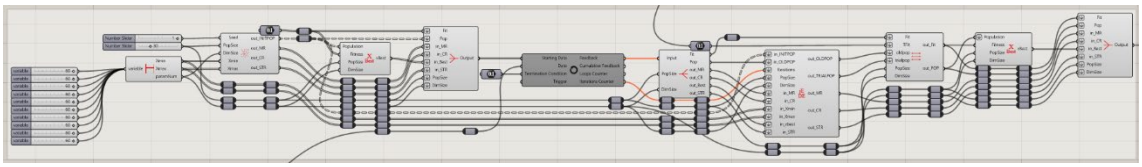

Figure 102 Implementation of the Optimus script without the optimization process. It eventually did not lead to faster convergence.

Additionally, Optimus was tested as an optimization strategy (Figure 102). The paper by the authors: *OPTIMUS: Self-Adaptive Differential Evolution with Ensemble of Mutation Strategies for Grasshopper Algorithmic Modeling (2019)* states that it outperforms the RFBOpt algorithm in finite element related tasks. (Cubukcuoglu, Ekici, Tasgetiren, & Sariyildiz, 2019) Optimus implements a self-adaptive differential evolution algorithm with an ensemble of mutation strategies (jEDE). As there is no free lunch, explorative studies were performed to test the performance of various optimization algorithms. The explorative studies verified the conclusion from the literature study. Model-based optimization becomes more optimal as the script becomes computationally more expensive.

5.7.2.8 Structural verification

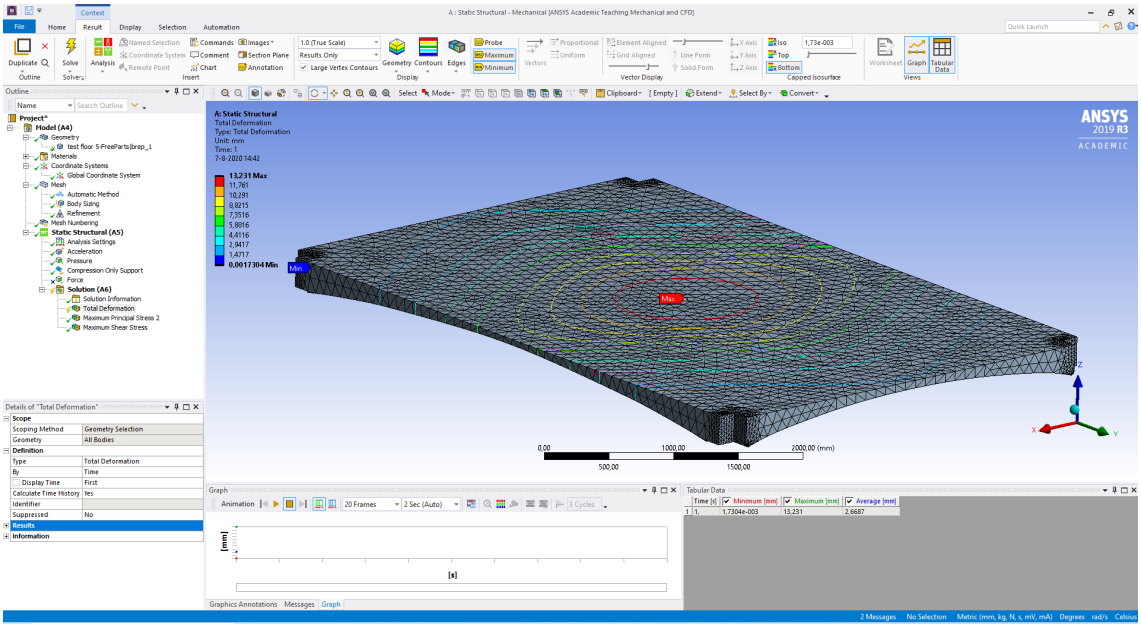

Figure 103 – Verification of the floorslab in ansys mechanical with an refinement of the mesh near the supports

The last step consists of structural verification of the rationalized fabrication aware structure. This is done by a finite element analysis performed in ANSYS. Due to the limitations of mesh size for the student editions, the floor slab consisted of a mesh size of 150mm with a refinement at the supports. As shown in Figure (103)

In the finite element analysis, the self-weight of the structure was simulated by giving the floor an acceleration. The support conditions of the dry concrete connection were simulated by plates only taking axial compression. This resulted in a critical shear and compression stresses in the corner for up to 79 Mpa (Figure 104). The illustration shows that it is a local increase at the intersection of the compression-only support plates.

In the actual structure, a value of this hight is unlikely. The critical shear and compression have been takin into account in the design of the connection node. This resulted in a steel shoe, that "catches" the axial membrane forces in the corner.

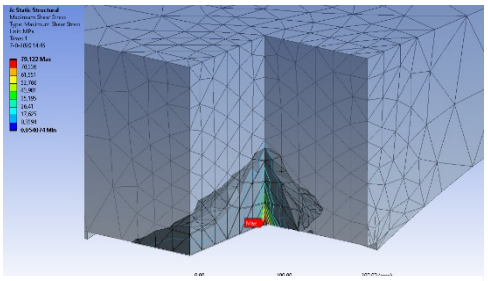

Figure 104 - image showcasing the critical position of the concentrated loads, in the same position as the overall optimization

Besides the concentrated local increase of load, the solid finite element analysis verified the structural integrity of the floor slab. Showing no critical forces outside of the corner element for all load cases. The working of the shoe and the actual shear forces can be best verified by design by testing. This same test can be used to test the rigidity of the connection together with the steel tension ties.

Structural verification of critical point loads

Additionally a script was written to test the potential for critical point loads not integrated within the optimization script. This happened in Karamba3D, with the same script which was used to find the critical position of the load-cases. Which varied a concentrated load over 250 positions of the floor trying to find the highest occurring critical stress. This, resulted in the same critical positions of the load at the positions where the floor is thinnest, not exceeding the tensile stresses of the initial optimization.

This verifies that the critical position for an variable thickness shell is in the parts where the flooring area is minimal. (e.g. the middle point and at the middle edges)

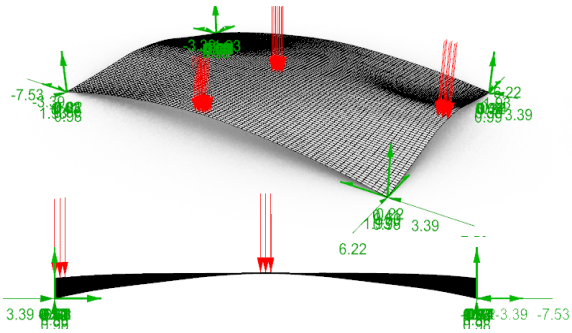

Figure 105 - The final critical positions leading to the maximal stresses

5.7.3 C | Design to fabrication

The design to fabrication workflow flowchart shows the earlier proposed fabrication method (annex). While not the primary focus of this thesis, different moulding techniques are evaluated and one method seems optimal for the fabrication of a sustainable and robust thin-shell system: Stay-in-place fabric formwork.(figure 106)

A unreinforced concrete shell shows brittle behaviour, what is unwanted for building structures. Additionally concentrated loads will likely result in critical tensile stresses in the bottom layer of the shell. Therefore the shell needs to be reinforced, giving a good case for stay-in-place formwork.

For stay-in-place fabric formwork to be effective the fabric formwork needs to have enough load bearing capacity to carry its self-weight and the load of the wet concrete. Additionally by using high-strength fibrous materials for knitted textiles, the formwork can act as a reinforcement in the final state. (Lee, Mata-Falcón, Popescu, Block, & Kaufmann, 2020) This has several advantages:

- the use of non-corrosive materials as reinforcement allows for thinner shells, as there is no need for steel coverage to protect the reinforcement.
- The clinker percentage can be reduced as a high PH value of the concrete is not required to prevent the steel from corroding, Resulting in a further reducing the environmental impact.
- The stay-in-place fabric formwork provides robustness to the structural system because textile reinforced shells do not show brittle failure. (Tsangouri et al., 2020)
- Textile reinforcement provides extra tensile capacity further increasing the structural efficiency of the system, as this is likely a guiding failure mode in relative low thin-shells.
- Provide robustness by providing alternative loading paths, ductility and increased tensile strength.

Herein the stay in place formwork can be easily prefabricated using CNC knitting machines. Which results in double curved surfaces by locally varying the length and width of the textile during production. (Popescu, Rippmann, Van Mele, & Block, 2018) Currently an opensource package is created within the COMPAS framework, which allows for the generation of knitted formwork for double curved surfaces (Van Mele, Liew, Mendez, & Rippmann, 2017) This allows for an easy generation of the input for the CNC knitting machine, for the stay in place formwork.

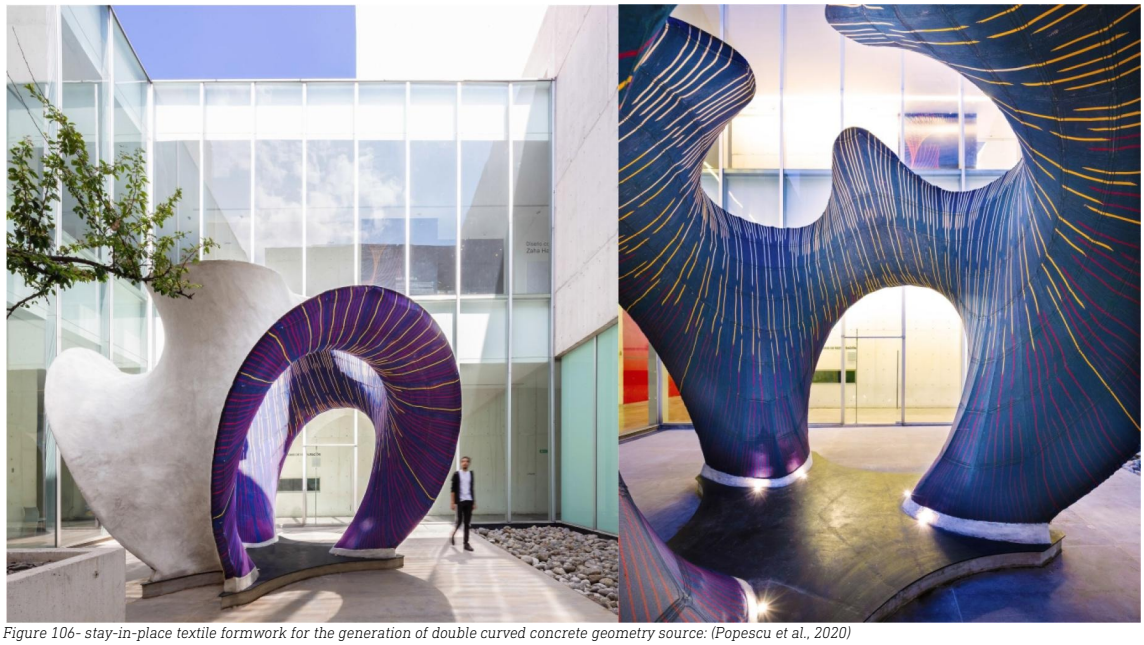

Figure 106- stay-in-place textile formwork for the generation of double curved concrete geometry source: (Popescu et al., 2020)

5.7.4 D | Fabrication

While not the primary focus of this graduation thesis, a short description is given of the proposed fabrication procedure. The fabrication starts with generation of the knitting pattern for the formwork, this can be done using compas_knit, a package developed using python which can be directly implemented within rhino3D, and create a knitting pattern based on a 3D input geometry. (Van Mele et al., 2017)

Afterwards the knitting pattern is tensioned in an external scaffolding frame, and coated with only a thin layer of cement paste, giving it the strength required to carry the dead weight of the wet concrete. It also improves the adhesion between the formwork and the final structure, allowing for an optimal use of the fibre reinforcement.

After this the concrete of the thin-shell is casted, with the support shoes and the tensioning cables in place, which allows for the transportation of the element after pre-fabrication. With the curing strength of CEMIII/B cement this allows for demoulding after a day, resulting in the prefabricated floor with integrated fabric formwork.

5.7.4.1 Resulting floor slabs of optimization

To verify the working of the optimization script two floor slabs have been generated to verify the hypothesis. The script (Figure 107) ran for the spans 2400x3600 and 5400x3600. The total design input is shown in Chapter 5.8.1 (Verification of the design input) This chapter shows the results of both of the floor slabs and forms the input for the evaluation of the floor slabs in section III. As the floor slab exhibits two-dimensional curvature, it hard to visualize the results in regular drawing sets or sections; therefore, two additional methods are generated to document the final geometry, Bitmap based, and Nurbs surface-based.

Each floor slab will be documented with the relevant information, including; results of the finite element analysis, environmental impact data for the two concrete mortars as a primary material, and the bitmap describing the final geometry.

Bitmap image as a means of describing a double-curved floor slab

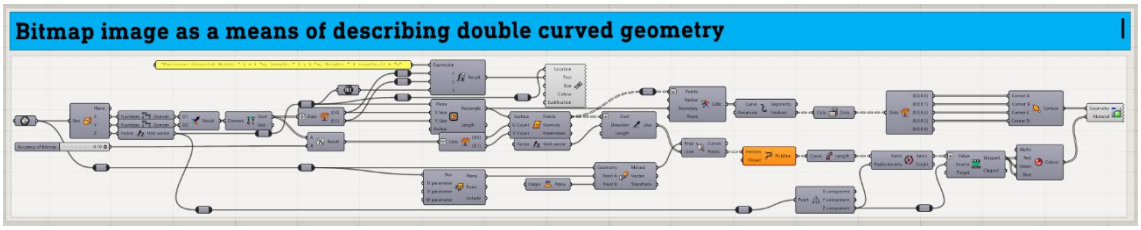

Figure 107 Script that describes the geometry of the floor slab by and bitmap image

With the difficulty of describing double curvature with regular drawing sets, a script was developed, explaining floor slabs by bitmap images. Floor slabs require a flat-top surface; therefore, the geometry can be described from that plane as a 2D extrusion. The script shown in Figure 107 does precisely that. It describes the designed floor slab by the height difference from the bottom layer. Interestingly this method of describing height difference in geometry is already used within computer graphics, known as mapping (Figure 108).

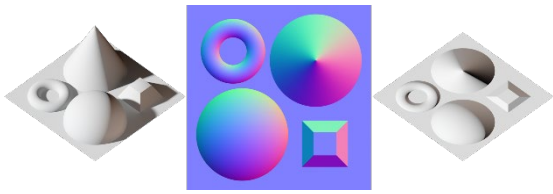

Figure 108 Image showcasing the information density of image mapping strategies, Source: Wikipedia.

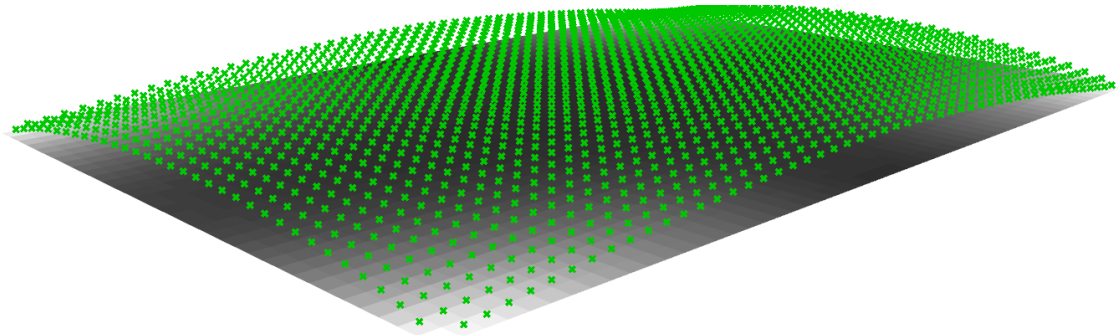

Figure 109 - showing the geometry generation based on the bitmap image. This image shows bitmaps are an accurate way of describing the floor slab

Bitmap images allow for a high density of information on an easy to handle a file. In the automatization process of the fabrication of the floor slab, it would be a good information carrier between systems to describe the to be fabricated flooring system. Figure 109 shows the geometry generation based on the bitmap image.

Nurbs based description of the geometry.

Another way to document the floor slab is by generating a NURBS surface describing the bottom of the shell. Description for this surface consists of a set of control points describing the double-curved bottom accurately. The results are inverted, and the minimum thickness is added to the control points, thereby the surface description also includes the minimal thickness of the floor. This results in points describing the geometry. The number of points in the {u} direction can be derived from the X values.

A correct approximation with the least amount of variables is important, for a similar approximation, as shown in 101, 2035 coordinates of points need to be accurately described or approximated by the surface. Therefore the generated bitmap representation seems more fitting due to the high amount of information density, the ease of use, and the insight it fives into the curvature of the geometry. (figure 110)

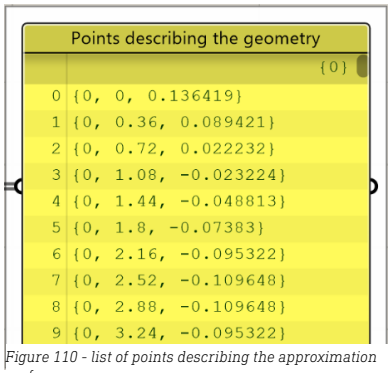

Figure 110 - list of points describing the approximation surface.

5.7.5 3600x2400 floor slab

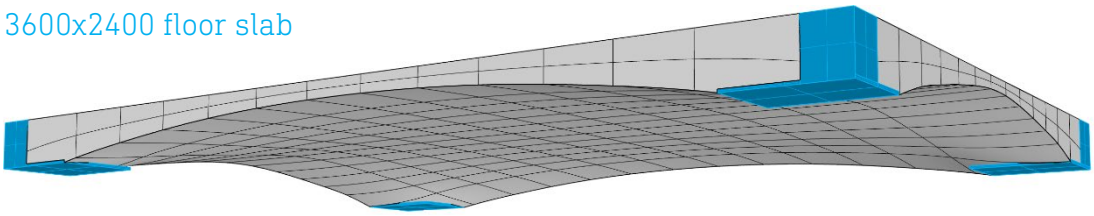

Figure 111 - image of one of the initial optimized slabs for the span of 3600x2400mm with fixed supports, blue is steel, grey is concrete.

The optimization process of the 3600x2400mm floor slab started with setting the right parameters. This related to the material, the loading conditions the mesh size and the boundary conditions of the floor. Every optimization process started with an explorative study based on a rough mesh. Hereby the floor converged to 160mm thickness, this. Based on this, the boundary was set to 100mm to 200mm for the span of 3600x2400mm. The minimal floor thickness is defined by the aggregate size D_{max} 16mm. This resulted in a minimum thickness of 40mm. Table 10 summarizes the other set parameters for the optimization process.

TABLE 10: INPUT PARAMETERS FOR THE OPTIMIZATION PROCESS OF THE FLOORSLAB.

Material description	Description	**Script parameters**	Explanation	**Loading conditions**	Description
Name	Concrete mortar c20/25 XC1	Floor span	3600x2400 mm	Dead load	5.37 kn/mm2
Specific weight kg/m3	2300 kg/m^3	Minimal floor height	100 mm	Live load	2 kn
Youngs modulus n/mm2	31476 N/mm^2	Maximum floor height	200 mm	Self-weight	Defined by floor
Poisson ratio [-]	0.2 [-]	Minimal thickness	40 mm		
Compressive strength n/mm2	20 N/mm^2	Mesh size	50 mm		
Tensile strength n/mm^2	1.5 N/mm^2				

The optimization process of the floor slab was run for 2650 iterations, taking 9,71 hours. This is primarly due to the integration of four different load cases in the optimization and the thickness optimization for the primary load case. After the optimization, manual optimization (increasing the maximum compressive utilization of the thickness-optimization to 0.55 and doubling the cross-sectional step size to 51) resulted in the final optimal geometry for the 2400x3600mm span. This manual optimization step further reduced the volume of the shell by 7,4%. Table 11 shows the final results of the optimization.

TABLE 11: RESULTS OPTIMIZATION PROCESS

Results	Description	**Unity checks**	Description	Description
Max compression stress P1 [N/mm2]	-2,91 N/mm2	Unity check	0.1455 [-]	Passed UC > 1
Max compression stress P2 [N/mm2]	-10,5 N/mm2	Unity check	0.525 [-]	Passed UC > 1
Max tensile stress P1 [N/mm2]	1.48 N/mm2	Unity check	0,99 [-]	Critical UC (Passed)
Max tensile stress P2 [N/mm2]	0.45 N/mm2	Unity check	0.3 [-]	Passed UC > 1
Max tensile stress LC 1 [N/mm2]	1,06 N/mm2	Unity check	0.71 [-]	Passed UC > 1
Max tensile stress LC 2 [N/mm2]	1,02 N/mm2	Unity check	0.68 [-]	Passed UC > 1
Max tensile stress LC 3 [N/mm2]	1,37 N/mm2	Unity check	0.91 [-]	Passed UC > 1
X (horizontal) resultant force [kN]	96,75 kN	Diameter steel wire	12 mm	DIN3064 6x36 warrington-seale+steelcore cable (eurocable)
Y (horizontal) resultant force [kN]	61,99 kN	Diameter steel wire	9 mm	DIN3064 6x36 warrington-seale+steelcore cable (eurocable)
Z (vertical) resultant force [kN]	60.96 kN	Vertical load Z [kN]	58,2 kN	
Weight castable shell [kg]	1182,91 kg	Volume	0,514 m^3	
Reduction of weight vs hollowcore [%]	48,91%	Comparison floor	VBI 150mm	0,99 [-]
Reduction of weight vs solid floor [%]	70,24%	Comparison floor	200mm 2300kg concrete	

The maximum tensile stress in principle direction 1 is critical and defines the optimal shape. Figure 112 shows the compressive and tensile forces in the bottom layer of the structure in principle direction one. This shows that the critical stress occurs at the short edges in the middle. Interestingly the corners are still in compression, which shows that the floor successfully carries the load through membrane action. For the tensile stress of 1.5 kN, uncracked concrete was assumed. In the actual structure textile-reinforced concrete or fiber reinforced concrete can be used to further optimize the structure as tensile stresses are guiding.

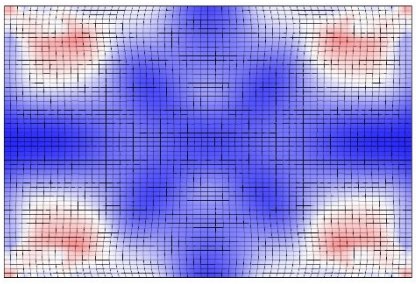

Figure 112 – principle stress in the bottom layer of the structure, blue is tension red is compression.

5.7.6 3600x5400 floor slab

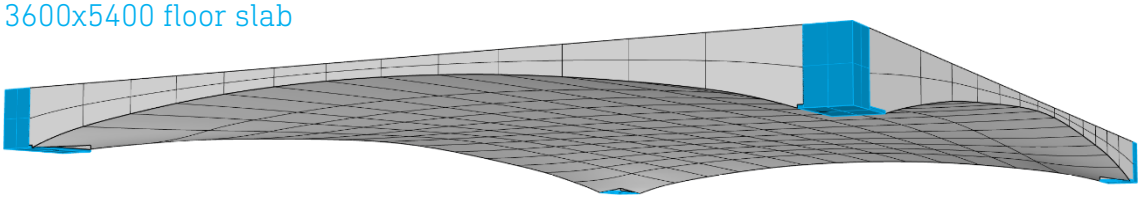

Figure 113 - image of one of the initial optimized slabs for the span of 3600x5400mm with fixed supports, blue is steel, grey is concrete.

The optimization process of the 3600x5400mm floor slab started similar with setting the right parameters. Due to the bigger span, the mesh size had to be finer for the 3600x5400mm floor slab. The final average mesh size was 45mm, resulting in 22200 elements and computation time of 22 seconds for one calculation.

Interestingly the explorative optimization for thickness also resulted in a range of 100mm to 200mm for the span of 3600x5400mm. This is primarily caused by the extra concrete due to the set casting constraints. The parameters for the 3600x5400 are mostly similar, table 12 summarizes the parameters of the optimization process.

TABLE 12: INPUT PARAMETERS FOR THE OPTIMIZATION PROCESS OF THE FLOORSLAB.

Material description	Description	**Script parameters**	Explanation	**Loading conditions**	Description
Name	Concrete mortar c20/25 XC1	Floor span	3600x5400 mm	Dead load	5.37 kN/mm2
Specific weight kg/m3	2300 kg/m^3	Minimal floor height	100 mm	Live load	2 kN
Youngs modulus n/mm2	31476 N/mm^2	Maximum floor height	200 mm	Self-weight	Defined by floor
Poisson ratio [-]	0.2 [-]	Minimal thickness	40 mm		
Compressive strength n/mm2	20 N/mm^2	Mesh size	45 mm		
Tensile strength n/mm^2	1.5 N/mm^2				

The optimization process of the floor slab was run for 4500 iterations, taking 27,5 hours. After the automated optimization process, manual optimization (increasing the maximum compressive utilization of the thickness-optimization to 0.80 and doubling the cross-sectional step size to 51) resulted in the final optimal geometry for the 5400x3600mm span. This manual optimization step further reduced the volume of the shell by 2,9%. Table 13 shows the final results of the optimization.

TABLE 13: RESULTS OPTIMIZATION PROCESS

Results	Description	**Unity checks**	Description	Description
Max compression stress P1 [N/mm2]	-4,14 N/mm2	Unity check	0.207 [-]	Passed UC > 1
Max compression stress P2 [N/mm2]	-16,7 N/mm2	Unity check	0.89 [-]	Passed UC > 1
Max tensile stress P1 [N/mm2]	1,47 N/mm2	Unity check	0.98 [-]	Critical UC
Max tensile stress P2 [N/mm2]	0,06 N/mm2	Unity check	0.04 [-]	Passed UC > 1
Max tensile stress LC 1 [N/mm2]	1,22 N/mm2	Unity check	0.81 [-]	Passed UC > 1
Max tensile stress LC 2 [N/mm2]	0,96 N/mm2	Unity check	0.64 [-]	Passed UC > 1
Max tensile stress LC 3 [N/mm2]	1,48 N/mm2	Unity check	0.99 [-]	Passed UC > 1
X (horizontal) resultant force [kN]	143,66 kN	Diameter steel wire	14 mm	DIN3064 6x36 warrington-seale+steelcore cable (eurocable)
Y (horizontal) resultant force [kN]	218,22 kN	Diameter steel wire	17 mm	DIN3064 6x36 warrington-seale+steelcore cable (eurocable)
Z (vertical) resultant force [kN]	36,25 kN	Total horizontal force	145 kN	
Weight castable shell [kg]	3313,61 kg	Volume	1.44 m^3	
Reduction of weight vs. hollow-core [%]	36,4%	Comparison of floor	VBI 150mm	
Reduction of weight vs. solid floor [%]	69,12%	Comparison of floor	240 mm 2300kg concrete	

The maximum tensile stress in principle direction 1 is critical together with concentrated load in LC3. Interestingly the critical tensile stress P1 happens at the top of the surface at the short span side (Figure 1`4). The stress is the result of the double-curved shape (negative gaussian curvature). The double curvature allows for the shorter span to help carry the load of the longer span.

The concentrated load (LC3) is also critical in the short span. Tensile stresses occur in the bottom layer (Figure 114). Similarly to the other floor slab textile or fiber reinforced concrete can further reduce the environmental impact.

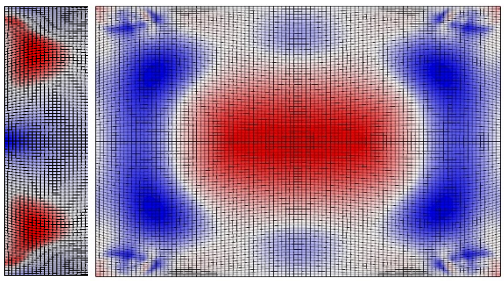

Figure 114 – Illustration of both critical loadcases left is LC3, bottom layer of the structure Right is LC0 top. blue = tension red = compression

5.7.7 Verification of the load

As a verification of the load cases, the resulting forces in the z-direction will be compared to a hand calculated q-load. This will be done by multiplying the load over the surface area of the floor and then adding the self-weight of the floor in kN. This results in:

- 3600x2400mm Total vertical load = 5.37*3.6*2.4+1175,86/100 = 58,2 kN
- 3600x5400mm Total vertical load = 5.37*3.6*5.4+3313,91/100 = 137,5 kN

TABLE 14: RESULTS OPTIMIZATION PROCESS

Description	value	Hand calculation	Description	Accuracy
Z (vertical) Total resultant force [kN] 3600x 2400mm	60.96 kN	Vertical load Z [kN]	58,2 kN	+ 3,9%
Z (vertical) Total resultant force [kN] 3600x 5400mm	145 kN	Vertical load Z [kN]	137,5 kN	+ 5,2%

Table 14 shows the values and the hand calculation. The relatively small positive difference shows that the applied force is calculated correct and conservative, and that the assumptions in the process result in an accurate view of the reality.

5.7.8 Drawing and bitmap representation

This chapter shows the final shape of the floors, including a bitmap representation of the bottom surface. This can be used to successfully recreate the surface based on the value of each pixel. By remapping the color value (0-255) to the range of the total height (annotated in the bitmap). The calculations of the total environmental impact can be found in Chapter 6.1

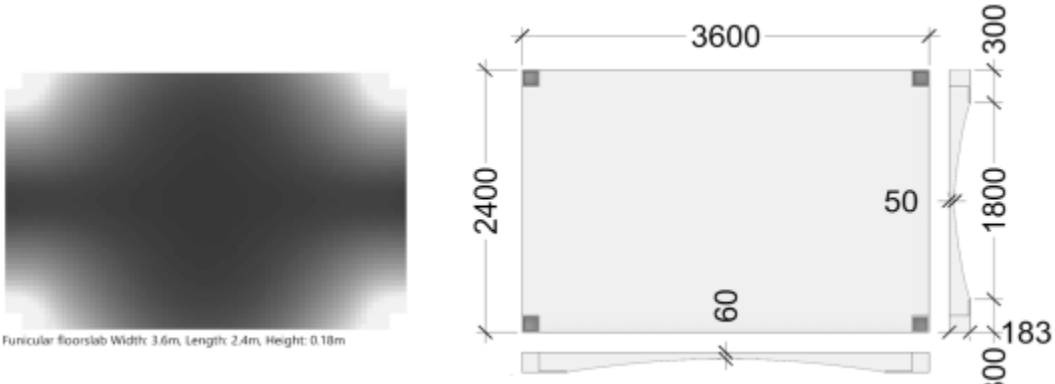

Figure 115 - bitmap representation and drawing of the 2400x3600mm floorslab

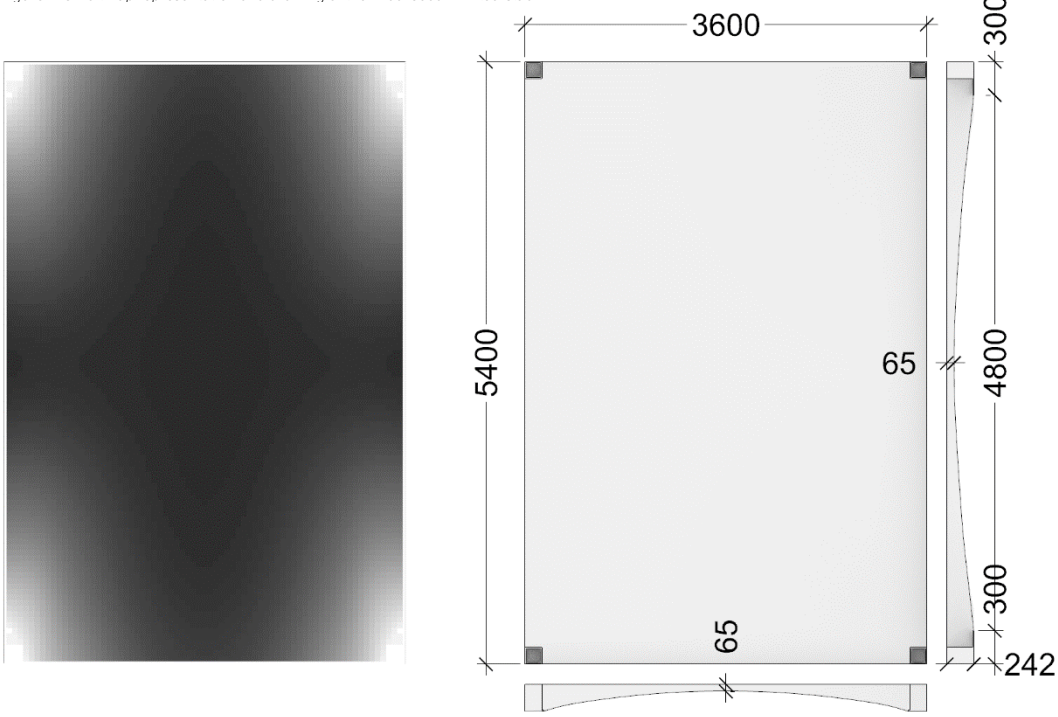

Figure 116 - bitmap representation and drawing of the 5400x3600mm floorslab

5.8 Section II: Summary and key findings

Section II focused on the generation of the floor slabs to test the hypothesis. This resulted in a derivative-free optimization methodology for the optimization of floor-slabs, - inspired by thin shells - combining shape and size optimization, whereby the global optimum was found using a surrogate-based optimization solver. This all results in two optimized floor-slabs for the evaluation of the hypothesis in section III. Section II builds upon the research from Section I, the key findings of the research through design are:

- The optimization methodology shows that the conclusion from the literature research into structural optimization was correct. A parametric model, in combination with a derivative-free optimization method, allows for the integration of casting constraints and multiple load cases. This bridges the difficulties of concurrent optimization by a derivative-free approach.

- Funicular form-finding methods (e.g., Catenary based optimization, particle spring methods) for the shape optimization result in a significantly faster convergence, but do not contain the optimal solution within the solution space, as their solution space does not benefit from a variable thickness. This also verifies the literature study.

- Particle spring methods are able to simulate multiple structural systems (e.g., groin vaults). And the variable thickness could be integrated into the form of variable spring stiffness, but this results in a complex topology with a lot of parameters. Additionally, the input topology of dynamic relaxation methods defines the outcome of the shape. Therefore, it is unlikely that it will converge to the optimal solution as assumptions define the outcome of the optimization process.

- The combination of shape and size optimization is an effective methodology for finding thin-shell structures with a variable thickness as the generated thin-shell floor slabs with the integration of casting constraints result in significant material savings while keeping the occurring stresses within the material limits.

- The results of the optimization show that the minimum cement content of concrete of 260kg/m^3 is not defined by the required structural strength in the proposed floor slab, but by the regulation (XC1). This regulation is based on the corrosion risk of reinforcement. This annotates the importance of the integration of non-corrosive materials as reinforcement in an attempt to further reduce the environmental impact of flooring systems. Stay-in-place fabric formwork show a lot of potential in this regard and should be further evaluated.

- Minimizing material does not always result in a lower environmental impact; constructability constraints require a higher water percentage, resulting in a higher amount of clinker for the same structural strength. The optimal minimal thickness for floor slabs aimed at reducing environmental impact is 40mm, based on the manufacturability and the aggregate size.

- The optimization process of the 2400 x 3600 mm and 5400 x 3600 mm floor-slabs results in structures that not only work in membrane action but also utilized bending. This shows the relationship between structural optimality versus minimizing material with casting constraints.

- The optimized result of the 5400 x 3600 mm floor showed double curvature with critical tensile stresses occurring on the top surface. This is likely due to a slight negative Gaussian curve, which allows the short span to carry the load of the longer span. Initially, I would have never thought of the optimal solution of concrete to exhibit Gaussian curvature.

- Bitmaps are an effective way to represent the casted flooring systems In a 2D medium. Tests within grasshopper showed they also provide an effective way to represent double-curved surfaces, which can accurately be translated to the original 3D solid by an algorithmic approach.

Section II's primary goal was the generation of the floor slabs that addresses the set hypothesis. This, in turn forms the bases of Section III, where the generated floor slabs will be evaluated in a virtual office building.

SECTION III

Comparison and evaluation

Image Source: https://www.tugraz.at/index.php?id=36358

6 Section III: Comparison and evaluation

This section starts with an elaboration on the floor slabs and the assumptions within the calculation. The environmental assessment will then be carried out. After this, the newly designed floor slab will be assessed by comparing it to ten conventional flooring systems and evaluating the new flooring system in a hypothetical office building.

For the environmental assessment, two different approaches will be applied here. The first approach is based on a reduction of CO_2 emissions. The second method is a fast track LCA analysis comparing the floor slab to other flooring systems. The primary focus will be on the 5400 mm x 3600 mm floor slab based on the availability of data.

- Approach 1: Reduction of CO_2 emissions in kg
- Approach 2: LCA comparison with other floor slabs

The first measure of sustainability is CO_2 emissions in the product stage A1–A3. The second is a fast track LCA analysis. The reason for using two methods is data availability and the impossibility of doing a full LCA of different flooring systems. In a fast track analysis, small inaccuracies might occur as the LCA evaluations are carried by various entities (NIBE and NMD 2.3), and the background information on LCA is not publicly available.

Both of these methods will give a good indication of whether the environmental impact of concrete construction can be reduced. Additionally, the floor slab will be compared in a hypothetical office building to show its effective impact on a building scale. Throughout the process, assumptions will be elaborated.

6.1 LCA analysis of the new floor

The environmental impact from the production stage (A1–A3) of the given floor slabs results from the raw material supply, the transport, and the manufacturing of the concrete floor slabs. The data used to calculate the environmental impact is primarily based on the amount of material required and the data provided by the NMD 2.3. This includes:

- Process emissions in the production of the material
- Additional auxiliary materials and additives needed to produce the material up to a mass percentage of 1%
- Transport, storage of the material, and potential failure of the product
- Cleaning processes of water and air (also when required externally)
- Recycling and processing of the production waste
- Production, maintenance, and disposal of equipment (if greater than 5%).
- Overhead processes (offices, etc.) are disregarded
- All processes from the direct suppliers related to the material
- Transport of the product from the supplier to the producer
- Return transport of the empty trucks

As stated earlier, the product stage accounts for 60% to 80% of the environmental-related emissions. It is critical that in the processing of the materials, the material is handled efficiently because it is hard to indicate the production losses, material efficiency, and the impact of the reusable formwork during the prefabrication of the floor slab. Additionally, the impact is location-dependent, making a precise comparison of products difficult. A conservative 20% increase in emissions is therefore assumed, which is primarily based on:

- Material losses during the fabrication process of the structural floor (5%)
- Emissions related to the auxiliary materials and reusable formwork (5%)
- Emissions related to the transport of the product (5%)
- Unforeseen emissions, such as packaging, cleaning processes, rationalization of the design (5%)

The total calculation will give a conservative value of the environmental impact of a floor slab system in the product stage (A1–A3). To put the 20% safety factor in perspective, (Kong, Kang, He, Li, & Wang, 2020) studied the impact of the emissions of the raw materials in the entire construction process of prefabricated floor slabs. They concluded that the raw material accounts for 85.4% of total emissions in the product stage (A1–A3) and nearly 83% in the entire construction process.

6.1.1 Calculation of the structural weight

As stated earlier, environmental impact is based on material-related emissions, including a 20% increase in emissions due to material loss, formwork, unforeseen emissions, and transport. The material-related emissions are, in turn, based on the volume in the structure and the data provided by the NMD 2.3. This relates to the two materials in the floor slab system: concrete and steel.

- *Concrete volume in the floor*
  The volume of concrete is calculated based on the volume of the B-rep presentation of the floor slab. This was one of the primary objective values and can be directly exported from the script

- *Steel volume in the floor*
  The steel volume consists of two parts of the floor, the steel connection nodes, and the steel tension ties. The thickness of the structural nodes is not optimized within the process. For the calculations here, they are assumed to be twice the thickness of the steel tension tie, resulting in a minimum thickness of 34 mm. The resulting node is shown in Figure 117.

  The dimension of the steel tension ties is calculated automatically based on the strength of the DIN3064 6 x 36 Warrington-Seale+Steelcore cable. While the volume and weight are easily calculated, there is a third issue: the unavailability of the environmental impact data of DIN3064 steel. Thus, its environmental impact will be assumed here based on the data available for reinforcement steel in NMD 2.3and modified with a safety factor of 2.

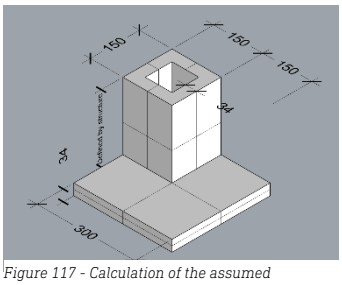

Figure 117 - Calculation of the assumed thickness for the connection node of the 3600 mm x5400 mm floor slab

Life cycle assessment data in the NMD is based on the weight in kg. Therefore the volumes have to be converted to weight. The density of steel varies from 7.75 to 8.05 g/cm^3, and the most conservative weight value is 8050 kg/m^3. For the concrete, a density of 2300 kg/m^3 is used, which is the same value given in the optimization process of both floor slabs. The weight of the DIN3064 tension ties is described by the supplier (Euro Cable) The resulting weight of the elements are summarized in table 15.

Table 15: Volume and the resulting weight of the floor slabs

Floor slabs	Volume of the concrete [M3]	Volume of the steel nodes [M3]	Steel: wires DIN3064 [-]	Weight of the concrete [kg]	Weight of the steel nodes [kg]	Weight of steel wire DIN 3064 [kg]
Floor slab 3600 mm x 2400 mm	5.14E-01	2.14E-01	3.8m x 9mm 7.2m x 12mm	1.19E+03	1.73E+02	5.95E+00
Floor slab 3600 mm x 5400 mm	1,44E+00	2,52E-01	7,2m x 14mm 10,8m x 17mm	3.31E+03	2.03E+02	1.67E+01

Now that we know the weight of the individual materials within the structure, we can calculate the environmental impact. Table 16 shows the data on the life cycle impact of the materials used and the associated shadow cost of each impact category. The shadow cost can expressed the environmental impact in comparable values, which allows for the evaluation of the cost of overall environmental impact, as explained in the background study, thereby comparing different LCA categories.

Table 16: LCA environmental impact of different materials.

Impact category	ABRR.		NMD 2.3 Concrete mortar C20/25 XC1 1 kg	Betonhuis: Concrete mortar c20/25 XC1 1 kg	Steel ecoinvent 3.4, 1 kg	Steel wire DIN 6468 (assumption: 1 kg)	Associated shadow cost in euros
Global warming potential	GWP	kg CO_2 eq.	2.20E+02	1.36E-03	1.36E-03	2.72E-03	€ 0.06
Ozone depletion potential	ODP	kg CFC-11 eq.	1.93E-05	0.00E+00	0.00E+00	0.00E+00	€ 30.40
Human toxicity potential	HTP	kg 1.4-DCB eq.	5.07E+01	1.82E-01	1.82E-01	3.64E-01	€ 0.16
Freshwater aquatic ecotoxicity	FWAE	kg 1.4-DCB eq.	1.13E+00	3.20E-03	3.20E-03	6.40E-03	€ 0.04
Marine aquatic ecotoxicity	MEA	kg 1.4-DCB eq.	5.30E-01	2.26E+01	2.26E+01	4.52E+01	€ 0.01
Terrestrial ecotoxicity	TE	kg 1.4-DCB eq.	9.94E-02	1.70E-03	1.70E-03	3.40E-03	€ 8.89
Photochemical oxidation	PO	kg C_2H_4 eq.	9.94E-01	5.40E-03	5.40E-03	1.08E-02	€ 2.10
Acidification potential	AP	kg SO_2 eq.	1.66E-01	6.00E-04	6.00E-04	1.20E-03	€ 5.40
Eutrophication potential	EP	kg PO_4 eq.	0.00E+00	0.00E+00	0.00E+00	0.00E+00	€ 311
Abiotic depletion potential	ADP	kg PO_4 eq.	2.20E+02	8.60E-03	8.60E-03	1.72E-02	€ 0.16

6.1.2 Environmental impact of the newly proposed system

Now that we have all the necessary information, we can calculate the environmental impact of the floor slabs. The calculation is done based on two different datasets, the NMD 2.3 and Betonhuis concrete. The calculations show that NMD 2.3 concrete is the more sustainable option, which is a mixture based on 280 kg/m^3 CEM III/B cement.[1] The resulting CO_2 emissions are calculated for a 3600 mm x2400 mm floor slab.

The integration of the extra 20% emissions results in 94.69 or 264.32 kg CO_2, respectively, and a total shadow cost of 133,43, 264 euros for the 3600 mm x5400 mm floor slab. The overall environmental impact and the results for the NMD 2.3 flooring system are shown in the table 17. The calculation of the floor slab based on the mixture of Betonhuis can be found in the appendix.

Table 17: Results Floor slab 3600 mm x 2400 mm NMD 2.3

			Emissions concrete	Emissions steel	Emissions steel	Total emissions per LCA category	Associated shadow cost
Global warming potential	GWP	kg CO_2 eq.	7.84E+01	8.09E-03	4.70E-01	7.89E+01	€ 4.50
Ozone depletion potential	ODP	kg CFC-11 eq.	6.88E-06	0.00E+00	0.00E+00	6.88E-06	€ 0.00
Human toxicity potential	HTP	kg 1,4-DCB eq.	1.81E+01	1.08E+00	6.29E+01	8.20E+01	€ 12.96
Freshwater aquatic ecotoxicity	FWAE	kg 1.4-DCB eq.	4.02E-01	1.90E-02	1.11E+00	1.53E+00	€ 0.06
Marine aquatic ecotoxicity	MEA	kg 1.4-DCB eq.	2.50E+03	1.34E+02	7.81E+03	1.04E+04	€ 78.90
Terrestrial ecotoxicity	TE	kg 1.4-DCB eq.	1.89E-01	1.01E-02	5.87E-01	7.87E-01	€ 6.99
Photochemical oxidation	PO	kg C_2H_4 eq.	3.55E-02	3.21E-02	1.87E+00	1.93E+00	€ 4.06
Acidification potential	AP	kg SO_2 eq.	3.55E-01	3.57E-03	2.07E-01	5.66E-01	€ 3.05
Eutrophication potential	EP	kg PO_4 eq.	5.91E-02	0.00E+00	0.00E+00	5.91E-02	€ 0.18
Abiotic depletion potential	ADP	kg PO_4 eq.	0.00E+00	5.12E-02	2.97E+00	3.02E+00	€ 0.48
			TOTAL CO_2 emissions:	94.69 kg		TOTAL SHADOW COST:	€ 133.09

Table 18: Results Floor slab 3600 mm x 5400 mm NMD 2.3

			Emissions concrete	Emissions steel	Emissions steel	Total emissions per LCA category	Associated shadow cost
Global warming potential	GWP	kg CO_2 eq.	2.20E+02	2.27E-02	5.52E-01	2.20E+02	€ 12.56
Ozone depletion potential	ODP	kg CFC-11 eq.	1.93E-05	0.00E+00	0.00E+00	1.93E-05	€ 0.00
Human toxicity potential	HTP	Kg 1,4-DCB eq.	5.07E+01	3.03E+00	7.39E+01	1.28E+02	€ 20.16
Freshwater aquatic ecotoxicity	FWAE	kg 1,4-DCB eq.	1.13E+00	5.33E-02	1.30E+00	2.48E+00	€ 0.09
Marine aquatic ecotoxicity	MEA	kg 1,4-DCB eq.	6.99E+03	3.77E+02	9.18E+03	1.65E+04	€ 125.07
Terrestrial ecotoxicity	TE	kg 1,4-DCB eq.	5.30E-01	2.83E-02	6.90E-01	1.25E+00	€ 11.10
Photochemical oxidation	PO	kg C_2H_4 eq.	9.94E-02	9.00E-02	2.19E+00	2.38E+00	€ 5.00
Acidification potential	AP	kg SO_2 eq.	9.94E-01	1.00E-02	2.44E-01	1.25E+00	€ 6.74
Eutrophication potential	EP	kg PO_4 eq.	1.66E-01	0.00E+00	0.00E+00	1.66E-01	€ 0.52
Abiotic depletion potential	ADP	kg PO_4 eq.	0.00E+00	1.43E-01	3.49E+00	3.63E+00	€ 0.58
			TOTAL CO_2 emissions:	264.32 kg		TOTAL SHADOW COST:	€ 218.19

While conservative, the resulting total shadow costs of € 133.09 and € 218.19, respectively, look promising. For comparison, a lattice girder floor slab of 200 mm, with a span of 3600 mm x 5400 mm, results in 1823.47 kg of CO_2 and a shadow cost of € 382.04[2] (Haas, 2020).

[1] This means further optimization is possible.

[2] This calculation is based on the environmental impact data from Nederlands Instituut voor Bouwbiologie en Ecologie together with the shadow-cost from CE Delft (De Bruyn et al., 2018).

6.2 LCA analysis of conventional floors

As mentioned previously, in order to put these environmental emissions into perspective, other flooring systems must be compared. This will consist of flooring systems from the NMD 2.3 and the database of Environmental Classifications Construction products by "NIBE Nederlands Instituut Voor Bouwbiologie en Ecologie" (2019).

This chapter will start with an introduction and summary of each flooring system, with their respective environmental impact, CO_2 emissions, and shadow cost for a span of 3600 mm x 5400 mm . Once we know their impact, we can compare them with the new system inspired by thin-shell design proposed here. The data behind the life cycle assessment comes mostly from the NIBE. The shadow cost is calculated in accordance with the environmental price handbook by (De Bruyn et al., 2018).

The NIBE performs its environmental impact assessment based on the CML2-baseline. This is the same model on which the NMD 2.3 basis its calculations, therefore resulting in relatively good comparability. Additionally, NIBE focuses on flooring systems with a span of 5.4 m, which is the same span as the optimized floor slabs.

6.2.1 VBI hollow-core slab 150 mm green

VBI Hollow-core slab 150 mm green		
GWP	4.69E+02	€ 26.74
ODP	0.00E+00	€ 0.00
HTP	1.32E+02	€ 20.84
FWAE	3.50E+00	€ 0.13
MEA	1.91E+04	€ 144.37
TE	4.20E+00	€ 37.34
PO	2.00E-01	€ 0.42
AP	2.00E+00	€ 10.80
EP	4.00E-01	€ 1.24
ADP	2.30E+00	€ 0.37
Source NMD 2.3	Total CO_2 emissions	Associated shadow cost
	469.20 kg	**€ 242.25**

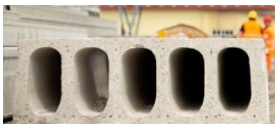

Image source: vbi.nl

Hollow-core slabs are known for their tubular voids, resulting in material saving and structural efficiency. This makes them a highly competitive flooring system when it comes to sustainability with a relatively low shadow cost and CO_2 footprint.

The VBI green is a hollow-core slab flooring system optimized for sustainability by the Dutch manufacturer VBI that aims on reducing CO_2. The use of this flooring system results in a relatively low CO_2 footprint of 469.20 kg per 19.44 meter for an area of 3600 mm x 5600 mm.(table to left).

More background information and an illustration of the hollow-core concept can be found in Chapter 5.3.3.

6.2.2 Dycore hollow-core slab 150 mm

Dycore Hollow-core slab 150 mm		
GWP	6.99E+02	€ 39.87
ODP	0.00E+00	€ 0.00
HTP	1.06E+02	€ 16.70
FWAE	3.40E+00	€ 0.13
MEA	1.69E+04	€ 127.82
TE	4.90E+00	€ 43.56
PO	0.00E+00	€ 0.00
AP	2.10E+00	€ 11.34
EP	4.00E-01	€ 1.24
ADP	2.60E+00	€ 0.42
Source NMD 2.3	Total CO_2 emissions	Associated shadow cost
	699.40 kg	**€ 241.07**

Image source: nbd-online.nl

The Dycore hollow-core slab is a regular hollow-core system by the manufacturer Dycore, which shares many similarities with the VBI hollow-core slab. In general, hollow-core systems are known for their low self-weight, the possibility of erecting long spans up to around 18 m, and their ease of constructability.

Interestingly, when comparing the VBI and Dycore flooring system, the resulting shadow costs turn out to be comparable (table to left). This shows that the "green" option is not automatically the most sustainable option.

6.2.3 Wooden hollow-core slab 280 mm

Wooden Hollow-core slab 280 mm		
GWP	9.18E+01	€ 5.23
ODP	0.00E+00	€ 0.00
HTP	3.60E+02	€ 56.82
FWAE	1.45E+01	€ 0.54
MEA	2.94E+04	€ 222.57
TE	2.70E+00	€ 24.00
PO	1.20E+00	€ 2.52
AP	4.50E+00	€ 24.30
EP	1.10E+00	€ 3.42
ADP	3.00E-01	€ 0.05
Source NMD 2.3	Total CO_2 emissions	Associated shadow cost
	91.80 kg	**€ 339.45**

Image source: biobasedbouwen.nl

Wooden hollow-core systems consist of wooden plates glued together, creating a rigid whole. The primary strength of wood-based systems is the reduction of CO_2 emissions. It should be noted that, the total environmental impact most often turns out to be worse due to the glue required in creating the flooring system.

Similar results also shows up when comparing the wooden system to the other floor slabs. While the CO_2 emissions are 4 to 5 times lower than the hollow-core alternatives, the overall shadow cost of the environmental emissions is higher due to the processing of the wood (table to left) (See also Chapter 6.3.)

6.2.4 European softwood beam floor 246 mm

European softwood beam floor 246 mm		
GWP	1.88E+02	€ 10.69
ODP	0.00E+00	€ 0.00
HTP	2.61E+02	€ 41.22
FWAE	9.50E+00	€ 0.35
MEA	3.46E+04	€ 261.88
TE	2.40E+00	€ 21.34
PO	9.00E-01	€ 1.89
AP	3.10E+00	€ 16.74
EP	8.00E-01	€ 2.49
ADP	1.40E+00	€ 0.22
Source NMD 2.3	Total CO_2 emissions	Associated shadow cost
	187.50 kg	**€ 356.82**

Image source: cobouw.nl

European softwood beam flooring systems have a long tradition in Dutch houses before 1980. After this date, they have mostly been used as flooring systems for attics. This is primarily due to the weight and the sound insulation properties of the wood. Similar to the wooden hollow-core system, their CO_2 emissions are significantly lower than the hollow-core systems.

Comparing wood and concrete shows the relationship between emissions and the used material. Once again, in addition to the reduction of CO_2 emissions, the structure results in a higher shadow-cost than with hollow-core construction systems (table to left).

6.2.5 Solid wooden floor 200 mm

Solid wooden floor 200 mm		
GWP	1.23E+03	€ 70.14
ODP	1.40E-04	€ 0.00
HTP	3.81E+02	€ 60.20
FWAE	1.28E+01	€ 0.47
MEA	4.16E+04	€ 314.51
TE	2.62E+00	€ 23.33
PO	1.08E+00	€ 2.26
AP	5.37E+00	€ 28.97
EP	9.29E-01	€ 2.89
ADP	3.42E-03	€ 0.00
Source NIBE	Total CO_2 emissions	Associated shadow cost
	1230.55 kg	**€ 502.78**

Image source: joostdevree.nl

Solid wooden floors are made of Cross Laminated Timber (CLT) plates. This results in a significant structural strength which, in turn, allows for lower heights of the flooring system. The key issue here is again the environmental impact of the adhesive used in the structural system which results in a significantly higher environmental footprint (table to left).

As of yet, there is no sustainable alternative to the adhesives. The products based on dowel laminated timber look the most promising, but an assessment of the environmental impact of rotational welding and high-temperature mechanical compression should be evaluated before drawing conclusions in regards to sustainability (Sotayo et al., 2020).

6.2.6 In-situ concrete floor (thickness 250 mm)

In-situ concrete floor 250 mm		
GWP	1.76E+03	€ 100.17
ODP	1.22E-04	€ 0.00
HTP	2.08E+02	€ 32.87
FWAE	7.25E+00	€ 0.27
MEA	2.86E+04	€ 216.04
TE	2.16E+00	€ 19.18
PO	3.83E-01	€ 0.80
AP	4.84E+00	€ 26.14
EP	8.53E-01	€ 2.65
ADP	1.77E-03	€ 0.00
Source NMD 2.3	Total CO_2 emissions	Associated shadow cost
	1757.40 kg	**€ 398.13**

Image source: skyrisecities.com

In-situ concrete floors are one of the more commonly used, conventional way of fabrication of floor slabs. They are formed by pouring concrete on-site, often within wooden formwork. It usually includes reinforcement across its entire area, resulting in a monolithic flat plate.

Simplicity is the primary strength of in-situ systems, which can be applied to any shape or object. No cranes are needed during construction. As the in-situ systems result in a monolithic slab, they are not known for good environmental impact. This is also evident in their total CO_2 emissions and the associated shadow cost (table to left)

6.2.7 Aerated concrete floor (thickness 200 mm)

In-situ concrete floor 250 mm		
GWP	1.58E+03	€ 90.20
ODP	8.03E-05	€ 0.00
HTP	1.92E+02	€ 30.41
FWAE	5.31E+00	€ 0.20
MEA	2.41E+04	€ 182.24
TE	1.93E+00	€ 17.20
PO	3.13E-01	€ 0.66
AP	3.44E+00	€ 18.58
EP	5.17E-01	€ 1.61
ADP	1.96E-03	€ 0.00
Source NMD 2.3	Total CO_2 emissions	Associated shadow cost
	1582.42	**€ 341.08**

Image source: skyrisecities.com

Aerated concrete floors exist of lightweight, precast, foam (concrete) blocks. The floor slab is made with regular cement with the addition of aluminum powder and chalk. This results in air bubbles within the slab. Due to the enclosed air, it has several advantages over regular concrete blocks such as good sound and heat insulation. Additionally, the air, significantly reduces the density to around 300 to 800 kg/m^3.

This allows for easy construction and handling. Additionally, it is easy to be shaped. When it comes to the environmental impact, it is lower than regular concrete, but higher when corrected it for its strength (table to left). Therefore it is not the best solution for sustainable construction systems.

6.2.8 Lattice girder floor slab (thickness 200 mm)

Lattice girder floor slab 200mm		
GWP	1.88E+03	€ 107.26
ODP	1.15E-04	€ 0.00
HTP	2.88E+02	€ 45.46
FWAE	7.25E+00	€ 0.27
MEA	3.27E+04	€ 246.90
TE	2.33E+00	€ 20.74
PO	5.83E-01	€ 1.22
AP	6.16E+00	€ 33.28
EP	9.35E-01	€ 2.91
ADP	1.39E-03	€ 0.00
Source NMD 2.3	Total CO_2 emissions	Associated shadow cost
	1881.792	**€ 458.04**

Image source: bft-international.com

The lattice girder floor slab is the successor of the in-situ flooring system. Basically, it consists of a prefabricated concrete slab with reinforcement embedded, which acts as a formwork for the cast in-site concrete. It shares most of the same advantages as in-situ fabrication but allows for a quicker fabrication onsite.

While sustainable fabrication is possible, the prefabrication often happens with high cementitious concretes for faster construction speed. This results in a higher environmental impact than in-situ fabrication (table to left).

All the above flooring systems were selected based on their comparability and their strengths. Several other flooring systems were included in the initial evaluation, but did not make it to the final comparison. These flooring systems and their environmental impact can be found in the excel in the appendix AA

6.3 LCA analysis of a hypothetical office building

A hypothetical office building will be used to assess here the performance of the floor slab with the integration of boundary conditions. This office building will be designed with three structural flooring systems: the new flooring system proposed in this thesis, a lattice girder floor, and a hollow-core slab system. (figure 118) The loading will be in accordance with Eurocode as defined earlier in Chapter 4.2.2.

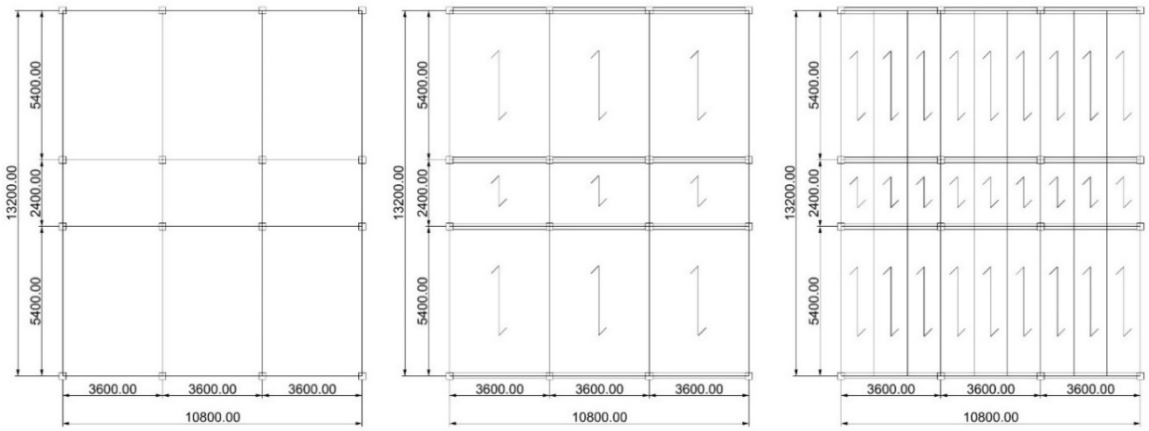

Figure 118 - Floorplan of the three flooring systems: left, the new flooring system proposed here; center, the lattice girder system; right the hollow-core slab system

6.3.1 Optimized flooring system

Two different spans were optimized for the hypothetical office building of the thin-shell inspired floor system, 2400 mm x 3600 mm, and 3600 mm x 5400 mm (Chapter 5.10). The environmental impact of these flooring systems is calculated in Chapter 6.1. The floor slab's environmental impact is based on data from the NMD 2.3 with CEMIII/B concrete.

In comparing emissions, aquatic ecotoxicity will not be taken into account as the number is entirely dominated by the inclusion of hydrogen fluoride (HF) emissions. This is often overlooked in the environmental assessments of the material or product and cannot be verified, as the background data of the NIBE and the NMD 2.3 is unavailable. Table 19 and 20 summarize the environmental impact of the floor slab in the product stage (A1–A3), without the inclusion of aquatic ecotoxicity.

Table 19: Overview of environmental impact optimized floor slab 3600 mm x 2400 mm (NMD 2.3 CEM III/B)											Source NMD 2.3
Impact category	GWP	ODP	HTP	FWAE	TE	PO	AP	EP	ADP		
Emissions floor slab	5,5	6.88E-06	8.20E+01	1.53E+00	7.87E-01	1.93E+00	5.66E-01	5.91E-02	3.02E+00	Total CO_2 emissions	94.68 kg
Shadow cost:	€ 4.50	€ 0.00	€ 12.96	€ 0.06	€ 7.00	€ 4.05	€ 3.06	€ 0.18	€ 0.48	Associated shadow cost	€ 38.74

Table 20: Overview of environmental impact optimized floor slab 3600 mm x 5400 mm (NMD 2.3 CEM III/B)											Source NMD 2.3
Impact category	GWP	ODP	HTP	FWAE	TE	PO	AP	EP	ADP		
Emissions floor slab	2.20E+02	1.93E-05	5.07E+01	1.13E+00	5.30E-01	9.94E-02	9.94E-01	1.66E-01	0.00E+00	Total CO_2 emissions	264.00 kg
Shadow cost:	€ 12.56	€ 0.00	€ 20.16	€ 0.09	€ 11.10	€ 5.00	€ 6.74	€ 0.52	€ 0.58	Associated shadow cost	€ 68.10

The full span of the floor requires the following elements:

- 6x Optimized floor slab: 3600 mm x 5400 mm (NMD 2.3 CEM III/B)
- 3x Optimized floor slab: 3600 mm x 2400 mm (NMD 2.3 CEM III/B)

This in total results in 1868 kg of CO_2 emissions and a total shadow cost of € 342.28 for the product stage (A1–A3) emissions of the hypothetical office building built with the new flooring system proposed here.

6.3.2 Lattice girder floor slab

The lattice girder floor slab is a prefabricated slab with reinforcement, which serves as permanent formwork for the final cast floor.

The lattice girder slab used in the hypothetical building consists of a 50 mm reinforced prefabricated slab, with continuous lattice girders acting as reinforcement (*Figure 119*). Lattice girder systems with a span of 5.4 meters result in 150 mm in-situ concrete with a 50 mm prefabricated slab, which together form a monolithic floor slab.

The lattice girder flooring system exists within the database of the NIBE (Nederlands Instituut voor Bouwbiologie en Ecologie) for a span of 5.4 meters. The NIBE will be used as a basis for calculating the environmental impact excluding aquatic ecotoxicity. The shadow cost will be calculated based on the environmental prices handbook by (De Bruyn et al., 2018).

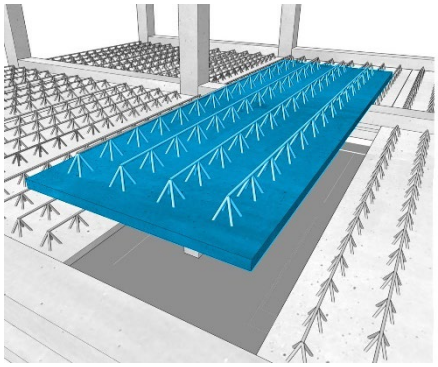

Figure 119 – Lattice girder system. Adapted from: Saraschok.com

Table 21: Lattice girder 3600 mm x 5400 mm (calculated by NIBE)										Source NMD 2.3	
Impact category	GWP	ODP	HTP	FWAE	TE	PO	AP	EP	ADP		
Environmental emissions	1.88E+03	1.15E-04	2.88E+02	7.25E+00	2.33E+00	5.83E-01	6.16E+00	9.35E-01	1.39E-03	Total CO_2 emissions	1881.8 kg
Shadow cost:	€ 107.26	€ 0.00	€ 45.46	€ 0.27	€ 20.74	€ 1.22	€ 33.28	€ 2.91	€ 0.00	Associated shadow cost	€ 211,.14

Table 21 shows the environmental impact and shadow cost of the 3600 mm x 5400 mm floor span. The floor slab of the 3600 mm x 2400 mm can most likely be optimized for a lower structural depth, and therefore lower emissions, but for an accurate comparison, the same structural depth will be used. This resulted in the following environmental impact for the 3600 mm x 2400 mm floor slab. (table 22)

Table 22: Lattice girder 3600 mm x 2400 mm (calculated by NIBE)										Source NMD 2.3	
Impact category	GWP	ODP	HTP	FWAE	TE	PO	AP	EP	ADP		
Environmental emissions	8.36E+02	5.11E-05	1.28E+02	3.22E+00	1.04E+00	2.59E-01	2.74E+00	4.16E-01	6.19E-04	Total CO_2 emissions	836.4 kg
Shadow cost	€ 47.67	€ 0.00	€ 20.20	€ 0.12	€ 9.22	€ 0.54	€ 14.79	€ 1.29	€ 0.00	shadow cost	€ 93.84

The lattice girder floor slab, as calculated by NIBE, is based on CEM I concrete for faster construction speed. CEM I releases 2.3 times more CO_2 emissions than CEMIII/B (Chapter 5.5.3). Therefore, the lattice girder system will also be optimized using hand calculations. A lattice girder floor system (span 5400 mm) contains around 480 kg concrete and 18.9 kg of reinforcing steel (Haas, 2020). Using the same concrete as in the optimized floor slab results in the following environmental emissions and shadow cost. (Table 23/24)

Table 23: Lattice girder 3600 mm x 5400 mm (NMD 2.3 CEM III/B concrete)										Source NMD 2.3	
Impact category	GWP	ODP	HTP	FWAE	TE	PO	AP	EP	ADP		
Emissions concrete	6.19E+02	5.43E-05	1.43E+02	3.17E+00	1.49E+00	2.80E-01	2.80E+00	4.67E-01	0.00E+00		
Emissions steel	5.00E-01	0.00E+00	6.69E+01	1.18E+00	6.25E-01	1.98E+00	2.20E-01	0.00E+00	3.16E+00	Total CO_2 emissions	619.00 kg
Shadow cost	€ 35.31	€ 0.00	€ 33.16	€ 0.16	€ 18.80	€ 4.75	€ 16.31	€ 1.45	€ 0.51	shadow cost	€ 110.45

Table 24: Lattice girder 3600 mm x 2400 mm (NMD 2.3 CEM III/B concrete)										Source NMD 2.3	
Impact category	GWP	ODP	HTP	FWAE	TE	PO	AP	EP	ADP		
emissions Concrete	2.76E+02	2.42E-05	6.37E+01	1.41E+00	6.64E-01	1.25E-01	1.25E+00	2.08E-01	0.00E+00		
Emissions steel	2.23E-01	0.00E+00	2.98E+01	5.26E-01	2.78E-01	8.82E-01	9.80E-02	0.00E+00	1.41E+00	Total CO_2 emissions	275.68 kg
Shadow cost:	€ 15.73	€ 0.00	€ 14.77	€ 0.07	€ 8.37	€ 2.11	€ 7.26	€ 0.65	2.25E-01	shadow cost	€ 49.19

The difference in emissions between the two materials shows the importance of decoupling construction speed from the curing time of concrete. This is a good example of the advantages of prefabrication. It should be noted that the construction with the CEMIII/B concrete is unlikely, as the speed of setting is not decoupled from the construction speed in lattice girder floor slabs. This comparison does give insight into the impact of the material. Thus, the CEMIII/B based floor will also be used in the evaluation of the floor slabs. The total flooring system will consist of the following elements:

- 6x Lattice girder 3600 mm x 5400 mm
- 3x Lattice girder 3600 mm x 2400 mm
- 43.2 m Beam to support the lattice girder

6.3.3 Hollow-core slab

Hollow-core slabs are another alternative to monolithic slabs. The slab has tubular voids over the entire length of the slab, thereby resulting in a lighter flooring system (Chapter 6.2). The lower weight produces by a reduction in material reduces the environmental impact and transportation costs. The slabs are typically 1200 mm wide, 150 mm to 400 mm thick, and are prefabricated. Hollow-core slabs are known for their material efficiency and hence their sustainability. For comparison, two different flooring systems will be compared:

- Dycore hollow-core slab 150 mm
- VBI hollow-core slab 150 mm green

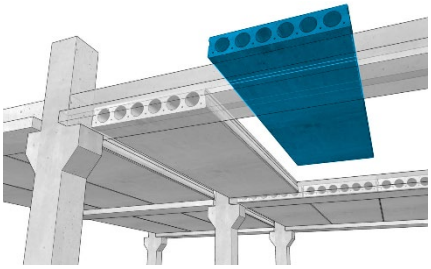

Figure 120 – Lattice girder system. Adapted from: Saraschok.com

The hollow-core slab fabricated by VBI is optimized for sustainability and thus the perfect candidate for comparison. Both flooring systems exist within the NMD database. Like the other floor slabs, the shadow cost is calculated by the shadow cost defined by CE Delft. Table 25 and 26 show the environmental impact of one Dycore Hollow-core floor slab (1200 mm x 150 mm) for the floor span of 3600 x 5400 mm.[1]

Table 25: Dycore hollow-core slab 5400 mm x 1200 mm x 150 mm											Source NMD 2.3
Impact category	GWP	ODP	HTP	FWAE	TE	PO	AP	EP	ADP		
Environmental emissions	2.33E+02	0.00E+00	3.52E+01	1.13E+00	1.63E+00	0.00E+00	7.00E-01	1.33E-01	8.67E-01	Total CO_2 emissions	233.13 kg
Shadow cost	€ 13.29	€ 0.00	€ 5.57	€ 0.04	€ 14.52	€ 0.00	€ 3.78	€ 0.41	€ 0.14	Associated shadow cost	€ 37.75

Table 26: Dycore hollow-core slab 2400 mm x 1200 mm x 150 mm											Source NMD 2.3
Impact category	GWP	ODP	HTP	FWAE	TE	PO	AP	EP	ADP		
Environmental emissions	9.99E+01	0.00E+00	1.51E+01	4.86E-01	7.00E-01	0.00E+00	3.00E-01	5.71E-02	3.71E-01	Total CO_2 emissions	99.91 kg
Shadow cost	€ 5.70	€ 0.00	€ 2.39	€ 0.02	€ 6.22	€ 0.00	€ 1.62	€ 0.18	€ 0.06	shadow cost	€ 16.18

Table 27 and 28 summarize the environmental impact of the hollow-core slab (1200 mm x 150 mm) green by VBI.

Table 27: VBI hollow-core green slab 5400 mm x 1200 mm x 150 mm											Source NMD 2.3
Impact category	GWP	ODP	HTP	FWAE	TE	PO	AP	EP	ADP		
Environmental emissions	1.56E+02	0.00E+00	4.40E+01	1.17E+00	1.40E+00	6.67E-02	6.67E-01	1.33E-01	7.67E-01	Total CO_2 emissions	156.40 kg
Shadow cost	€ 8.91	€ 0.00	€ 6.95	€ 0.04	€ 12.45	€ 0.14	€ 3.60	€ 0.41	€ 0.12	shadow cost	€ 32.63

Table 28: VBI hollow-core green slab 2400 mm x1200 mm x 150 mm											Source NMD 2.3
Impact category	GWP	ODP	HTP	FWAE	TE	PO	AP	EP	ADP		
Environmental emissions	6.70E+01	0.00E+00	1.88E+01	5.00E-01	6.00E-01	2.86E-02	2.86E-01	5.71E-02	3.29E-01	Total CO_2 emissions	67.03 kg
Shadow cost	€ 3.82	€ 0.00	€ 2.98	€ 0.02	€ 5.33	€ 0.06	€ 1.54	€ 0.18	€ 0.05	shadow cost	€ 13.98

Like the lattice girder floor, the hollow-core flooring system requires additional support beams. The total flooring system based on hollow-core slabs consists of the following elements:

- 18 x Dycore/VBI hollow-core slab 5400 mm x 1200 mm x 150 mm (data from NMD 2.3)
- 9 x Dycore/VBI hollow-core slab 2400 mm x 1200 mm x 150 mm (data from NMD 2.3)
- 43.2 m Beam to support the hollow-core slabs

[1] Floor slabs can also have a span covering the total flooring length, but this results in a higher environmental impact due to the extra height required. Hence, the same span will be used as in the lattice girder system.

6.3.4 The impact on the building scale

As shown in Figure 121, the hollow-core and the lattice girder have different support conditions than the hollow-core based system. Thus, an appropriate support beam must be fitted to meet the required support conditions.

6.3.4.1 Support condition

The beam used as support for the two flooring systems was selected for a calculated Q-load of 38 kN and optimized for weight. This resulted in a THQ 150 mm x 5 mm to190 mm x 12 mm to 400 mm x 8 mm beam as the best option, with a weight of 55.8 kg/m. SFB, and IFB beams resulted in more steel, and therefore a higher environmental impact. For the edge beams, the Q-load is a factor 0.75 lower, 30.4kN. As the difference is minor and the difference in environmental impact neglectable, the same THQ 150 beam will be used. To calculate the environmental impact of the support beam, the structural weight was used as input data for an environmental assessment. Table 29 the environmental impact of the THQ 150 mm x 5 mm to 190 mm x 12 mm 400 mm x 8 mm beam per meter.

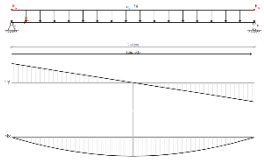

Figure 121 - Simple calculation for supported beam

Table 29: THQ 150 mm x 5 mm to 190 mm x 12mm to 400 mm x 8 mm beam											Source NMD 2.3	
Impact category	GWP	ODP	HTP	FWAE	TE	PO	AP	EP	ADP	GWP		
Environmental emissions	7.59E-02	0.00E+00	1.02E+01	1.79E-01	1.26E+03	9.49E-02	3.01E-01	3.35E-02	0.00E+00	4.80E-01	Total CO_2 emissions	00.08 kg
Shadow cost	€ 0.00	€ 0.00	€ 1.60	€ 0.01	€ 9.53	€ 0.84	€ 0.63	€ 0.18	€ 0.00	€ 0.08	Associated shadow cost	€ 12.88

Now that we know the environmental impact of the individual flooring elements and support beams, we can now calculate the impact of the overall flooring systems.

6.3.4.2 Optimized flooring system

The optimized flooring system of the following elements:

- 6x Optimized floor slab: 3600 mm x 5400 mm (NMD 2.3 CEM III/B)
- 3x Optimized floor slab: 3600 mm x 2400 mm (NMD 2.3 CEM III/B)

The new floor slab results in a total CO_2 emission of 1868 kg and a shadow cost of 343.28 euros. Table 30 shows the impact of the individual elements of the floor slab and the shadow costs related to individual impact categories.

Table 30: Overall impact of the optimized floor slab (NMD 2.3 CEM III/B)										Source NMD 2.3	
Impact category	GWP	ODP	HTP	MEA	TE	PO	AP	EP	ADP		
3600 mm x 5400 mm floor x6	1.32E+03	1.16E-04	3.04E+02	6.78E+00	3.18E+00	5.96E-01	5.96E+00	9.96E-01	0.00E+00		
3600 mm x 2400 mm floor x3	2.37E+02	2.06E-05	2.46E+02	4.59E+00	2.36E+00	5.79E+00	1.70E+00	1.77E-01	9.06E+00	Total CO_2 emissions	1868.0 kg
Shadow cost total floor	€ 88.73	€ 0.00	€ 86.93	€ 0.42	€ 49.26	€ 13.41	€ 41.37	€ 3.65	€ 1.45	shadow cost	€ 342.28

6.3.4.3 Lattice girder flooring system

The total lattice girder flooring system consists of the following elements:

- 6x Lattice girder 3600 mm x 5400 mm
- 3x Lattice girder 3600mm x 2400mm
- 43.2 m THQ 150x5 - 190x12 - 400x8 beam

- The CEMI based lattice girder floor slab results in a carbon footprint of 13,803 kg and a total shadow cost of 1693.05euros. Table 31 shows the impact of the individual elements of the floor slab and the shadow costs related to individual impact categories.

Table 31: Overall impact of the lattice girder flooring system (CEMI NIBE)										Source NMD 2.3	
Impact category	GWP	ODP	HTP	MEA	TE	PO	AP	EP	ADP		
3600 mm x 5400 mm floor x6	1.13E+04	6.89E-04	1.73E+03	4.35E+01	1.40E+01	3.50E+00	3.70E+01	5.61E+00	8.36E-03		
3600 mm x 2400 mm floor x3	2.51E+03	1.53E-04	3.84E+02	9.67E+00	3.11E+00	7.78E-01	8.22E+00	1.25E+00	1.86E-03		
43.2 m beam	3.28E+00	0.00E+00	4.39E+02	7.71E+00	4.10E+00	1.30E+01	1.45E+00	0.00E+00	2.07E+01	Total CO_2 emissions	13,803 kg
Shadow cost Total floor	€ 786.78	€ 0.03	€ 402.68	€ 2.25	€ 188.51	€ 36.32	€ 251.84	€ 21.33	€ 3.32	Associated shadow cost	€ 1,693.05

As stated earlier, the impact of clinker replacement in the production process of lattice girder floors was also evaluated. Table 32 shows the results of the CEMIII/B based lattice girder flooring system.

Table 32: Overall impact of the lattice girder flooring system (CEMIII/B concrete)											Source NMD 2.3
Impact category	GWP	ODP	HTP	FWAE	TE	PO	AP	EP	ADP		
3600 mm x 5400 mm floor x6	3.72E+03	3.26E-04	1.26E+03	2.61E+01	1.27E+01	1.36E+01	1.81E+01	2.80E+00	1.90E+01		
3600 mm x 2400 mm floor x3	8.28E+02	7.25E-05	2.80E+02	5.81E+00	2.83E+00	3.02E+00	4.03E+00	6.24E-01	4.22E+00		
43,2 m beam	3.28E+00	0.00E+00	4.39E+02	7.71E+00	4.10E+00	1.30E+01	1.45E+00	0.00E+00	2.07E+01	Total CO_2 emissions	**4548,0 kg**
Shadow cost total floor	€ 259.23	€ 0.01	€ 312.61	€ 1.46	€ 174.37	€ 62.15	€ 127.45	€ 10.65	€ 7.03	Associated shadow cost	**€ 954.97**

These results show a significant reduction of the carbon footprint and shadow cost. The CEMIII/B based floor has a total CO_2 emissions of 4547.98 kg, and a total shadow cost of 954.97 euros.

The decrease in emissions confirms the results of the literature research in this thesis into concrete manufacturing that indicate that integrating material-related aspects will result in a significant reduction in environmental impact (Chapter 4.6).

6.3.4.4 Hollow-core slab flooring system

The total flooring system based on hollow-core slabs consists of the following elements:

- 18 x Dycore/VBI hollow-core slab 5400 mm x 1200 mm x 150 mm (data from NMD 2.3)
- 9 x Dycore/VBI hollow-core slab 2400 mm x 1200 mm x 150 mm (data from NMD 2.3)
- 43.2 m THQ 150x5 - 190x12 - 400x8 beam

The flooring system based on Dycore hollow-core slabs results in total CO_2 emissions of 5098.91 kg and a total shadow cost of 969.81 euros. The calculation and the impact of the individual elements is shown in table 33.

Table 33: Overall impact of Dycore hollow-core slab flooring system											Source NMD 2.3
Impact category	GWP	ODP	HTP	FWAE	TE	PO	AP	EP	ADP		
3600 mm x 5400 mm floor x6	4.20E+03	0.00E+00	6.34E+02	2.04E+01	2.94E+01	0.00E+00	1.26E+01	2.40E+00	1.56E+01		
3600 mm x 2400 mm floor x3	8.99E+02	0.00E+00	1.36E+02	4.37E+00	6.30E+00	0.00E+00	2.70E+00	5.14E-01	3.34E+00		
43.2 m beam	3.28E+00	0.00E+00	4.39E+02	7.71E+00	4.10E+00	1.30E+01	1.45E+00	0.00E+00	2.07E+01	Total CO_2 emissions	**5098,91 kg**
Shadow cost total floor	€ 290.64	€ 0.00	€ 190.99	€ 1.20	€ 353.80	€ 27.34	€ 90.43	€ 9.06	€ 6.35	Associated shadow cost	**€ 969.81**

As stated earlier, the floor was also tested for the VBI green hollow-core slabs, which are optimized to reduce environmental impact,primarily CO_2. The results are shown in table 34

Table 34: Overall impact of VBI hollow-core slab flooring system											Source NMD 2.3
Impact category	GWP	ODP	HTP	MEA	TE	PO	AP	EP	ADP		
3600 mm x 5400 mm floor x6	2.82E+03	0.00E+00	7.91E+02	2.10E+01	2.52E+01	1.20E+00	1.20E+01	2.40E+00	1.38E+01		
3600 mm x 2400 mm floor x3	6.03E+02	0.00E+00	1.70E+02	4.50E+00	5.40E+00	2.57E-01	2.57E+00	5.14E-01	2.96E+00		
43.2 m beam	3.28E+00	0.00E+00	4.39E+02	7.71E+00	4.10E+00	1.30E+01	1.45E+00	0.00E+00	2.07E+01	Total CO_2 emissions	**3421.7 kg**
Shadow cost total floor	€ 195.04	€ 0.00	€ 221.15	€ 1.23	€ 308.46	€ 30.40	€ 86.50	€ 9.06	€ 6.00	Associated shadow cost	**€ 857.84**

This resulted in a reduction of the carbon footprint of 5098.9 kg to 4321.7 kg and a reduction of the carbon footprint from 969.81 to 857.84 euros. Now that we know all the information about the floor slabs, the results can be evaluated (see Chapter 6.5). However, the optimized floor slabs will first be compared to 10 conventional flooring systems.

6.4 Comparison of flooring systems (3600 mm x 5400 mm)

This chapter focuses on comparing the new flooring system proposed here to the ten flooring systems introduced earlier. As before, the comparison focuses on the product stage and includes a 20% increase in the emissions of the new floor slab (Chapter 6.2). It compares the floor slabs in regard to CO_2 reduction and total environmental impact.

6.4.1 Comparison of CO_2 emissions of floor slabs 3600 mm x 5400 mm

Table 35 shows the amount of CO_2 pollution in kg resulting from the production stage of ten 3600 mm x 5400 mm floor slabs. In evaluating the different floors, there is a clear relationship between the material used and the CO_2 emissions of the floor slabs. The figure below shows the environmental impact in a bar chart to allow for better comparability.

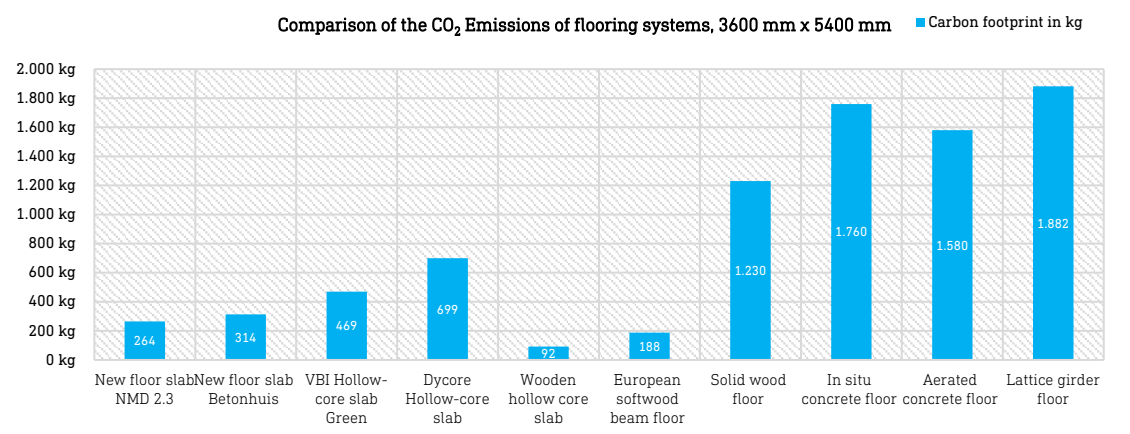

The bar chart shows that wooden systems allow for a significant reduction in CO_2 emissions. Additionally, the difference between hollow-core systems and in-site concrete floors shows the potential of reducing the impact by reduce the amount of material required.

Table 35: Comparison of the carbon footprint of the flooring systems	New floor slab NMD 2.3	New floor slab Betonhuis	VBI hollow-core slab Green	Dycore hollow-core slab	Wooden hollow-core slab	European softwood beam floor	Solid wood floor	In situ concrete floor	Aerated concrete floor	Lattice girder floor
Carbon footprint in kg	264,32 kg	313,71 kg	469,20 kg	699,40 kg	91,80 kg	188,00 kg	1230,00 kg	1760,00 kg	1580,00 kg	1881,79 kg
Overall reduction in CO_2	0,00%	-15,74%	-43,67%	-62,21%	187,93%	40,60%	-78,51%	-84,98%	-83,27%	-85,95%

Table 35 shows the reduction of CO_2 emissions of the newly proposed floor slabs in percentages. The new proposed floor slab proposed here made with the NMD 2.3 CEMIII/B concrete shows a significant decrease in CO_2 emissions compared to other concrete flooring systems. When compared to conventional flooring systems of concrete, a minimal reduction of 43.67% in CO_2 (hollow-core slab) will yield up to an 85.95% reduction of CO_2 emissions compared to the lattice girder flooring systems.[1]

Interestingly, there is a material impact of the floor built from the Betonhuis concrete mixture when compared to the mixture based on the NMD 2.3 of up to a 15.74% reduction in CO_2. This reduction is purely material based and shows the impact of optimizing the mixture. Structural engineers mostly optimize for the design strength class, for example, C20/C25). Changing this to designing with sustainability in mind, in collaboration with a concrete technologist, could easily reduce the environmental impact of concrete, especially if the environmental impact of CEM I types of cement, which are still commonly used worldwide, is taken into consideration.

Table 35 also shows that wood excels in reducing carbon emissions. The new floor slabs proposed here cannot compete against most wood-based flooring systems. The new floor slab shows an increase of 139.94% in CO_2 emissions compared to wooden hollow-core slabs, as well as an increase of 17% compared to European softwood beam flooring systems.

This is primarily due to the fact that wood-based systems perform really well in regard to CO_2 emissions, as trees absorb CO_2 through photosynthesis. Some wood-based systems even show a negative footprint in the product stage

[1] It should be noted that lattice girder flooring systems are still widely used. For example, the new Zalmhaven Toren (7500 m^2) in Rotterdam is built with lattice girder floor slabs. Changing the structural system of this tower could potentially reduce carbon emissions by 640,984 kg of CO_2 emissions.

(A1–A3), as the biogenic carbon that flows in plants can be accounted for in the removal of carbon dioxide from the atmosphere (Tellnes et al., 2017).

Interestingly, comparison based on CO_2 emissions also shows that the reduction of CO_2 emissions of wood-based systems cannot be generalized, as solid wood systems (CLT) result in significantly more carbon emissions due to process-related carbon emissions. Thus, while wooden hollow-core slabs and softwood wooden beam-floor systems perform better, a solid (CLT) system results in 87.48% more CO_2 emissions than the new flooring system proposed in this thesis.

In summary, the average reduction of the new flooring system is 58.19% compared to concrete based systems, even including a 20% safety factor. In the wooden floor system, the reduction varies from an increase of 139.94% to a reduction of 87.48% of emissions. It can be concluded that especially wooden hollow-core systems show excellent performance when it comes to the environmental emissions of CO_2, and as the biogenic carbon flows may even result in a positive carbon footprint. Concrete optimized floors, with a carbon sequestration curing process, will likely never be able to reach similar numbers.

6.4.2 Comparison of overall environmental impact (LCA)

The carbon footprint analyzed here is a subset of the larger environmental impact of a floor slab. While there is currently intense focus on CO_2 emissions due to the 2015 Paris Climate Change Conference (Rhodes, 2016), there are many other factors that are important. This is where the life cycle assessment comes into play, as a life cycle assessment systematically evaluates multiple environmental impacts of, in this case, a floor slab. Table 36 summarizes the environmental impact of the ten flooring systems that were calculated in Chapter 6.1 and 6.2

Table 36: Comparison of the environmental impactper category	New floor slab NMD 2.3 (240 mm)	New floor slab Betonhuis (240 mm)	VBI hollow-core slab Green (150 mm)	Dycore hollow-core slab (150 mm)	Wooden hollow-core slab (280 mm)	European softwood beam floor (246 mm)	Solid wood floor (200 mm)	In situ concrete floor (250 mm)	Aerated concrete floor (200 mm)	Lattice girder floor (200 mm)
Global warming potential	2.20E+02	3.14E+02	4.69E+02	6.99E+02	9.18E+01	1.88E+02	1.23E+03	1.76E+03	1.58E+03	1.88E+03
Ozone depletion potential	1.93E-05	1.51E-05	0.00E+00	0.00E+00	0.00E+00	0.00E+00	1.40E-04	1.22E-04	8.03E-05	1.15E-04
Human toxicity potential	1.28E+02	1.19E+02	1.32E+02	1.06E+02	3.60E+02	2.61E+02	3.81E+02	2.08E+02	1.92E+02	2.88E+02
Fresh water aquatic ecotoxicity	2.48E+00	2.34E+00	3.50E+00	3.40E+00	1.45E+01	9.50E+00	1.28E+01	7.25E+00	5.31E+00	7.25E+00
Marine aquatic ecotoxicity	1.65E+04	1.64E+04	1.91E+04	1.69E+04	2.94E+04	3.46E+04	4.16E+04	2.86E+04	2.41E+04	3.27E+04
Terrestrial ecotoxicity	1.25E+00	1.71E+00	4.20E+00	4.90E+00	2.70E+00	2.40E+00	2.62E+00	2.16E+00	1.93E+00	2.33E+00
Photochemical oxidation	2.38E+00	2.38E+00	2.00E-01	0.00E+00	1.20E+00	9.00E-01	1.08E+00	3.83E-01	3.13E-01	5.83E-01
Acidification potential	1.25E+00	1.28E+00	2.00E+00	2.10E+00	4.50E+00	3.10E+00	5.37E+00	4.84E+00	3.44E+00	6.16E+00
Eutrophication potential	1.66E-01	8.62E-02	4.00E-01	4.00E-01	1.10E+00	8.00E-01	9.29E-01	8.53E-01	5.17E-01	9.35E-01
Abiotic depletion potential	3.63E+00	5.62E+00	2.30E+00	2.60E+00	3.00E-01	1.40E+00	3.42E-03	1.77E-03	1.96E-03	1.39E-03

Because individual impact categories are not easily comparable, the shadow cost of the environmental impact is calculated here. This results in the comparability of the different environmental impact categories as equivalent values. As stated earlier, the comparison was made with the exclusion of aquatic ecotoxicity because hydrogen fluoride is often overlooked although it has a significant impact. Since it cannot be verified if the datasets include hydrogen fluoride, it is best if it is not included here.[1]

Table 37: Comparison of the environmental impact per category	New floor slab NMD 2.3 (240 mm)	New floor slab Betonhuis (240 mm)	VBI hollow-core slab Green (150 mm)	Dycore hollow-core slab (150 mm)	Wooden hollow-core slab (280 mm)	European softwood beam floor (246 mm)	Solid wood floor (200 mm)	In situ concrete floor (250 mm)	Aerated concrete floor (200 mm)	Lattice girder floor (200 mm)
Global warming potential	€ 12,56	€ 17,88	€ 26,74	€ 39,87	€ 5,23	€ 10,72	€ 70,11	€ 100,32	€ 90,06	€ 107,26
Ozone depletion potential	€ 0,00	€ 0,00	€ 0,00	€ 0,00	€ 0,00	€ 0,00	€ 0,00	€ 0,00	€ 0,00	€ 0,00
Human toxicity potential	€ 20,16	€ 18,86	€ 20,84	€ 16,70	€ 56,88	€ 41,24	€ 60,20	€ 32,86	€ 30,34	€ 45,46
Fresh water aquatic ecotoxicity	€ 0,09	€ 0,09	€ 0,13	€ 0,13	€ 0,54	€ 0,35	€ 0,47	€ 0,27	€ 0,20	€ 0,27
Terrestrial ecotoxicity	€ 11,10	€ 15,17	€ 37,34	€ 43,56	€ 24,00	€ 21,34	€ 23,29	€ 19,20	€ 17,16	€ 20,74
Photochemical oxidation	€ 5,00	€ 5,00	€ 0,42	€ 0,00	€ 2,52	€ 1,89	€ 2,27	€ 0,80	€ 0,66	€ 1,22
Acidification potential	€ 6,74	€ 6,92	€ 10,80	€ 11,34	€ 24,30	€ 16,74	€ 29,00	€ 26,14	€ 18,58	€ 33,28
Eutrophication potential	€ 0,52	€ 0,27	€ 1,24	€ 1,24	€ 3,42	€ 2,49	€ 2,89	€ 2,65	€ 1,61	€ 2,91
Abiotic depletion potential	€ 0,58	€ 0,90	€ 0,37	€ 0,42	€ 0,05	€ 0,22	€ 0,00	€ 0,00	€ 0,00	€ 0,00
	€ 56,75	**€ 65,08**	**€ 97,88**	**€ 113,25**	**€ 116,94**	**€ 94,98**	**€ 188,23**	**€ 182,25**	**€ 158,59**	**€ 211,14**

The table above shows the overall environmental impact of the ten flooring systems. To better understand the relationship between the materials and the environmental impact category, the relative impact of each category is visualized within the table.

[1] Note that wood-based construction systems often perform poorly in this category due to the adhesives required.

Figure 74 shows total environmental impact in a stacked bar chart to allow for easy comparison between the different types of floor slabs. Interestingly, the impact of wood-based systems becomes significantly worse when looking at the overall environmental impact versus the carbon footprint. This is primarily caused by the wood adhesives and VOC's required that result in high human toxicity and impact on human health (Jensen, Larsen, Mhave, Hansen, & Knudsen, 2001). The figure underneath compares overall emissions of the different types flooring systems and the primary source of the environmental impact. Table 38 shows the total shadow cost of the ten flooring systems, including the reduction in the environmental impact of the new flooring system proposed.

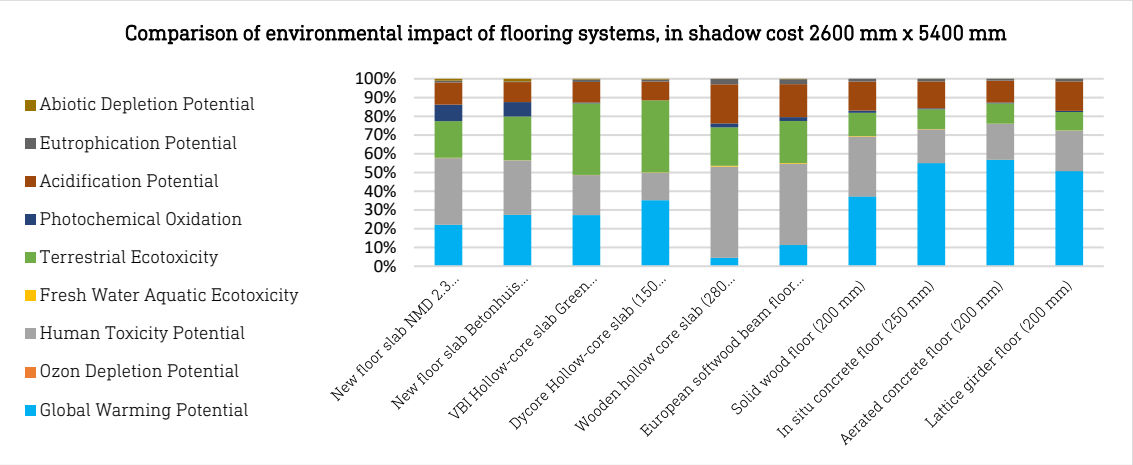

Interestingly, the reduction in the global warming potential due to the CEMIII/B is visible, the reduction in CO_2 means that it is no longer the primary source of pollution emitting from the floor slab. Instead, the potential for human toxicity is a major factor. What is also evident in the figure above is that the new floor slab proposed in this thesis requires less reinforcement steel than hollow-core slabs, which results in a lower percentage in terrestrial ecotoxicity. This shows the interesting relationship between the material and the environmental impact. Additionally, there is a considerable impact of human toxicity potential on the environmental footprint of wood-based construction, which accounts for 40% to 45% of the overall environmental impact.

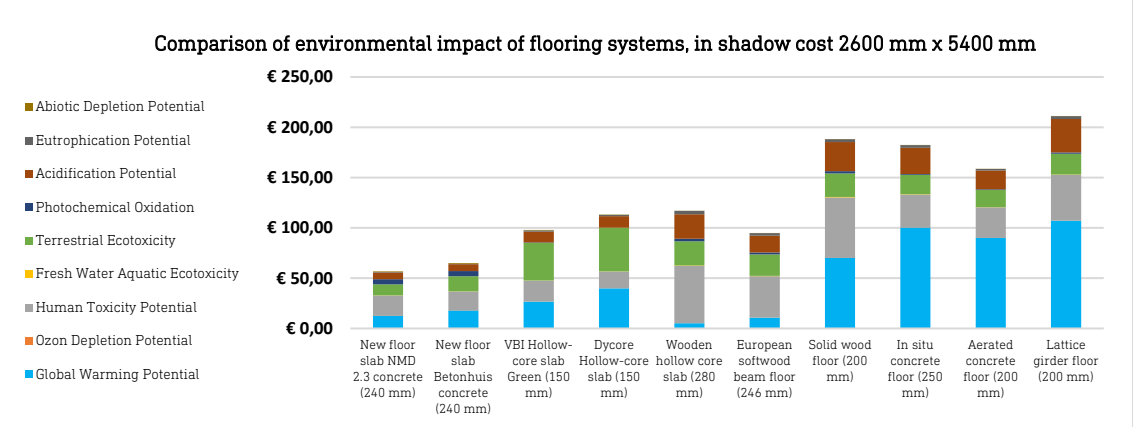

Table 38: Comparison of the carbon footprint of the flooring systems	New floor slab NMD 2.3	New floor slab Betonhuis	VBI hollow-core slab Green	Dycore hollow-core slab	Wooden hollow-core slab	European softwood beam floor	Solid wood floor	In situ concrete floor	Aerated concrete floor	Lattice girder floor
Total shadow cost:	€ 68.10	€ 93.71	€ 97.88	€ 113.25	€ 116.94	€ 94.98	€ 188.23	€ 182.25	€ 158.59	€ 211.14
Reduction in shadow cost:	0.00%	-27.33%	-30.43%	-39.87%	-41.76%	-28.30%	-63.82%	-62.63%	-57.06%	-67.75%

When comparing the total environmental impact by percentages in Table 38, it becomes clear that the new floor slab proposed in this thesis drastically reduces the overall shadow cost. The floor slab based on NMD 2.3 concrete shows a minimal reduction of 28.30% compared to the European softwood beam floor, a 30.43% reduction compared to the VBI flooring system, and up to a 67.75% reduction of emission compared to a lattice girder floor slab.

The reduction of environmental emissions shows the significance of integrating the material aspect and structural optimization in addressing climate-related issues. Additionally, it informs us that we should not blindly stare at the reduction of a carbon footprint because it may not automatically result in more sustainable construction.

Another factors that should be noted are the boundary conditions of the environmental impact analysis and the flooring systems. One example of this is the reduction of heating and cooling requirements by the addition of thermal mass in a building, which will reduce the energy requirements in the use stage of the building. Additionally, the flooring systems require different support conditions, thereby resulting in a larger environmental impact on the scale of a building.

6.5 Comparison of the flooring systems in a hypothetical office building

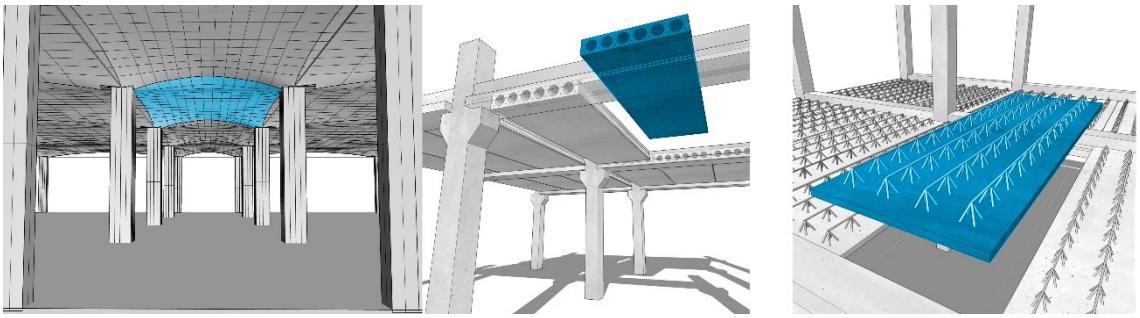

Figure 122 – Illustration of the three flooring systems: (left, the new flooring system proposed; center, the lattice girder system; right, the hollow-core slab system.

As stated earlier, the new flooring system proposed in this thesis will be compared to hollow-core slab and lattice girder systems in a hypothetical office building. The building consists of modules of a 10,080 mm x 13,200 mm grid, whereby the span is based on the required office standards and comparable building systems. Figure 122 offers a schematic rendering of the different structural systems. The systems are selected based on their comparability, performance, airtightness, and fire safety. It should be noted that monolithic floors (the lattice girder) are expected to have significantly more disk action than other flooring systems. In general, this is only a problem when disk action is required for stability, in which case a reinforced compression layer of 50 mm can be applied to the hollow-core system and the new flooring system. However, in general, no additional pressure layer is required for a regular office building with 5.4 m spans. Figure 122 shows a comparable office building with spans similar to those of the hypothetical office building.

6.5.1 Comparison of CO_2 emissions

The bar chart in Figure shows the carbon footprint in kg CO_2 of the flooring system in the hypothetical office buildings. Similar to the comparison of the floor slabs without support conditions, the new floor slab proposed in this thesis shows a significant decrease in CO_2 emissions compared to other flooring concrete flooring systems (Table 38). In the hypothetical office building, there is slightly better performance compared to the comparison of the individual floor slabs. This difference is likely caused by the optimization of the 2400 mm x 3600 mm spans, separately from the 5400 mm x 3600 mm span, as this results in a reduction of 304 kg CO_2.

Figure 123 - Construction of a building, in which the structure does not require a pressure layer.

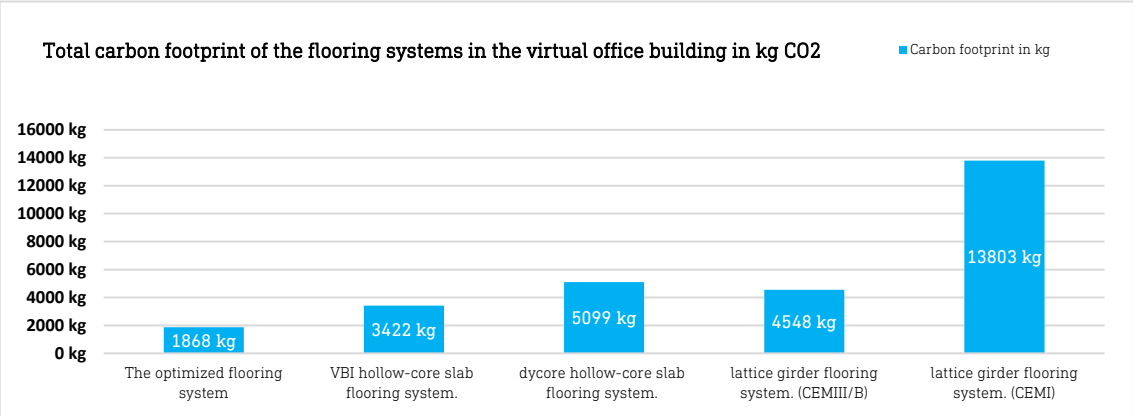

Table 38: Comparison of the carbon footprint of the flooring systems on a building scale	The optimized flooring system	VBI hollow-core slab flooring system.	dycore hollow-core slab flooring system.	lattice girder flooring system. (CEMIII/B)	lattice girder flooring system. (CEMI)
Carbon footprint in kg	1868 kg	3422 kg	5099 kg	4548 kg	13803 kg
Reduction in carbon footprint (%)	0.00%	-45.41%	-63.36%	-58.93%	-86.47%

The new floor slab has a CO_2 footprint of 1868 kg, which amounts to a reduction of 86.47% compared to lattice girder floor slabs (13,803 kg) and a 45.41% reduction compared to hollow-core systems optimized for a reduction of CO_2 (VBI Green 3422 kg). Interestingly, the lattice girder flooring system built with CEMIII/B cement results in a significant decrease in carbon emissions, even outperforming the Dycore hollow-core slab. This emphasizes the significance of clinker replacement strategies in addressing the carbon footprint (Chapter 4.4.3), which optimizes structures for early strength instead of 27-day strength. (Chapter 5.1.4).

6.5.2 Comparison of overall environmental impact (LCA)

As mentioned earlier, the carbon footprint analyzed here is a subset of the larger environmental impact of a floor slab. Table 39 shows the environmental impact of each LCA category. As in the earlier study, aquatic ecotoxicity will not be taken into account in the shadow costs, due to the impossibility of validating the dataset.

Table 39: Environmental emissions per category	Optimized flooring system	VBI hollow-core slab flooring system.	Dycore hollow-core slab flooring system.	Lattice girder flooring system. (CEMIII/B)	Lattice girder flooring system. (CEMI)
Global warming potential	1.87E+03	3.42E+03	5.10E+03	4.55E+03	1.51E+04
Ozone depletion potential	1.64E-04	0.00E+00	0.00E+00	3.98E-04	9.19E-04
Human toxicity potential	6.60E+02	1.40E+03	1.21E+03	1.98E+03	2.74E+03
Freshwater aquatic ecotoxicity	1.36E+01	3.32E+01	3.25E+01	3.96E+01	6.57E+01
Terrestrial ecotoxicity	6.65E+00	3.47E+01	3.98E+01	1.96E+01	2.28E+01
Photochemical oxidation	7.66E+00	1.45E+01	1.30E+01	2.96E+01	1.77E+01
Acidification potential	9.19E+00	1.60E+01	1.67E+01	2.36E+01	5.07E+01
Eutrophication potential	1.41E+00	2.91E+00	2.91E+00	3.43E+00	7.48E+00
Abiotic depletion potential	1.09E+01	3.75E+01	3.97E+01	4.39E+01	2.07E+01

In turn, Table 40 translates the environmental impact to the respective shadow cost of each category.

Table 40: Environmental emissions per category	The optimized flooring system	VBI hollow-core slab flooring system.	dycore hollow-core slab flooring system.	lattice girder flooring system. (CEMIII/B)	lattice girder flooring system. (CEMI)
Global warming potential	€ 106,48	€ 195,04	€ 290,64	€ 259,23	€ 858,28
Ozone depletion potential	€ 0,00	€ 0,00	€ 0,00	€ 0,01	€ 0,03
Human toxicity potential	€ 104,32	€ 221,15	€ 190,99	€ 312,61	€ 432,99
Fresh water aquatic ecotoxicity	€ 0,50	€ 1,23	€ 1,20	€ 1,46	€ 2,43
Terrestrial ecotoxicity	€ 59,11	€ 308,46	€ 353,80	€ 174,37	€ 202,34
Photochemical oxidation	€ 16,09	€ 30,40	€ 27,34	€ 62,15	€ 37,13
Acidification potential	€ 49,65	€ 86,50	€ 90,43	€ 127,45	€ 274,03
Eutrophication potential	€ 4,38	€ 9,06	€ 9,06	€ 10,65	€ 23,26
Abiotic Depletion potential	€ 1,74	€ 6,00	€ 6,35	€ 7,03	€ 3,32
	€ 342,28	**€ 857,84**	**€ 969,81**	**€ 954,97**	**€ 1.833,81**

Carbon emissions and their potential for global warming are the most significant polluter in cement-based construction systems, but by replacing clinker content, the effect of the carbon emissions can be reduced. This makes the effects of toxic substances on the human environment more significant in total shadow cost. Additionally, table 40 shows that the hollow-core systems show a higher terrestrial ecotoxicity than the other floor slabs. The reduction of concrete results in higher steel content which, in turn, results in higher terrestrial ecotoxicity.

Thus, an equilibrium exists with the optimization for overall environmental impact. Interestingly, this could mean that clinker replacement could result in lattice girder systems to become more sustainable than hollow-core alternatives, as was shown by the lattice girder flooring system based on CEMIII/B concrete.

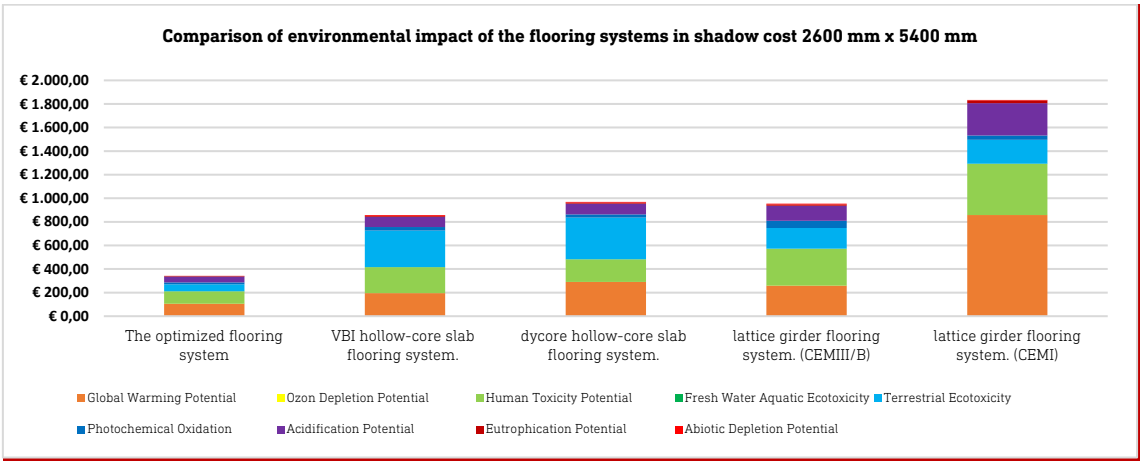

Table 41: Comparison of the carbon footprint of the flooring systems on a building scale	Optimized flooring system	VBI hollow-core slab flooring system.	Dycore hollow-core slab flooring system.	Lattice girder flooring system. (CEMIII/B)	Lattice girder flooring system. (CEMI)
Total Shadow cost: (euros)	€ 342.30	€ 857.80	€ 969.80	€ 955.00	€ 1693.00
Reduction of shadow cost (percentage)	0.00%	-60.10%	-64.71%	-64.16%	-79.78%

The bar chart together with table 41 compares the environmental impact of the flooring systems. The new floor slab proposed in this thesis shows a total shadow cost of 343.3 euros. The environmental footprint in shadow cost from the conventional structures ranges from 857.80 euros (VBI green hollow-core system) to 1693.80 euros (lattice girder system). This is a reduction in environmental impact of 60.10% to 79.78%, respectively. Interestingly, the lattice girder floor based on CEMIII/B cement outperformed the Dycore flooring system when it comes to overall environmental impact. This shows the impact of the material. It also illustrates that less optimized structural systems could result in a lower footprint by using cement with a lower clinker content.

6.6 Section III: Conclusion and key findings.

Section III focussed on a verification of the hypothesis by comparing the floor based on CO_2 and shadow cost, which is determined by performing an LCA analysis of the product stage (A1-A3). Herein the focus was on the comparison with conventional floor slabs for the span 5400 x 3600 mm and the performance in a hypothetical office building. Key findings from the comparison with 10 conventional flooring systems are:

- The new flooring system results in a reduction of 43.67% to 85.95% in carbon emissions compared to other concrete flooring systems. Additionally it shows an 30.43% to 67,75% reduction in overall environmental footprint. Whereby the VBI green hollow-core slab is the runner up in both shadow cost and CO_2.

  The new flooring system cannot compete against wooden-based flooring systems when it comes to CO_2 footprint. This is primarily as trees absorb CO_2 through photosynthesis, which is taken into account in the product phase. When compared on overall environmental impact the new flooring system performs better with a reduction of 28.30% in overall shadow cost. This shows the importance of an holistic approach to sustainability.

- The new flooring system results in a reduction of 28.30% to 67.75% reduction in overall environmental emissions. The most competitive floor slabs are the European softwood beam floor (28.30% increase) and the VBI hollow-core floor system. (43.57% increase)

Additionally, the floor is compared in a hypothetical office building to conventional concrete flooring systems. This resulted in the following key findings:

- In an office building the overall environmental footprint reduction ranges from 60.1% to 79.8%, to the hollow-core slab and lattice girder floor respectively. The reduction in carbon footprint also shows considerable saving. Reducing the footprint with a 45.4% to 68% respectively.

- The evaluation of the two lattice girder floors based on CEMI and CEMIII/b cement, verifies the literature research. A reduction in clinker content in the material significantly reduces the carbon footprint. This shows the importance of optimizing for early strength. (low clinker cements)

To summarize, thin-shell flooring systems result in a significant savings in both carbon footprint and shadow cost (overall footprint). When considering wooden systems, the floor is outperformed when it comes to CO_2 Emissions. But results in a lower shadow cost. This means that the structure is not only architecturally interesting, (figure 124) but also competes against both wooden-based and concrete flooring systems.

Figure 124 - illustration of the new flooring system applied within a hypothetical office building

Discussion

Limitations and future research

Image source: https://block.arch.ethz.ch/brg/project/full-scale-construction-prototype-nest-hilo-shell-roof

7 Discussion

This thesis showcased a derivative free approach on shape and size optimization using linear finite element analysis, to optimize floor slabs. Which focuses on the design of optimized floor-slabs in the early design phase. This chapter will focus on the limitations within the current optimization process and will set out directions for further research.

7.1 Limitations and suggestions for further research

Within the optimization process, several assumptions have been made. These include fixed supports, linear material behavior, and an approximation of the final form of the floor slab by a variable thickness shell. Initially, design by testing was within the scope of this thesis, verifying the structural calculations in Ansys and Karamba3D. The critical aspects regarding the thin-shell inspired floor slabs are listed below, with potential solutions and suggestions:

- *Robustness, brittle failure and ductility*
  Uncracked concrete without reinforcement is assumed in the optimization process of the shell, which would result in brittle behavior if failure occurs. Further studies should be carried out on the influence of fiber or textile reinforcements, as textile-reinforced shells do not result in a brittle failure modes (Tsangouri et al., 2020). Additionally, the increased tensile capacity provides robustness to the structure, and alternative loading paths through localized bending behaviour, Additionally it could result in a further reduction of material as tensile stresses are the critical stresses in both optimized flooring systems, with integrated casting constraints.

- *Diaphragm action*
  Floors usually also function as a medium to transfer the horizontal forces through diaphragm action. This often results in structural toppings in hollow-core slabs as integrating shear ties is difficult within the extrusion process. Similarly, it might result in a structural topping in the proposed flooring system, offsetting the saved emissions compared to lattice girder systems. While groin vaults are known for being able to transfer horizontal loads exceptionally well, the diaphragm action of the floor should be further studied to verify the material savings. Additionally, when a structural topping is required it results in a higher Q-load within the structure, therefore the optimization of the floor slab should be ran individually for the new situation to maximize the material savings.

- *Asymmetric loading*
  Unfavourable asymmetric distributed loads are often a critical loading condition in thin-shell systems. Possible localized stress concentrations or bending will result in critical tensile stresses as the failure mode for the flooring systems. Additionally non-linear behaviour and punching shear might occur due to asymmetric loading. This should be further evaluated using non-linear analysis.

- *Acoustic and vibration performance*
  The mass and minimal thickness of the structure is low. This reflects structural efficiency, but may have a detrimental impact on the acoustic and vibration performance. While the floor slab is thicker than most funicular flooring proposals, future studies should verify the vibration and acoustical performance of the floor slab.

- *Support displacement*
  The horizontal forces require steel tension ties with a high e-modulus to prevent lateral movement of the supports; this will become critical in structures serving larger spans. As the lateral restrain allows for the membrane action and prevents failure due to punching shear. Additionally, issues might arise with differential settlements of the support while serving limited issues in small displacements, because problems occur in thin shells for larger settlements (Hawkins, Orr, Ibell, & Shepherd, 2020).

- *Environmental impact analysis*
  While the best effort is made to perform a critical life cycle assessment of the different flooring systems, background information on the data from the NMD 2.3 and the NIBE is unavailable. The accuracy of the data can contribute to the inaccuracy of the environmental assessment. This is also the primary reason why freshwater ecotoxicity was excluded from the research. For a less conservative assessment, there is a need to produce accurate and transparent datasets for the Netherlands.

7.2 Future research

Key areas for future research, to bring the building sector one step closer to sustainability are listed below:

- The design, testing, and fabrication of thin shell flooring systems, with the focus on stay-in-place knitted formwork of non-corrosive materials. To act as reinforcement and to allow for a further reduction of clinker percentages, by decoupling steel and concrete in building structures.

- Verification of the structural concept in textile-reinforced shells, in a design by the testing framework. Additionally, testing the acoustic, dynamic, and vibration performance of the floor slab. To bring it one step closer to application.

- The investigation of the possibility of integrating the optimization process within a design for automatic fabrication framework. This is important as it allows for getting a good overview of the potentials to reduce carbon emissions and is an investigation in the scalability and cost of the concept.

- Research into the integration of horizontal restraining systems in conventional flooring systems allowing for membrane action to happen, as it can significantly increase the strength of flooring systems.

- Investigation of the influence of support displacements, what is the maximal span to height ratio for a floor system which works in membrane action, and when do systems which are optimized for bending become more efficient. Additionally the risk of punching shear increases with a reduction in lateral restraint, thereby likely being one of the primary failure modes as a result of support displacements for larger spans.

- Research into sustainable building materials, with the focus on increasing tensile strength while reducing the environmental impact. Additionally research should focus on the early strength development of materials as this is a key factor which withholds additive manufacturing from having a significant impact.

- Future studies should be on the cost efficient fabrication of columns with including column heads, as it allows for a significant material reduction in floor slabs by reducing the effective span. Especially hybrid approaches combining casting and additive manufacturing show potential.

Conclusions

Conclusion of the thesis

Image Source: https://www.tugraz.at/index.php?id=36358

8 Conclusions

This thesis focuses on the environmental impact of concrete construction by a hypothesis-driven design process. This final chapter presents the conclusions of the Masters thesis.

First, the research questions from the literature research are revisited and answered. Second, the results of the hypothesis-driven design will be summarized, and the effectivity of the proposed thin-shell inspired flooring system will be discussed. Afterwards, a critical overview of limitations and challenges is provided, together with the scientific and societal relevance. The thesis will conclude with a general discussion and potential further research.

8.1 Revisiting the research questions

This section gives detailed answers to the subquestions, each of which addresses an aspect of the primary research question: *In what manner can we use structural optimization and additive manufacturing in the building sector to address the environmental impact of concrete construction?*

The primary research question resulted in the following subquestions.

- *In what manner can we use additive manufacturing to address the environmental impact of concrete construction?*
- *In what manner can we use structural optimization to address the environmental impact of concrete construction?*
- *What are the different ways in which the environmental impact of concrete construction can be addressed?*

8.1.1 Additive manufacturing

Additive manufacturing techniques are unlikely to address the environmental impact of concrete construction as a primary fabrication method. For additive manufacturing to become game-changing, reinforcement, scalability, life cycle cost, and process-related material requirements need to be solved. Without solutions to these challenges, it is unlikely that innovative manufacturing methods will disrupt the industry towards a more sustainable paradigm.

The literature research and the current applications show that we should remain critical about the application of additive manufacturing as a sustainable solution. The focus should be on the process-related material requirements. Key examples are the requirement of the set-on-demand concretes of thin-shell hybrids manufacturing methods and an increase in clinker content to a minimum of 800kg/m^3 in 3DCP, which would result in environmental emissions of more than threefold compared to conventional construction. Future research should center on additive manufacturing with low emissions materials and the integration of the process-related material constraints.

8.1.2 Structural optimization

Raw material accounts for 85% of the overall emissions prefabricated concrete construction (Kong et al., 2020). Structural optimization aims for the efficient use of material within a structure. Therefore, structural optimization can already be considered as one of the key ways of addressing the environmental impact of concrete construction. Interestingly, the research into additive manufacturing illustrates the relationship between process-related material requirements and the environmental impact of the required material. This shows the importance of integrating the construction, design, and material constraints within the structural optimization process.

While much research is dedicated to concurrent manufacturability-oriented structural optimization, concurrent optimization processes come with the difficulty of remaining a clear objective function. Thus, derivative-free structural optimization methodologies – integrating the material related aspects – offer the greatest potential in addressing the environmental impact of concrete construction in the short term, whereby finite element analysis (FEA) or iso-geometric analysis (IGA) is used to define the objective values for structural performance. In turn, the global optimum can be best found using (surrogate) model-based optimization algorithms, because FEA and IGA calculations are computationally costly.

8.1.3 Concrete manufacturing process

In the production process of the raw material, it has been shown in this thesis that 90% of the emissions are related to the fabrication of the binder. This makes the binder generation process responsible for around 76% of the total environmental impact of concrete construction. Optimizing the binder manufacturing process would, therefore, be a highly effective way to reduce the environmental impact of concrete construction.

Several measures to optimize the binder production process are: decarbonizing transportation, increasing electricity efficiency, the use of alternative fuels, increasing kiln efficiency, and carbon capture and storage (CSS). Additionally, several optimization strategies are identified to reduce the amount of binder necessary, thereby decreasing the environmental impact of concrete construction:

- Optimizing the structure to reduce the quantity of concrete required
- Optimizing the structure to use concrete mortar with a lower binder percentage
- Optimizing the mix design with alternative binders

8.2 Conclusions on hypothesis-driven design

This research aimed to explore the potential in reducing the environmental impact of concrete construction. Based on hypothesis-driven design, the following hypothesis was explored: *Fabrication-aware, structurally optimized floor slabs can significantly reduce the environmental impact of concrete construction.*

The primary focus in the hypothesis-driven design is on simplicity over complexity, prefabrication, modularization, and casting as a primary manufacturing method in compliance with the current building regulations. This resulted in a derivative-free optimization methodology combining shape and size optimization, whereby the global optimum was found using a surrogate-based optimization solver.

This addressed a current gap in the literature in derivative-free concurrent optimization processes that took into account fabrication constraints to address the environmental impact of structures (Section II), The hypothesis put forth here was verified by creating two optimized floor slabs and comparing these floors to conventional flooring systems in a hypothetical office building.

Section III showed that a thin-shell inspired optimization process results in an overall environmental footprint reduction that ranges from 60.1% to 79.8%, compared to hollow-core slabs and a lattice girder floor, which support the hypothesis. When comparing the carbon emissions of the floor slab, the optimized flooring system also shows considerable savings, reducing the carbon footprint from 45.4% to 86.5%. This shows the impact of increasing the structural efficiency of the environmental footprint of structures.

This verifies the success of flooring systems inspired by thin-shells and confirms the hypothesis put forth in this thesis. Additionally, the proposed floor slab does not require support beams, providing extra structural efficiency while simultaneously minimizing the complexity of construction.

8.3 Societal relevance

To mitigate the increasing severity of climate change, we need to reduce greenhouse gas emissions by 55% to 85% before the year 2050 (Fisher & Nakicenovic, 2007). Concrete is responsible for around 8% of worldwide environmental emissions (Andrew, 2019), of which 50% is used within the building sector (Favier et al., 2018). Specifically, 59% of the concrete in building engineering is used in flooring (Wight & MacGregor, 2009). This makes concrete floors responsible for around 2.39% of environmental emissions. With a reduction of 45.4% to 86.5% of CO_2 emissions when compared to conventional flooring systems, this thesis emphasizes the potential of variable thickness, optimized shell-inspired flooring systems.

8.4 Scientific relevance

Recent publications show the scientific relevance of the subject of this thesis. For example, Liew, et al. (2017) generated a rib vaulted funicular slab resulting in 70% material savings (Liew, López, Van Mele, & Block, 2017). Similarly, Meibodi, et al. (2018) produced a smart slab, which also resulted in 70% material savings (Meibodi et al., 2018). These projects show the importance of an integrated design approach, as the rib vaulted funicular slab was built with 1000 kg/m^3 CEM I cement, completely offsetting the environmental impact, and the Smart Slab required four different manufacturing techniques.

While the structural concepts above show the effectivity of structural optimization, they also show the importance of integrating material and fabrication related aspects. Hawkins (2020) recently did his doctoral thesis on a similar investigation with fabrication in mind on constant thickness textile-reinforced shells that resulted in a reduction of 53% to 58% (Hawkins et al., 2020)

My thesis shows the potential of further reduction in concrete emissions with the inclusion of the infill – casting constraints – into the optimization process, resulting in a variable thickness shell. Additionally, it takes into account the material-related constraints, thereby allowing for clinker replacement.

Additionally, in the field of structural optimization, the research shows the strength of parametric modeling in combination with derivative-free optimization strategies to include fabrication constraints within structural optimization processes.

8.5 Concluding remarks

This Masters thesis started with the quote: "Although reinforced concrete has been used for over a hundred years and with increasing interest during the last decades, few of its properties and potentialities have been fully exploited so far. Apart from the unconquerable inertia of our own minds, which do not seem to be able to adapt freely any new ideas, the main cause of this delay is a trivial technicality: The need to prepare wooden frames." – Nervi, 1956

However, more than 50 years later, I am sad to report that we are still dependent on formwork. We, as the building industry, are currently entrusted with an immense responsibility when it comes to sustainability, which requires a paradigm shift in the way we build, manufacture, select, and use materials.

We do not necessarily need to eliminate formwork, but we do need to learn from the past. This works aims to inspire engineers and architects to follow the footsteps towards a paradigm with less environmental emissions.

9 References

Abergel, T., Dean, B., Dulac, J., & Hamilton, I. (2017). Global Status Report. Towards a zero-emission, efficient, and resilient buildings and construction sector. *International Energy Agency*.

Adriaenssens, S., Block, P., Veenendaal, D., & Williams, C. (2014). *Shell structures for architecture: form finding and optimization*: Routledge.

Ahangar, P., Cooke, M. E., Weber, M. H., & Rosenzweig, D. H. (2019). Current biomedical applications of 3D printing and additive manufacturing. *Applied sciences, 9*(8), 1713.

Allaire, G., & Jakabčin, L. (2018). Taking into account thermal residual stresses in topology optimization of structures built by additive manufacturing. *Mathematical Models and Methods in Applied Sciences, 28*(12), 2313-2366.

Amir, S. (2014). Compressive membrane action in prestressed concrete deck slabs.

Amir, S., van der Veen, C., Walraven, J., & de Boer, A. (2015). Punching shear capacity of bridge decks regarding compressive membrane action. *HERON, 60*(3), 235.

Andrade, C. (2019). Propagation of reinforcement corrosion: principles, testing and modelling. *Materials and Structures, 52*(1), 2.

Andrew, R. M. (2019). Global CO2 emissions from cement production, 1928–2018. *Earth System Science Data*, 1675-1710.

Anton, A., Jipa, A., Reiter, L., & Dillenburger, B. (2020). *Fast Complexity: Additive Manufacturing for Prefabricated Concrete Slabs*. Paper presented at the RILEM International Conference on Concrete and Digital Fabrication.

Asprone, D., Menna, C., Bos, F. P., Salet, T. A., Mata-Falcón, J., & Kaufmann, W. (2018). Rethinking reinforcement for digital fabrication with concrete. *Cement and Concrete Research, 112*, 111-121.

Attia, S., Hamdy, M., O'Brien, W., & Carlucci, S. (2013). Assessing gaps and needs for integrating building performance optimization tools in net zero energy buildings design. *Energy and Buildings, 60*, 110-124.

Austern, G., Capeluto, I. G., & Grobman, Y. J. (2018). Rationalization methods in computer aided fabrication: A critical review. *Automation in construction, 90*, 281-293.

Barbosa, F., Woetzel, J., & Mischke, J. (2017). *Reinventing Construction: A Route of Higher Productivity*. Retrieved from

Barbosa, F., Woetzel, J., Mischke, J., Ribeirinho, M. J., Sridhar, M., Parsons, M., . . . Brown, S. (2017). Reinventing construction: a route to higher productivity. *McKinsey Global Institute*.

Barnes, M. R. (1999). Form finding and analysis of tension structures by dynamic relaxation. *International journal of space structures, 14*(2), 89-104.

Beersaerts, G., Lucas, S. S., & Pontikes, Y. (2020). *An Fe-Rich Slag-Based Mortar for 3D Printing*. Paper presented at the RILEM International Conference on Concrete and Digital Fabrication.

Beheshti, Z., & Shamsuddin, S. M. H. (2013). A review of population-based meta-heuristic algorithms. *Int. J. Adv. Soft Comput. Appl, 5*(1), 1-35.

Bendsøe, M. P. (1989). Optimal shape design as a material distribution problem. *Structural optimization, 1*(4), 193-202.

Bendsoe, M. P., & Sigmund, O. (2013). *Topology optimization: theory, methods, and applications*: Springer Science & Business Media.

Benhelal, E., Zahedi, G., Shamsaei, E., & Bahadori, A. (2013). Global strategies and potentials to curb CO2 emissions in cement industry. *Journal of cleaner production, 51*, 142-161.

Blaauwendraad, J., & Hoefakker, J. H. (2013). *Structural Shell Analysis: Understanding and Application* (Vol. 200): Springer Science & Business Media.

Bos, F., Dezaire, S., Ahmed, Z., Hoekstra, A., & Salet, T. (2020). *Bond of reinforcement cable in 3D printed concrete*. Paper presented at the RILEM International Conference on Concrete and Digital Fabrication.

Bos, F., Wolfs, R., Ahmed, Z., & Salet, T. (2016). Additive manufacturing of concrete in construction: potentials and challenges of 3D concrete printing. *Virtual and Physical Prototyping, 11*(3), 209-225.

Brun, F., Gaspar, F., Mateus, A., Vitorino, J., & Diz, F. (2020). *Experimental Study on 3D Printing of Concrete with Overhangs*. Paper presented at the RILEM International Conference on Concrete and Digital Fabrication.

Buchanan, A. H., & Abu, A. K. (2017). *Structural design for fire safety*: John Wiley & Sons.

Buswell, R. A., da Silva, W. L., Bos, F. P., Schipper, H., Lowke, D., Hack, N., . . . Roussel, N. (2020). A process classification framework for defining and describing Digital Fabrication with Concrete. *Cement and Concrete Research, 134*, 106068.

Buswell, R. A., Silva, W. R. L. d., Jones, S. Z., & Dirrenberger, J. (2018). 3D printing using concrete extrusion: A roadmap for research. *Cement and concrete research : SI: Digital concrete 2018*, 37-49.

Butscher, A., Bohner, M., Hofmann, S., Gauckler, L., & Müller, R. (2011). Structural and material approaches to bone tissue engineering in powder-based three-dimensional printing. *Acta biomaterialia, 7*(3), 907-920.

Celani, G., & Vaz, C. E. V. (2012). CAD scripting and visual programming languages for implementing computational design concepts: A comparison from a pedagogical point of view. *International Journal of Architectural Computing, 10*(1), 121-137.

Challener, C. (2007). Fire safety with specialt coating. *JCT coatingstech, 4*(9), 78-84.

Chana, P., & Desai, S. (1992). Membrane action, and design against punching shear. *Structural Engineer, 70*(19).

Christensen, P. W., & Klarbring, A. (2008). *An introduction to structural optimization* (Vol. 153): Springer Science & Business Media.

Coenders, J., & Bosia, D. (2006). Computational tools for design and engineering of complex geometrical structures: From a theoretical and a practical point of view. *Game Set And Match II. On Computer Games, Advanced Geometries, and Digital Technologies. Episode Publishers*, 006.

Costa, A., & Nannicini, G. (2014). RBFOpt: an open-source library for black-box optimization with costly evaluations. *ht_tp://www_. optimization-online. org/DB_FILE/2014/09/4538. pdf*.

Craveiroa, F., Duartec, J. P., Bartoloa, H., & Bartolod, P. J. (2019). Additive manufacturing as an enabling technology for digital construction: A perspective on Construction 4.0. *sustainable development, 4*, 6.

Crippa, M., Oreggioni, G., Guizzardi, D., Muntean, M., Schaaf, E., Lo Vullo, E., . . . Vignati, E. (2019). Fossil CO2 and GHG emissions of all world countries. *Luxemburg: Publication Office of the European Union*.

Cubukcuoglu, C., Ekici, B., Tasgetiren, M. F., & Sariyildiz, S. (2019). OPTIMUS: Self-Adaptive Differential Evolution with Ensemble of Mutation Strategies for Grasshopper Algorithmic Modeling. *Algorithms, 12*(7), 141.

De Bruyn, S., Ahdour, S., Bijleveld, M., De Graaff, L., Schep, E., Schroten, A., & Vergeer, R. (2018). Environmental prices handbook 2017-methods and numbers for valuation of environmental impacts. *Delft: CE Delft*, 05-2018.

De Schutter, G., & Feys, D. (2016). Pumping of fresh concrete: insights and challenges. *RILEM Technical Letters, 1*, 76-80.

Derby, B. (2010). Inkjet printing of functional and structural materials: fluid property requirements, feature stability, and resolution. *Annual Review of Materials Research, 40*, 395-414.

Dillenburger, B., & Hansmeyer, M. (2014). Printing architecture: castles made of sand. *Gramazio, F. Kohler, M. and Langenberg, S.(eds) FABRICATE: negotiating design & making. Eidgenössische Technische Hochschule Zürich*.

Dillenburger, B., & Hansmeyer, M. (2019). Digital Grotesque II. In *Robotic Building: Architecture in the Age of Automation* (pp. 48-50): DETAIL.

Eisenbach, P. (2017). *Processing of Slender Concrete Shells-Fabrication and Installation*: kassel university press GmbH.

Environment, U., Scrivener, K. L., John, V. M., & Gartner, E. M. (2018). Eco-efficient cements: Potential economically viable solutions for a low-CO2 cement-based materials industry. *Cement and Concrete Research, 114*, 2-26.

Eschenauer, H. A., & Olhoff, N. (2001). Topology optimization of continuum structures: a review. *Appl. Mech. Rev., 54*(4), 331-390.

Favier, A., De Wolf, C., Scrivener, K., & Habert, G. (2018). *A sustainable future for the European Cement and Concrete Industry: Technology assessment for full decarbonisation of the industry by 2050*. Retrieved from

Fisher, B., & Nakicenovic, N. (2007). *Issues related to mitigation in the long-term context*. Retrieved from Cambridge:

Fu, J., Li, H., Gao, L., & Xiao, M. (2019). Design of shell-infill structures by a multiscale level set topology optimization method. *Computers & Structures, 212*, 162-172.

Gartner, E., & Sui, T. (2018). Alternative cement clinkers. *Cement and Concrete Research*, 27-39.

Gee, M., Ramm, E., & Wall, W. A. (2005). Parallel multilevel solution of nonlinear shell structures. *Computer Methods in Applied Mechanics and Engineering, 194*(21-24), 2513-2533.

Georgopoulos, C., & Minson, A. (2014). *Sustainable concrete solutions*: John Wiley & Sons.

Gervasio, H., & Dimova, S. (2018). Model for Life Cycle Assessment (LCA) of buildings. In: EUR.

Gibson, I., Rosen, D. W., & Stucker, B. (2014). *Additive manufacturing technologies* (Vol. 17): Springer.

Global Status Report: Towards a zero-emission, efficient and resilient buildings and construction sector. (2018). Retrieved from Paris:

Griffin, C. T., Reed, B., Hsu, S., & Cruz, P. (2010). Comparing the embodied energy of structural systems in buildings. *Struct. Archit*, 1367-1373.

Gutmann, H.-M. (2001). A radial basis function method for global optimization. *Journal of Global Optimization, 19*(3), 201-227.

Haas, M. (2020). NIBE-Milieuclassificatie Bouwmaterialen. *Naarden: Nederlands Instituut voor Bouwbiologie en Ecologie*.

Haber, R., & Abel, J. (1982). Initial equilibrium solution methods for cable reinforced membranes part I—formulations. *Computer Methods in Applied Mechanics and Engineering, 30*(3), 263-284.

Hafele, F. (2012). Soma architecture · New Foyer and Adaption of the Building Academy. .

Hasançebi, O., Çarbaş, S., Doğan, E., Erdal, F., & Saka, M. (2009). Performance evaluation of metaheuristic search techniques in the optimum design of real size pin jointed structures. *Computers & Structures, 87*(5-6), 284-302.

Häßler, M., Häßler, D., Hothan, S., & Krüger, S. (2019). Fire tests of steel tension rod systems with intumescent coating. *Journal of Structural Fire Engineering*.

Hawkins, W. (2019). Thin-shell Concrete Floors for Sustainable Buildings.

Hawkins, W., Orr, J., Ibell, T., & Shepherd, P. (2020). A design methodology to reduce the embodied carbon of concrete buildings using thin-shell floors. *Engineering Structures, 207*, 110195.

Huang, X., & Xie, M. (2010). *Evolutionary topology optimization of continuum structures: methods and applications*: John Wiley & Sons.

Ilunga, G., & Leitão, A. (2018). *Derivative-free Methods for Structural Optimization.* Paper presented at the Proceedings of the 36th eCAADe Conference, Lodz, Poland.

International Renewable Energy Agency. (2020). *Renewable Power Generation Costs in 2019*. Retrieved from

Irungu, S. N., Muchiri, P., & Byiringiro, J. B. (2017). The generation of power from cement kiln waste gases: a case study of a plant in Kenya. *Energy Science & Engineering*, 90-99.

ISO/ASTM 17296 Standard on additive manufacturing (AM) Technologies. (2015). In.

Jabi, W. (2013). *Parametric design for architecture*: Laurence King Publishing.

Jacobsen, S., & Jahren, P. (2002). *Binding of CO2 by carbonation of Norwegian OPC concrete.* Paper presented at the CANMET/ACI international conference on sustainability and concrete technology, Lyon.

Jaillon, L., & Poon, C. S. (2009). The evolution of prefabricated residential building systems in Hong Kong: A review of the public and the private sector. *Automation in construction, 18*(3), 239-248.

Jensen, L. K., Larsen, A., Mhave, L., Hansen, M. K., & Knudsen, B. (2001). Health evaluation of volatile organic compound (VOC) emissions from wood and wood-based materials. *Archives of Environmental Health: An International Journal, 56*(5), 419-432.

Jipa, A., Bernhard, M., Ruffray, N., Wangler, T., Flatt, R., & Dillenburger, B. (2019, 14 (1)). Fabricação de forma livre para uma canoa de concreto. *Gestão & Tecnologia De Projetos,* 25-44.

Jipa, A., Giacomarra, F., Giesecke, R., Chousou, G., Pacher, M., Dillenburger, B., . . . Leschok, M. (2019). *3D-printed formwork for bespoke concrete stairs: from computational design to digital fabrication.* Paper presented at the Proceedings of the ACM Symposium on Computational Fabrication.

Kajaste, R., & Hurme, M. (2016). Cement industry greenhouse gas emissions–management options and abatement cost. *Journal of cleaner production, 112*, 4041-4052.

Kong, A., Kang, H., He, S., Li, N., & Wang, W. (2020). Study on the Carbon Emissions in the Whole Construction Process of Prefabricated Floor Slab. *Applied sciences, 10*(7), 2326.

Koziel, S., & Yang, X.-S. (2011). *Computational optimization, methods and algorithms* (Vol. 356): Springer.

La Rosa, A. D., Recca, G., Summerscales, J., Latteri, A., Cozzo, G., & Cicala, G. (2014). Bio-based versus traditional polymer composites. A life cycle assessment perspective. *Journal of cleaner production, 74*, 135-144.

Lee, M., Mata-Falcón, J., Popescu, M., Block, P., & Kaufmann, W. (2020). *Potential Approaches for Reinforcing Complex Concrete Structures with Integrated Flexible Formwork.* Paper presented at the RILEM International Conference on Concrete and Digital Fabrication.

Lehne, J., & Preston, F. (2018). Making Concrete Change. *Innovation in Low-carbon Cement and Concrete*.

Lehne, J., & Preston, F. (2018). Making concrete change: Innovation in low-carbon cement and concrete. *Chatham House Reports, Energy environment and resources department*, 1-66.

Liew, A., López, D. L., Van Mele, T., & Block, P. (2017). Design, fabrication and testing of a prototype, thin-vaulted, unreinforced concrete floor. *Engineering Structures, 137*, 323-335.

Lilliestam, J., Bielicki, J. M., & Patt, A. G. (2012). Comparing carbon capture and storage (CCS) with concentrating solar power (CSP): Potentials, costs, risks, and barriers. *Energy policy, 47*, 447-455.

Lin, S.-H. E., & Gerber, D. J. (2014). Designing-in performance: A framework for evolutionary energy performance feedback in early stage design. *Automation in construction, 38*, 59-73.

Liu, J., Gaynor, A. T., Chen, S., Kang, Z., Suresh, K., Takezawa, A., . . . Wang, C. C. (2018). Current and future trends in topology optimization for additive manufacturing. *Structural and Multidisciplinary Optimization, 57*(6), 2457-2483.

Llatas, C. (2011). A model for quantifying construction waste in projects according to the European waste list. *Waste management 31(6),* 1261-1276.

Lloret, E., Shahab, A. R., Linus, M., Flatt, R. J., Gramazio, F., Kohler, M., & Langenberg, S. (2015, March). Complex concrete structures: Merging existing casting techniques with digital fabrication. *Computer-aided Design V.60,* 40-49.

López-Mesa, B., Pitarch, Á., Tomás, A., & Gallego, T. (2009). Comparison of environmental impacts of building structures with in situ cast floors and with precast concrete floors. *Building and Environment, 44*(4), 699-712.

Lowke, D., Dini, E., Perrot, A., Weger, D., Gehlen, C., & Dillenburger, B. (2018). Particle-bed 3D printing in concrete construction–possibilities and challenges. *Cement and Concrete Research, 112*, 50-65.

Lowke, D., Talke, D., Dressler, I., Weger, D., Gehlen, C., Ostertag, C., & Rael, R. (2020). Particle bed 3D printing by selective cement activation–Applications, material and process technology. *Cement and Concrete Research, 134*, 106077.

Lu, W., & Yuan, H. (2013). Investigating waste reduction potential in the upstream processes of offshore prefabrication construction. *Renewable and Sustainable Energy Reviews, 28*, 804-811.

Lucherini, A., & Maluk, C. (2019). Intumescent coatings used for the fire-safe design of steel structures: A review. *Journal of Constructional Steel Research, 162*, 105712.

Malaeb, Z., Hachem, H., Tourbah, A., Maalouf, T., Zarwi, N. E., & Hamzeh, F. (2015). 3D concrete printing: Machine and mix design. *IJCIET*, 14-22.

Malmqvist, J., Axelsson, R., & Johansson, M. (1996). *A comparative analysis of the theory of inventive problem solving and the systematic approach of pahl and beitz.* Paper presented at the Proceedings of the 1996 ASME Design Engineering Technical Conferences.

Mao, C., Shen, Q., Shen, L., & Tang, L. (2013). Comparative study of greenhouse gas emissions between off-site prefabrication and conventional construction methods: Two case studies of residential projects. *Energy and Buildings, 66*, 165-176.

Mao, C., Xie, F., Hou, L., Wu, P., Wang, J., & Wang, X. (2016). Cost analysis for sustainable off-site construction based on a multiple-case study in China. *Habitat International, 57*, 215-222.

Marchal, V., Dellink, R., Van Vuuren, D., Clapp, C., Chateau, J., Magné, B., & Van Vliet, J. (2011). OECD environmental outlook to 2050. *Organization for Economic Co-operation and Development, 8*, 397-413.

Mariappan, T. (2016). Recent developments of intumescent fire protection coatings for structural steel: A review. *Journal of fire sciences, 34*(2), 120-163.

McCollum, D. L., Gould, G., & Greene, D. L. (2010). Greenhouse gas emissions from aviation and marine transportation: Mitigation potential and policies.

Mechtcherine, V., Bos, F. P., Perrot, A., da Silva, W. L., Nerella, V., Fataei, S., . . . Roussel, N. (2020). Extrusion-based additive manufacturing with cement-based materials–Production steps, processes, and their underlying physics: A review. *Cement and Concrete Research, 132*, 106037.

Meibodi, M. A., Jipa, A., Giesecke, R., Shammas, D., Bernhard, M., Leschok, M., . . . Dillenburger, B. (2018). Smart Slab. Computational design and digital fabrication of a lightweight concrete slab.

Meier, C., Weissbach, R., Weinberg, J., Wall, W. A., & Hart, A. J. (2019). Critical influences of particle size and adhesion on the powder layer uniformity in metal additive manufacturing. *Journal of Materials Processing Technology, 266*, 484-501.

Menna, C., Mata-Falcón, J., Bos, F. P., Vantyghem, G., Ferrara, L., Asprone, D., . . . Kaufmann, W. (2020). Opportunities and challenges for structural engineering of digitally fabricated concrete. *Cement and Concrete Research, 133*, 106079.

Miller, D., Doh, J.-H., Guan, H., Mulvey, M., Fragomeni, S., McCarthy, T., & Peters, T. (2013). Environmental impact assessment of post tensioned and reinforced concrete slab construction.

Miller, D., Doh, J.-H., & Mulvey, M. (2015). Concrete slab comparison and embodied energy optimisation for alternate design and construction techniques. *Construction and Building Materials, 80*, 329-338.

Miyanaji, H., Zhang, S., & Yang, L. (2018). A new physics-based model for equilibrium saturation determination in binder jetting additive manufacturing process. *International Journal of Machine Tools and Manufacture, 124*, 1-11.

Mohan, M. K., Rahul, A., Van Tittelboom, K., & De Schutter, G. (2020). *Evaluating the Influence of Aggregate Content on Pumpability of 3D Printable Concrete.* Paper presented at the RILEM International Conference on Concrete and Digital Fabrication.

Mostafaei, A., Elliott, A. M., Barnes, J. E., Li, F., Tan, W., Cramer, C. L., . . . Chmielus, M. (2020). Binder jet 3D printing–process parameters, materials, properties, and challenges. *Progress in Materials Science*, 100707.

Motro, R. (2009). *An anthology of structural morphology*: World scientific.

Motta, E. (1999). *Reusable components for knowledge modelling: Case studies in parametric design problem solving* (Vol. 53): IOS press.

Nouri-Baranger, T. (2004). Computational methods for tension-loaded structures. *Archives of Computational Methods in Engineering, 11*(2), 143.

Odaglia, P., Voney, V., Dillenburger, B., & Habert, G. (2020). *Advances in Binder-Jet 3D Printing of Non-cementitious Materials.* Paper presented at the RILEM International Conference on Concrete and Digital Fabrication.

Osher, S., & Sethian, J. A. (1988). Fronts propagating with curvature-dependent speed: algorithms based on Hamilton-Jacobi formulations. *Journal of computational physics, 79*(1), 12-49.

Oxman, R. (2006). Theory and design in the first digital age. *Design studies, 27*(3), 229-265.

Pan, W., Gibb, A. G., & Dainty, A. R. (2012). Strategies for integrating the use of off-site production technologies in house building. *Journal of Construction Engineering and Management, 138*(11), 1331-1340.

Pegna, J. (1997). Exploratory investigation of solid freeform construction. *Automation in construction, 5*(5), 427-437.

Piegl, L., & Tiller, W. (2012). *The NURBS book*: Springer Science & Business Media.

Piker, D. (2013). Kangaroo: form finding with computational physics. *Architectural Design, 83*(2), 136-137.

Plaut, R. H. (2015). Snap-through of arches and buckled beams under unilateral displacement control. *International Journal of Solids and Structures, 63*, 109-113.

Popescu, M., Rippmann, M., Liew, A., Reiter, L., Flatt, R. J., Van Mele, T., & Block, P. (2020). *Structural design, digital fabrication and construction of the cable-net and knitted formwork of the KnitCandela concrete shell.* Paper presented at the Structures.

Popescu, M., Rippmann, M., Van Mele, T., & Block, P. (2018). Automated generation of knit patterns for non-developable surfaces. In *Humanizing Digital Reality* (pp. 271-284): Springer.

Preisinger, C. (2015). Karamba3D. *Version, 1*(2), 25.

Rahman, A., Rasul, M., Khan, M. M. K., & Sharma, S. (2015). Recent development on the uses of alternative fuels in cement manufacturing process. *Fuel, 145*, 84-99.

Recast, E. (2010). Directive 2010/31/EU of the European Parliament and of the Council of 19 May 2010 on the energy performance of buildings (recast). *Official Journal of the European Union, 18*(06), 2010.

Reiter, L., Wangler, T., Roussel, N., & Flatt, R. J. (2018). The role of early age structural build-up in digital fabrication with concrete. *Cement and Concrete Research, 112*, 86-95.

Rhodes, C. J. (2016). The 2015 Paris climate change conference: COP21. *Science progress, 99*(1), 97-104.

Rios, L. M., & Sahinidis, N. V. (2013). Derivative-free optimization: a review of algorithms and comparison of software implementations. *Journal of Global Optimization, 56*(3), 1247-1293.

Rippmann, M. (2016). *Funicular Shell Design: Geometric approaches to form finding and fabrication of discrete funicular structures.* ETH Zurich,

Rippmann, M., Liew, A., Van Mele, T., & Block, P. (2018). Design, fabrication and testing of discrete 3D sand-printed floor prototypes. *Materials Today Communications, 15*, 254-259.

Rippmann, M., Van Mele, T., & Block, P. (2018). Design, fabrication and testing of discrete 3D sand-printed floor prototypes. *Materials Today Communications Volume 15, June 2018*, 254-259.

Roadmap to a Resource Efficient Europe (2011). Retrieved from Brussels:

Rutten, D. (2015). Grasshopper3D. In.

Ruuska, A., & Hakkinen, T. (2014). Material Efficiency of Building Construction. *Buildings, 4(3)*, 266-294.

Samuel, F. (2007). *Le Corbusier in detail*: Routledge.

Sanjayan, J. G., & Nematollahi, B. (2019). 3D concrete printing for construction applications. *3D concrete Printing Technology,* 1-11.

Saremi, S., Mirjalili, S., & Lewis, A. (2017). Grasshopper optimisation algorithm: theory and application. *Advances in Engineering Software, 105*, 30-47.

Seo, J. H., Amr, I. T., Park, S. M., Bamagain, R. A., Fadhel, B. A., Kim, G. M., . . . Lee, H. K. (2018). CO2 uptake of carbonation-cured cement blended with ground volcanic ash. *Materials, 11*(11), 2187.

Shafigh, P., Asadi, I., & Mahyuddin, N. B. (2018). Concrete as a thermal mass material for building applications-A review. *Journal of Building Engineering, 19*, 14-25.

Sigmund, O., Clausen, A., Groen, J. P., & Wu, J. (2017). *Topology optimization of structures and infill for additive manufacturing.* Paper presented at the Simulation for Additive Manufacturing.

Sigmund, O., & Maute, K. (2013). Topology optimization approaches. *Structural and Multidisciplinary Optimization, 48*(6), 1031-1055.

Sotayo, A., Bradley, D., Bather, M., Sareh, P., Oudjene, M., El-Houjeyri, I., . . . Haller, P. (2020). Review of state of the art of dowel laminated timber members and densified wood materials as sustainable engineered wood products for construction and building applications. *Developments in the Built Environment, 1*, 100004.

Suiker, A. S., Wolfs, R. J., Lucas, S. M., & Salet, T. A. (2020). Elastic buckling and plastic collapse during 3D concrete printing. *Cement and Concrete Research, 135*, 106016.

Szabó, L., Hidalgo, I., Císcar, J. C., Soria, A., & Russ, P. (2003). Energy consumption and CO2 emissions from the world cement industry. *European Commission Joint Research Centre, Report EUR, 20769*.

Tam, V. W., Butera, A., Le, K. N., & Li, W. (2020). Utilising CO2 technologies for recycled aggregate concrete: A critical review. *Construction and Building Materials, 250*, 118903.

Tam, V. W., Tam, C. M., & Ng, W. C. (2007). On prefabrication implementation for different project types and procurement methods in Hong Kong. *Journal of Engineering, Design and Technology*.

Taylor, M., Tam, C., & Gielen, D. (2006). Energy efficiency and CO2 emissions from the global cement industry. *Korea, 50*(2.2), 61.67.

Taylor, S., Rankin, G., & Cleland, D. (2001). Arching action in high-strength concrete slabs. *Proceedings of the Institution of Civil Engineers-Structures and Buildings, 146*(4), 353-362.

Tellnes, L. G., Ganne-Chedeville, C., Dias, A., Dolezal, F., Hill, C., & Zea Escamilla, E. (2017). Comparative assessment for biogenic carbon accounting methods in carbon footprint of products: A review study for construction materials based on forest products. *iForest: Biogeosciences and Forestry, 10*, 815-823.

Tregambi, C., Salatino, P., Solimene, R., & Montagnaro, F. (2018). An experimental characterization of Calcium Looping integrated with concentrated solar power. *Chemical Engineering Journal, 331*, 794-802.

Tsangouri, E., Van Driessche, A., Livitsanos, G., & Aggelis, D. G. (2020). Design, casting and fracture analysis of textile reinforced cementitious shells. *Developments in the Built Environment*, 100013.

Tuojy, P., McElroy, L., & Johnstone, C. (2005). *Thermal mass, insulation and ventilation in sustainable housing- An investigation across climate and occupancy*.

Turrin, M., Von Buelow, P., & Stouffs, R. (2011). Design explorations of performance driven geometry in architectural design using parametric modeling and genetic algorithms. *Advanced Engineering Informatics, 25*(4), 656-675.

Valeri, P., Guaita, P., Baur, R., Fernández Ruiz, M., Fernández-Ordóñez, D., & Muttoni, A. (2020). Textile reinforced concrete for sustainable structures: Future perspectives and application to a prototype pavilion. *Structural Concrete*.

van Dijk, N. P., Maute, K., Langelaar, M., & Van Keulen, F. (2013). Level-set methods for structural topology optimization: a review. *Structural and Multidisciplinary Optimization, 48*(3), 437-472.

Van Mele, T., Liew, A., Mendez, T., & Rippmann, M. (2017). COMPAS: A framework for computational research in architecture and structures. In.

Van Oss, H. G., & Padovani, A. C. (2002). Cement manufacture and the environment: part I: chemistry and technology. *Journal of Industrial Ecology, 6*(1), 89-105.

Van Ruijven, B. J., Van Vuuren, D. P., Boskaljon, W., Neelis, M. L., Saygin, D., & Patel, M. K. (2016). Long-term model-based projections of energy use and CO2 emissions from the global steel and cement industries. *Resources, Conservation and Recycling, 112*, 15-36.

Vecchio, F., & Collins, M. (1990). Investigating the Collapse of a Warehouse. *Concrete International, March, 3*.

Veenendaal, D., & Block, P. (2012). An overview and comparison of structural form finding methods for general networks. *International Journal of Solids and Structures, 49*(26), 3741-3753.

Vizcaíno-Andrés, L., Sánchez-Berriel, S., Damas-Carrera, S., Pérez-Hernández, A., Scrivener, K., & Martirena-Hernández, J. (2015). Industrial trial to produce a low clinker, low carbon cement. *Materiales de Construcción, 65*(317), 045.

VOBN. (2013). Betonmortel specificaties voor de bestelling. In.

Vogtlander, J. G. (2016). A practical guide to LCA for students designers and business managersL Cradle-to-Grave and Cradle-to-craddle. *Delft Academic Press*.

Wang, W., Munro, D., Wang, C. C., van Keulen, F., & Wu, J. (2020). Space-time topology optimization for additive manufacturing. *Structural and Multidisciplinary Optimization, 61*(1), 1-18.

Wangler, T., Lloret, E., Reiter, L., Hack, N., Gramazio, F., Kohler, M., . . . Roussel, N. (2016). Digital concrete: opportunities and challenges. *RILEM Technical Letters, 1*, 67-75.

Watts, J. (2019, Februari 25). Concrete: the most destructive material on Earth. *The Guardian,* 1.

Wight, J. K., & MacGregor, J. G. (2009). Reinforced concrete: Mechanics and design. *Prentice hall.*

Wijte, S. (2019). Influence of sustainable cement alternatives on the design and construction of concrete structures.

Wolpert, D. H., & Macready, W. G. (1997). No free lunch theorems for optimization. *IEEE transactions on evolutionary computation, 1*(1), 67-82.

Wortmann, T., Costa, A., Nannicini, G., & Schroepfer, T. (2015). Advantages of surrogate models for architectural design optimization. *Artificial Intelligence for Engineering Design, Analysis and Manufacturing: AI EDAM, 29*(4), 471.

Wortmann, T., & Nannicini, G. (2016). Black-box optimization for architectural design: An overview and quantitative comparison of metaheuristic, direct search, and model-based optimization methods. *Living Systems and Micro-Utopias*, 177-186.

Wright, M. H. (1996). Direct search methods: Once scorned, now respectable.

Wu, J., Aage, N., Westermann, R., & Sigmund, O. (2017). Infill optimization for additive manufacturing—approaching bone-like porous structures. *IEEE transactions on visualization and computer graphics, 24*(2), 1127-1140.

Wu, J., Aage, N., Lefebvre, S., & Wang, C. (2017). Topology optimization for computational fabrication (2017). In: Eurographics tutorials.

Wu, P., Wang, J., & Wang, X. (2016). A critical review of the use of 3-D printing in the construction industry. *Automation in construction, 68*, 21-31.

Yang, K.-H., Seo, E.-A., & Tae, S.-H. (2014). Carbonation and CO2 uptake of concrete. *Environmental Impact Assessment Review, 46*, 43-52.

Yang, X.-S. (2010). *Engineering optimization: an introduction with metaheuristic applications*: John Wiley & Sons.

Zhang, P., Liu, J., & To, A. C. (2017). Role of anisotropic properties on topology optimization of additive manufactured load bearing structures. *Scripta Materialia, 135*, 148-152.

Zhang, Y., Wang, W., & Hughes, T. J. (2012). Solid T-spline construction from boundary representations for genus-zero geometry. *Computer Methods in Applied Mechanics and Engineering, 249*, 185-197.

10 Appendix

AA appendix: Excel calculation emissions of floor slabs

BB appendix: Excel calculation emissions of virtual office buildings

CC appendix: Design to fabrication flowchart

DD appendix: Derivative-free concurrent optimization process

Appendix AA: Excel calculation emissions of 3600 x 5400mm Floor slabs

Z	Global Warming Potential	Ozone Depletion Potential	Human Toxicity Potential	Fresh Water Aquatic Ecotoxicity	Terrestrial Ecotoxicity	Photochemical Oxidation	Acidification Potential	Eutrophication Potential	Abiotic Depletion Potential
	GWP	ODP	HTP	FWAE	TE	PO	AP	EP	ADP
	kg CO 2 eq.	kg CFC-11 eq.	Kg 1,4-DCB eq.	kg 1,4-DCB eq.	kg 1,4-DCB eq.	kg C 2 H 4 eq.	kg SO 2 eq.	kg PO4 eq.	kg PO4 eq.
	€ 0,06	€ 30,40	€ 0,16	€ 0,04	€ 8,89	€ 2,10	€ 5,40	€ 3,11	€ 0,16

	GWP	ODP	HTP	FWAE	TE	PO	AP	EP	ADP	Source NMD 2.3	
Proposed floorslab NMD 2.3 concrete 240mm	2,20E+02	1,93E-05	1,28E+02	2,48E+00	1,25E+00	2,38E+00	1,25E+00	1,66E-01	3,63E+00	Total CO2 emissions	**264,32 kg**
	€ 12,56	€ 0,00	€ 20,16	€ 0,09	€ 11,10	€ 5,00	€ 6,74	€ 0,52	€ 0,58	Associated Shadow cost	**€ 218,19**
	GWP	ODP	HTP	FWAE	TE	PO	AP	EP	ADP	Source NMD 2.3	
New floor slab 240mm (Betonhuis concrete)	3,14E+02	1,51E-05	1,19E+02	2,34E+00	1,71E+00	2,38E+00	1,28E+00	8,62E-02	5,62E+00	Total CO2 emissions	**376,45 kg**
	€ 17,88	€ 0,00	€ 18,86	€ 0,09	€ 15,17	€ 5,00	€ 6,92	€ 0,27	€ 0,90	Associated shadow cost	**€ 226,68**
	GWP	ODP	HTP	FWAE	TE	PO	AP	EP	ADP	Source NMD 2.3	
VBI Hollow-core slab 150mm Green	4,69E+02	0,00E+00	1,32E+02	3,50E+00	4,20E+00	2,00E-01	2,00E+00	4,00E-01	2,30E+00	Total CO2 emissions	**469,20 kg**
	€ 26,74	€ 0,00	€ 20,84	€ 0,13	€ 37,34	€ 0,42	€ 10,80	€ 1,24	€ 0,37	Associated shadow cost	**€ 242,25**
	GWP	ODP	HTP	FWAE	TE	PO	AP	EP	ADP	Source NMD 2.3	
Dycore Hollow-core slab 150mm	6,99E+02	0,00E+00	1,06E+02	3,40E+00	4,90E+00	0,00E+00	2,10E+00	4,00E-01	2,60E+00	Total CO2 emissions	**699,40 kg**
	€ 39,87	€ 0,00	€ 16,70	€ 0,13	€ 43,56	€ 0,00	€ 11,34	€ 1,24	€ 0,42	Associated shadow cost	**€ 241,07**
	GWP	ODP	HTP	FWAE	TE	PO	AP	EP	ADP	Source NMD 2.3	
Wooden hollow core slab 280mm	9,18E+01	0,00E+00	3,60E+02	1,45E+01	2,70E+00	1,20E+00	4,50E+00	1,10E+00	3,00E-01	Total CO2 emissions	**91,80 kg**
	€ 5,23	€ 0,00	€ 56,82	€ 0,54	€ 24,00	€ 2,52	€ 24,30	€ 3,42	€ 0,05	Associated shadow cost	**€ 339,45**
	GWP	ODP	HTP	FWAE	TE	PO	AP	EP	ADP	Source NIBE	
European softwood beam floor 246mm	1,88E+02	0,00E+00	2,61E+02	9,50E+00	2,40E+00	9,00E-01	3,10E+00	8,00E-01	1,40E+00	Total CO2 emissions	**187,50 kg**
	€ 10,69	€ 0,00	€ 41,22	€ 0,35	€ 21,34	€ 1,89	€ 16,74	€ 2,49	€ 0,22	Associated shadow cost	**€ 356,82**
	GWP	ODP	HTP	FWAE	TE	PO	AP	EP	ADP	Source NIBE	
Solid wood floor 200 mm	1,23E+03	1,40E-04	3,81E+02	1,28E+01	2,62E+00	1,08E+00	5,37E+00	9,29E-01	3,42E-03	Total CO2 emissions	**1230,55 kg**
	€ 70,14	€ 0,00	€ 60,20	€ 0,47	€ 23,33	€ 2,26	€ 28,97	€ 2,89	€ 0,00	Associated shadow cost	**€ 502,78**
	GWP	ODP	HTP	FWAE	TE	PO	AP	EP	ADP	Source NIBE	
In situ concrete floor 250 mm	1,76E+03	1,22E-04	2,08E+02	7,25E+00	2,16E+00	3,83E-01	4,84E+00	8,53E-01	1,77E-03	Total CO2 emissions	**1757,40 kg**
	€ 100,17	€ 0,00	€ 32,87	€ 0,27	€ 19,18	€ 0,80	€ 26,14	€ 2,65	€ 0,00	Associated shadow cost	**€ 398,13**
	GWP	ODP	HTP	FWAE	TE	PO	AP	EP	ADP	Source NIBE	
Aerated concrete floor	1,58E+03	8,03E-05	1,92E+02	5,31E+00	1,93E+00	3,13E-01	3,44E+00	5,17E-01	1,96E-03	Total CO2 emissions	**1582,42**
	€ 90,20	€ 0,00	€ 30,41	€ 0,20	€ 17,20	€ 0,66	€ 18,58	€ 1,61	€ 0,00	Associated shadow cost	**€ 341,08**
	GWP	ODP	HTP	FWAE	TE	PO	AP	EP	ADP	Source NIBE	
Lattice girder floor (200mm)	1,88E+03	1,15E-04	2,88E+02	7,25E+00	2,33E+00	5,83E-01	6,16E+00	9,35E-01	1,39E-03	Total CO2 emissions	**1881,792**
	€ 107,26	€ 0,00	€ 45,46	€ 0,27	€ 20,74	€ 1,22	€ 33,28	€ 2,91	€ 0,00	Associated shadow cost	**€ 458,04**
	GWP	ODP	HTP	FWAE	TE	PO	AP	EP	ADP	Source NIBE	
Lattice girder floor (200mm)	1,88E+03	1,15E-04	2,88E+02	7,25E+00	2,33E+00	5,83E-01	6,16E+00	9,35E-01	1,39E-03	Total CO2 emissions	**1881,792**
	€ 107,26	€ 0,00	€ 45,46	€ 0,27	€ 20,74	€ 1,22	€ 33,28	€ 2,91	€ 0,00	Associated shadow cost	**€ 458,04**
	GWP	ODP	HTP	FWAE	TE	PO	AP	EP	ADP	Source NIBE	
Precast concrete shell with I-profiles (IPE 270 at 1200 mm centers)	1,31E+03	7,95E-05	1,67E+02	5,07E+00	1,54E+00	4,00E-01	4,41E+00	6,80E-01	8,50E-04	Total CO2 emissions	**1308,312**
	€ 74,57	€ 0,00	€ 26,35	€ 0,19	€ 13,67	€ 0,84	€ 23,83	€ 2,12	€ 0,00	Associated shadow cost	**€ 298,83**
	GWP	ODP	HTP	FWAE	TE	PO	AP	EP	ADP	Source NIBE	
Hollow-core slab floor incl pressure layer (thickness 200 mm)	1,55E+03	1,00E-04	2,02E+02	5,73E+00	1,96E+00	3,73E-01	4,20E+00	7,21E-01	1,32E-03	Total CO2 emissions	**1553,256**
	€ 88,54	€ 0,00	€ 31,94	€ 0,21	€ 17,45	€ 0,78	€ 22,67	€ 2,24	€ 0,00	Associated shadow cost	**€ 340,21**
	GWP	ODP	HTP	FWAE	TE	PO	AP	EP	ADP	Source NIBE	
Climate floor (thickness 260 mm)	1,76E+03	1,22E-04	2,08E+02	7,25E+00	2,16E+00	3,83E-01	4,84E+00	8,53E-01	1,77E-03	Total CO2 emissions	**1757,376**
	€ 100,17	€ 0,00	€ 32,87	€ 0,27	€ 19,18	€ 0,80	€ 26,14	€ 2,65	€ 0,00	Associated shadow cost	**€ 398,13**
	GWP	ODP	HTP	FWAE	TE	PO	AP	EP	ADP	Source NIBE	
Bubble deck floor (thickness 230mm)	1,94E+03	1,04E-04	2,80E+02	7,50E+00	2,26E+00	6,59E-01	6,14E+00	9,02E-01	1,30E-03	Total CO2 emissions	**1944**
	€ 110,81	€ 0,00	€ 44,23	€ 0,28	€ 20,05	€ 1,38	€ 33,17	€ 2,81	€ 0,00	Associated shadow cost	**€ 458,16**
	GWP	ODP	HTP	FWAE	TE	PO	AP	EP	ADP	Source NIBE	
Cassette floor (thickness 220 mm)	2,02E+03	1,67E-04	5,21E+02	3,95E+01	3,58E+00	7,81E-01	8,48E+00	1,22E+00	8,13E-02	Total CO2 emissions	**2021,76**
	€ 115,24	€ 0,01	€ 82,32	€ 1,46	€ 31,80	€ 1,64	€ 45,77	€ 3,80	€ 0,01	Associated shadow cost	**€ 846,39**

Appendix BB: Excel calculation emissions of hypothetical office building

	GWP	ODP	HTP	FWAE	TE	PO	AP	EP	ADP	Source NMD 2.3	
optimized floorslab: 3600mm x 5400mm (NMD 2.3 CEM III/B)	2,20E+02	1,93E-05	5,07E+01	1,13E+00	5,30E-01	9,94E-02	9,94E-01	1,66E-01	0,00E+00	Total CO2 emissions	**264,00 kg**
	€ 12,56	€ 0,00	€ 20,16	€ 0,09	€ 11,10	€ 5,00	€ 6,74	€ 0,52	€ 0,58	Associated shadow cost	**€ 68,10**
	GWP	ODP	HTP	FWAE	TE	PO	AP	EP	ADP	Source NMD 2.3	
optimized floorslab: 3600mm x 2400mm (NMD 2.3 CEM III/B)	7,89E+01	6,88E-06	8,20E+01	1,53E+00	7,87E-01	1,93E+00	5,66E-01	5,91E-02	3,02E+00	Total CO2 emissions	**94,68 kg**
	€ 4,50	€ 0,00	€ 12,96	€ 0,06	€ 7,00	€ 4,05	€ 3,06	€ 0,18	€ 0,48	Associated shadow cost	**€ 38,74**
	GWP	ODP	HTP	FWAE	TE	PO	AP	EP	ADP	Source NMD 2.3	
Overall impact of the optimized floor slab (NMD 2.3 CEM III/B)	1,56E+03	1,36E-04	5,50E+02	1,14E+01	5,54E+00	6,39E+00	7,66E+00	1,17E+00	9,06E+00	Total CO2 emissions	1868,0 kg
	€ 88,73	€ 0,00	€ 86,93	€ 0,42	€ 49,26	€ 13,41	€ 41,37	€ 3,65	€ 1,45	Associated shadow cost	€ 342,28
	GWP	ODP	HTP	FWAE	TE	PO	AP	EP	ADP	Source NMD 2.3	
VBI hollowcore slab 5400x1200x150mm green	1,56E+02	0,00E+00	4,40E+01	1,17E+00	1,40E+00	6,67E-02	6,67E-01	1,33E-01	7,67E-01	Total CO2 emissions	**156,40 kg**
	€ 8,91	€ 0,00	€ 6,95	€ 0,04	€ 12,45	€ 0,14	€ 3,60	€ 0,41	€ 0,12	Associated shadow cost	**€ 32,63**
	GWP	ODP	HTP	FWAE	TE	PO	AP	EP	ADP	Source NMD 2.3	
VBI hollowcore green slab 2400x1200x150mm	6,70E+01	0,00E+00	1,88E+01	5,00E-01	6,00E-01	2,86E-02	2,86E-01	5,71E-02	3,29E-01	Total CO2 emissions	**67,03 kg**
	€ 3,82	€ 0,00	€ 2,98	€ 0,02	€ 5,33	€ 0,06	€ 1,54	€ 0,18	€ 0,05	Associated shadow cost	**€ 13,98**
	GWP	ODP	HTP	FWAE	TE	PO	AP	EP	ADP	Source NMD 2.3	
THQ 150x5-190x12-400x8 beam	7,59E-02	0,00E+00	1,02E+01	1,79E-01	9,49E-02	3,01E-01	3,35E-02	0,00E+00	4,80E-01	Total CO2 emissions	0,1 kg
	€ 0,00	€ 0,00	€ 1,60	€ 0,01	€ 0,84	€ 0,63	€ 0,18	€ 0,00	€ 0,08	Associated shadow cost	€ 3,35
	GWP	ODP	HTP	FWAE	TE	PO	AP	EP	ADP	Source NMD 2.3	
Overall impact of VBI hollowcore slab	4,96E+03	1,54E+03	4,96E+03	3,56E+03	3,53E+03	3,49E+03	3,48E+03	3,46E+03	3,66E+03	Total CO2 emissions	3421,7 kg
	€ 195,04	€ 0,00	€ 221,15	€ 1,23	€ 308,46	€ 30,40	€ 86,50	€ 9,06	€ 6,00	Associated shadow cost	€ 857,84
	GWP	ODP	HTP	FWAE	TE	PO	AP	EP	ADP	Source NMD 2.3	
Dycore hollow-core slab 5400x1200x150mm	1,56E+02	0,00E+00	4,40E+01	1,17E+00	1,40E+00	6,67E-02	6,67E-01	1,33E-01	5,00E-01	Total CO2 emissions	**156,40 kg**
	€ 8,91	€ 0,00	€ 6,95	€ 0,04	€ 12,45	€ 0,14	€ 3,60	€ 0,41	€ 0,12	Associated shadow cost	**€ 32,63**
	GWP	ODP	HTP	FWAE	TE	PO	AP	EP	ADP	Source NMD 2.3	
Dycore hollow-core slab 2400x1200x150mm	9,99E+01	0,00E+00	1,51E+01	7,00E-01	0,00E+00	3,00E-01	5,71E-02	3,71E-01	4,86E-01	Total CO2 emissions	**99,91 kg**
	€ 5,70	€ 0,00	€ 2,39	€ 6,22	€ 0,00	€ 1,62	€ 0,18	€ 0,06	€ 0,05	Associated shadow cost	**€ 16,16**
	GWP	ODP	HTP	FWAE	TE	PO	AP	EP	ADP	Source NMD 2.3	
THQ 150x5-190x12-400x8 beam	7,59E-02	0,00E+00	1,02E+01	1,79E-01	9,49E-02	3,01E-01	3,35E-02	0,00E+00	4,80E-01	Total CO2 emissions	0,1 kg
	€ 0,00	€ 0,00	€ 1,60	€ 0,01	€ 0,84	€ 0,63	€ 0,18	€ 0,00	€ 0,08	Associated shadow cost	€ 3,35
	GWP	ODP	HTP	FWAE	TE	PO	AP	EP	ADP	Source NMD 2.3	
Overall impact of Dycore hollow-core slab	5,10E+03	0,00E+00	1,21E+03	3,98E+01	1,30E+01	1,67E+01	2,91E+00	3,97E+01	3,66E+03	Total CO2 emissions	5098,9 kg
	€ 290,64	€ 0,00	€ 190,99	€ 353,80	€ 27,34	€ 90,43	€ 9,06	€ 6,35	€ 6,35	Associated shadow cost	€ 968,61
	GWP	ODP	HTP	FWAE	TE	PO	AP	EP	ADP	Source NMD 2.3	
Lattice girder 3600mm x 5400mm	6,20E+02	5,43E-05	2,10E+02	4,35E+00	2,12E+00	2,26E+00	3,02E+00	4,67E-01	3,16E+00	Total CO2 emissions	**619,00 kg**
	€ 35,31	€ 0,00	€ 33,16	€ 0,16	€ 18,80	€ 4,75	€ 16,31	€ 1,45	€ 0,51	Associated shadow cost	**€ 110,45**
	GWP	ODP	HTP	FWAE	TE	PO	AP	EP	ADP	Source NMD 2.3	
Lattice girder 3600mm x 2400mm	2,76E+02	2,42E-05	9,35E+01	1,94E+00	9,42E-01	1,01E+00	1,34E+00	2,08E-01	1,41E+00	Total CO2 emissions	**275,68 kg**
	€ 15,73	€ 0,00	€ 14,77	€ 0,07	€ 8,37	€ 2,11	€ 7,26	€ 0,65	€ 0,23	Associated shadow cost	**€ 49,19**
	GWP	ODP	HTP	FWAE	TE	PO	AP	EP	ADP	Source NMD 2.3	
THQ 150x5-190x12-400x8 beam	7,59E-02	0,00E+00	1,02E+01	1,79E-01	9,49E-02	3,01E-01	3,35E-02	0,00E+00	4,80E-01	Total CO2 emissions	0,1 kg
	€ 0,00	€ 0,00	€ 1,60	€ 0,01	€ 0,84	€ 0,63	€ 0,18	€ 0,00	€ 0,08	Associated shadow cost	€ 3,35
	GWP	ODP	HTP	FWAE	TE	PO	AP	EP	ADP	Source NMD 2.3	
Overall impact of Dycore hollow-core slab	4,55E+03	3,98E-04	1,98E+03	3,96E+01	1,96E+01	2,96E+01	2,36E+01	3,43E+00	4,39E+01	Total CO2 emissions	4548,0 kg
	€ 259,23	€ 0,01	€ 312,61	€ 1,46	€ 174,37	€ 62,15	€ 127,45	€ 10,65	€ 7,03	Associated shadow cost	€ 954,97
	GWP	ODP	HTP	FWAE	TE	PO	AP	EP	ADP	Source NIBE	
Lattice girder 3600mm x 5400mm (CEMI NIBE)	1,88E+03	1,15E-04	2,88E+02	7,25E+00	2,33E+00	5,83E-01	6,16E+00	9,35E-01	1,39E-03	Total CO2 emissions	**1881,79 kg**
	€ 107,26	€ 0,00	€ 45,46	€ 0,27	€ 20,74	€ 1,22	€ 33,28	€ 2,91	€ 0,00	Associated shadow cost	**€ 211,14**
	GWP	ODP	HTP	FWAE	TE	PO	AP	EP	ADP	Source NIBE	
Lattice girder 3600mm x 2400mm (CEMI NIBE)	8,36E+02	5,11E-05	1,28E+02	3,22E+00	1,04E+00	2,59E-01	2,74E+00	4,16E-01	6,19E-04	Total CO2 emissions	**836,35 kg**
	€ 47,67	€ 0,00	€ 20,20	€ 0,12	€ 9,22	€ 0,54	€ 14,79	€ 1,29	€ 0,00	Associated shadow cost	**€ 93,84**
	GWP	ODP	HTP	FWAE	TE	PO	AP	EP	ADP	Source NIBE	
THQ 150x5-190x12-400x8 beam	7,59E-02	0,00E+00	1,02E+01	1,79E-01	9,49E-02	3,01E-01	3,35E-02	0,00E+00	4,80E-01	Total CO2 emissions	0,1 kg
	€ 0,00	€ 0,00	€ 1,60	€ 0,01	€ 0,84	€ 0,63	€ 0,18	€ 0,00	€ 0,08	Associated shadow cost	€ 3,35
	GWP	ODP	HTP	FWAE	TE	PO	AP	EP	ADP	Source NIBE	
Overall impact of the lattice girder flooring system (CEMI NIBE)	1,65E+04	2,72E+03	1,65E+04	1,40E+04	1,39E+04	1,39E+04	1,39E+04	1,38E+04	1,38E+04	Total CO2 emissions	13803,1 kg
	€ 786,78	€ 0,03	€ 402,68	€ 2,25	€ 188,51	€ 36,32	€ 251,84	€ 21,33	€ 3,32	Associated shadow cost	€ 1.693,05

Appendix CC: Design to fabrication flowchart of the proposed floorslab based on conventional casting

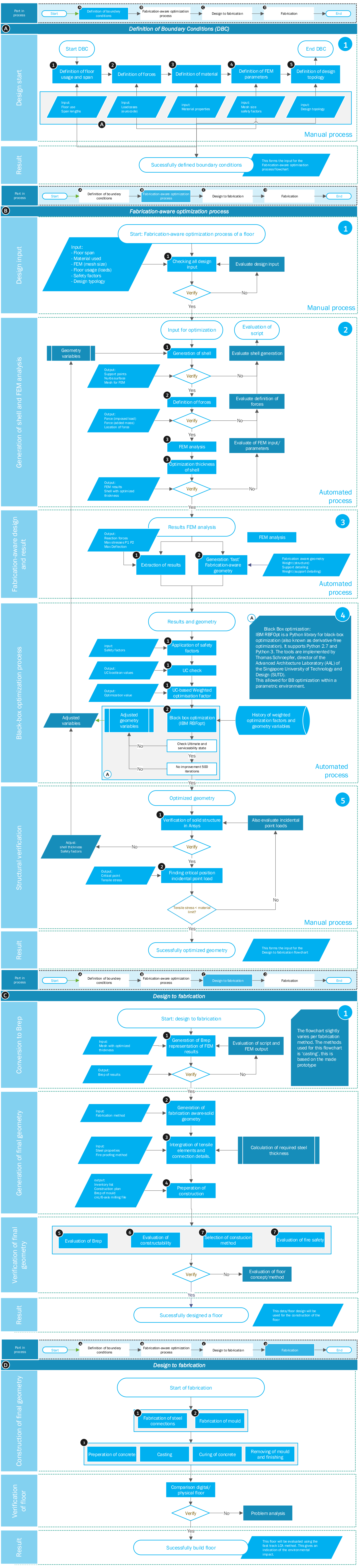
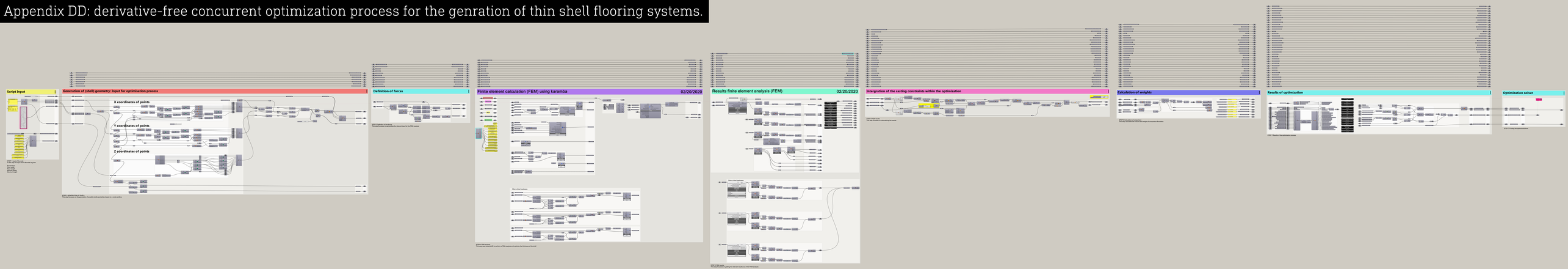
Appendix DD: derivative-free concurrent optimization process for the genration of thin shell flooring systems.